

**Reconstruction of past changes in ocean salinity –
a compound specific stable hydrogen isotope
approach**

Sebastian Kasper

ISBN 978-94-6203-839-4

Printed by Wöhrmann Print Service, Zutphen.

cover image: Ocean surface salinity map from Ocean Atlas 2009
generated in Ocean Data View

**Reconstruction of past changes in ocean salinity –
a compound specific stable hydrogen isotope approach**

**Reconstructie van saliniteitsveranderingen van de Oceaan in het verleden –
een component specifieke stabiele waterstof isotopen benadering**
(met een samenvatting in het Nederlands)

**Rekonstruktion der Salinitätveränderungen vergangener Ozeane –
ein komponentenspezifischer stabiler Wasserstoff Isotopen Ansatz**
(mit einer Zusammenfassung in deutscher Sprache)

Proefschrift

ter verkrijging van de graad van doctor aan de Universiteit Utrecht op gezag van
de rector magnificus, prof.dr. G.J. van der Zwaan, ingevolge het besluit van het
college voor promoties in het openbaar te verdedigen op dinsdag 23 juni 2015
des avonds te 6.00 uur

door

Sebastian Kasper

geboren op 25 september 1983 te Heinsberg, Duitsland

Promotoren: Prof. dr. ir. S. Schouten
Prof. dr. ir. J.S. Sinninghe Damsté

Copromotor: Dr. M.T.J. van der Meer

For my brothers.

Table of contents

Chapter 1	Introduction and general outline	7
PART I		
Chapter 2	Salinity changes in the Agulhas leakage area recorded by stable Hydrogen isotopes of C ₃₇ alkenones during Termination I and II	19
Chapter 3	Salinity changes in the southern Agulhas Current since the Last Glacial Maximum	35
Chapter 4	Past salinity changes in the eastern tropical Atlantic as recorded by the stable hydrogen isotope composition of alkenones and $\delta^{18}\text{O}$ of planktonic foraminifera	51
Chapter 5	Evaluating the impact of lateral transport on alkenones using sea surface temperature reconstructions and D/H ratios in the Atlantic sector of the Southern Ocean	63
PART II		
Chapter 6	Testing the alkenone D/H ratio as a paleo indicator of sea surface salinity in a coastal ocean margin (Mozambique Channel)	73
Chapter 7	A 135 ka long record of ocean salinity as recorded by C ₃₇ alkenone hydrogen isotope ratios from offshore Southeast Australia	85
PART III		
Chapter 8	Compound specific stable hydrogen isotopes as tool for past ocean salinity reconstruction - A synthesis and outlook	97
References		107
Summary		127
Samenvatting		131
Zusammenfassung		135
Acknowledgments		139
Curriculum Vitae		140

Chapter 1

Introduction and general outline

1.1. Climate variability and ocean circulation

The increased release of anthropogenic CO_2 to the atmosphere over the past decades is shown to have resulted in a global warming trend (Karl and Trenberth, 2003), which is expected to continue, resulting in future warming of the air and the surface of the oceans (Diffenbaugh et al., 2005; IPCC, 2007). However, the extent of the warming and the consequent implications for the global climate are still heavily debated. For the extrapolation of future climate trends, complex global climate models are used, simulating the interaction between the atmosphere, the oceans (hydrosphere), the land surface (geosphere) and the ice (cryosphere) (Manabe et al., 1979; Bony and Dufresne, 2005; Reichler and Kim, 2008). Ocean circulation and the interaction at the ocean and atmosphere interface play an important role in these models (Webster et al., 1999), since the oceans make up earth's largest storage for energy in the form of momentum, moisture and heat. Changes in ocean currents circulation will, therefore, directly cause changes in the global climate (Ramanathan, 1981; Rahmstorf, 2002; Soden and Held, 2006). Besides the wind-driven ocean currents, an important mechanism of the overall large scale ocean circulation is the heat and salt driven thermohaline circulation (THC) (Figure 1) (Broecker, 1991; Rudnick and Ferrari, 1999; Rahmstorf, 2003). The THC is particularly sensitive to fresh water influx by, for example, melting of the Greenland ice sheets in the Atlantic (Rahmstorf, 1995) or changes in salinity in the Southern Ocean (Keeling and Stephens, 2001).

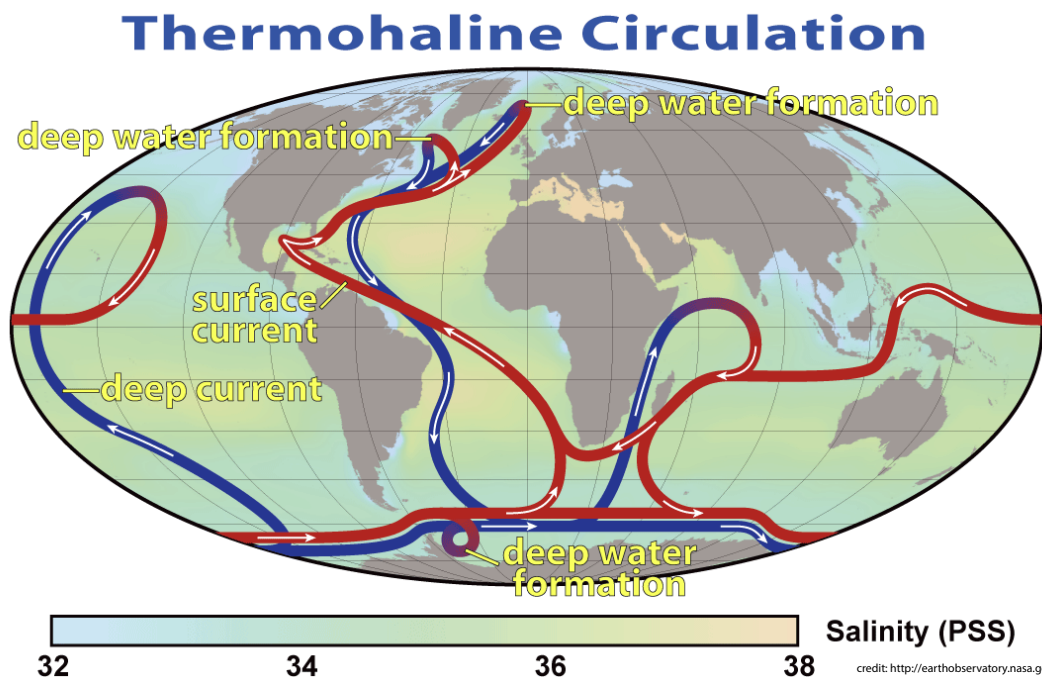


Figure 1. A map showing a simplified model of the global Thermohaline Circulation. Red indicates surface currents and blue deep sea currents. Source: earthobservatory.nasa.gov, date of access 22.12.2014.

In modern day oceans, sea surface salinity (SSS) naturally ranges between 33 – 37 (psu) varying with latitude (Gross, 1987; Antonov et al., 2006) (Figure 2). The latitudinal distribution of SSS is primarily caused by the balance between evaporation and transpiration through atmospheric convection driven by the latitudinal insolation gradient (Libes, 2009). Therefore, SSS is generally elevated in low- to mid-latitudes ($0 - 60^\circ$), where insolation is higher and thus net evaporation exceeds precipitation. Accordingly, higher latitudes ($30 - 90^\circ$) with lower insolation and higher net precipitation are regions of lower SSS (Figure 2) (Antonov et al., 2006). Exceptions of this latitudinal effect are found in semi-enclosed marginal seas, such as the Mediterranean Sea (Brasseur et al., 1996) with elevated net evaporation, i.e. higher salinity, and oppositely in coastal regions with lower salinity due to their closer proximity to freshwater sources, e.g. large rivers and groundwater (Le Vine et al., 1998; Siddorn et al., 2001; Dávila et al., 2002). Besides the latitudinal effect, SSS gradients occur also between Oceans, e.g. the salinity in the Atlantic is generally higher than in the Pacific Ocean (Figure 2) (Antonov et al., 2006). This gradient is generated by the permanent net export of water vapor from the Atlantic to the Pacific and Indian Ocean via the Trade wind system as well as the transport of saline water via the THC (Broecker, 1991).

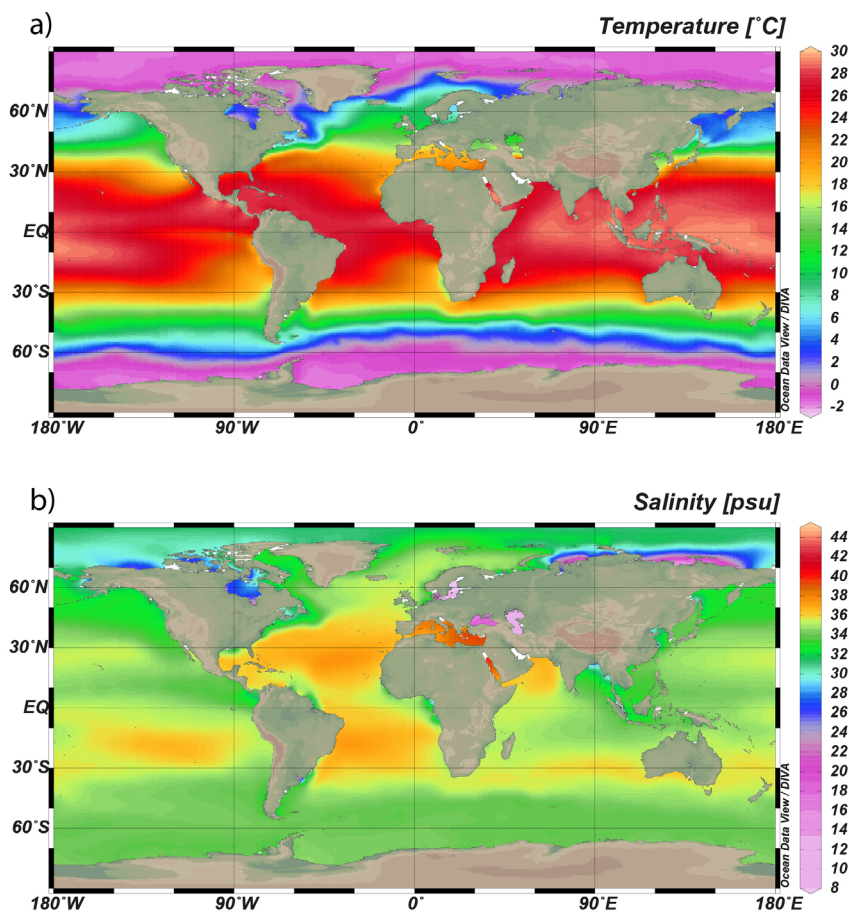


Figure 2. Maps showing a) global mean annual sea surface temperature and b) global mean sea surface salinity, based on the World Ocean Atlas (Antonov et al., 2006; Locarnini, 2010).

An important branch of the THC is the Atlantic Meridional Overturning Circulation (AMOC), transporting salt and heat from the southern hemisphere across the Atlantic to the polar and subpolar North Atlantic and Nordic Seas (Gordon, 1986). There, the released heat from the ocean drives the atmospheric circulation, whereby the remaining cold and salt water sinks to form the source of the North Atlantic Deep Water (NADW) (Cunningham et al., 2007). The strength of the AMOC, thus, significantly influences the climatic conditions over Europe and central North Africa (Rahmstorf, 2002; Ganachaud and Wunsch, 2003; Bryden et al., 2005). An important mechanism for the supply of warm and saline to the Atlantic Ocean is the Agulhas Current, located at the southern tip of the African continent. While the vast majority of the warm and saline Indian Ocean water is reflected back into the Indian Ocean via the Agulhas Return Current (Lutjeharms and Ansorge, 2001), a significant amount of approximately 2 – 15 Sv is released annually into the South Atlantic Ocean by the spinoff of so-called “Agulhas rings” (Lutjeharms, 2006). The variability in the Agulhas leakage, on the other hand, is closely related to the position of the Southern Hemisphere westerly winds and the oceanic subtropical fronts (de Ruijter et al., 1999; Beal et al., 2011). Results for global climate modelling studies, however, predict a weakening of the AMOC and the associated cross-Atlantic heat and salt transport due to the increasing freshwater input into the North Atlantic via the melting of the polar ice sheet as well as an expected shifting of the Southern Hemisphere westerlies, (Stocker and Schmittner, 1997; Wood et al., 1999; Vellinga and Wood, 2002; Sijp and England, 2009). The implied slowdown of oceanic and atmospheric convection eventually will lead to modifications not only in European, but also in the global climate with implications largely unknown (Clark et al., 2002).

In order to validate the ocean-atmosphere circulation models, continuous time series of observational data for temperature and salinity are required. Unfortunately, these instrumental data records only reach as far back as approximately 150 years to the mid-19th century (Brohan et al., 2006), and make the validation of long-term modeling experiments beyond the instrumental period complicated. Therefore, the extension of oceanographic parameters to the past, i.e. beyond observational data, has become a crucial task, in order to make comprehensive predictions of future climate development. In particular the reconstruction of the two most important physical factors determining the water density, i.e. temperature and salinity, are essential for the study of past ocean current dynamics (Pawlowicz, 2013). While past ocean temperatures can be reconstructed relatively accurately from various independent methods, the accurate reconstruction of past ocean salinity has proven to be more difficult.

1.2. The reconstruction of past ocean temperature

Paleoceanographic proxies represent the measurable analogues of non-measurable climatic variables (Fischer and Wefer, 1999) and provide an excellent way of evaluating past climatic conditions. These proxies are commonly based on the analyses of organic and inorganic remnants of organisms preserved in sediments. Ideally, the proxy material has preserved its original structure and composition from the time of its creation. The most extensively used inorganic ocean temperature proxies are based on the oxygen isotope composition of carbonate shells from benthic and planktonic foraminifera ($\delta^{18}\text{O}_{\text{foram}}$) (Urey et al., 1951; Epstein et al., 1953;

Shackleton, 1967; Bemis et al., 1998), the ratio between Mg/Ca of the planktonic foraminifera shells (Nürnberg et al., 1996; Lea et al., 1999; Mashiotta et al., 1999; Lear et al., 2002) and faunal transfer functions (McIntyre and Cline, 1981). Temperature calibrations derived from cultivation studies, from sediment traps and sedimentary core tops enable a translation of a measured proxy value into a temperature value (Bemis et al., 1998; Anand et al., 2003; Kucera et al., 2005).

A second group of proxies employed for temperature reconstruction is provided by lipid biomarkers derived from specific groups of organisms. For paleoceanographic studies there are two frequently applied organic proxies available. The first proxy is based on the ratio between C_{37} di- and tri-unsaturated long-chain alkenones (U_{37}^k index) produced by a limited number of species of photosynthetic haptophyte algae of the class Prymnesiophyceae (Volkman et al., 1980; Marlowe et al., 1984a). The U_{37}^k index is defined as:

$$U_{37}^k = \frac{[C_{37:2}]}{[C_{37:2}] + [C_{37:3}]}$$

(Prahl and Wakeham, 1987). It is based on the observation that with increasing ambient water temperature in which the haptophyte algae synthesized the alkenones, the relative abundance of the tri-unsaturated C_{37} alkenone decreases relative to the di-unsaturated C_{37} alkenone (Brassell et al., 1986; Prahl and Wakeham, 1987). Hence, with increasing temperature the index increases. The strong linear correlation found for values of the U_{37}^k index, obtained from global sediment core top studies correlated with annual mean sea surface temperatures (SST), allows the translation of any measured value for the U_{37}^k directly to absolute values for SST (Müller et al., 1998).

The second commonly applied organic temperature proxy is based on the relative distribution of the cyclopentane moieties in glycerol dialkyl glycerol tetraethers (GDGTs) produced by archaea in relation to ambient seawater temperature (Schouten et al., 2002). It is defined as the index of molecules with 4 ether bonds, tetraethers, consisting of 86 carbon atoms (TEX_{86}):

$$TEX_{86} = \frac{[GDGT - 2] + [GDGT - 3] + [Crenarchaeol \text{ regio-isomer}]}{[GDGT - 1] + [GDGT - 3] + [Crenarchaeol \text{ regio-isomer}]}$$

where GDGT-1 contains one cyclohexane moiety, GDGT-2 two and GDGT-3 three cyclohexane moieties (Schouten et al., 2002; Kim et al., 2008; 2010). The crenarchaeol regio-isomer is a specific tricyclic biphytane, which has been linked to the group of Thaumarchaeota (Schouten et al., 2000; Sinninghe Damsté et al., 2002). A global core top calibration revealed a significant non-linear relationship between TEX_{86} values and SST (Kim et al., 2008). This calibration allows, similarly to the U_{37}^k SST calibration, the calculation of absolute temperatures from any measured TEX_{86} index (Kim et al., 2010). Kim et al. (2010) developed two indices, which correlated statistically better with the lower (TEX_{86}^L) and upper end (TEX_{86}^H) of the temperature calibration. In the index the crenarchaeol regio-isomer is excluded. Absolute temperature reconstructions based on TEX_{86}^L were shown to be the most realistic in subpolar and polar oceans, since the crenarchaeol regio-isomer is likely to be less influential for temperature adaptation in these regions (Kim et al., 2010). The TEX_{86}^H index, on the other hand, is defined as the logarithmic function of the

TEX₈₆ and has been found to correlate best with SST when the data from the subpolar oceans is excluded, and hence was recommended to be applied for temperatures above 15 °C (Kim et al., 2010). Thus, there is a large variety in proxies available for the reconstruction of past SST with relatively low calibration errors, (1-3 °C for the Quaternary) based on substantially different approaches. This has the added benefit that several of these proxies can be used simultaneously and may provide more confidence in the temperature reconstructions.

1.3. Past ocean salinity reconstructions

While the measurement of the distribution of salinity in modern oceans is relatively simple to obtain with a high level of accuracy, the reconstruction of past SSS remains the single most important oceanographic parameter which still cannot be quantified with reasonable accuracy from sedimentary records (Schmidt, 1999a; Rohling, 2000; 2007). However, this information is crucial for the understanding of past global ocean current dynamics and changes therein. The most common approach for the reconstruction of past SSS is based on the measurement of the stable oxygen isotope composition of planktonic foraminiferal carbonate ($\delta^{18}\text{O}_{\text{foram}}$), which is a function of the oxygen isotope composition of the ambient sea water ($\delta^{18}\text{O}_{\text{sw}}$) and the calcification temperature (Epstein et al., 1953; Shackleton, 1974; Bemis et al., 1998). The latter is normally corrected for, by using one of the temperature proxies described earlier, preferentially Mg/Ca based temperatures from the same carbonate shell. The temperature-corrected $\delta^{18}\text{O}$ is thus assumed to reflect the ambient $\delta^{18}\text{O}_{\text{sw}}$ (Duplessy et al., 1991; Rostek et al., 1993). Due to its strong linear correlation with salinity (Figure 3a) (Craig and Gordon, 1965), as both are affected by evaporation and condensation, reconstructed $\delta^{18}\text{O}_{\text{sw}}$ can then be used to calculate past SSS. However, besides an isotopic fractionation effect during the evaporation of sea water, the isotopic composition of precipitation is also controlled by isotopic distributional factors including differences in the altitude, latitude and an amount effect (Craig, 1961; Craig and Gordon, 1965), consequently yielding temporal and spatial inconsistencies in the $\delta^{18}\text{O}_{\text{sw}}$ – salinity relationship (Rohling and Bigg, 1998; Rohling, 2000). Furthermore, the transition from glacial to interglacial periods is accompanied by large changes in ice volume, which cause an additional global isotope effect on seawater, that requires a correction of the $\delta^{18}\text{O}_{\text{sw}}$ prior to the reconstruction of long-term SSS records (Rostek et al., 1993). This so-called ice volume effect is caused by the preferential accumulation of the lighter ¹⁶O isotopes into the large ice sheets during the glacial periods and, vice versa, a relative depletion of ¹⁸O in seawater occurring with the melting of the ice during interglacial periods (Shackleton, 1987; Waelbroeck et al., 2002). As a consequence of the sum of uncertainties from the required corrections, absolute SSS reconstructions based on $\delta^{18}\text{O}_{\text{foram}}$ contain a relatively large error margin estimated to be ± 2 for absolute salinity values (Duplessy et al., 1993; Rohling and Bigg, 1998; Schmidt, 1999a; Rohling, 2000).

1.4. Hydrogen isotopes of organic matter

Evaporation and condensation of sea water does not only affect the oxygen isotopes of water but also the hydrogen isotopic composition. Since the underlying fractionation processes

are quite similar, the hydrogen isotope composition of the seawater (δD_{sw}) is closely correlated with the $\delta^{18}O_{sw}$, firstly described by Craig (1961) in the global Meteoric Water Line (MWL) (Figure 3b):

$$\delta D_{sw} = 8 * \delta^{18}O_{sw} + 10$$

As a result, the hydrogen isotope composition of the seawater may provide an alternative to reconstruct salinity under the assumption that the past hydrogen isotope composition of the water can be recorded in organic matter. Indeed, an initial study on sapropel deposition in the Tyrrhenian Basin in the Mediterranean Sea showed the hydrogen isotope composition of bulk organic matter to be depleted in D in sapropels, indicating an ocean freshening at the time of the sapropel formation (Krishnamurthy et al., 2000). However, using the δD of the bulk organic

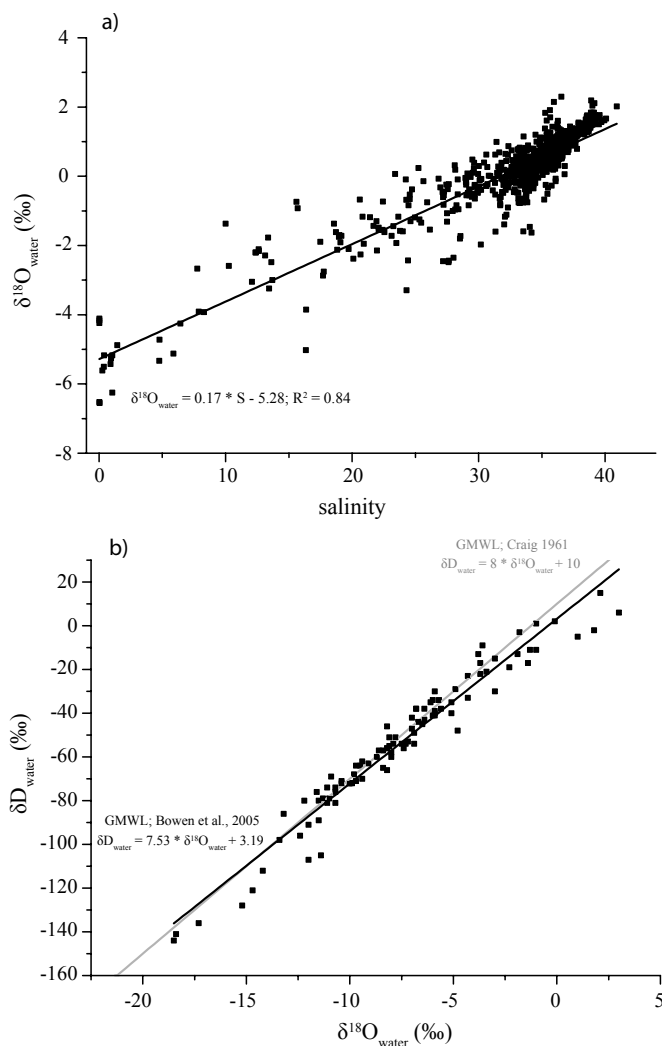


Figure 3. Panel a) shows the linear relationship between sea surface salinity (depth < 50 m) between -50 to $130^{\circ}E$ and -45 to $45^{\circ}N$ and the $\delta^{18}O_{water}$ (Schmidt, 1999b); b) shows the global hydrogen and oxygen isotope variation in water from Bowen et al. (2005) together with the global Meteoric Waterline (grey line) of Craig (1961) as reference.

matter of sediments is problematic due to the exchange of the labile hydrogen of the organic matter with ambient hydrogen (Schimmelmann et al., 1999).

Since the availability of compound-specific hydrogen isotope measurements in the late 90's, specific molecules, rather than the bulk organic matter, were targeted for the reconstruction of past δD of organic matter and water (Xie et al., 2000; Andersen et al., 2001; Sauer et al., 2001). Sessions et al. (2004) demonstrated that the covalently bound hydrogen in lipids, such as sterols, n-alkanes, n-alcohols and n-acids, is less likely to be exchanged over geological time scales and, therefore, might be a suitable method for the reconstruction of the past δD_{sw} . In particular, the hydrogen isotopic composition of the C_{37} long chain alkenones ($\delta D_{alkenone}$), compounds already used for the $U^{K^2}_{37}$ index, appeared well suited for reconstructing past ocean δD_{sw} as it is analyzable by GC, rarely co-elutes with other compounds and has no readily exchangeable hydrogen (Paul, 2002; Englebrecht and Sachs, 2005). First measurements of the δD of the $C_{37.2}$ alkenones produced by *Emiliania huxleyi* showed a constant offset with ambient δD_{sw} of ~ 232 ‰ (Paul, 2002), suggesting a constant fractionation between the alkenones and the ambient water (Figure 4a). A similar, apparently constant, fractionation between the $\delta D_{alkenone}$ and the δD_{sw} of ~ 225 ‰ was reported by Englebrecht and Sachs (2005) and consequently applied for the determination of sediment provenances (Figure 4a). However, Schouten et al. (2006) demonstrated in culture experiments with the two common open ocean haptophyte algae species, *E. huxleyi* and *Gephyrocapsa oceanica*, that the hydrogen isotope fractionation of the combined $C_{37.2-3}$ alkenones is not constant. Instead the hydrogen isotope fractionation factor α between the alkenones and the ambient water, calculated as:

$$\alpha_{alkenone-water} = \frac{1000 + \delta D_{alkenone}}{1000 + \delta D_{water}}$$

also depends on salinity and, to a lesser extent, growth rate of the alkenone producers (Figure 4b) (Schouten et al., 2006). These culture experiments showed a ~ 3 ‰ increase in the hydrogen fractionation in the alkenones for 1 unit decrease in salinity, amplifying the salinity related changes in the δD of the water recorded in the $\delta D_{alkenone}$ (Schouten et al., 2006). For this reason, the $\delta D_{alkenone}$ appeared to be a good candidate for reconstructing past ocean SSS. Indeed, initial applications of $\delta D_{alkenone}$ as a tool for reconstructing past ocean salinity for the eastern Mediterranean and Black Sea (van der Meer et al., 2007; 2008) and the Panama Basin (Pahnke et al., 2007) led to reasonable results and demonstrated the potential of the $\delta D_{alkenone}$ as a paleosalinity proxy. However, it has not been applied in real open ocean settings, where salinity changes are small, nor coastal areas where salinity changes can be highly variable.

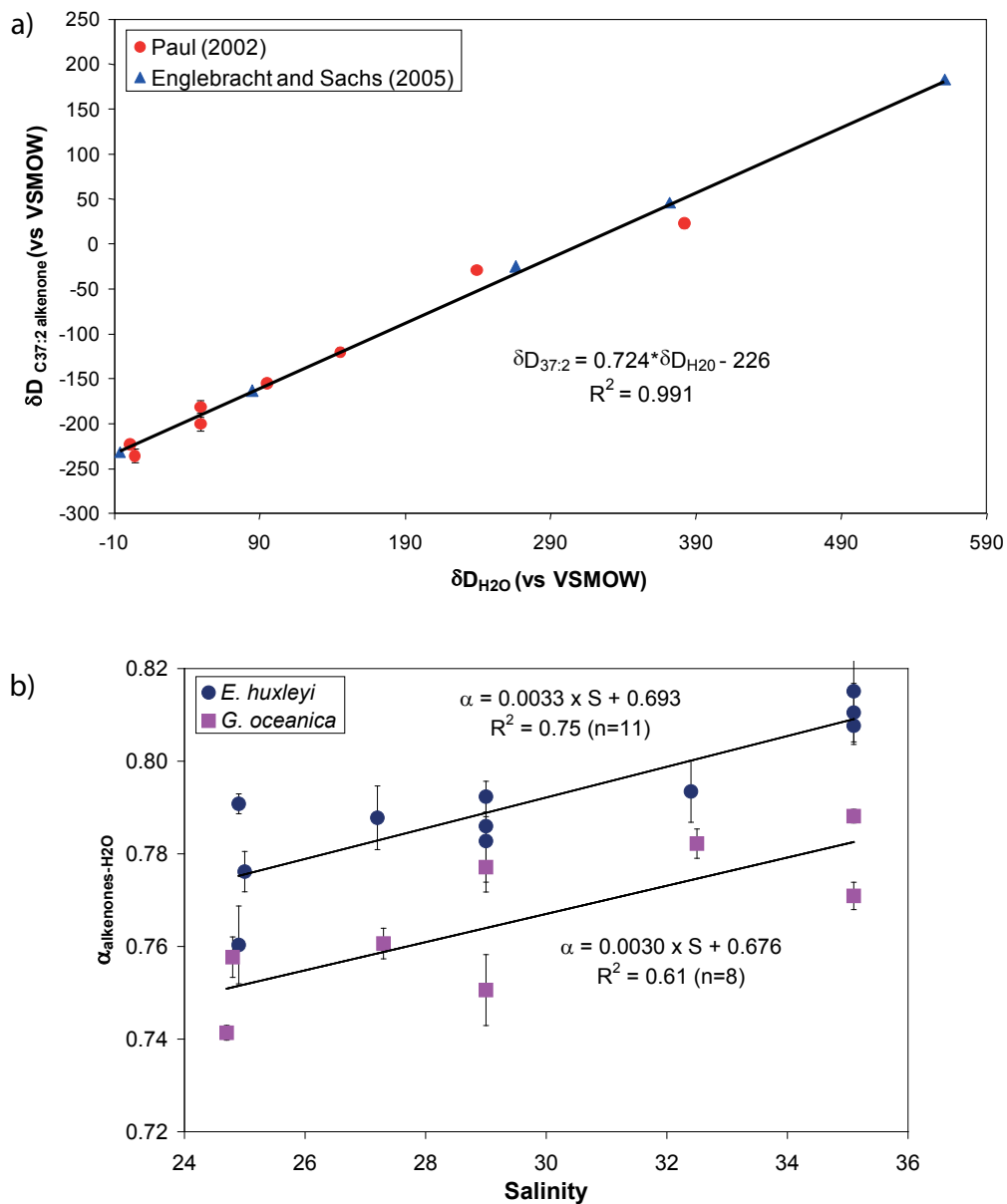


Figure 4. Results for δD of $C_{37:2}$ alkenones vs δD of the water for the studies of Paul (2002) (red circles) and Englebracht and Sachs (2005) (blue triangles); b) results for the relationship of the fractionation factor $\alpha_{\text{alkenone-water}}$ for culture studies from *E. huxleyi* (blue dots) and *G. oceanica* (purple squares) vs. salinity are reported by Schouten et al. (2006).

1.5 Scope of this thesis

The research presented in this thesis is focused on the reconstruction of past ocean salinity using the stable hydrogen isotope composition of the $C_{37:2-3}$ alkenones. Although pilot studies demonstrated reasonable reconstructions of past ocean salinity changes in selected settings (Pahnke et al., 2007; van der Meer et al., 2007; 2008), further application of the $\delta D_{\text{alkenone}}$ in more diverse open oceanic settings and comparison with the more established $\delta^{18}O_{\text{sw}}$ based on foraminifera are required to constrain the potential of this proxy. Thus, the aim of the first part of the thesis (Chapters 2 – 5) is to study the applicability of the $\delta D_{\text{alkenone}}$ proxy in open ocean settings with an expected large variation in salinity over glacial – interglacial stages, derived from highly dynamical ocean current systems, such as the Agulhas Current. Since it is not clear how large freshwater contributions, for instance from river discharge, and a close proximity to the coast will affect the $\delta D_{\text{alkenone}}$, the second part of the thesis (Chapters 6-7) investigates the effects on $\delta D_{\text{alkenone}}$ from ocean margin settings which are affected by freshwater input via river discharge. The last part (Chapter 8) concludes the research carried out during the thesis research and it will give a brief outlook on potential future research possibilities for the development of the $\delta D_{\text{alkenone}}$ as salinity proxy.

Chapter two describes the glacial–interglacial hydrogen isotope variability measured in two sediment cores, one spanning Termination II from MIS 6 to 5 and one spanning Termination I from MIS 3 to 1, located in the Agulhas Leakage area, south of the African continent. This region has been shown to be subject to relatively large changes in salinity and temperature during glacial – interglacial transitions in response to the leakage efficiency of warmer and more saline Indian Ocean water into the Atlantic. Reconstruction of sea surface temperatures and $\delta D_{\text{alkenone}}$ in comparison with planktonic foraminifera proxies shows clear freshening and cooling trends during glacial terminations as response to an increase in Indian Ocean water leakage into the Atlantic Ocean.

Chapter three shows the paleosalinity variability in the wider Agulhas region by using a multiproxy data-model integration study utilizing SSS reconstruction, based on $\delta D_{\text{alkenone}}$ and planktonic foraminifera-derived $\delta^{18}O_{\text{sw}}$, since the Last Glacial Maximum (LGM). These reconstructions indicate that higher SSS prevailed during the LGM compared to the Holocene. During Heinrich Stadial 1 SSS simultaneously increased in the Agulhas Current as well as in the Indian–Atlantic Ocean Gateway consistent with a quasi-inter-hemispheric salt seesaw response, an analogue to the thermal bipolar seesaw. Numerical modelling results reveal that the salt accumulation in the Agulhas System is most likely Atlantic sourced and occurs via salt advection throughout the Southern Hemisphere super gyre in response to a reduced cross-hemispheric heat and salt exchange during times of abrupt climate change.

Chapter four presents a multiproxy approach using $\delta^{18}O_{\text{sw}}$ reconstructions based on planktonic foraminifera and the hydrogen isotope fractionation of long-chain alkenones versus seawater ($\alpha_{\text{alkenone-sw}}$) from sediment record located on the Guinea Plateau Margin off the coast of Northwest Africa spanning 190 ka to investigate the response of subtropical Atlantic Ocean salinity to AMOC variability. Both $\delta^{18}O_{\text{sw}}$ and $\alpha_{\text{alkenone-sw}}$ indicate increased salinity at times of weakened AMOC, such as during glacial MIS 6. Reconstructed relative salinity estimates from

$\delta^{18}\text{O}_{\text{ruber}}$ and $\delta\text{D}_{\text{alkenone}}$ indicate a shift in salinity of ca. 2-4 towards fresher conditions during Termination II. A comparison with $\delta^{18}\text{O}_{\text{sw}}$ reconstructions from the western subtropical Atlantic (core ODP-999A) shows a fairly good agreement with the Guinea Plateau Margin record and suggests that changes in salinity variability might have been a general phenomenon across the subtropical Atlantic.

Chapter five discusses potential effects of resuspension and lateral transport of alkenones at the subtropical and sub-polar fronts between the South Atlantic Gyre and the Antarctic Circumpolar Current from a 25 ka long record for SST and alkenone δD . These records are compared with temperature reconstructions from and previously published temperature estimates based on planktonic foraminiferal Mg/Ca ratios and the foraminiferal species assemblage based Modern Analogue Technique. Anomalous warm temperatures, diverging from foraminiferal temperature reconstructions during the last Glacial suggest that alkenones were synthesized in a different water mass and subsequently transported to the core site. The record of $\delta\text{D}_{\text{alkenone}}$ indicates relatively D-enriched values during the last glacial co-occurring with elevated alkenone accumulation rates followed by a glacial-interglacial shift in $\delta\text{D}_{\text{alkenone}}$ only slightly higher than the expected shift based on the ice volume effect. This suggests that allochthonous alkenones were likely synthesized in warmer water masses with similar or slightly higher salinity during the glacial.

In **Chapter six**, a $\delta\text{D}_{\text{alkenone}}$ record from the Zambezi river fan delta in the Mozambique channel spanning 40 ka is investigated. Due to the sea level low stand during the glacial the coast line was at that time in close proximity to the core site, thereby increasing the effect of freshwater run off as indicated by increased input of terrestrial organic matter, reflected in the Branched and Isoprenoid Tetraether (BIT) index. The $\delta\text{D}_{\text{alkenone}}$ shows no clear glacial – interglacial trend, which could be attributed to the core site being affected by freshwater run off resulting in lower salinities and therefore lower $\delta\text{D}_{\text{alkenone}}$ than typically observed during a glacial. A significant positive correlation between $\delta\text{D}_{\text{alkenone}}$ with BIT values during the glacial and elevated C_{37}/C_{38} ratios suggest that haptophyte species changes may additionally have affected the hydrogen isotopic composition of the C_{37} alkenones during the glacial when the core location was closest to the coast.

Chapter seven investigates the $\delta\text{D}_{\text{alkenone}}$ in comparison with a record of planktonic foraminifera $\delta^{18}\text{O}_{\text{foram}}$ in a sedimentary record from the upper Murray Canyon area, south of Australia spanning 135 ka. The core location is influenced by both Southern and Indian Ocean water, and occasionally the warm and low salinity Leeuwin Current. During glacial sea level low stand, river discharge via the River Murray increasingly affected conditions at the core site. However, the records of $\delta\text{D}_{\text{alkenone}}$, $\delta^{18}\text{O}_{\text{foram}}$ and SST correspond well with each other showing parallel glacial-interglacial variability, while the lack of correlation between $\delta\text{D}_{\text{alkenone}}$ with the BIT index suggests no major influence of rivers on the alkenone δD . To reconstruct local salinity variability, both the $\delta^{18}\text{O}_{\text{sw}}$ and $\delta\text{D}_{\text{alkenone}}$ were corrected for the ice volume effect. However, the ice volume corrected $\delta^{18}\text{O}_{\text{sw}}$ shows a somewhat opposite trend from the ice volume corrected $\delta\text{D}_{\text{alkenone}}$, the former suggesting lower ocean salinity conditions during glacial periods. This is probably caused by overcorrecting for calcifying temperatures due to the use of alkenone-based SST, derived from haptophyte algae, rather than foraminiferal based temperature proxies. This study shows the benefit of using multiple proxies for the same parameter, in this case salinity.

Chapter eight provides a synthesis of the research on alkenone δD as a potential paleosalinity proxy and an outlook on the further development of this proxy. This includes combining δD measurements on multiple lipid biomarkers, such as for instance phytol, which in preliminary experiments has been shown not to be substantially affected by salinity. This could be a new potential tool for paleo salinity estimates independent of the hydrogen isotopic composition of the seawater and therefore the whole conversion of $\delta^{18}O_{\text{foram}}$ to δD_{sw} .

In summary, the results described in this thesis show that the $\delta D_{\text{alkenone}}$ can be a useful tool for reconstructing past salinity variability in open ocean settings. However, the use of this method in coastal settings with a significant influence of terrestrial input, i.e. freshwater runoff via river discharge, may increasingly lead to an effect of species composition and haptophyte algae growth rates on the $\delta D_{\text{alkenone}}$ and thus making the interpretation solely as indicator for salinity complicated. Nevertheless, the $\delta D_{\text{alkenone}}$ as proxy for past ocean salinity can be applied at sites of relatively low terrestrial influence and can yield valuable paleoclimatic information, which will add to already established paleoceanographic proxies.

Chapter 2

Salinity changes in the Agulhas leakage area recorded by stable hydrogen isotopes of C₃₇ alkenones during Termination I and II

Sebastian Kasper, Marcel T.J. van der Meer, Anhelique Mets, Rainer Zahn, Jaap S. Sinninghe Damsté, Stefan Schouten, 2014, *Climate of the Past*, 10, 251 - 260

Abstract.

At the southern tip of Africa, the Agulhas Current reflects back into the Indian Ocean causing so-called 'Agulhas rings' to spin off and release relatively warm and saline water into the South Atlantic Ocean. Previous reconstructions of the dynamics of the Agulhas current, based on paleo sea surface temperature and sea surface salinity proxies, inferred that Agulhas leakage from the Indian Ocean to the South Atlantic was reduced during glacial stages as a consequence of shifted wind fields and a northwards migration of the subtropical front. Subsequently, this might have led to a build-up of warm saline water in the southern Indian Ocean. To investigate this latter hypothesis, we reconstructed sea surface salinity changes using alkenone δD , and paleo sea surface temperature using TEX^H₈₆ and U^K₃₇, from two sediment cores (MD02-2594, MD96-2080) located in the Agulhas leakage area during Termination I and II. Both U^K₃₇ and TEX^H₈₆ temperature reconstructions indicate an abrupt warming during the glacial terminations while a shift to more negative $\delta D_{\text{alkenone}}$ values of approximately 14‰ during glacial Termination I and II is also observed. Approximately half of the isotopic shift can be attributed to the change in global ice volume, while the residual isotopic shift is attributed to changes in salinity, suggesting relatively high salinities at the core sites during glacials, with subsequent freshening during glacial terminations. Approximate estimations suggest that $\delta D_{\text{alkenone}}$ represents a salinity change of ca. 1.7 - 1.9 during Termination I and Termination II. These estimations are in good agreement with the proposed changes in salinity derived from previously reported combined planktonic foraminifera $\delta^{18}O$ values and Mg/Ca-based temperature reconstructions. Our results confirm that the δD of alkenones is a potentially suitable tool to reconstruct salinity changes independent of planktonic foraminifera $\delta^{18}O$.

2.1 Introduction

Approximately 2-15 Sv of warm and saline Indian Ocean water is annually released into the South Atlantic Ocean by the Agulhas Current, an ocean current system that is confined by the Subtropical Front (STF) and the Southern African Coast (Lutjeharms 2006). The Agulhas Current is fed by warm, saline Indian Ocean water from two sources; the Mozambique Channel, between Madagascar and the East African Coast, and the East Madagascar Current, which merges with the Mozambique Channel flow at approximately 28°S (Penven et al. 2006). When this warm, saline water reaches the Agulhas corridor at the tip of Africa, the vast majority is transported back into the Indian Ocean via the Agulhas Return Current (Figure 1). However, between 5 and 7 rings of warm, saline water are released into the Atlantic Ocean per year, termed Agulhas Leakage (Lutjeharms 2006). These Agulhas rings of Indian Ocean waters have been shown to play an important role in the heat and salt budget in the Atlantic Ocean, thereby impacting the Atlantic Meridional Overturning Circulation (AMOC) (Peeters et al. 2004, Biastoch et al. 2008, Bard and Rickaby 2009, Haarsma et al. 2011, van Sebille et al. 2011).

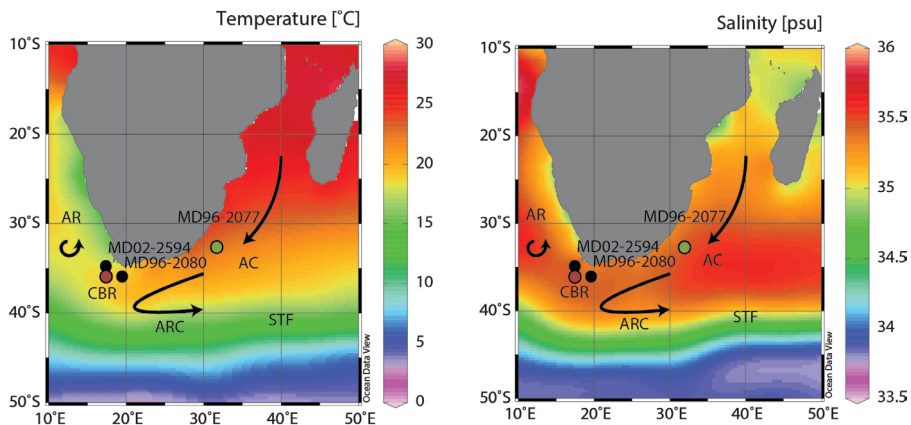


Figure 1. Location of the cores MD02-2594 and MD96-2080 (black dots) and reference sites Cape Basin record (CBR, red dot) (Peeters et al. 2004), MD96-2077 (green dot) (Bard and Rickaby 2009) and oceanographic setting on a) a map of modern sea surface temperatures and b) a map of modern sea surface salinity. Agulhas Current (AC), Agulhas Return Current (ARC), Agulhas rings (AR), Subtropical Front (STF) and Sub Antarctic Front (SAF). The underlying maps of modern sea surface temperatures and salinity were compiled with high resolution CTD data from <http://www.nodc.noaa.gov> and the Ocean Data View software version 4.3.7 by Schlitzer, R., Ocean Data View (<http://odv.awi.de>), 2010.

The magnitude of Agulhas Leakage into the Atlantic Ocean depends on the strength of the Agulhas Current as well as the position of the retroflection (Lutjeharms 2006). However, the effect of Agulhas Current strength on the Agulhas leakage efficiency is still debated. For instance, Rouault et al. (2009) suggested that, based on recent temperature observations and modeling experiments, increased Agulhas leakage of warm and saline waters into the South Atlantic Ocean can be associated with increased Agulhas Current transport, while modeling experiments performed by van Sebille et al. (2009) suggested increased Agulhas leakage to be associated with a weakened Agulhas Current.

Previous studies have shown that during glacial stages a weakened and more variable Agulhas Current occurs together with reduced Agulhas Leakage (Peeters et al. 2004, Franzese et al. 2006). Peeters et al. (2004) found relatively low contributions of ‘Agulhas leakage fauna’ in the Cape Basin, suggesting a reduced Agulhas Leakage during glacial stages (Rau et al. 2002, Peeters et al. 2004), coinciding with low sea surface temperatures. This suggests a restriction in the Agulhas leakage during cold periods (Peeters et al. 2004). Furthermore, deep-ocean stable carbon isotope gradients have been applied in combination with sea surface temperature reconstructions as indicators for a connection between deep-water ventilation and Agulhas leakage strength (Bard and Rickaby 2009). The results demonstrate a reduced leakage typically correlates with reduced deep ventilation (Bard and Rickaby 2009).

A northward shift of the STF and eastward forcing of the retroflexion during glacial periods may have led to an increased back transport of warm, saline water into the Indian Ocean during glacial periods (Peeters et al. 2004). Martinez-Mendez et al. (2010) showed increased sea water oxygen isotopes ($\delta^{18}\text{O}_{\text{sw}}$) values derived from paired planktonic foraminifera $\delta^{18}\text{O}$ and Mg/Ca analysis of *Globigerina bulloides*, in the Agulhas leakage area throughout marine isotope stage 6 (MIS6) and marine isotope stage 3 (MIS3) and early marine isotope stage 2 (MIS2). These elevated $\delta^{18}\text{O}_{\text{sw}}$ values are likely indicative for increased salinity (Martinez-Mendez et al. 2010). However, it should be noted that salinity reconstructions, based on planktonic foraminifera $\delta^{18}\text{O}_{\text{sw}}$ values, carry some uncertainties that are difficult to constrain, e.g. assumed constancy for the transfer functions of $\delta^{18}\text{O}_{\text{sw}}$ to salinity over space and time (Rohling and Bigg 1998, Rohling 2000).

Martinez-Mendez et al. (2010) further reported that reconstructed SST, derived from the planktonic foraminifera Mg/Ca of *G. bulloides*, displayed a gradual warming trend starting in the early MIS6 and MIS2 (Martinez-Mendez et al. 2010). This is, however, in contradiction with temperature reconstructions based on U^{K}_{37} paleothermometry (Peeters et al. 2004, Martinez-Mendez et al. 2010), which showed cooler sea surface temperatures during glacial periods, followed by a rapid warming at the onset of the interglacial stages. These differences may be related to uncertainties associated with the different temperature proxies (Bard 2001). Planktonic foraminiferal Mg/Ca ratios have been shown to not only reflect temperature, but also salinity (Ferguson et al. 2008; Arbuszewski et al. 2010, Hönisch et al. 2013). This has been demonstrated in high salinity environments such as the Mediterranean Sea (Ferguson et al. 2008), and in open ocean settings such as the tropical Atlantic ocean (Arbuszewski et al. 2010). Furthermore, U^{K}_{37} - SST relationships are derived from photosynthetic haptophyte algae with different growth seasons and (depth) habitats than the planktonic foraminifera *G. bulloides*, potentially recording different temperature ranges (Prah et al 1987, Bard 2001).

We use the hydrogen isotope composition of the combined $\text{C}_{37:2-3}$ alkenones ($\delta\text{D}_{\text{alkenone}}$), produced by haptophyte algae, as a proxy for relative changes in sea surface salinity (SSS). Culture experiments for two common open ocean haptophyte species, *Emiliania huxleyi* and *Gephyrocapsa oceanica*, have shown that the hydrogen isotope composition of alkenones is mainly dependent on salinity, the hydrogen isotope composition of the growth media and, to a lesser extent, growth rate (Englebrecht and Sachs 2005, Schouten et al., 2006). Furthermore, van der Meer et al. (2013) showed that measuring the combined $\text{C}_{37:2-3}$ $\delta\text{D}_{\text{alkenone}}$ rather than separated $\text{C}_{37:2}$ and $\text{C}_{37:3}$ alkenones yields a more robust water δD and salinity signal, possibly by reducing biosynthetic effects related

to the synthesis of the $C_{37:3}$ alkenones from the $C_{37:2}$ (Rontani et al 2006). Application of the hydrogen isotope composition of alkenones has resulted in reasonable salinity reconstructions for the eastern Mediterranean and Black Sea (van der Meer et al. 2007, 2008) and hydrological reconstructions in the Panama Basin (Pahnke et al 2007). Here, we apply the $\delta D_{\text{alkenone}}$ to estimate relative salinities of the Agulhas system focusing on Termination I and Termination II using the same cores used by Martinez-Mendez et al. (2010), situated in the Agulhas Leakage area, off the coast of South Africa (Figure 1). In order to assess the effect of growth rates on $\delta D_{\text{alkenone}}$, we measure the stable carbon isotope composition of the combined $C_{37:2-3}$ alkenones ($\delta^{13}C_{\text{alkenones}}$) on samples from glacial and interglacials (Rau et al. 1996, Bidigare et al. 1997, Schouten et al. 2006). Furthermore, we reconstruct SST using the TEX^H_{86} proxy (Schouten et al. 2002, Kim et al. 2010) and compare this with the U^{K}_{37} and Mg/Ca record of the planktonic foraminifera *G. bulloides* for the same sediment cores (Martinez-Mendez et al. 2010).

2.2 Material and Methods

2.2.1. Setting

Sediment samples were taken from cores MD96-2080 (36°19.2'S; 19°28.2'E, 2488 m water depth) and MD02-2594 (34°42.6'S; 17°20.3'E, 2440 m water depth) from the Agulhas Bank slope off the coast of southern South Africa (Figure 1). Core MD02-2594 was taken during the RV Marion Dufresne cruise MD128 “SWAF” (Giraudeau et al. 2003). Core MD96-2080 was obtained during the IMAGES II Campaign “NAUSICAA” (Bertrand et al., 1997). Age models and records of *Globigerina bulloides* $\delta^{18}O$ and Mg/Ca have previously been established for both sediment cores (Martinez-Mendez et al. 2008, 2010). The sampled interval of core MD02-2594 covered the period 3 to 42 ka (MIS1 to mid MIS3) and included Termination I. Core MD96-2080 covered the period between 117– 182 ka (MIS5e to MIS6) and included Termination II (Table 1, Table 2).

Table 1. Results for combined $C_{37:2-3}$ alkenone stable hydrogen isotope ($\delta D_{\text{alkenone}}$, ‰), stable carbon isotope ($\delta^{13}C_{\text{alkenone}}$), TEX_{86}^H SST and $U_{37}^{K'}$ SST analyses for core MD96-2080.

Age (ka)	$U_{37}^{K'}$	TEX_{86}^H	$\delta D_{\text{alkenone}}$ (‰) ^{a)}	$\delta^{13}C_{\text{alkenone}}$ (‰) ^{a)}
117.7	0.819	-0.276	-197 ±2	
119.9	0.819	-0.272	-196 ±2	
123.1	0.856	-0.277	-180	
125.4	0.864	-0.278	-193 ±4	-24.7±0.5
126.5	0.833	-0.273	-194 ±1	-25.4±0.2
127.0	0.829	-0.274	-198 ±0	
127.9	0.845	-0.275	-188 ±1	-25.1±0.8
128.7	0.851	-0.266	-194 ±4	-25.6±0.4
129.8	0.828	-0.248	-194 ±0	
131.3	0.821	-0.253	-192 ±3	
132.8	0.798	-0.250	-189 ±2	-24.2±0.4
133.6	0.819	-0.238	-190 ±0	-23.9±0.1
135.1	0.776	-0.235	-182 ±2	
137.3	0.750	-0.251	-182 ±4	-24.5±0.1
137.7	0.749	-0.256	-183 ±1	-24.1±0.4
141.2	0.709	-0.321	-179 ±1	
142.2	0.710	-0.320	-177 ±3	
145.0	0.717	-0.325	-180 ±1	-24.9±0.1
147.5	0.726	-0.309		
151.5	0.707	-0.314	-184 ±2	-24.8±0.6
152.0	0.734	-0.314	-182 ±0	
154.7	0.724	-0.330	-186 ±1	-24.6±0.2
158.0	0.738	-0.290	-177 ±0	
162.3	0.745	-0.332	-179 ±3	
168.8	0.745	-0.314	-191 ±2	
177.9	0.714	-0.292	-190 ±3	
182.7	0.707	-0.303	-187 ±3	

^{a)}The error is defined as the range of duplicated measurements.

Table 2. Results for combined C_{37:2-3} alkenone stable hydrogen isotope ($\delta D_{\text{alkenone}}$, ‰), stable carbon isotope ($\delta^{13}C_{\text{alkenone}}$), TEX^H₈₆ SST and U^K₃₇ SST analyses for core MD02-2594.

Age (ka)	U ^K ₃₇	TEX ^H ₈₆	$\delta D_{\text{alkenone}}$ (‰) ^{a)}	$\delta^{13}C_{\text{alkenone}}$ (‰) ^{a)}
3.5	0.724	-0.305	-192 ±2	-24.1±0.1
5.6	0.723	-0.307	-184 ±2	
6.3	0.746	-0.309	-189 ±4	
6.9	0.736	-0.311	-182 ±1	
8.6	0.753	-0.308	-191 ±3	
12.0	0.762	-0.282	-178 ±2	-24.1±0.8
18.0	0.685	-0.308	-179 ±1	
18.5	0.677	-0.366	-171 ±2	
21.1	0.672	-0.336	-173 ±3	-24.2±1.1
22.3	0.686	-0.352	-178 ±2	
26.7	0.686	-0.328	-166 ±2	
28.4	0.682	-0.333	-173 ±0	
29.5	0.686	-0.339	-172 ±1	
30.8	0.715	-0.313	-179 ±2	
31.5	0.692	-0.332	-173 ±2	-23.6±0.1
32.0	0.696	-0.315	-177 ±1	
37.4	0.728	-0.312	-171 ±3	
42.1	0.676	-0.343	-180 ±2	

^{a)}The error is defined as the range of duplicated measurements.

2.2.2. Sample preparation

Sediment samples were freeze dried and homogenized with a mortar and pestle. The homogenized material was then extracted using the accelerated solvent extractor method (ASE) with dichloromethane (DCM):methanol 9:1 (v/v) and a pressure of 1000 psi in 3 extraction cycles. The total lipid extract was separated over an Al₂O₃ column into a apolar, ketone and polar fraction using hexane:DCM 9:1, hexane:DCM 1:1 and DCM:methanol 1:1, respectively. The ketone fraction was analyzed for U^K₃₇ using gas chromatography. Gas chromatography/high-temperature conversion/isotope ratio mass spectrometry (GC/TC/irMS) was used to measure the combined hydrogen isotope composition of the di- and tri-unsaturated C₃₇alkenones. The polar fraction was analyzed for TEX^H₈₆ using high performance liquid chromatography mass spectrometry (HPLC/MS). Stable carbon isotopes of the combined di- and tri-unsaturated C₃₇ alkenones were analyzed using GC/combustion/irMS.

2.2.3. U_{37}^K analysis

Ketone fractions were analyzed by gas chromatography (GC) using an Agilent 6890 gas chromatograph with a flame ionization detector and a Agilent CP Sil-5 fused silica capillary column (50 m x 0.32 mm, film thickness=0.12 μm) with helium as the carrier gas. The GC-oven was programmed to subsequently increase the temperature from 70 to 130°C at 20°C min^{-1} , and then at 4°C min^{-1} to 320°C, at which it was held isothermal for 10 min. U_{37}^K values were calculated according to Prahl and Wakeham (1987). Subsequently, SST was calculated using the core top calibration established by Müller et al. (1998).

2.2.4. δD of alkenone analysis

Alkenone hydrogen isotope analyses were carried out on a Thermo – Finnigan DELTA^{Plus} XL GC/TC/irMS. The temperature conditions of the GC increased from 70 to 145°C at 20°C min^{-1} , then to 320°C at 4°C min^{-1} , at which it was held isothermal for 13 min using an Agilent CP Sil-5 column (25 m x 0.32 mm) with a film thickness of 0.4 μm and 1 ml min^{-1} helium at constant flow. The thermal conversion temperature was set to 1425°C. The H_3^+ correction factor was determined daily and ranged between 10 and 14. Isotopic values for alkenones were standardized against pulses of H_2 reference gas, which was injected three times at the beginning and two times at the end of each run. A set of standard n-alkanes with known isotopic composition (Mixture B prepared by Arndt Schimmelmann, University of Indiana) was analyzed daily prior to each sample batch in order to monitor the systems performance. Samples were only analyzed when the alkanes in Mix B had an average deviation from their off-line determined value of <5%. Squalane was co-injected as an internal standard with each sample to monitor the precision of the alkenone isotope values. The squalane standard yielded an average δD - value of $-167\text{‰} \pm 4.5$, which compared favorably with its offline determined δD -value of -170‰ . Alkenone δD values were measured as the combined peak of the $\text{C}_{37:2}$ and $\text{C}_{37:3}$ alkenones (van der Meer et al. 2013) and fractions were analyzed in duplicates if a sufficient amount of sample material was available. Standard deviations of replicate analyses varied from $\pm 0.1\text{‰}$ to $\pm 5.9\text{‰}$.

2.2.5. $\delta^{13}\text{C}$ of alkenone analyses

Combined $\text{C}_{37:2-3}$ alkenones were analyzed using a Thermo Delta V isotope ratio monitoring mass spectrometer coupled to an Agilent 6890 GC. Samples were dissolved in hexane and analyzed using a GC temperature program starting at 70°C, then increasing to 130°C at 20°C min^{-1} , and then to 320°C at 4°C min^{-1} , where it was held for 20 min. The stable carbon isotope compositions for $\delta^{13}\text{C}_{\text{alkenone}}$ are reported relative to Vienna Pee Dee Belemnite (VDPB). The $\delta^{13}\text{C}_{\text{alkenone}}$ values are averages of at least two runs. GC-irMS performance was checked daily by analyzing a standard mixture of n-alkanes and fatty acids, including two fully perdeuterated alkanes with a known isotopic composition. These perdeuterated alkanes were also co-injected

with every sample analysis and yielded an average $\delta^{13}\text{C}$ value of $-32.5\pm 0.5\text{‰}$ and $-27.0\pm 0.5\text{‰}$ for $n\text{-C}_{20}$ and $n\text{-C}_{24}$, respectively. This compared favorably with their offline determined $\delta^{13}\text{C}$ -values of -32.7‰ and -27.0‰ for $n\text{-C}_{20}$ and $n\text{-C}_{24}$, respectively.

2.2.6. $\text{TEX}^{\text{H}}_{86}$ analysis

Analyses for $\text{TEX}^{\text{H}}_{86}$ were performed as described by Schouten et al. (2007). In summary, an Agilent 1100 series HPLC/MS equipped with an auto-injector and Agilent Chemstation chromatography manager software was used. Separation was achieved on an Alltech Prevail Cyano column (2.1 x 150 mm, $3\mu\text{m}$), maintained at $30\text{ }^{\circ}\text{C}$. Glycerol dibiphytanyl glycerol tetraethers (GDGTs) were eluted with 99% hexane and 1% propanol for 5 min, followed by a linear gradient to 1.8% propanol in 45 min, followed by back-flushing hexane/propanol (9:1, v/v) at 0.2ml/min for 10 min. Detection was achieved using atmospheric pressure positive ion chemical ionization mass spectrometry (APCI-MS) of the eluent. Conditions for the Agilent 1100 APCI-MS were as follows: nebulizer pressure of 60 psi, vaporizer temperature of $400\text{ }^{\circ}\text{C}$, drying gas (N_2) flow of 6 L/min and temperature $200\text{ }^{\circ}\text{C}$, capillary voltage of -3 kV and a corona of $5\ \mu\text{A}$ ($\sim 3.2\text{ kV}$). GDGTs were detected by Single Ion Monitoring (SIM) of their $[\text{M}+\text{H}]^+$ ions (dwell time = 234 ms) (Schouten et al., 2007) and quantified by integration of the peak areas. The $\text{TEX}^{\text{H}}_{86}$ values and absolute temperatures were calculated according to Kim et al. (2010). This calibration is recommended for temperature reconstruction above $15\text{ }^{\circ}\text{C}$ (Kim et al. 2010) and therefore appears to be the most suitable model for reconstructing subtropical temperatures, as found in the Agulhas leakage area.

2.3. Results

2.3.1. Sea surface temperature proxies

The U^{K}_{37} record of MD96-2080 indicated constant temperatures of $20.7\pm 0.5\text{ }^{\circ}\text{C}$ throughout MIS6 (138 - 182 ka) (Table 1, Figure 2). With the onset of Termination II at approximately 138 ka, temperatures began to increase to a maximum of $\sim 25\text{ }^{\circ}\text{C}$ during early MIS5e ($\sim 125\text{ ka}$), followed by a slight decrease in temperature towards $\sim 23\text{ }^{\circ}\text{C}$ at about 120 ka. The U^{K}_{37} SST record for MD02-2594 indicated relatively constant temperatures of $20\pm 0.5\text{ }^{\circ}\text{C}$ throughout MIS3 and early MIS2 (Table 2, Figure 3). With the onset of Termination I during mid - MIS2 ($\sim 18\text{ ka}$), temperatures showed a slight warming towards $\sim 22\text{ }^{\circ}\text{C}$ at the beginning of MIS1. Throughout MIS1, temperatures slightly decreased to approximately $21\text{ }^{\circ}\text{C}$.

The overall pattern in the $\text{TEX}^{\text{H}}_{86}$ records for the two cores indicated that absolute temperatures were cooler by up to $5\text{ }^{\circ}\text{C}$ compared to U^{K}_{37} temperatures during glacial and interglacial stages MIS5e and MIS6, as well as MIS3/MIS2 and MIS1. During MIS6, $\text{TEX}^{\text{H}}_{86}$ temperatures were relatively stable at $17\pm 1\text{ }^{\circ}\text{C}$, although less stable than U^{K}_{37} SST (Table 1, Figure 2). At the initial termination of the glacial MIS6 (ca. 135 – 138 ka), reconstructed $\text{TEX}^{\text{H}}_{86}$ temperatures increased

rapidly to about 22°C, which is similar in absolute terms compared to $U^{K'}_{37}$ SST (Figure 2). Subsequently, TEX^H_{86} SST decreased rapidly to ~20 °C and remained constant during MIS5e. During MIS3 and early MIS2, TEX^H_{86} SST showed a trend towards cooler temperatures from approximately 17 °C at ~38 ka to 14 °C at the start of Termination I (18 ka) (Table 2, Figure 3). At the onset of Termination I, TEX^H_{86} SSTs abruptly increased. Temperatures reached a maximum

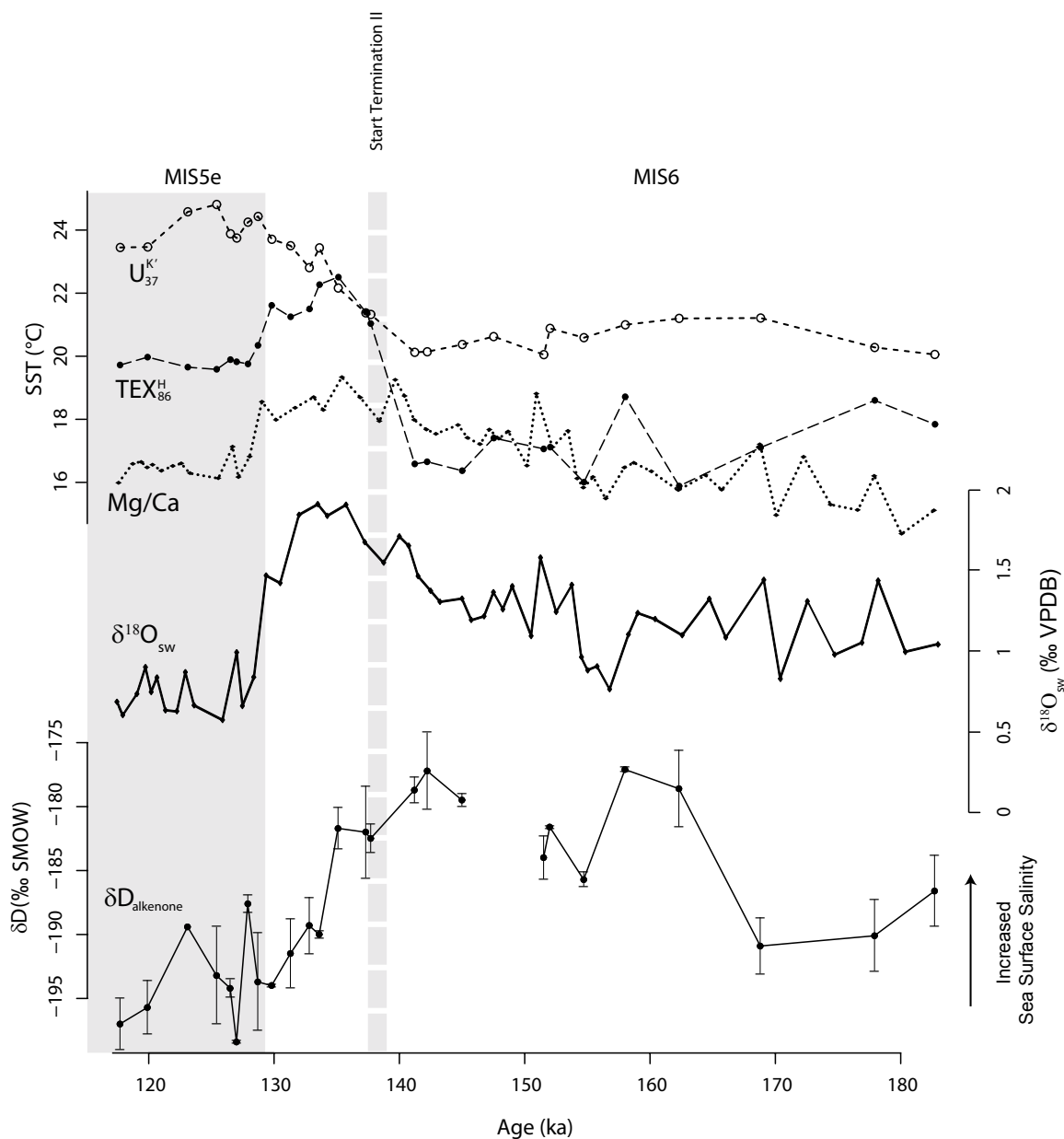


Figure 2. Reconstructed SST of $U^{K'}_{37}$ (dashed line, open circles), TEX^H_{86} (dashed line, closed circles), Mg/Ca of *G. bulloides* (dotted line, closed circles, Martinez-Mendez et al., 2010), reconstructed $\delta^{18}O_{sw}$ from *G. bulloides* (solid line, diamonds, Martinez-Mendez et al., 2010) and hydrogen isotope composition of $C_{37:2-3}$ alkenones (solid line, closed circles) for core MD96-2080.

of 19 °C at the beginning of MIS1 (11 ka) and decreased again to relatively constant temperatures of ca. 18 °C throughout MIS1. This trend is comparable to the $U_{37}^{K'}$ SST record, albeit with a negative offset of approximately 4 °C throughout MIS3/MIS2 and MIS1, and approximately 2°C during the glacial termination phase (11 – 18 ka) (Figure 3).

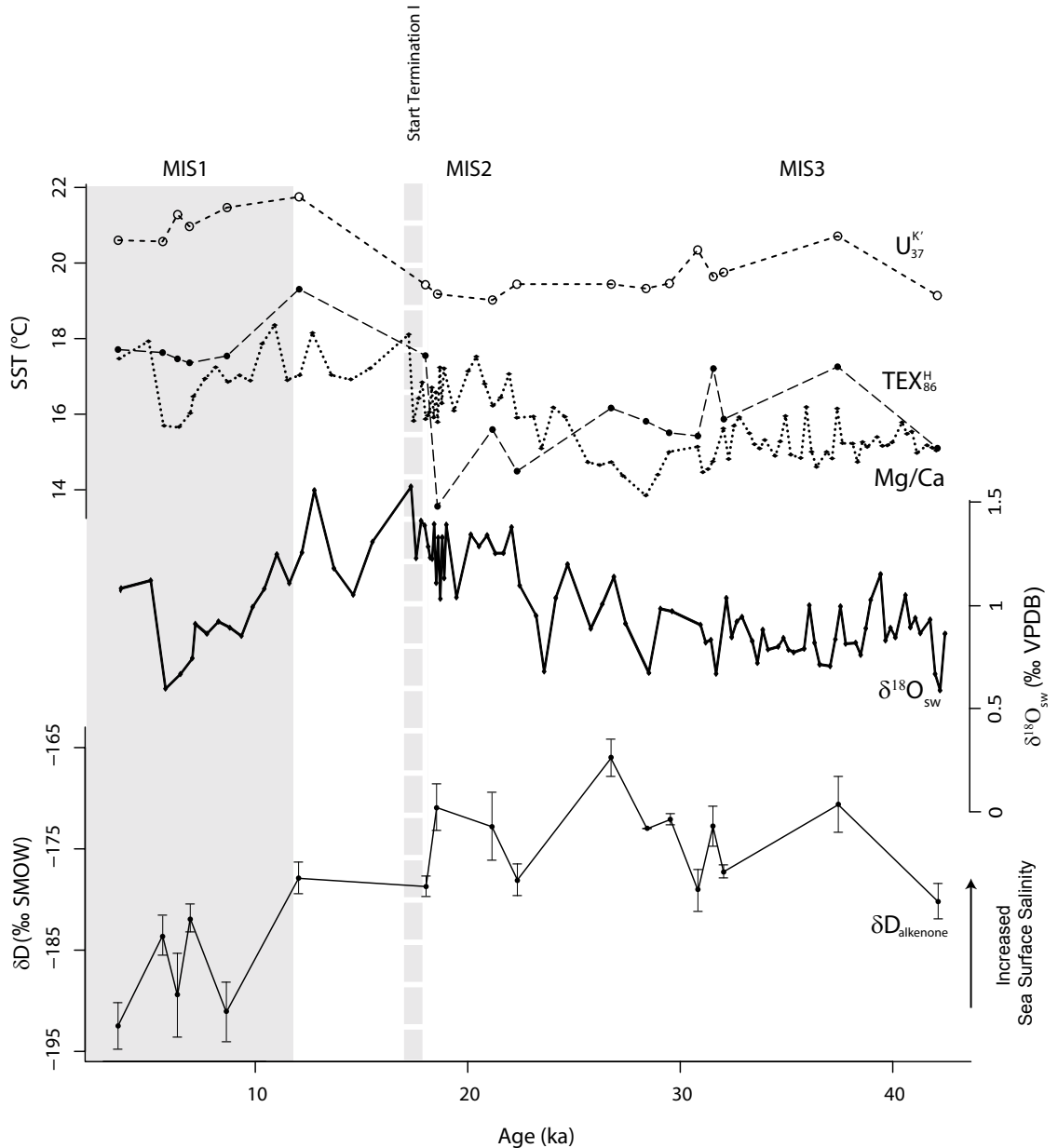


Figure 3. Reconstructed SST of $U_{37}^{K'}$ (dashed line, open circles), TEX_{86}^{H} (dashed line, closed circles), Mg/Ca of *G. bulloides* (dotted line, closed circles, Martinez-Mendez et al., 2010), reconstructed $\delta^{18}O_{sw}$ from *G. bulloides* (solid line, diamonds, Martinez-Mendez et al., 2010) and hydrogen isotope composition of $C_{37:2-3}$ alkenones (solid line, closed circles) for core MD02-2594.

2.3.2. Stable hydrogen and carbon isotope composition of $C_{37:2-3}$ alkenones

The $\delta D_{\text{alkenone}}$ values in core MD96-2080 ranged between -177 to -198‰ (Table 1). During early MIS6 (169 to 181 ka), $\delta D_{\text{alkenone}}$ values were approximately $-189 \pm 2\text{‰}$ and shifted to more positive values of ca. -177‰ at 158 ka. In the time interval between 142 to 162 ka (MIS6), $\delta D_{\text{alkenone}}$ decreased to $-180 \pm 3\text{‰}$. During glacial Termination II (130 to 138 ka) the $\delta D_{\text{alkenone}}$ values decreased abruptly to approximately $-194 \pm 3\text{‰}$ for MIS5e (118 -130 ka) (Figure 2). The $\delta D_{\text{alkenone}}$ values in core MD02-2594 ranged between -166 to -192‰ (Table 2). In the time interval from 12 to 41 ka (MIS3 and MIS2), values for $\delta D_{\text{alkenone}}$ were relatively constant at approximately $-174 \pm 4\text{‰}$ (Figure 3). At ca. 11 ka (onset of MIS1), $\delta D_{\text{alkenone}}$ values shifted to more negative values with an average of $-188 \pm 5\text{‰}$ for the time period of 3 to 9 ka (MIS1) (Figure 3).

The stable carbon isotope composition of the alkenones ($\delta^{13}C_{\text{alkenone}}$) was analyzed from selected sediment samples before, within and after each glacial termination stage (Table 1, 2). In the time period before the termination phase of glacial MIS6 (141-152 ka) the alkenones had an average $\delta^{13}C$ value of $-24.9 \pm 0.3\text{‰}$. Within the termination phase (133 – 138 ka), $\delta^{13}C_{\text{alkenone}}$ values were slightly more enriched in ^{13}C , i.e. $-24.2 \pm 0.3\text{‰}$. During MIS5e, $\delta^{13}C_{\text{alkenone}}$ values became more negative and were on average $-25.3 \pm 0.4\text{‰}$ (Table 1). For core MD02-2594, the $\delta^{13}C_{\text{alkenone}}$ values were fairly constant between -23.6 to -24.1‰ (Table 2).

2.4. Discussion

2.4.1. Development of sea surface temperatures during Terminations I and II

Application of the U^{K}_{37} proxy resulted in higher reconstructed temperatures compared to the TEX^{H}_{86} and Mg/Ca SST reconstructions (Figure 2, 3). Difference in absolute temperatures may be explained by a variety of reasons such as growth seasons and/or depth habitats between the alkenone producers, the Thaumarchaeota (GDGT producers) and the planktonic foraminifera (Müller et al. 1998, Bard 2001, Karner et al. 2001, Wuchter et al. 2006, Lee et al. 2008, Saher et al. 2009, dos Santos et al. 2010, Fallett et al. 2011, Huguet et al. 2011).

Both U^{K}_{37} and TEX^{H}_{86} temperatures suggest cooler conditions throughout stages MIS6 and MIS3/2 (Figure 2, 3). This is followed by an abrupt warming during succeeding glacial terminations, leading to warmer conditions in the interglacial stages MIS5e and MIS1. The pattern fits well with U^{K}_{37} derived temperature reconstructions from other sediment cores in the area of this study site (Figure 4) (Schneider et al. 1995, Peeters et al. 2004, Bard and Rickaby 2009). Temperature reconstructions based on Mg/Ca and TEX^{H}_{86} show that maximum temperatures occurred during the deglaciations. However, U^{K}_{37} temperature reconstructions showed that the SST maximum occurred approximately 5 ka later than in Mg/Ca and TEX^{H}_{86} based reconstructions. This temperature increase could possibly point towards an increased influence of warm Indian Ocean waters, and hence increased Agulhas Leakage. This increased leakage in turn is likely related to a

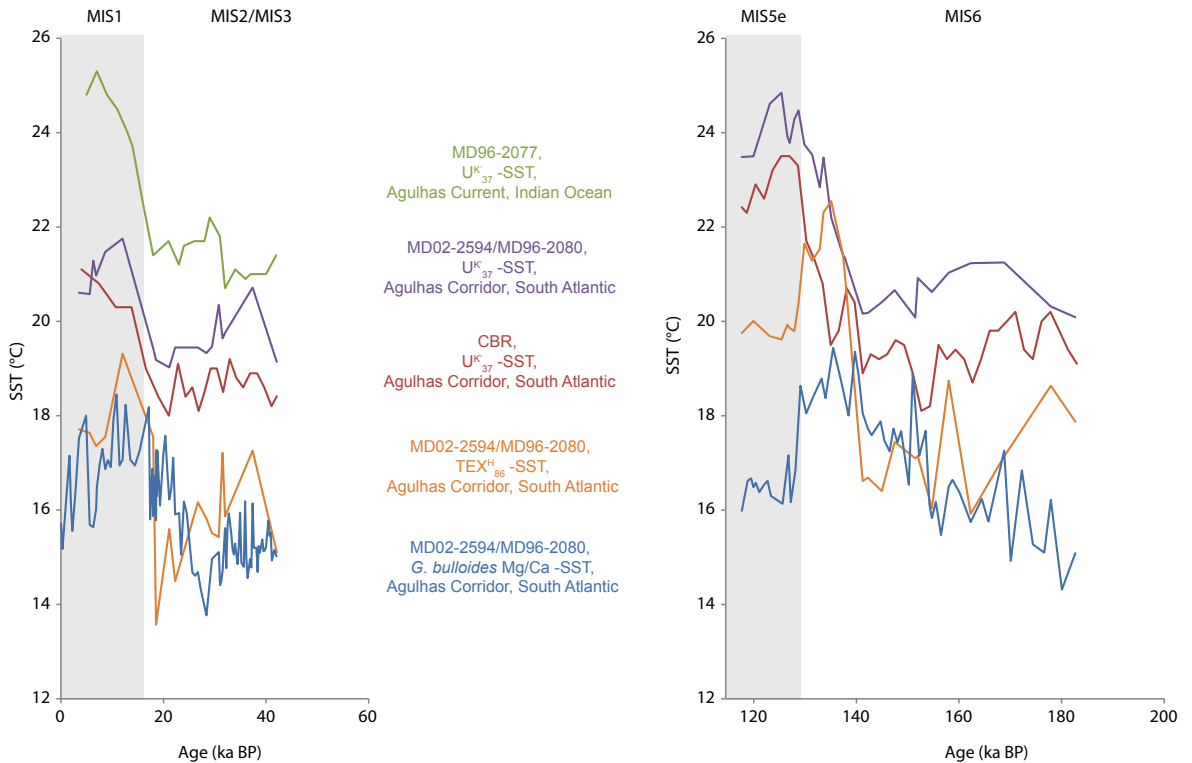


Figure 4. Comparison of U^{k}_{37} SST, TEX^{H}_{86} SST and *G. bulloides* Mg/Ca SST (Martinez-Mendez et al. 2010) of a) MIS3- 1 (MD02-2594) and b) MIS6-5 (MD96-2080) (see Figure 1 for core location) with U^{k}_{37} SST of MD96-2077 in the Agulhas Current, Indian Ocean (Bard and Rickaby 2009) and U^{k}_{37} SST of Cape Basin record in the Agulhas Corridor, South Atlantic (Peeters et al. 2004).

southward shift of the sub-tropical front due to shifting wind fields and a southward migration of the land ice shields (Peeters et al. 2004). Nevertheless, these observations do not necessarily imply a buildup of warm Indian Ocean waters prior to glacial terminations at the core site.

Strikingly, the timing of the beginning of the warming trend reflected in the foraminifera Mg/Ca record of *G. bulloides* (Martinez-Mendez et al. 2010) is different from the U^{k}_{37} and TEX^{H}_{86} records, as well as other U^{k}_{37} records in the region (Figure 4) (Peeters et al., 2004). The Mg/Ca SST record identifies a warming trend starting in the early glacial periods and gradually extending over the glacial termination phases (Martinez-Mendez et al. 2010). Furthermore, a recent study by Marino et al. (2013) also showed a discrepancy between Mg/Ca of the planktonic foraminifer *Globigerinoides ruber* and U^{k}_{37} SST. It has been reported that changes in salinity can also affect the Mg/Ca ratios in foraminifera shells, specifically during glacial periods when salinity was likely elevated (Ferguson et al. 2008, Arbuszewski et al. 2010). Thus, the observed trends in foraminiferal Mg/Ca may result from a combined salinity and temperature signal (Hönisch et al. 2013).

2.4.2. Salinity changes during Terminations I and II

The $C_{37:2-3}$ alkenone hydrogen isotope records consistently show a substantial decrease toward more deuterium depleted values during the glacial terminations and the interglacial stages MIS5e and MIS1 (Figure 2, 3). We quantified changes from glacial to interglacial stages by averaging time intervals from before and after each termination. We observed average shifts in $\delta D_{\text{alkenone}}$ of approximately 14‰ for both Termination I and II (Table 3). These shifts in the $\delta D_{\text{alkenone}}$ values can be caused by a number of factors such as: decreasing δD of sea water (δD_{sw}) as an effect of decreasing global ice volume during the Terminations (Rohling 2000); ocean salinity; algal growth rate; haptophyte species composition (Schouten et al. 2006); differences in the hydrogen isotope composition of the $C_{37:2}$ and $C_{37:3}$ alkenones (D’Andrea et al. 2007, Schwab and Sachs 2009). However, the latter factor is likely unimportant as for the range of $U^{K^{27}}$ values observed in this study we expect a maximum difference of 4‰ in the hydrogen isotope composition between $C_{37:2}$ and $C_{37:3}$, which falls within the accuracy of the GC/TC/irMS (van der Meer et al. 2013).

Table 3. Average values for the hydrogen isotope composition of the $C_{37:2-3}$ alkenones, the global $\delta^{18}O_{\text{ice vol.}}$ (Waelbroeck et al., 2002), $\delta D_{\text{ice vol.}}$ (Srivastava et al., 2010) and the local δD_{sw} derived from $\delta^{18}O$ of *G. bulloides* (Martinez-Mendez et al., 2010) for the intervals of before and after Termination I and II.

	Time interval	$\delta D_{\text{alkenone}}$ (‰)	$\delta^{18}O_{\text{ice vol}}$ (‰)	$\delta D_{\text{ice vol.}}$ (‰)	δD_{sw} (‰)
Term. I	before (3.5-8.6 ka, n=5)	-188±5	0.06 ±0.05	0.7 ±0.4	-0.4 ±0.9
	after (18-37.4 ka, n=11)	-174±4	0.83 ±0.16	6.3 ±1.2	6.5 ±2.6
Term. II	before (117.7-129.8 ka, n=9)	-194±3	0.00±0.05	0.3±0.4	-0.5±2.7
	after (141.2-162.3 ka, n=8)	-180±3	0.88±0.13	6.7±0.9	9.6±2.4

In order to assess changes in growth rate for the haptophytes, we measured the stable carbon isotope composition of the combined $C_{37:2-3}$ alkenones ($\delta^{13}C_{\text{alkenone}}$) (Table 1, 2). Our results show relatively small changes of about -0.6‰ and -0.3‰ in $\delta^{13}C_{\text{alkenone}}$ during Termination I and II, respectively. The fractionation of stable carbon isotopes is mainly controlled by physiological factors like growth rate, cell size and geometry, as well as by the supply of dissolved CO_2 (Rau et al. 1996, Bidigare et al. 1997). The more depleted alkenone $\delta^{13}C$ values during interglacials suggest either slightly higher dissolved CO_2 concentrations or lower growth rates. We suggest that higher dissolved CO_2 concentrations likely explains the more depleted alkenone $\delta^{13}C$ values as CO_2 concentrations were higher during interglacials compared to glacials (Curry and Crowley, 1987). Since reduced growth rates would result in decreasing hydrogen isotopic fractionation, our observed increase in hydrogen isotopic fractionation during interglacials compared to glacials cannot be explained by growth rate changes (Schouten et al., 2006).

Species changes could also explain the observed hydrogen isotope shift. Assemblage studies in the Agulhas Leakage have shown an increasing abundance of the predominant haptophyte *E. huxleyi* from the beginning of MIS7 towards MIS1, with a maximum relative abundance observed at the onset of MIS1 (Flores et al. 1999). *G. oceanica*, however, reaches maximum relative abundances during Termination II (Flores et al. 1999). Changes in the coccolithophore assemblage toward a larger fraction of *G. oceanica* could have resulted in more negative $\delta D_{\text{alkenone}}$ values during that time since *G. oceanica* fractionates more against D than *E. huxleyi* (Schouten et al. 2006). However, the abundance of *G. oceanica* never exceeded the relative abundance of *E. huxleyi* and it is therefore unlikely that species composition changes had a large impact on $\delta D_{\text{alkenone}}$ values during Termination II. During Termination I *E. huxleyi* reached its maximum relative abundances compared to *G. oceanica* (Flores et al. 1999) possibly resulting in more positive $\delta D_{\text{alkenone}}$ values rather than the observed trend toward more depleted values (Schouten et al. 2006). Therefore, the observed trends towards more depleted values in the $\delta D_{\text{alkenone}}$ during the glacial Terminations are most likely not affected significantly by changes in the coccolithophore species composition.

Thus, our observed isotope shifts can likely only be explained by a shift in the δD of water, through global ice volume changes, and/or salinity. We estimate the effect of changes in global ice volume on the $\delta D_{\text{alkenone}}$ by using the global mean ocean $\delta^{18}\text{O}_{\text{sw}}$ record based on benthic foraminifera (Waelbroeck et al. 2002) and calculated an equivalent δD_{sw} record by applying a local Indian Ocean meteoric waterline (Srivastava et al. 2010). Changes in global δD_{sw} due to the ice volume effect are estimated to be approximately -6‰ during both Terminations (Table 3). This shift is smaller than that observed in $\delta D_{\text{alkenone}}$, suggesting an increase in hydrogen isotopic fractionation during the two Terminations.

The residual $\delta D_{\text{alkenone}}$ shift likely reflects changes in sea surface salinity. We find alkenones relatively enriched in D during the glacials MIS6 and MIS2/3 and relatively depleted in D during MIS5e and MIS1, suggesting lower salinities during interglacials compared to glacials (Figure 2, 3). Indeed, reconstructed $\delta^{18}\text{O}_{\text{sw}}$ from the planktonic foraminifera *G. bulloides* also indicates higher salinity throughout the glacials MIS6 and MIS3/MIS2 (Figures 2, 3) (Martinez-Mendez et al. 2010). However, alkenone δD values begin to shift toward more depleted values shortly before the start of Termination II, at approximately 135 ka, whereas the initial freshening recorded in the $\delta^{18}\text{O}_{\text{sw}}$ begins at about 133 ka (Figure 2). Similar diverging trends are noted for reconstructed $\delta^{18}\text{O}_{\text{sw}}$ derived from the planktonic foraminifera *G. ruber* (Marino et al. 2013). The most depleted values are reached in both reconstructed $\delta^{18}\text{O}_{\text{sw}}$ and $\delta D_{\text{alkenone}}$ during early MIS5e at about 128 ka (Figure 2). Higher salinity conditions are also observed throughout MIS3/MIS2 in reconstructed $\delta^{18}\text{O}_{\text{sw}}$ and $\delta D_{\text{alkenone}}$ (Figure 3) followed by freshening trends starting during early Termination I (~ 18ka). The offset in timing of the start of the freshening trends between the different proxies is similar to that observed in the Mg/Ca and U^{K}_{37} temperature records. This might be explained by differences in depth habitat between haptophyte algae and the foraminifera and/or salinity effects on Mg/Ca and consequently the reconstructed $\delta^{18}\text{O}_{\text{sw}}$ record. Despite the discrepancy in the timing of the start of the freshening events, an overall increase in salinity is recorded in both $\delta^{18}\text{O}_{\text{sw}}$ and $\delta D_{\text{alkenone}}$ during glacial stages MIS6 and MIS3/5. This is followed by a rapid decrease in salinity during the Terminations. The fresher conditions prevail during the subsequent interglacial stages.

Absolute salinity estimates are difficult to obtain from the $\delta D_{\text{alkenone}}$ due to the uncertainties in both the slope and intercept of the culture calibrations and other variables (Rohling 2007). However, by estimating relative salinity changes only, using the slope of the $\delta D_{\text{alkenone}}$ -salinity relationship, we avoid uncertainties related to the intercept. This provides an added advantage that the slopes for *E. huxleyi* or *G. oceanica* are nearly identical, i.e. 4.8‰ and 4.2‰ $\delta D_{\text{alkenone}}$ per salinity unit, respectively (Schouten et al. 2006). Estimations for relative salinity changes from $\delta D_{\text{alkenone}}$ result in a freshening trend of approximately 1.7 - 1.9 salinity units during the course of Termination I and II. These results are in fairly good agreement with the estimated salinity shift of 1.2 – 1.5 based on combined Mg/Ca SST estimates and $\delta^{18}O$ of *G. bulloides* for these time periods (Martinez-Mendez et al. 2010). However, they both seem to differ from the $\delta^{18}O_{\text{sw}}$ record based on *G. ruber* which indicates no salinity difference between glacial-interglacial and only an intermittent shift during the Terminations (Marino et al., 2013).

2.4.3. Paleoceanographic implications

Based on the reconstructed SST and relative SSS records, we suggest that increased salinity during glacial periods and subsequent freshening during the glacial terminations can be explained by the efficiency of the Agulhas Leakage, i.e. the volume transport of water from the Indian Ocean to the South Atlantic. According to Peeters et al. (2004), U^{K}_{37} SST maxima correspond to maximum Agulhas Leakage, as seen in the planktonic foraminifera Agulhas Leakage Fauna, during glacial Termination I and II. We observe enriched $\delta D_{\text{alkenone}}$ values, suggesting increased salinity, coinciding with reduced Agulhas Leakage during glacial stages MIS6 and MIS2/3. We suggest that with reduced through-flow and increased residence time of Indian Ocean water, the surface waters become relatively more saline and cooler in the Agulhas region, including the Agulhas leakage area. In contrast, with higher transport rates the surface waters will retain more of the original temperature and salinity resulting in the reconstructed lower salinities and higher temperatures. Thus, temperature and salinity are likely decoupled in this setting. In this case, heat loss is enhanced when water masses flow pole wards. Salinity, however, will be retained and during low through-flow situations in relative dry glacial periods evaporation will increase sea surface salinity. At the same time, the limited precipitation and river run off in this region will not counteract this increase sufficiently. However, the absolute amount of salt that is released into the Atlantic Ocean would still increase during terminations due to the increased flow, even though the surface waters are becoming less saline. Consequently, this would lead to increasing the Atlantic Meridional Overturning Circulation (Bard and Rickaby 2009, Haarsma et al. 2011).

2.5. Conclusions

In this study, we analyzed two sediment cores from the Agulhas leakage area covering Terminations I and II. We combined TEX^{H}_{86} and U^{K}_{37} SST reconstructions with a previously reported SST record based on Mg/Ca of the planktonic foraminifera *G. bulloides* (Martinez-Mendez et al. 2010). Sea surface temperatures reconstructed from three different proxies indicated relatively low temperature conditions throughout the late glacials MIS6 and MIS2/3 in the

Agulhas Leakage area and at the onset of the de-glaciation (Termination I and II) temperatures increase significantly. Relative salinity changes were reconstructed using $\delta D_{\text{alkenone}}$, which showed a shift from more positive values to more negative values during Termination I and Termination II suggesting elevated salinities during glacial periods, with subsequent freshening during glacial Terminations. Similar trends in glacial to interglacial salinity changes were also observed based on planktonic foraminifera $\delta^{18}O_{\text{sw}}$ reconstructions. Estimated salinity changes, based on $\delta D_{\text{alkenone}}$, range from 1.7 to 1.9 salinity units for Termination I and II. This is in fairly good agreement with salinity shifts based on the paired Mg/Ca and $\delta^{18}O$ approach of the planktonic foraminifera *G. bulloides*. Our results therefore suggest an increased release of slightly less saline Indian Ocean water to the South Atlantic Ocean during the Terminations than during the glacial, but with a net increase in salt transport during interglacials due to the higher through flow.

Acknowledgments

We acknowledge financial support from The Seventh Framework Programme PEOPLE Work Programme, Grant 238512 (Marie Curie Initial Training Network 'GATEWAYS'). The Netherlands Organization for Scientific Research (NWO) is acknowledged for funding Marcel van der Meer (VIDI) and Stefan Schouten (VICI). S.K. would like to thank Craig A. Grove (Royal NIOZ, the Netherlands) and David Chivall (Royal NIOZ, the Netherlands) for their input to this manuscript.

Chapter 3

Salinity changes in the southern Agulhas Current since the Last Glacial Maximum

Margit H. Simon, Conor Purcell, Ian R. Hall, Martin Ziegler, Stephen Barker, Gregor Knorr, Marcel T. J. van der Meer, Sebastian Kasper, Stefan Schouten, in preparation

Abstract.

Every year approximately 5-7 Agulhas rings are shed into the South Atlantic (SA) causing a salt anomaly there of $\sim +0.2$. The northward propagation of these density anomalies to the Norwegian–Greenland Seas have been considered to be important for the stability of the Atlantic Meridional Overturning Circulation (AMOC) on decadal-to millennial timescales. However, the origin of the salt oscillations associated with the ring shedding events in the Indian-Atlantic Ocean Gateway (I-AOG) remains equivocal. In this study we compare multi-proxy paleosalinity records since the Last Glacial Maximum (LGM) with results of model simulations using the fully coupled Community Earth System Model. We find that higher salinities prevailed in the southern Agulhas Current as well as in the I-AOG during the LGM compared to the Holocene. Additionally, during Heinrich Stadial 1 salinities simultaneously increased in both areas consistent with a quasi-inter-hemispheric salt seesaw response, analogous to the thermal bipolar see-saw. Interestingly, these hydrographic shifts can be recognised in the wider South Atlantic-Southern Ocean region which implies that salinity anomalies are not purely restricted to the Agulhas Current System itself. In fact, the numerical modelling results reveal that the salt accumulation in the Agulhas System is most likely Atlantic sourced and occurs via salt advection throughout the Southern Hemisphere super gyre in response to a reduced cross-hemispheric heat and salt exchange during times of abrupt climate change/weakened AMOC. Despite the fact that more saline upstream Agulhas waters were propagated to the I-AOG during Heinrich Stadial 1, as evident from both data and model results, no significant change in the actual salt-flux through the I-AOG into the SA is evident in the model.

3.1. Introduction

The large-scale ocean circulation is driven partly by global density gradients created by surface heat and freshwater fluxes (Rahmstorf, 1996; Rahmstorf, 2000). Thus, density-controlled circulation is key to transporting heat in the ocean and maintaining Earth's climate on different timescales. Broecker et al. (1990) hypothesized that millennial-scale Atlantic Meridional Overturning Circulation (AMOC) changes were modulated by sea surface salinity (SSS) oscillations altering ocean water density (buoyancy) in the proximity of the NADW formation sites (Renold et al., 2010).

An increasing number of studies have focussed on salt transport through the Indian-Atlantic Ocean Gateway (I-AOG), via the Agulhas leakage, which is considered as one potential controlling factor impacting on the North Atlantic salt budget (Lutjeharms, 2006; Beal et al., 2011). The Agulhas leakage of $\sim 5\text{--}15$ Sv is considered as a dominant source of the upper branch of the AMOC, connecting the southern tip of Africa to the North Atlantic (Gordon, 1986; Lutjeharms, 2006; Beal et al., 2011). The warm and saline Agulhas rings contribute salt and heat to the South Atlantic thermocline waters at a rate of up to 2.5×10^6 kg s^{-1} (salt) and 0.045 PW (heat), assuming a yearly total of six eddies (van Ballegooyen et al., 1994), causing a salinity anomaly of +0.2 in the South Atlantic thermocline (Gordon, 1985). The northward propagation of this salt anomaly across the Atlantic constitutes the warm water route of the global overturning circulation that feeds the renewal of NADW in the Northern Hemisphere (Gordon, 2001; Speich et al., 2001). The principal carrier of Agulhas leakage, the Agulhas Rings, decay rapidly in the Cape Basin (Schmid et al., 2003; van Sebille et al., 2010) thereby losing their anomalous surface thermal content quickly to the atmosphere (van Aken et al., 2003). What remains is the enhanced salt content, which persists for longer and contributes to the overall densification of the South Atlantic on advective timescales (Biaostoch et al., 2008; Biaostoch and Böning, 2013). The advection of salt is communicated north within 2–4 decades (Weijer et al., 2002; van Sebille et al., 2011; Rühls et al., 2013) suggesting the potential for a close coupling between Agulhas leakage and the AMOC with importance for global climate variability.

Paleosalinity is the single most important oceanographic parameter, which currently can still not be accurately quantified from sedimentary records. To date, the most promising tool to estimate paleosalinity variations combines reconstructions of paleotemperature and foraminiferal $\delta^{18}\text{O}$ (Rohling, 2000). Foraminiferal $\delta^{18}\text{O}$ varies as a function of temperature and ambient seawater $\delta^{18}\text{O}$ which is directly coupled to seawater salinity (Rohling and Bigg, 1998). Similar to seawater $\delta^{18}\text{O}$, seawater deuterium (D) content (δD) is also coupled to salinity. The hydrogen of seawater is incorporated into algal biomarker lipids during photosynthesis and these can be extracted from seafloor sediments. Thus, the δD of algal biomarker lipids is reflecting the δD of sea water. Furthermore, the biological hydrogen isotopic fractionation of photosynthetic organisms as measured in their biomarker lipids, is negatively correlated to salinity, thereby amplifying the sensitivity of the correlation between δD lipid and salinity (Schouten et al., 2006; M'boule et al., 2014). Thus, δD analyses on algal biomarker lipids could provide an alternative proxy for sea surface paleosalinity (Schouten et al., 2006).

The interest of the palaeoclimate community in Agulhas leakage arose from the finding that peak Agulhas leakage, based on the continuous presence of subtropical planktonic foraminifera in the South Atlantic (the so-called Agulhas Leakage Fauna (ALF)), occurred during glacial terminations (Peeters et al., 2004) and plausibly aided the AMOC to shift to its full-strength interglacial mode (Knorr and Lohmann, 2003; 2007). This hypothesis builds on a variety of records from within the Agulhas leakage pathway, which inferred fluctuations in the strength of Agulhas leakage (volume transport) over the late Pleistocene epoch based on a variety of geochemical proxy reconstructions (Peeters et al., 2004; Franzese et al., 2006; Martínez-Méndez et al., 2010; Rackebrandt et al., 2011; Caley et al., 2012; Marino et al., 2013; Scussolini and Peeters, 2013; Scussolini et al., 2013; Kasper et al., 2014; Scussolini et al., 2015).

However, proxy reconstructions of the last glacial termination from the I-AOG reveal an inconsistent picture. Peak Agulhas leakage inferred from ALF maxima occurred in the Holocene rather than during the last termination (Peeters et al., 2004). Salinity oscillations based on a $\delta^{18}\text{O}_{\text{sw}}$ record in the I-AOG display high variability, but are lacking distinct evidence for a maximum in salinity during the last termination and, hence, peak Agulhas leakage (Dyez et al., 2014). Moreover, a recent study hinted at the fact that the interpretation of Agulhas leakage strengthening or weakening, as previously inferred from SST, ALF and $\delta^{18}\text{O}_{\text{sw}}$ variability observed in records from the I-AOG (Peeters et al., 2004; Caley et al., 2012; Marino et al., 2013), may be a result of water mass property changes of the Agulhas Current without changing the actual amount of leakage (volume transport) (Simon et al., 2013). Therefore, the question arising is: do proxy records in the I-AOG strictly represent Agulhas leakage (volume) variability or are the observed oscillations part of a wider South Atlantic-Southern Ocean (SASO) signal during glacial terminations?

Here we explore this question by determining the nature of salinity changes in the Agulhas Current System with focus on the southern Agulhas Current since the Last glacial Maximum (LGM; 19–23 kyr BP) (Mix et al., 2001). Salinity changes are derived from organic (hydrogen isotope composition of long chain (C_{37}) alkenones ($\delta\text{D}_{\text{alkenone}}$)) and inorganic ($\delta^{18}\text{O}$ seawater reconstructed from $\delta^{18}\text{O}$ of planktonic foraminifera corrected for calcification temperature using Mg/Ca ratio based temperature) proxies in the same core. These proxies are compared to records from the I-AOG, previously interpreted to reflect changes in Agulhas salt-leakage. Furthermore, recent modelling studies (Purcell et al., in review) are used to better understand what might have driven the observed salinity pattern in the wider Agulhas Current system.

3.2. Core location and regional oceanography

Marine sediment core CD154-10-06P (31°10.36' S, 032° 08.91' E, 3076 m water depth) was retrieved from the southwest Indian Ocean ~160 km off the KwaZulu-Natal province coast (Fig. 1). Surface waters at the core site are dominated by the Agulhas Current, which transports about 70–78 Sv (1 Sv=10⁶m³s⁻¹) of tropical and subtropical waters along the south-eastern coast of Africa from 27 °S to 40 °S (Lutjeharms, 2006). These waters are characterised by high SSTs (23–26 °C) and high surface salinities (35.4), (Gordon et al., 1987).

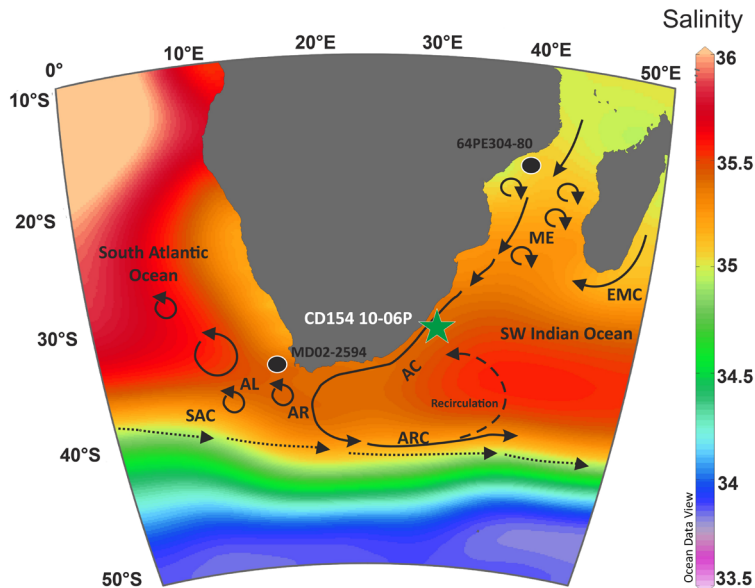


Figure 1. Location of the core CD154 10-06P this study (green star) and reference sites (black dots), I-AOG MD02-2594 (Kasper et al. [2014]), 64PE304-80 [Kasper et al., 2015] in the Mozambique Channel and oceanographic setting on a map of modern sea surface salinity. Mozambique Eddies (ME), East Madagascar Current (EMC) Agulhas Current (AC), Agulhas Return Current (ARC), Agulhas Retroflection (AR), Agulhas Leakage in form of Agulhas rings, and South Atlantic Current (SAC). The underlying map of modern sea surface salinity was compiled with high-resolution CTD data from <http://www.nodc.noaa.gov> and the Ocean Data View software version 4.3.7 by Schlitzer, R., Ocean Data View (<http://odv.awi.de>), 2010.

The Agulhas Current system is fed by various water sources. Most of its waters derive from the Mozambique Channel, from the southward flow to the east of Madagascar, from the Red Sea and from inertial recirculation in the southwest Indian Ocean (Beal et al., 2006). Studies have shown that the sources of the Agulhas Current are not dominated by the Mozambique Current (Saetre and Da Silva, 1984) or by the East Madagascar Current (Lutjeharms, 1988), but mostly by the recirculation in the Southwest Indian Ocean sub-gyre (SWIOSG), (Stramma and Lutjeharms, 1997). The Agulhas Current surface layer transports Indian Tropical Surface Water with potential temperature above 20 °C and salinity values between 34.7 and 35.3, along with South Indian Ocean Subtropical Surface Water with temperature above 17 °C and salinity values about 35.6 (Gordon et al., 1987). The excess of precipitation over evaporation in the tropical latitudes of the Indian Ocean can explain the lower salinities of Indian Tropical Surface Water (Gordon et al., 1987). The South Indian Ocean Subtropical Surface Water is found in the Agulhas Current as a subsurface salinity maximum with the high salinities arising from the high evaporation within the subtropical gyre (Beal et al., 2006). Red Sea Intermediate Water (RSIW) is also part of the intermediate layer constituting the Agulhas Current and has been shown to move down the current as distinct lenses (Roman and Lutjeharms, 2009). A further component of the Agulhas Current is the southwest Indian Ocean Central Water with roughly 13% volume amount within the current,

temperature range between 8°- 15°C and salinities between 34.6 and 35.5 (Lutjeharms, 2006). It seems obvious that changes in the proportions of these source waters could create different salinity signals in the current itself with variability through time. For example a higher intrusion of low salinity sub-Antarctic surface waters via enhanced recirculation, normally located south of the thermal STF (Fig. 1) could lower surface salinities. On the other hand, a higher proportion of saline subtropical Indian Ocean waters due to the excess of evaporation could increase salinities on the other hand (Fig.1).

3.3. Methods

3.3.1. Age model CD154-10-06P

The age model for the core was developed using ten ^{14}C accelerator mass spectrometer (AMS) dates measured from samples containing approximately 1000 tests of *G. ruber* (>250-315 μm). Radiocarbon measurements were made at the Natural Environment Research Council (NERC) Radiocarbon Laboratory. The radiocarbon ages were converted into calendar years using the Marine09 data set (Reimer et al., 2009) with the global mean reservoir correction of (R) 405 years (Bard, 1988). The core chronology was constructed using the statistical package BChron (Parnell et al., 2008; Parnell et al., 2011) using a Bayesian approach to calculate the 95% (2σ) uncertainty on the calibrated ages and the 95% probability envelope for the time period studied. In the range of the ^{14}C dates (1.9 -27.9 ka) relatively constant sedimentation rates of $\sim 4.0 \text{ cm ka}^{-1}$ (4.8-1.9 cm ka^{-1}) and a sample integration of ~ 300 years for every 1 cm sample is implied.

3.3.2. Inorganic proxies

Planktonic foraminifera $\delta^{18}\text{O}$ and Mg/Ca measurements

Paired stable oxygen isotope ($\delta^{18}\text{O}$) and Mg/Ca measurements in planktonic foraminifera species *G. ruber* are used to reconstruct changes in the surface salinities of the southern Agulhas Current (Fig. 1). Around 30 individuals were picked from the 250–315 μm size fraction every 1 cm in the upper part of the core (0-76cm), providing a temporal resolution of ~ 0.2 kyr over the last 21 kyr. Stable isotopes were measured using either a ThermoFinnigan MAT 252 mass spectrometer linked online to a Carbo Kiel-II carbonate preparation device (long-term external precision is 0.06‰ for $\delta^{18}\text{O}$ and 0.02‰ $\delta^{13}\text{C}$) or a Thermo Scientific Delta V Advantage mass spectrometer coupled with a Gas Bench III automated preparation device (long-term external precision is 0.08‰ for $\delta^{18}\text{O}$ and 0.06‰ $\delta^{13}\text{C}$) depending on the sample size. The stable isotope measurements were expressed relative to the Vienna Peedee Belemnite scale (VPDB) through calibration with the NBS-19 carbonate standard.

Mg/Ca measurements

Magnesium-to-calcium ratios (Mg/Ca) measurements in planktonic foraminifer *G. ruber* have been used to reconstruct changes in the surface temperature of the Agulhas Current (Fig. 1). *G. ruber* is a warm water species, highly abundant in the tropical-subtropical waters of the Indian Ocean and makes up to 40-60 % of the planktonic foraminiferal assemblage of the Agulhas Current today (Simon et al., 2013). A study of calcification depths of planktonic foraminifera in the tropical Indian Ocean showed that *G. ruber* calcifies within the mixed-layer, between 20-50 m (Mohtadi et al., 2009). Samples for Mg/Ca analysis were prepared and cleaned following the protocol outlined by Barker et al. (2003). The samples were analysed using a Thermo Element XR High ICP-MS with a long-term precision of element ratios, determined by replicate analyses of standard solutions containing Mg/Ca = 1.15 mmol mol⁻¹ and Mg/Ca = 6.9 mmol mol⁻¹, of ± 1.25 % relative standard deviation (RSD) and ± 0.52 % RSD, respectively. The Mg/Ca of *G. ruber* were converted to calcification temperature using the sediment trap calibration of Anand et al. (2003): $T = (1/0.09) * \ln((\text{Mg/Ca})/0.449)$. The standard error associated with this calibration is ± 1.1 °C on the calcification temperature estimates.

Mg/Ca content of foraminiferal calcite is particularly sensitive to dissolution (Rosenthal et al., 2004; Barker et al., 2005) and a previous study from the southwest Indian Ocean demonstrated that core material from that area is affected by post-depositional dissolution and needs to be adjusted (Simon et al., 2013). We therefore follow the same approach and applied the dissolution adjustment of Rosenthal and Lohmann (2002) in which the pre-exponential constant of the paleothermometry equation is a function of the shell weight of *G. ruber* with a modified exponential constant A in this study: $(\text{Mg/Ca})_{G. ruber} = (0.025 * \text{shell weight} + 0.11) e^{0.090T}$. Measured shell weights are a composite signal of dissolution related weight loss (Lohmann, 1995; Broecker and Clark, 2001) superimposed upon initial shell weight variability (Barker and Elderfield, 2002) which adds further uncertainty on corrected Mg/Ca values.

For error estimates the average standard deviation of 0.2mmol/mol (7.2% RSD) was used to account for artefacts associated with picking, cleaning, and natural variability of the *G. ruber* populations which was derived from duplicate measurements of 34 Mg/Ca samples of core CD154 17-17K (Simon et al., 2013). Trace element analyses on material from core CD154 10-06P were performed in the same manner, on the same species *G. ruber* and analytical facilities as for core CD154 17-17K. Hence, a standard error propagation calculation for a quadratic paleotemperature equation is followed in order to propagate these uncertainties along with those associated with the conversion of Mg/Ca to calcification temperatures (± 1.1 °C) and the analytical procedures involved in the Mg/Ca measurements (0.88% RSD = ± 0.1 °C). The resulting mean error for past calcification temperature is ± 1.3 °C. The adjustment for dissolution contributes additional uncertainties which results in a mean total error for past dissolution adjusted calcification temperatures of ± 1.4 °C. The effect of changing carbonate ion concentration of the surface ocean and salinity on the *G. ruber* Mg/Ca data was not considered as an additional source of uncertainty here, given that the changes in these components during the geological past are not well constrained. However, a recent study suggests a Mg/Ca-sensitivity to salinity of $3.3 \% \pm 1.7$ % per salinity unit for the foraminiferal species *G. ruber* (Hönisch et al., 2013). Glacial salinity was

assumed to be globally $\sim 3\%$ higher compared to the modern ocean, hence the expected salinity effect on Mg/Ca in glacial foraminifera would result into an approximate temperature bias of $+0.3\text{-}0.5\text{ }^\circ\text{C}$ (Hönisch et al., 2013).

Seawater Oxygen Isotope Reconstruction ($\delta^{18}\text{O}_{\text{sw}}$)

The Mg/Ca-derived *G. ruber* calcification temperatures were used to determine the oxygen isotopic composition of seawater ($\delta^{18}\text{O}_{\text{sw}}$) by extracting the temperature component from the $\delta^{18}\text{O}$ of the calcite using the paleotemperature equation of Kim and O'Neil (1997), with a VPDB to Standard Mean Ocean Water (SMOW) $\delta^{18}\text{O}$ correction of $0.27\text{ }‰$ (Hut, 1987), (Supplementary Figure 4). The $\delta^{18}\text{O}_{\text{sw}}$ was corrected for changes in global ice-volume to produce ice-volume corrected local $\delta^{18}\text{O}_{\text{sw}}$ estimates ($\delta^{18}\text{O}_{\text{sw-ivc}}$) following Grant et al. (2012) assuming a glacial $\delta^{18}\text{O}$ -enrichment in seawater of $0.008\text{ }‰$ per meter sea level lowering (Schrag et al., 2002). Full error propagation (uncertainty associated with temperature estimation from Mg/Ca, with the $\delta^{18}\text{O}_{\text{calcite}}$ analysis of *G. ruber*, with the $\delta^{18}\text{O}_c$ paleotemperature equation, with the sea level estimates, with the conversion of sea level values to mean ocean $\delta^{18}\text{O}$ analytical) yields 1σ uncertainties for the $\delta^{18}\text{O}_{\text{sw-ivc}}$ data of $\pm 0.4\text{ }‰$. The conversion from $\delta^{18}\text{O}_{\text{sw}}$ to salinity is generally accompanied by large uncertainties (Rohling, 2000). Therefore all data is shown here in $\delta^{18}\text{O}_{\text{sw-ivc}}$ values. However, to provide an estimate for relative shifts in the $\delta^{18}\text{O}_{\text{sw}}$, the regional southern tropical Indian Ocean ($24^\circ\text{S}\text{-}44^\circ\text{S}$) $\delta^{18}\text{O}_{\text{sw}}$ -salinity relationship ($\delta^{18}\text{O}$ -SSS slope of 0.44 ± 0.03 ; $r^2=0.69$; $n=115$; significant at $p=0.99$, (Tiwari et al., 2013)) is used here. A $\delta^{18}\text{O}_{\text{sw}}$ change of $0.1\text{ }‰$ would translate into a shift of approximately 0.27 in salinity.

3.3.3. Organic proxies

Sample preparation

Forty sediment samples were freeze-dried and homogenized with a mortar and pestle. The homogenized material was then extracted using an accelerated solvent extractor with dichloromethane (DCM):methanol 9:1 (v/v) and a pressure of 6895 kPa in 3 extraction cycles. The total lipid extract was separated over an Al_2O_3 column into an apolar, ketone and polar fraction using hexane:DCM 9:1, hexane:DCM 1:1 and DCM:methanol 1:1 (v/v), respectively. The ketone fraction was analysed by gas chromatography (GC), GC-mass spectrometry (MS) and GC thermal conversion isotope ratio monitoring MS (GC/TC/irMS).

δD of alkenone analysis

Alkenone hydrogen isotope analyses were carried out on the ketone fraction using a Thermo-Finnigan DELTA V GC/TC/irMS coupled with an Agilent GC using a GC isolink and conflo

IV interface. The temperature of the GC increased from 70 to 145 °C with 20 °C min⁻¹, then to 200°C with 8 °C min⁻¹ and to 320 °C with 4 °C min⁻¹, at which it was held isothermal for 13 min. Separation was achieved on an Agilent CP Sil-5 column (25m×0.32mm) with a film thickness of 0.4 μm and a carrier gas flow of 1 ml min⁻¹ helium at constant flow. The thermal conversion reactor temperature was set to 1420 °C. Hydrogen isotope values for alkenones were standardized against pulses of H₂ reference gas, which was injected three times at the beginning and two times at the end of each run. Alkenone δD values were measured as the combined peak of the C_{37:2} and C_{37:3} alkenones (van der Meer et al., 2013) and the fractions were analysed in duplicate if a sufficient amount of sample material was available. Standard deviations of replicate analyses varied from ±0.1 ‰ to ±5.9 ‰. A set of standard n-alkanes with known isotopic composition (Mix B prepared by A. Schimmelmann, University of Indiana) was analysed daily prior to measuring samples in order to monitor system performance. Samples were only analysed when the n-alkanes in Mix B had an average deviation from their offline determined value smaller than 5 ‰. The effect of changes in global ice volume on the δD_{alkenone} were estimated by using the global mean ocean δ¹⁸O_{sw} record from Grant et al. (2012) assuming a glacial δ¹⁸O-enrichment in sea-water of 0.008 ‰ per meter sea level lowering (Schrag et al., 2002). The equivalent changes in δ¹⁸O_{sw} were calculated by applying a local Indian Ocean meteoric waterline (Srivastava et al., 2010) which was subsequently subtracted from the δD_{alkenone} record (δD_{alkenone-ivc}).

Absolute salinity estimates are difficult to obtain from the δD_{alkenone} due to the uncertainties in both the slope and intercept of the culture calibrations and other variables (Rohling, 2007). Nevertheless, relative salinity changes from δD_{alkenone} result can be roughly estimated since the slope of the δD_{alkenone} - salinity relationship is 4.8 ‰ for *E. huxleyi* and 4.2 ‰ for *G. oceanica* grown in batch cultures (Schouten et al., 2006).

3.3.4. Numerical model simulations

Comprehensive fully-coupled Earth System model simulations

In order to better evaluate the observed salinity changes during abrupt climate change in the wider Agulhas Current System, COSMOS (The Community Earth System model) (Jungclauss et al., 2006) was used to perform a North Atlantic freshwater perturbation experiment, analogous to the iceberg/meltwater discharge suggested to be associated with Heinrich Events (Heinrich, 1988). Results from COSMOS have been shown in Purcell et al. (in review) and further details regarding the experimental setup can be found there.

3.4. Results and discussion

3.4.1. Glacial –Interglacial salinity changes in the Agulhas Current and I-AOG since the LGM

The ice-volume corrected hydrogen isotopic composition of alkenones ($\delta D_{\text{alkenone-ivc}}$) in core CD 154 10-06P display an isotope shift from the LGM to the Holocene (core top) of approximately 10‰ with sub-orbital variability throughout the deglaciation (Fig. 2b). Several factors can affect hydrogen isotope fractionation in haptophyte algae and the $\delta D_{\text{alkenone}}$ values including: (1) regional salinity change; (2) algal growth rate and growth phase (3) haptophyte species composition (Schouten et al., 2006; Chivall et al., 2014; M'boule et al., 2014). A recent study from the I-AOG in the South Atlantic (Kasper et al., 2014) used $\delta D_{\text{alkenone}}$ to infer relative changes in SSS and demonstrated that changes in algal growth rate and haptophyte species composition did not seem to affect the reliability of the $\delta D_{\text{alkenone}}$ SSS estimates during TI in this setting. The core discussed here is located in the same current system as the cores discussed in Kasper et al. (2014) and (Kasper et al., 2015) downstream and upstream in the Agulhas system. On that basis, acknowledging potential uncertainties, we also assume here that the $\delta D_{\text{alkenone-ivc}}$ shifts predominantly reflect the relative changes in the regional SSS at the CD154 10-06P site rather than growth rate or species composition changes. This assumption is supported by the good agreement of the $\delta^{18}O_{\text{sw-ivc}}$ record, derived from the same core material, with the $\delta D_{\text{alkenone-ivc}}$ record (Fig. 2c).

Equally to the glacial-interglacial (G-I) changes evident in the $\delta D_{\text{alkenone-ivc}}$ data set an approximate 0.4 ‰ shift is displayed by the $\delta^{18}O_{\text{sw-ivc}}$ record (Fig. 2c), derived from the same core material. Translating the observed LGM-Holocene changes to absolute salinities would suggest more saline waters in the southern Agulhas Current of approximately 1 during the LGM based on $\delta^{18}O_{\text{sw-ivc}}$ values. Based on the $\delta D_{\text{alkenone-ivc}}$ shift of approximately 10‰ the LGM would have been 2 more saline than the Holocene. The here inferred relative regional G-I salinity changes in the southwest Indian Ocean are generally in keeping with estimated whole glacial ocean salinity changes (Adkins and Schrag, 2001; Adkins et al., 2002).

Comparison between the CD154 10-06P data set and Kasper et al., (2014) shows that the ice-volume corrected residual $\delta D_{\text{alkenone}}$ recorded similar relative changes in salinity within the I-AOG and the Agulhas Current (CD154 10-06P site) with hydrogen isotope changes of approximately 10‰ since the LGM (Fig. 2b). The general G-I trend from relatively elevated $\delta D_{\text{alkenone-ivc}}$ values during the LGM to lower $\delta D_{\text{alkenone-ivc}}$ values during the Holocene is evident at both locations which implies that surface waters during the LGM within the I-AOG (Kasper et al., 2014) as well as in the southern Agulhas Current were more saline than during the Holocene (Fig. 2). Previous studies from the I-AOG observed elevated $\delta D_{\text{alkenone-ivc}}$ values (Kasper et al., 2014), suggesting increased salinity, coinciding with assumed reduced Agulhas leakage (i.e., the volume transport of water from the Indian Ocean to the South Atlantic) during glacial stages (Peeters et al., 2004). If the amount of water exchanged between the two oceans was reduced during the LGM one would expect the southwest Indian Ocean to become more saline in comparison to the South Atlantic

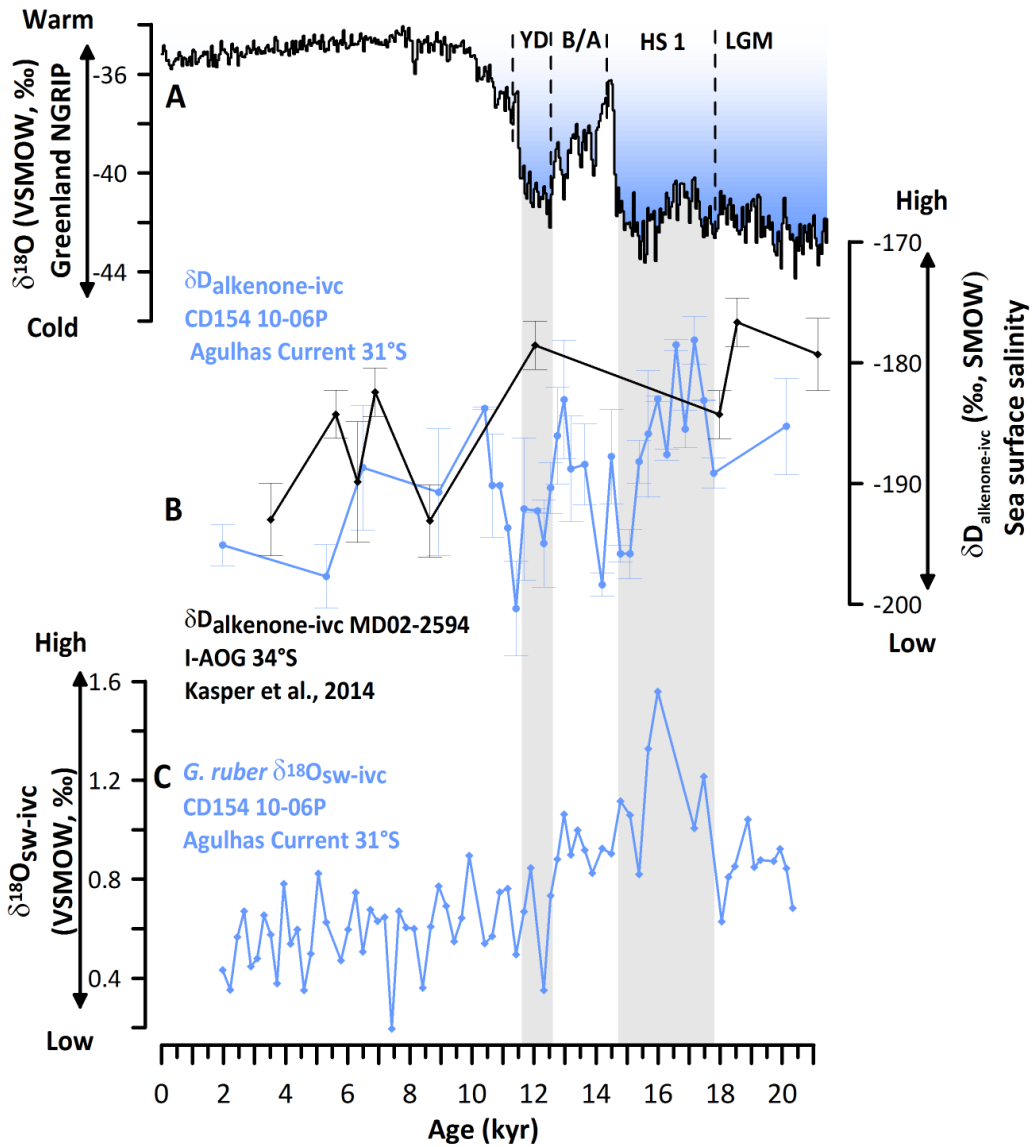


Figure 2. (a) $\delta^{18}\text{O}$ record from Greenland ice core NGRIP [NGRIP, 2004], (black, Speleo-age model presented in Barker et al. [2011]) displaying abrupt temperature variability in the North Atlantic. Underlying grey bars indicate Last Glacial Maximum (LGM), Heinrich Stadial 1 (HS1), Bølling-Allerød interstadial (B/A) and Younger Dryas (b) Hydrogen isotope composition of $\text{C}_{37:2-3}$ alkenones (blue), for core CD154 10-06P reflecting Sea Surface Salinity changes in the Agulhas Current and in the I-AOG core MD02-2594 (black), [Kasper et al., 2014]. Error bars indicate standard deviations based on replicate analyses of each sample (c) Ice-volume corrected $\delta^{18}\text{O}_{\text{sw}}$ reconstruction ($\delta^{18}\text{O}_{\text{sw-ivc}}$) for core CD154 10-06P.

due to increase residence time of Indian Ocean waters. However, the overall pattern in both $\delta\text{D}_{\text{alkenone-ivc}}$ records does not suggest that and might equally imply a downstream propagation of saltier (fresher) Agulhas Current waters during the LGM (Holocene) into the South Atlantic without any changes in leakage rates.

One could also consider that the G-I variability observed here in the southern Agulhas Current are a result of upstream source water changes for example in the Mozambique Channel (Fig. 1). However, a recently published $\delta D_{\text{alkenone}}$ record from the core 64PE304-80 (18° 14' 26.6274''S; 37° 52' 8.6874'' E, 1329 m water depth), located north of the Zambezi River Delta at the Mozambique shelf, shows no clear G-I shift in $\delta D_{\text{alkenone}}$ values (Kasper et al., 2015). It has been suggested that increased input of freshwater via the Zambezi River outflow (Schefuß et al., 2011), either via closer proximity to the coast or increased precipitation or a combination of both, would lead to a lowering in δD_{sw} at the 64PE304-80 core site and subsequently to a decrease in $\delta D_{\text{alkenone}}$ during the glacial. The lack of a clear G-I salinity shift in the Agulhas Current source area (Mozambique Channel) (Kasper et al., 2015) compared to the further downstream in the system (this study) moreover strengthens the assumption that upper ocean dynamics in the southern Agulhas Current area might have been crucial in determining the final leakage signature as opposed to its northern counterpart.

3.4.2. Millennial-scale salinity changes in the Agulhas Current

The last deglacial period (Termination I) witnessed several abrupt climatic shifts. During early Termination I (18–14.6 kyr ago), temperature records from Greenland and the North Atlantic reveal a cold interval (Heinrich stadial 1 (HS1)) during which the massive ice-rafting episode known as Heinrich event 1 occurred. This was followed by an abrupt and significant warming into the Bølling–Allerød (B/A) warm interval before a rapid return to near-glacial conditions during the Younger Dryas (YD) event (12.8–11.5 kyr ago). Interglacial conditions of the Holocene were reached by about 10 kyr ago.

During the course of the last deglaciation the $\delta D_{\text{alkenone-ivc}}$ values in core CD154 10-06P show a high degree of variability with the highest values present in the first half of HS1 ranging from ~ -180 and -185‰ suggesting relatively high salinity conditions at that time (Fig.2). In the second half of HS1 the $\delta D_{\text{alkenone-ivc}}$ values decreased to $\sim -195\text{‰}$, at the end of and just after HS1 indicating a freshening of surface waters. After HS1, during the B/A the $\delta D_{\text{alkenone-ivc}}$ values are initially relatively low suggest lower salinity during this period compared to most of HS1, but increase towards the end of the B/A to approximately -185‰ . During the YD, the ice volume corrected alkenone δD values decreased again to approximately -195‰ , suggesting relatively fresh conditions at the core site. After the YD, the hydrogen isotopic composition of the alkenones increase again, before slowly decreasing during the Holocene. Variability in the $\delta^{18}\text{O}_{\text{sw-ivc}}$ record, derived from the same core material, is in good agreement with the $\delta D_{\text{alkenone-ivc}}$ record (Fig. 2c). The overall pattern in the $d^{18}\text{O}_{\text{sw-ivc}}$ data fits with the $\delta D_{\text{alkenone-ivc}}$ indicating higher salinities during the LGM compared to the Holocene. During Termination I, with the onset of HS1 the $\delta^{18}\text{O}_{\text{sw-ivc}}$ values display an abrupt shift toward higher values, indicative of enhanced salinities. With the end of HS1 and the onset of the B/A, isotope values decreased, suggesting freshening of the surface Agulhas Current, however, values remained higher compared to the YD interval. Thereafter, values continuously decreased towards the late Holocene values of $\sim 0.4\text{‰}$ in that record (Fig. 2c).

Both proxies indicate that elevated salinity prevailed in the Agulhas Current during HS1 (Fig.2). Owing to the thermal bipolar seesaw behaviour, the South Atlantic-Southern Ocean (SASO) region warmed during Greenland stadials (GS) (Broecker, 1998; Stocker and Johnsen, 2003; Barker and Diz, 2014). A warming in the SASO region is accompanied by a salinification of the surface waters due to enhanced evaporation (Lohmann, 2003; Purcell et al., in review). Analogous to the thermal bipolar seesaw (Stocker and Johnsen, 2003), Lohmann (2003), based on modelling results, suggested the presence of an additional quasi-bipolar salt–seesaw that reflects changes in the salt advection throughout the Southern Hemisphere supergyre in response to the interhemispheric seesaw. It is possible that the Agulhas Current hydrography was influenced by such a salt–seesaw mechanism causing the salinification of the upper water layers. The lower resolution of the I-AOG record (Kasper et al., 2014) does not allow a direct comparison of both areas on shorter timescales over the last deglaciation. Notwithstanding, a previous comparison (Simon et al., 2013) between the variability in the $\delta^{18}\text{O}_{\text{sw}}$ records in the Agulhas Current and the I-AOG (Marino et al., 2013) during MIS 5 further strengthened the assumption that the observed salinity oscillations in the I-AOG could be a result of propagated upstream changes in the Agulhas Current.

Following the observations that Agulhas Current salinities are generally increasing during GS (Simon et al., 2013) one might expect the same pattern to occur during the YD. However, the YD seems to mark the point in the $\delta^{18}\text{O}_{\text{sw-ivc}}$ record when higher salinities during the last termination were dropping to lower interglacial values (Fig. 2c). More pronounced is the freshening of the surface waters in the $\delta\text{D}_{\text{alkenone-ivc}}$ record with a decrease of around approximately 15‰ during that interval (Fig. 2b). The reason for the observed lowered salinities during the YD remains equivocal, but could be related to a less pronounced salt–seesaw response in the Agulhas Current compared to the HS1 period. During HS1, cold conditions across the North Atlantic and warming over Antarctica were assumed to be associated with a strong reduction in overturning strength (McManus et al., 2004). A similar but less pronounced weakening occurred during the Younger Dryas. One could consider that a generally weak, but slightly more efficient AMOC compared to the HS1 interval secured more heat and salt exchange between the hemispheres resulting in reduced heat and salt build-up in the SASO region.

Another explanation could arise from a stronger contribution of fresher source waters feeding the Agulhas Current from the low-latitudes during the YD due to oceanic-atmospheric reorganisation during times of abrupt climate change. Schefuß et al. (2011) demonstrated that, during GSs, such as the YD and HS1, rainfall was enhanced in the Zambezi catchment area in response to a southwards forcing of the intertropical convergence zone. A higher proportion of these fresher waters from the coastal upstream areas and/or an increasing amount of Indian Tropical Surface Water having generally lower salinities could create lower densities in the Agulhas core region.

3.4.3. Simulated millennial time-scale climate variability in the Agulhas region

In order to test the general assumption that Northern Hemisphere climate variability forces hydrographical changes in the southwest Indian Ocean, an idealised North Atlantic freshwater perturbation experiment, analogous to the iceberg/meltwater discharge thought to be associated with a Heinrich Event (Heinrich, 1988), was performed using the COSMOS Earth System Model (Fig. 3). This numerical model simulation offers the opportunity to better evaluate the mechanism driving the observed salinity features in the multiproxy record of core CD154 10-06P. During the hosing experiment an upper level salinity increase of ~ 0.2 - 0.4 develops across the wider Agulhas Current system (Fig. 3). However, no significant change of I-AOG water transport is simulated during the experiment (Purcell et al., in review). Evident from the model output data is that the salinity increase is not exclusively restricted to the Agulhas System but is rather a feature in the wider South Atlantic-Southern Ocean (SASO). In fact, the signal is even more pronounced outside the Agulhas region i.e. the equatorial SA and the northern Indian Ocean (Fig. 3).

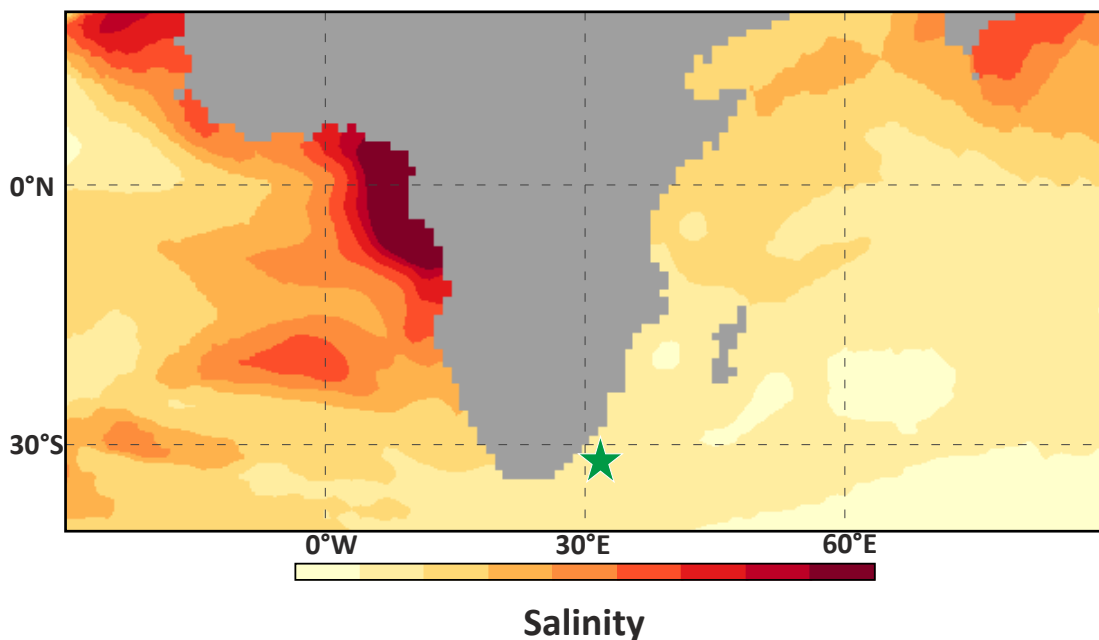


Figure 3. Modelled response to North Atlantic freshwater perturbation on LGM background state. Sea surface salinity anomaly. Location of the core CD154 10-06P (this study; green star) and reference site (black dot), I-AOG MD02-2594 [Kasper et al., 2014] are indicated.

Proxy based salinity reconstructions of core CD154 10-06P/CD154 17-17K (this study, Simon et al., 2013) and from the I-AOG (Marino et al., 2013) are consistent with the SSS increases around South Africa as well as in the Agulhas Current core region simulated by the model during the hosing experiment (Fig. 3). Marino et al. (2013) suggested that the increased salt-leakage might have acted as a source of negative buoyancy for the perturbed AMOC, possibly promoting its resumption. However, the idealised numerical modelling experiment suggests that the salt accumulation in the Agulhas system is most likely Atlantic-sourced and occurs via salt advection throughout the Southern Hemisphere supergyre in response to the quasi-bi-polar salt seesaw (Lohmann, 1995; Purcell et al., in review). This appears in response to the reduction of the AMOC (forced in the experiments by North Atlantic freshwater). The slowdown of the AMOC results in a reduced transport of salt across the equator in the Atlantic Ocean, and a recirculation throughout the South Atlantic Subtropical gyre system. This also results in a distribution of salt throughout the Southern Hemisphere supergyre and recirculation in the subtropical Indian Ocean Gyre system, effectively acting to increase salinity in the greater Agulhas region (Marino et al., 2013).

Future numerical modelling studies utilising Lagrangian analysis will be necessary in order to further investigate the dynamic relationship between the observed salt increase in the Agulhas Current/I-AOG and its impact on AMOC variability during millennial-scale climate change.

3.5. Conclusions

The general agreement between the organically and inorganically-derived proxy results confirms the application of $\delta D_{\text{alkenone}}$ for reconstructing past salinity changes in the wider Agulhas Current system. In detail, we find evidence that oscillation in upper water mass salinities in the southern Agulhas Current since the LGM are important for finally determining the Agulhas salt-leakage signal. That might imply that the Agulhas leakage signal south of Africa may in fact be controlled by upstream (southern Agulhas Current) dynamics, meaning that a change in the Agulhas leakage properties may occur even without a change in volume transport itself. In fact, more saline southern Agulhas Current waters were propagated to the I-AOG during times of abrupt climate change explaining proxy evidence in both regions. However, due to a reduced volume transport through the I-AOG no significant change in the actual I-AOG salt-flux into the SA is evident in the model (Purcell et al., in review). This implies that periods of higher salinity in the source region do not necessarily suggest that a greater fraction of Indian Ocean water entered the South Atlantic Ocean, as previously inferred from proxy records in the I-AOG.

Acknowledgements

We acknowledge funding from the European Commission 7th Framework Marie Curie People programme FP7/2007-2013 through funding of the Initial Training Network ‘GATEWAYS’ (www.gateways.itn.eu) under the grant number 238512 and the Climate Change Consortium of Wales. We thank the Captain, officers and crew of RRS Charles Darwin Cruise number 154, for which IH also gratefully acknowledge funding support from the Natural Environment Research Council. Radiocarbon measurements were performed at the NERC Radiocarbon Facility, East Kilbride, UK. Furthermore we acknowledge funding from the DAAD (German Academic Exchange Service) which supported the RISE (Research Internships in Science and Engineering) internship placement of Elisa Spreitzer who assisted together with Sebastian Steinig in carrying out laboratory and analytical work on core material CD154 10-06P. G. Rothwell and S. Maclachlan facilitated access and the measurement of CD154 10-06P on the ITRAX XRF scanning system at BOSCORF, National Oceanographic Centre, Southampton, UK. Alexandra Nederbragt, Lindsey Owen and Anabel Morte-Ródenas provided technical support with the isotope and trace element analysis at Cardiff University. Marcel van der Meer was funded by the Dutch Organization for Scientific Research (NWO) through a VIDI grant and Stefan Schouten was funded under the program of the Netherlands Earth System Science Centre (NESSC).

Chapter 4

Past salinity changes in the eastern tropical Atlantic as recorded by the stable hydrogen isotope composition of alkenones and $\delta^{18}\text{O}$ of planktonic foraminifera

Sebastian Kasper, Marcel T.J. van der Meer, Enno Schefuß, Stefan Mulitza,
Jaap S. Sinninghe Damsté, Stefan Schouten, in preparation

Abstract

The Atlantic Meridional Overturning Circulation (AMOC) is the major driver for the transport of heat and salt across the Atlantic Ocean towards the Northern Atlantic and Nordic Seas and is of key importance for the North African and European climate. On millennial time scales AMOC strength has been shown to vary in intensity, with weakened AMOC during glacial periods and Heinrich stadials. Eventually, this weakening may have led to a reduction of the south-north Atlantic surface transport of saltier and warmer water thereby changing the Atlantic salt and heat budget and potentially leading to a buildup of more saline surface waters across the entire subtropical Atlantic Ocean. To investigate the response of subtropical Atlantic Ocean salinity to AMOC variability, we reconstructed sea surface salinity variability for the period between 13 - 190 ka in an AMOC sensitive location on the Guinea Plateau Margin at the Northwest coast of Africa. We used a multiproxy approach with sea water $\delta^{18}\text{O}$ ($\delta^{18}\text{O}_{\text{sw}}$) reconstructions based on planktonic foraminiferal tests and the hydrogen isotope fractionation of long-chain alkenones versus seawater ($\alpha_{\text{alkenone-sw}}$) in sediment core GeoB9528-3. Both $\delta^{18}\text{O}_{\text{sw}}$ and $\alpha_{\text{alkenone-sw}}$ indicate increased salinity at times of weakened AMOC, such as glacial marine isotope stage 6. Reconstructed relative salinity estimates from both $\delta^{18}\text{O}_{\text{ruber}}$ and $\delta\text{D}_{\text{alkenone}}$ indicate a shift in salinity of ca. 2-4 towards fresher conditions during Termination II. A comparison with $\delta^{18}\text{O}_{\text{sw}}$ reconstructions from the western subtropical Atlantic (ODP-999A) shows a fairly good agreement and suggests that changes in salinity might have been a general phenomenon across the subtropical Atlantic.

4.1. Introduction

Vast amounts of salt and heat are transported around the globe via the global thermohaline circulation (Gordon, 1986). As part of this, the Atlantic Meridional Overturning Circulation (AMOC) transports salt and heat from the southern hemisphere across the Atlantic to the polar and subpolar North Atlantic and Nordic Seas, where the heat is released to the atmosphere (Rahmstorf, 2002; Ganachaud and Wunsch, 2003). The cooled, saline water sinks and forms the source of the southward flowing North Atlantic Deep Water (NADW) (Rahmstorf, 2002; Kuhlbrodt et al., 2007). On millennial time scales substantial variability occurs in AMOC strength depending on the positioning and depth of NADW formation during glacial and interglacial periods (Sarnthein et al., 1994; Alley and Clark, 1999; Lippold et al., 2012). Moreover, during Heinrich stadials the formation of NADW slows down in response to large meltwater discharges and the resulting freshening and cooling of the North Atlantic (Broecker, 1991; Elliot et al., 2002; Kuhlbrodt et al., 2007). This is evident in North Atlantic sea surface temperature (SST) and sea surface salinity (SSS) reconstructions from marine sediment cores (Lehman and Keigwin, 1992; Rahmstorf, 2002; McManus et al., 2004; Carlson et al., 2008). It is widely accepted that variation in AMOC strength directly impacts the global heat distribution, specifically affecting climatic conditions in Europe and central North Africa (Broecker, 1991; Rahmstorf, 2002; Bryden et al., 2005; Kuhlbrodt et al., 2007; Castañeda et al., 2009). During periods of weakened AMOC cold air is advected from high latitudes accompanied by an intensification of the northeast trade winds and a southward displacement of the intertropical convergence zone (ITCZ) leading to drier conditions in North Africa (Chiang et al., 2008; Mulitza et al., 2008; Castañeda et al., 2009). A weakened AMOC leads to a decreased northward transport of heat and salt, resulting in warming and increasing salinity in the tropical Atlantic Ocean (Manabe and Stouffer, 1997; Rühlemann et al., 1999; Schmidt et al., 2004; Chang et al., 2008) and deepening of the eastern tropical Atlantic thermocline (Lopes dos Santos et al., 2010). Conversely, relatively rapid climate warming like glacial to interglacial transitions, have been shown to correspond to increased polewards flow of warm and more saline Atlantic Ocean surface waters as response to AMOC strengthening, thereby reducing tropical Atlantic Ocean salinity (Lehman and Keigwin, 1992; McManus et al., 2004).

Although much is known of the thermal response to AMOC slowdown, much less is known about salinity changes, in particular for the tropical and subtropical North Atlantic. This is in part due to the limited number of proxies suitable to reconstruct past salinity changes. To assess past ocean salinity variations, the stable oxygen isotopic composition of the planktonic foraminifera *Globigerina ruber* ($\delta^{18}\text{O}_{\text{ruber}}$) corrected for calcification temperatures has been used to obtain the local sea water oxygen isotope composition ($\delta^{18}\text{O}_{\text{sw}}$) of e.g. the tropical North Atlantic (Duplessy et al., 1991; Schmidt et al., 2004). The $\delta^{18}\text{O}_{\text{sw}}$ is further corrected for global ice volume changes by subtracting a mean global ocean $\delta^{18}\text{O}_{\text{sw}}$ estimate (Waelbroeck et al., 2002). Variations in the resulting ice volume corrected $\delta^{18}\text{O}_{\text{sw}}$ ($\delta^{18}\text{O}_{\text{ic-sw}}$) are thus thought to solely reflect salinity (Rostek et al., 1993). However, there are uncertainties in planktonic foraminifera derived salinity estimates, i.e. in the transfer functions for the applied temperature correction and the $\delta^{18}\text{O}$ - salinity relationship, which relies on the assumption of temporal and spatial consistency (Rohling

and Bigg, 1998; Schmidt, 1999a; Rohling, 2000). More recently, the stable hydrogen isotope ratios of long-chain (C_{37}) alkenones ($\delta D_{\text{alkenone}}$) have been applied to estimate the variability of past ocean salinity as the hydrogen isotope composition of the combined $C_{37:2-3}$ alkenones, produced by haptophyte algae, has been shown to depend on salinity and the hydrogen isotope composition of the growth water. However, it has also been shown to depend on growth rate (Schouten et al., 2006) as well as growth phase and species composition (Chivall et al., 2014; M'Boule et al., 2014). Thus far, $\delta D_{\text{alkenone}}$ has been applied as proxy for past salinity changes in the eastern Mediterranean and Black Sea (van der Meer et al., 2007; 2008; Coolen et al., 2013), the Panama Basin (Pahnke et al., 2007), the Agulhas Leakage area at the southern tip of the African continent (Kasper et al., 2014) and the Mozambique channel (Kasper et al., 2015).

Here, we have used the $\delta^{18}O$ of the planktonic foraminifera *Globigerina ruber* and the δD of alkenones as two independent paleo salinity proxies to assess salinity variability off the coast of tropical West Africa over the last 190 ka in relation to glacial-interglacial cycles and AMOC strength variability. Modelling experiments have shown that this region reacts with particular sensitivity to AMOC strength variability by e.g. thermocline adjustment (Lopes dos Santos et al., 2010). We used core GeoB9528-3, which has previously been shown to record changes in climatic patterns over Northern Africa and ocean temperature variation associated with AMOC strength (Mulitza et al., 2008; Castañeda et al., 2009; Lopes dos Santos et al., 2010).

4.2. Material and Methods

4.2.1. Study site and oceanographic setting

We have analyzed core GeoB9528-3, located on the Guinea plateau margin ($09^{\circ}09.96'N$, $17^{\circ}39.81'W$, 3057 m depth) (Figure 1), for the hydrogen isotope composition of the combined $C_{37:2-3}$ alkenones (van der Meer et al., 2013) and the $\delta^{18}O$ of *G. ruber* for the time period covering 13 – 190 ka. The age model for the last 190 ka of core GeoB9528-3 is based on the age model of Castañeda et al. (2009) revised by Govin et al. (2014) using the AICC2012 ice core chronology (Veres et al., 2013). Core GeoB9528-3 is located outside of the Guinea Dome (GD), a thermal upwelling dome located near $10^{\circ}N$, $22^{\circ}W$ in the eastern tropical Atlantic off the coast of Guinea (Mazeika, 1967) (Figure 1). The Guinea coast is influenced by several surface and subsurface currents, of which the predominant systems are the Canary Current (CC), which transports year-round cool waters from $30^{\circ}N$ toward the equator along the West African coast (Knoll et al., 2002). The westwards flowing North Equatorial Current (NEC) transports mainly cooler Northeast Atlantic waters between $10 - 20^{\circ}N$ (Flores et al., 2000). A substantial contributor of warmer and more saline water to the core site is the Equatorial Under Current (EUC), an eastward flowing subsurface current at depths of about 100 m (Peterson and Stramma, 1991). Seasonally the intense, eastward flowing North Equatorial Countercurrent (NECC) appears at the southern boundary of the NEC (Richardson and Reverdin, 1987) and is fed by the retroflexion of surface waters (100 m) from the North Brazil Current (NBC) between $5 - 8^{\circ}N$ (Bourles et al., 1999). At

present day annual sea surface salinity ranges between ca. 35 – 35.5 at the study site (Dessier and Donguy, 1994). It receives Antarctic Intermediate Water (AIW) with a salinity of 34.6 – 34.9 at a depth of approximately 800 m underlain (< 1500 m) by North Atlantic Deep Water with a salinity between 34.9 – 35 (Mulitza et al., 2006).

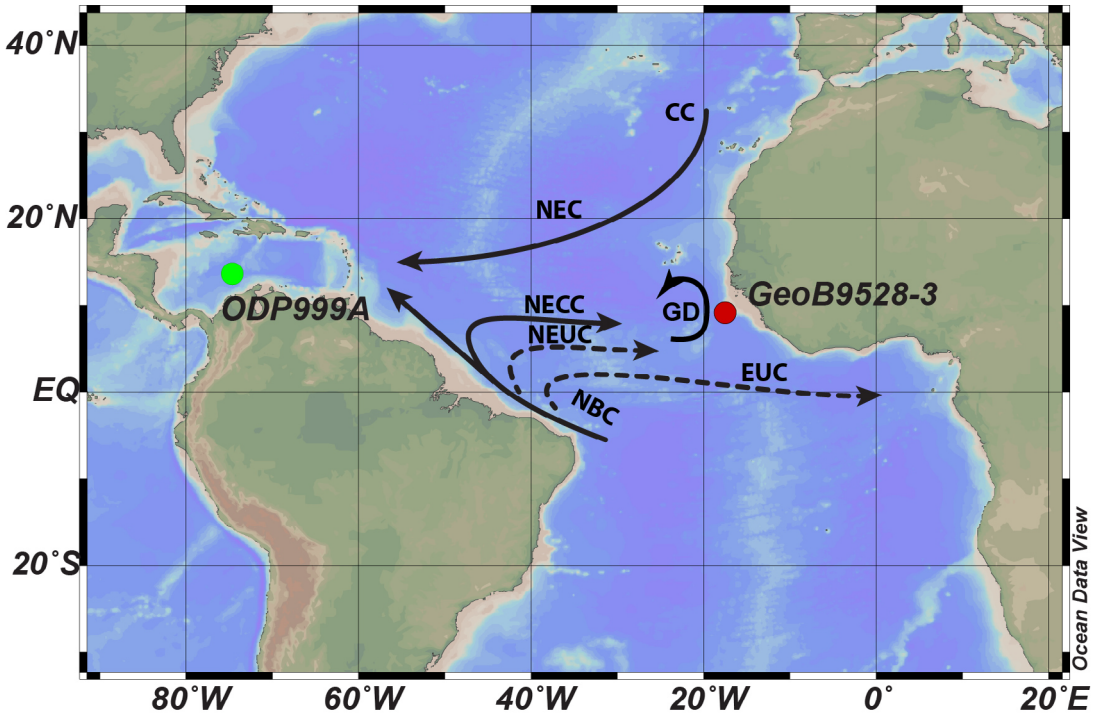


Figure 1: Location of core GeoB9528-3 in the eastern tropical Atlantic and core ODP-999A in the Cariaco basin (Schmidt et al., 2004). Major ocean surface currents (solid arrows) and subsurface currents (dashed arrows) are: Canary Current (CC), North Equatorial Current (NEC), North Equatorial Counter Current (NECC), North Equatorial Under Current (NEUC), Guinea Dome (GD), Equatorial Under Current (EUC) and the North Brazil Current (NBC). Figure based on Lopes dos Santos et al., 2010.

4.2.2 Foraminifera $\delta^{18}\text{O}$

Oxygen isotopes of the planktonic foraminifer *G. ruber* (pink) were measured at MARUM - Center for marine environmental science (Gemmeke, 2010) at the University of Bremen. Depending on the down-core availability, 7 to 25 specimens were picked from the >150 μm fraction. The size range of the shells, measured individually under the binocular along the longest axis of the shell, was in most depth intervals between about 300 and 550 μm . Isotope measurements have been done with a Finnigan MAT 252 using an automated carbonate preparation line (Kiel type). The standard gas (BurgbrohlCO₂) was calibrated against NBS 18, 19 and 20. Precision based on replicates of an internal Solnhofen limestone standard is better than 0.07 ‰.

4.2.3 Alkenone δD

Hydrogen isotope analyses on previously extracted alkenones from sediment core GeoB9528-3 (Lopes dos Santos et al., 2010) were carried out on a gas chromatograph (GC) linked by a GC Isolink and Conflo IV to a Thermo – Scientific DELTA V mass spectrometer with an Agilent CP Sil-5 column (25 m x 0.32 mm) with a film thickness of 0.4 μm and helium as carrier gas at 1 ml min^{-1} (constant flow). The temperature conditions of the GC increased from 70 to 145°C at 20°C min^{-1} , then at 8°C min^{-1} to 200°C and to 320°C at 4°C min^{-1} , at which it was held isothermal for 13 min. The high temperature conversion reactor was set at a temperature of 1420°C. The H_3^+ correction factor was determined daily and was constant at 4.7 ± 0.3 . A set of standard n-alkanes with known isotopic composition (Mixture B prepared by Arndt Schimmelmann, University of Indiana) was analyzed daily prior to analyzing samples in order to monitor the systems performance. Samples were analyzed when the alkanes in Mix B had an average deviation from their off-line determined value of $<5\%$. Squalane was co-injected as an internal standard with each sample to monitor the accuracy of the alkenone isotope values. The squalane standard yielded an average δD of $-162\% \pm 2.1$, which compared reasonably with its offline determined δD of -170% . Alkenone fractions were analyzed in duplicate unless insufficient sample material was available (2 out of 68 samples). Standard deviations of replicate analyses were $\pm 6\%$ at maximum.

4.3 Results

4.3.1 Foraminifera $\delta^{18}\text{O}$

The record of measured $\delta^{18}\text{O}$ of *G. ruber* ($\delta^{18}\text{O}_{\text{ruber}}$) shows a typical glacial-interglacial pattern (Figure 2c). The $\delta^{18}\text{O}_{\text{ruber}}$ ranges between -1.65 to 0.08% and increases from ca. -1.2% at 190 ka to ca. -0.03% at 166 ka. Between 130 – 161 ka [mid to late marine isotope stage 6 (MIS6)] values are relatively stable around $-0.27 \pm 0.16\%$ with the exception of a negative spike to -1.57% at 138 ka. During termination II (133 ka) $\delta^{18}\text{O}_{\text{ruber}}$ drops from -0.30% to -1.65% at 131 ka. Between 20 – 131 ka (MIS2 – MIS5e) values for $\delta^{18}\text{O}_{\text{ruber}}$ show an overall increase of $\sim 0.01\% \text{ ka}^{-1}$ toward the maximum of 0.1% at 20 ka. During this time period $\delta^{18}\text{O}_{\text{ruber}}$ shows a negative excursion at 81 ka (MIS5a) to about -1.29% and three positive excursions; at 68 ka (MIS4) to -0.38% ; at 47 ka (MIS3) to -0.31% and at 37 ka to -0.11% .

3.2 Alkenone δD

$\delta D_{\text{alkenone}}$ values range between ca. -205 to -174% (Figure 2g). The oldest part of the record at 190 ka shows $\delta D_{\text{alkenone}}$ values of -192% , which steadily increase to about -176% at 161 ka (mid MIS6; Figure 2g). Between 160 - 137 ka $\delta D_{\text{alkenone}}$ values are relatively constant at approximately $-179 \pm 3\%$. During Termination II at about 137 ka, $\delta D_{\text{alkenone}}$ values rapidly decrease by approximately 25% to about -206% at 131 ka (MIS5e). Between 131 to 100 ka (MIS5d/e) a peak can be

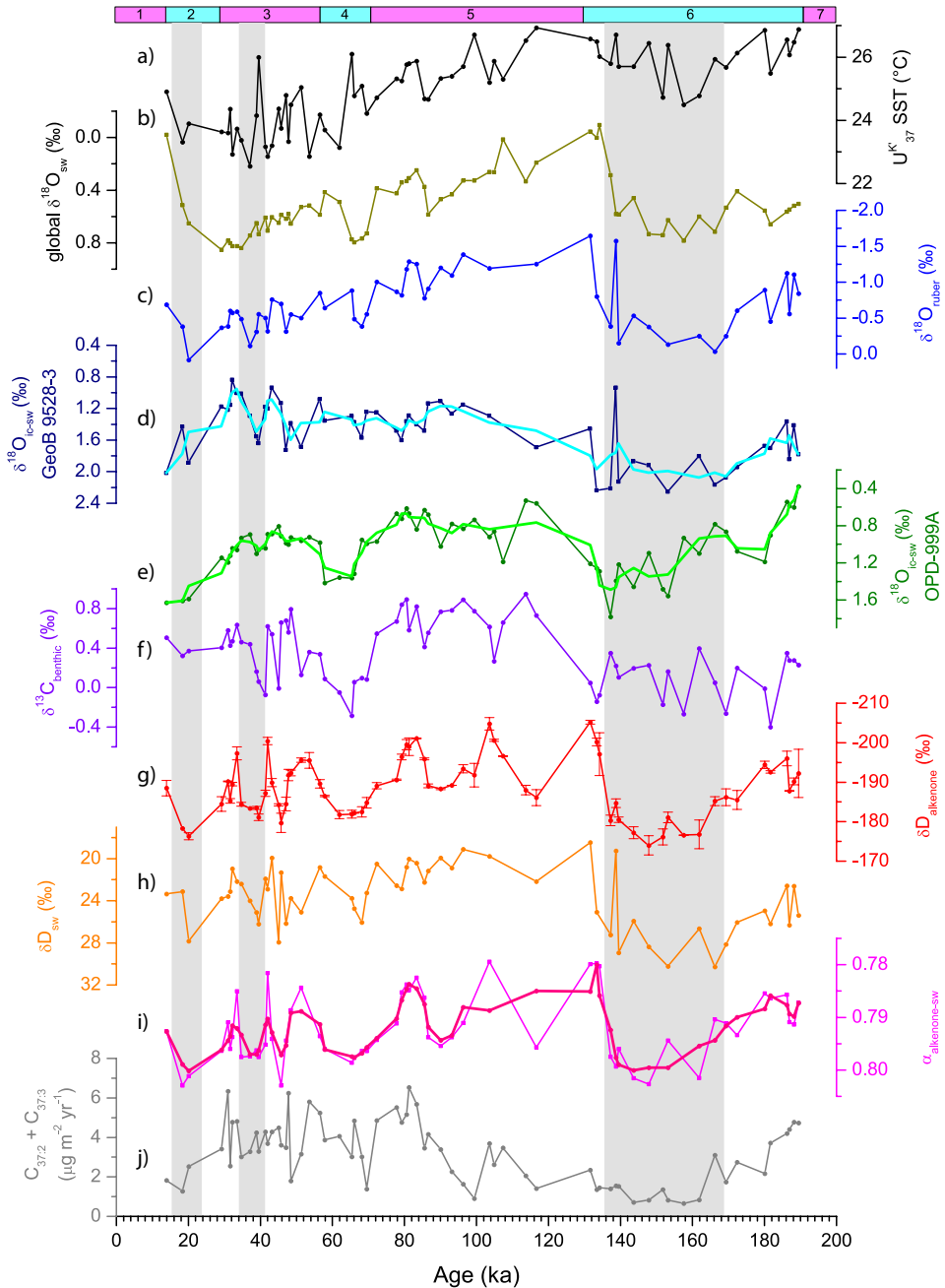


Figure 2: Geochemical records of the eastern tropical Atlantic core GeoB9528-3; (a) $U^{k'}_{37}$ SST (Castañeda et al., 2009); (b) global mean $\delta^{18}O_{sw}$ curve (Schrag et al., 2002; Rohling et al., 2009) (c) planktonic foraminifera *G. ruber* $\delta^{18}O$; (d) $\delta^{18}O_{ic-sw}$ or GeoB9528-3 (dark blue, axis reversed) with three point running mean (light blue); (e) $\delta^{18}O_{ic-sw}$ for ODP-999A (dark green, axis reversed) with three point running mean (light green) (Schmidt et al., 2004); (f) benthic foraminifera $\delta^{13}C$, (purple) (Castañeda et al., 2009); (g) $\delta D_{alkenone}$ with 1σ error bars for duplicate measurements (dark red); (h) δD_{sw} (orange) transferred from $U^{k'}_{37}$ SST corrected $\delta^{18}O_{ruber}$ using the global Meteoric Water line (Craig and Gordon, 1965); (i) $\alpha_{alkenone-sw}$ (pink, axis reversed) with three point running mean (dark pink); (j) $C_{37:2-3}$ alkenone accumulation rates (grey) (Lopes dos Santos, 2012). Grey shaded bars indicate periods of corresponding maximum values between $\delta D_{ic-alkenone}$ and $\delta^{18}O_{ic-sw}$. The resolution of all records has been scaled to the sampling interval of the $\delta D_{alkenone}$.

observed in the $\delta D_{\text{alkenone}}$ with relatively enriched values of about -186‰ at 117 ka (mid MIS5e). $\delta D_{\text{alkenone}}$ values decrease again to approximately -204 ‰ at ca. 103 ka. This is immediately followed by an increase in $\delta D_{\text{alkenone}}$ values to ~ -190 ‰ at 92 ka. Values remain relatively enriched in D until 86 ka, after which they start to rapidly decrease to ~ -201 ‰ at 83 ka (transition MIS5a / MIS5b). From 83 ka onward $\delta D_{\text{alkenone}}$ values steadily increase to approximately -181‰ at 68 ka (MIS4), after which they remain constant until 61 ka (Transition MIS3 / MIS4). After 61 ka $\delta D_{\text{alkenone}}$ values become more negative by approximately 14‰ at 54 ka (MIS3). At 51 ka values increase again to ~ -180 ‰ at 45 ka. Between 29 to 45 ka $\delta D_{\text{alkenone}}$ values show two strong negative spikes from an average $\delta D_{\text{alkenone}}$ value of ~ -183 ‰; the first is marked by a depletion in D to -200‰ at 42 ka; the second at 33 ka shows $\delta D_{\text{alkenone}}$ values of -197‰. At 29 ka (MIS2) $\delta D_{\text{alkenone}}$ values increase toward more enriched values of about -176‰ at 20 ka (Last Glacial Maximum; LGM). During termination I $\delta D_{\text{alkenone}}$ values decrease again to -188‰ at 12 ka.

4.4 Discussion

4.4.1. Sea surface salinity proxies at the Guinea Plateau Margin

In this study we use two salinity proxies: one based on the oxygen isotopic composition of sea water ($\delta^{18}\text{O}_{\text{sw}}$) calculated from the $\delta^{18}\text{O}$ of the planktonic foraminifera *G. ruber* (Figure 2c) and another based on the δD of C_{37} long chain alkenones from haptophyte algae (Figure 2g). For salinity estimates based on $\delta^{18}\text{O}_{\text{sw}}$, the $\delta^{18}\text{O}_{\text{ruber}}$ was first corrected for calcification temperatures, using previously published temperatures (Figure 2a) (Castañeda et al., 2009) and the calcification temperature equation for *G. ruber* (white) of Mulitza et al. (2003) [$T(^{\circ}\text{C}) = 14.20 - 4.44 * (\delta^{18}\text{O}_{\text{foram}} - (\delta^{18}\text{O}_{\text{sw}} - 0.27))$]] to estimate $\delta^{18}\text{O}_{\text{sw}}$. The correction for the global ice volume effect was achieved by subtracting a calculated global mean $\delta^{18}\text{O}_{\text{sw}}$ record derived from the sea level curve of Rohling et al. (2009) assuming an enrichment of 0.008‰ in ^{18}O per meter sea level lowering (Figure 2b) (Schrag et al., 2002). The resulting ice volume-corrected $\delta^{18}\text{O}_{\text{sw}}$ ($\delta^{18}\text{O}_{\text{ic-sw}}$; Figure 2d) record should reflect local salinity with more positive values equaling more saline conditions and vice versa (Rostek et al., 1993). The $\delta^{18}\text{O}_{\text{ic-sw}}$ record shows a variability of ca. 1.4‰ over the past 190 ka (Figure 2d). It increases from ca. 1.4‰ at 188 ka to ca. 2.2‰ at 166 ka and decreased during the transition from MIS6 to MIS5, indicating a freshening trend during termination II. During MIS5 $\delta^{18}\text{O}_{\text{ic-sw}}$ shows a relatively low variability with an average of 1.3 ± 0.2 ‰. At the transition from MIS4 to MIS3 (ca. 56 ka) the $\delta^{18}\text{O}_{\text{ic-sw}}$ increased marginally, potentially indicating an increase in salinity. During MIS3 two relatively large negative excursion in $\delta^{18}\text{O}_{\text{ic-sw}}$ of ca. -0.75 ‰ occur at 43 and 32 ka, respectively (Figure 2d). From 32 ka (MIS3) $\delta^{18}\text{O}_{\text{ic-sw}}$ shows a steady increase to the overall maximum value of 2.0‰ at 13 ka, suggesting steadily increasing salinity throughout the last glacial maximum (LGM) towards the Younger Dryas.

The $\delta D_{\text{alkenone}}$ record shows a glacial-interglacial pattern comparable to the $\delta^{18}\text{O}_{\text{ruber}}$ and they correlated significantly with each other (Figure 2g, 3a; $\delta^{18}\text{O}_{\text{ruber}} = 0.031 * \delta D_{\text{alkenone}} + 5.244$, $R^2 = 0.35$, $p\text{-value} < 0.00001$), although the former shows more pronounced variability during MIS5 to MIS2. Several factors control the alkenone δD , including seawater hydrogen isotope (δD_{sw})

variability. We estimate δD_{sw} from $\delta^{18}O_{sw}$ using the global meteoric water line (MWL; $\delta D = 8.0 * \delta^{18}O + 10 \text{‰}$) (Craig, 1961) (Figure 2h). Cross correlation of δD_{sw} and $\delta D_{alkenone}$ reveals a significant correlation ($\delta D_{alkenone} = 1.341 * \delta D_{sw} - 223.633$; $R^2 = 0.27$, $p\text{-value} < 0.0001$; Figure 3b), suggesting that variability in δD of alkenones is in part due to the variability in δD_{sw} . However, reconstructed δD_{sw} shows a maximum variability of ca. 12‰, which is substantially smaller than the 31‰ variability in $\delta D_{alkenone}$. This suggests that factors other than the δD_{sw} , such as salinity, growth rate (Schouten et al., 2006) or species composition (Chivall et al., 2014; M'Bole et al., 2014) substantially contributed to the variability in $\delta D_{alkenone}$.

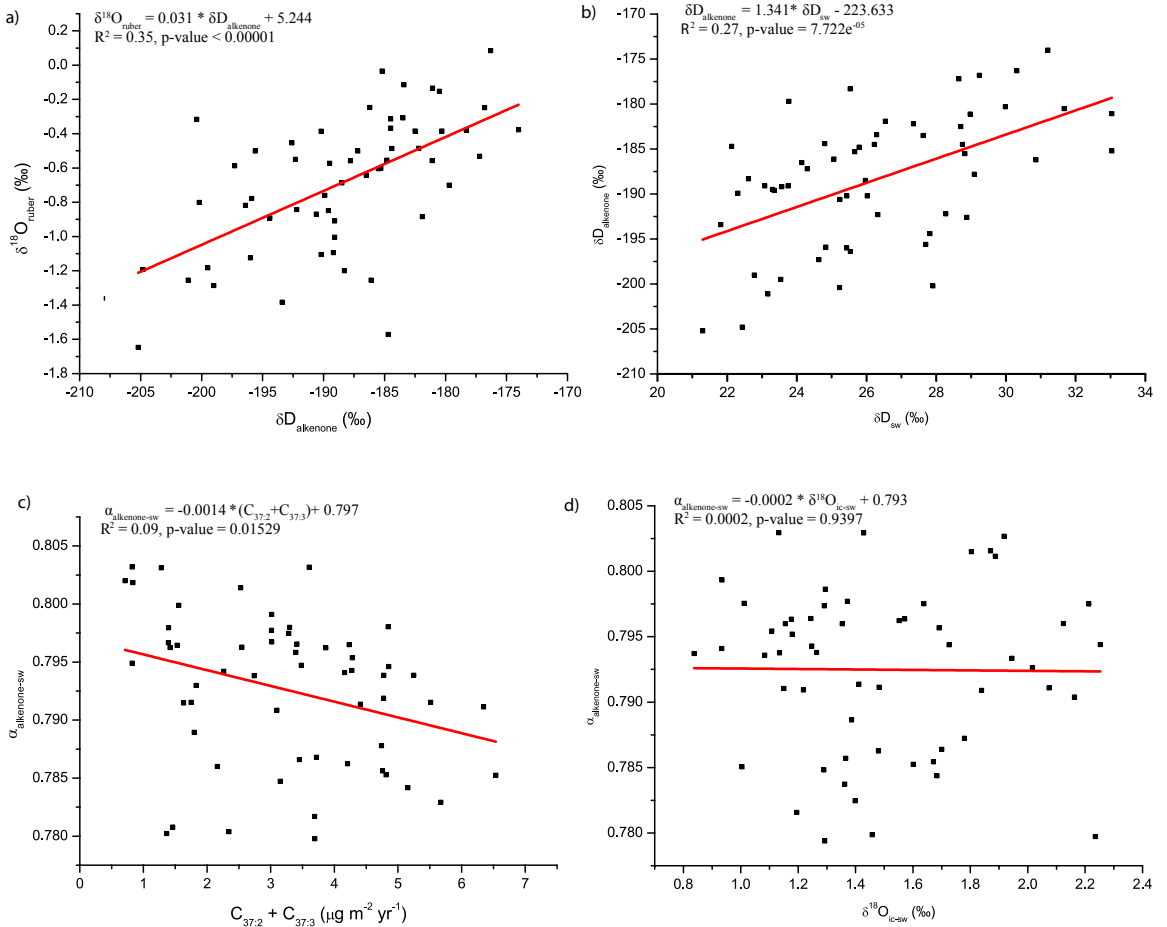


Figure 3. Cross plots and linear fitted lines (red) of (a) $\delta D_{alkenone}$ with $\delta^{18}O_{ruber}$; (b) reconstructed δD_{sw} and $\delta D_{alkenone}$; (c) alkenone accumulation rate $C_{37.2} + C_{37.3}$ and $\alpha_{alkenone-sw}$; (d) $\alpha_{alkenone-sw}$ and $\delta^{18}O_{ic-sw}$ for total data from core GeoB9528-3.

To correct for changes in δD_{sw} , we calculated the fractionation factor $\alpha_{alkenone-sw}$ ($\alpha_{alkenone-sw} = (1000 + \delta D_{alkenone}) / (1000 + \delta D_{sw})$) from measured $\delta D_{alkenone}$ and reconstructed δD_{sw} (from $\delta^{18}O_{sw}$). This fractionation factor varied between 0.780 and 0.803 (Figure 2i). The fractionation factor $\alpha_{alkenone-sw}$ shows variability that is in line with glacial – interglacial changes, similar to the $\delta D_{alkenone}$

record. We find $\alpha_{\text{alkenone-sw}}$ to be particularly elevated during the glacial stages MIS6, MIS4 and MIS2 as well as during one event in MIS5 at 90 ka. Below we explore potential causes for the variability in hydrogen isotope fractionation.

The offshore location of the core site makes a contribution of coastal haptophyte species, which are expected to produce generally more D-enriched alkenones compared to open ocean haptophyte species (M'Boule et al., 2014), unlikely. To test whether species composition changes may have occurred, we calculated the ratio for the total abundance of C_{37}/C_{38} alkenones, which has been reported to be higher in coastal haptophyte algae compared to open marine species (Marlowe et al., 1984b; Prahl et al., 1988; Schulz et al., 2000; Liu et al., 2011). However, C_{37}/C_{38} alkenone ratios show no substantial variation and are constant at 1.1 ± 0.1 for the period between 13 – 135 ka (data not shown). This suggests that no substantial changes in the haptophyte species composition occurred at the core location. Moreover, a study on the coccolithophorid assemblage from the eastern flank of the Mid-Atlantic Ridge and the eastern Ceara Rise in the western tropical Atlantic shows a relatively constant contribution of *Gephyrocapsa* species compared to *E. huxleyi* throughout the last 140 ka in the equatorial Atlantic Ocean, with only slightly increased contributions of *G. oceanica* during late MIS6, MIS4 and MIS2 (Kinkel et al., 2000). These changes in the relative contribution of *E. huxleyi* over the past 140 ka (Kinkel et al., 2000) do not resemble $\delta D_{\text{alkenone}}$ variability and, therefore, also suggest that changes in species composition might not have substantially affected the $\delta D_{\text{alkenone}}$ record.

Culture experiments have shown that lower growth rates result in increased $\alpha_{\text{alkenone-sw}}$ (Schouten et al., 2006) suggesting that growth rate could potentially affect isotopic fractionation. To investigate the impact of growth rate we compared $\alpha_{\text{alkenone-sw}}$ with alkenone accumulation rates (Figure 2j) (Lopes dos Santos, 2012) as a proxy for haptophyte productivity (Volkman et al., 1980; Marlowe et al., 1984b). Alkenone accumulation rates are relatively constant at a low value of $2 \pm 0.9 \mu\text{g m}^{-2} \text{yr}^{-1}$ during the transition of MIS6/MIS5 and slightly higher and more variable at $4 \pm 1.3 \mu\text{g m}^{-2} \text{yr}^{-1}$ during MIS4-MIS3. Cross correlation of $\alpha_{\text{alkenone-sw}}$ and the alkenone accumulation rates, however, only reveals a very weak correlation ($R^2 = 0.09$, p-value = 0.0153, Figure 3c), suggesting that growth rate might have exerted only a minor control on long term $\delta D_{\text{alkenone}}$ variability throughout the past 190 ka. Since species composition and growth rate changes do not seem to have affected the hydrogen isotopic fractionation significantly, we propose that glacial-interglacial variability in $\alpha_{\text{alkenone-sw}}$ is potentially mainly reflecting salinity. However, no clear statistical correlation between the two salinity proxy records of $\delta^{18}\text{O}_{\text{ic-sw}}$ and $\alpha_{\text{alkenone-sw}}$ is observed for the entire record ($\alpha_{\text{alkenone-sw}} = -0.0002 * \delta^{18}\text{O}_{\text{ic-sw}} + 0.793$, $R^2 = 0.0002$, p-value = 0.9397, Figure 3d).

Several factors can contribute to this apparent mismatch. First and foremost, the large uncertainties associated with the corrections used on the measured data leading to the estimations of $\alpha_{\text{alkenone-sw}}$ and $\delta^{18}\text{O}_{\text{ic-sw}}$. For instance, the temperatures used to correct for calcifying temperature in the seawater oxygen isotope calculations are based on long-chain alkenone temperature reconstructions and these alkenones are derived from haptophyte algae which might reflect a different depth habitat or growing season than the foraminifera (Nürnberg et al., 2000). For $\alpha_{\text{alkenone-sw}}$ the uncertainties are even larger as for this, the uncertain $\delta^{18}\text{O}_{\text{sw}}$ estimate is converted to δD_{sw} through a global meteoric water line which is likely to have varied on a regional scale and

through time. These cumulative corrections can lead to relatively large errors (Rohling, 2007; van der Meer et al., 2007) and could explain the relatively noisy character of both the $\delta^{18}\text{O}_{\text{ic-sw}}$ as well as $\alpha_{\text{alkenone-sw}}$ record compared to the measured $\delta^{18}\text{O}_{\text{ruber}}$ and $\delta\text{D}_{\text{alkenone}}$ which show more coherent changes.

To assess the long term variability in $\alpha_{\text{alkenone-sw}}$ and $\delta^{18}\text{O}_{\text{ic-sw}}$ we plot a three-point average and compare these records visually (Figure 2d, i). This comparison shows that more positive values in $\delta^{18}\text{O}_{\text{ic-sw}}$ correspond to higher values for $\alpha_{\text{alkenone-sw}}$ during glacial MIS6 and late MIS2, both suggesting elevated salinity during these stages. MIS5 shows slightly elevated $\delta^{18}\text{O}_{\text{ic-sw}}$ during MIS5e (117 ka), which is also evident in $\alpha_{\text{alkenone-sw}}$. $\delta^{18}\text{O}_{\text{ic-sw}}$ indicates relatively stable salinity conditions throughout the remaining MIS5 and MIS4, whereas $\alpha_{\text{alkenone-sw}}$ indicates more pronounced variability with positive excursions at 117 ka, 89 ka and 65 ka. During MIS3 both $\delta^{18}\text{O}_{\text{ic-sw}}$ and $\alpha_{\text{alkenone-sw}}$ show two shifts toward substantially lower values at ca. 42 and 33 ka. Thus, although some mismatches still occur, the two proxies do seem to roughly match on glacial-interglacial time scales.

4.4.2. $\delta^{18}\text{O}$ and δD based glacial-interglacial salinity shift estimates

To estimate average glacial-interglacial salinity shifts we calculated mean glacial and interglacial $\delta^{18}\text{O}_{\text{ic-sw}}$ and $\alpha_{\text{alkenone-sw}}$ for late MIS6 (137.2 – 153.2 ka), MIS5 (96.3 – 116.6 ka), MIS4 (57.8 – 66.1 ka) and MIS3 (47.1 – 51.3 ka) (Table 1). Salinity shifts were estimated from $\delta^{18}\text{O}_{\text{ic-sw}}$ using a slope of 0.22 for the salinity to $\delta^{18}\text{O}_{\text{sw}}$ relationship of the tropical Atlantic Ocean [$\delta^{18}\text{O}_{\text{sw}} = 0.22 * (\text{surface salinity}) - 6.95$; Watanabe et al. (2001)]. Assuming $\alpha_{\text{alkenone-sw}}$ reflects only salinity, relative salinity shifts can be calculated based on $\alpha_{\text{alkenone-sw}}$ using an average slope of 0.0028 per salinity unit as determined for culture calibrations of the open marine species *E. huxleyi* (PML B92/11) and *G. oceanica* (Schouten et al., 2006) and *E. huxleyi* (CCMP 1516) (M'Boule et al. (2014).

Table 1. Average values for the ice volume corrected $\delta^{18}\text{O}_{\text{ic-sw}}$ of ODP-999A (Schmidt et al., 2004); GeoB9528-3 and a $\delta\text{D}_{\text{sw}}$ equivalent derived from the global meteoric water line (Craig and Gordon, 1965); $\delta\text{D}_{\text{alkenone}}$ and the fractionation factor $\alpha_{\text{alkenone-sw}}$ (Schouten et al., 2006) for the designated time periods early MIS3, MIS4, MIS5d and late MIS6. The relative salinity shift is calculated from the difference between interglacial - glacial using a slope of 0.22‰ per change in 1 salinity unit for $\delta^{18}\text{O}_{\text{ic-sw}}$ (Watanabe et al., 2001) and 0.0028 per change in 1 salinity unit for $\alpha_{\text{alkenone-sw}}$ (Schouten et al., 2006), negative salinity shifts indicate freshening.

	Time interval	$\delta^{18}\text{O}_{\text{ic-sw}}$ (‰) ODP-999A	$\delta^{18}\text{O}_{\text{ic-sw}}$ (‰) GeoB9528-3	$\delta\text{D}_{\text{sw}}$ (‰) GeoB9528-3	$\delta\text{D}_{\text{alkenone}}$ (‰) GeoB9528-3	$\alpha_{\text{alkenone-sw}}$ GeoB9528-3
earlyMIS3 /	47.1 – 51.3 ka	0.96 ± 0.02 (n=4)	1.60 ± 0.19 (n=3)	27.6 ± 1.2 (n=3)	-191 ± 4 (n=4)	0.789 ± 0.005 (n=3)
MIS4	57.8 – 66.1 ka	1.30 ± 0.08 (n=4)	1.34 ± 0.04 (n=3)	26.0 ± 1.7 (n=3)	-183 ± 2 (n=4)	0.797 ± 0.001 (n=3)
salinity shift		-1.5 ± 0.4	1.1 ± 0.9			-2.9 ± 1.9
MIS5d	96.3 – 116.6 ka	0.83 ± 0.08 (n=7)	1.35 ± 0.24 (n=4)	23.2 ± 1.4 (n=3)	-195 ± 4 (n=7)	0.790 ± 0.007 (n=3)
Late MIS6	137.2 – 153.2 ka	1.37 ± 0.08 (n=7)	1.89 ± 0.49 (n=6)	29.4 ± 3.9 (n=6)	-180 ± 4 (n=7)	0.799 ± 0.003 (n=6)
salinity shift		-2.5 ± 0.5	-2.4 ± 2.5			-3.1 ± 2.9

For the transition of MIS6 to MIS5 we calculated a relative salinity shift of approximately 2.4 ± 2.5 toward fresher conditions from the $\delta^{18}\text{O}_{\text{ic-sw}}$ for the eastern tropical Atlantic (Table 1). The relative salinity change calculated from $\alpha_{\text{alkenone-sw}}$ also indicates a pronounced freshening of approximately 3.1 ± 2.9 for the transition between MIS6 / MIS5. Although the magnitude of the shift differs between proxies, this difference is well within uncertainty, particularly when accounting for the uncertainties associated with each method (Rohling, 2007) as well. A decrease in salinity in the eastern tropical Atlantic ocean of the magnitude of 2 - 4 during the transition from MIS6 to MIS5 as recorded in the $\delta\text{D}_{\text{alkenone}}$ and $\delta^{18}\text{O}_{\text{sw}}$ is in agreement with a proposed resumption of salt transport to the Northern Atlantic found in $\delta^{18}\text{O}_{\text{sw}}$ records along the western Atlantic Ocean in response to the gradual increase in AMOC strength after weakened glacial states (Broecker et al., 1990; Schmidt et al., 2004; Carlson et al., 2008). Furthermore, the observed coinciding excursions in $\delta^{18}\text{O}_{\text{ic-sw}}$ and $\alpha_{\text{alkenone-sw}}$ between 42 – 33 ka correspond to comparable changes in absolute salinity of 3 – 4 for both records (Figure 2d, i). For the transition of MIS4 to MIS3, we calculate a 2.9 ± 1.9 decrease in salinity from eastern Atlantic $\alpha_{\text{alkenone-sw}}$ (Table 1). However, the $\delta^{18}\text{O}_{\text{ic-sw}}$ salinity estimates for this record show only small variability during the transition of MIS 4 to MIS3, which would suggest a marginal increase in salinity of ca. 1.1 ± 0.9 for the same average intervals. Again this difference may well be within the uncertainty of both methods or could hint that one of them is affected by factors other than salinity, e.g. higher growth rates of the alkenone producers as suggested by the higher alkenone accumulation rates (Figure 2i, j) during this time leading to lower $\alpha_{\text{alkenone-sw}}$.

4.4.3. Paleoceanographic implications

U^{k7}_{37} based SST reconstructions for the tropical eastern Atlantic show a glacial – interglacial variability, which is in a relatively good overall agreement with reconstructed $\delta^{18}\text{O}_{\text{ic-sw}}$ and $\alpha_{\text{alkenone-sw}}$ (Figure 2a, d, i). These records indicate low salinity, i.e. relatively low $\alpha_{\text{alkenone-sw}}$ and more negative $\delta^{18}\text{O}_{\text{ic-sw}}$ values, coinciding with higher SSTs for most parts of the record (Castañeda et al., 2009), such as during MIS5e and early MIS4 (Figure 2). Vice versa, cool events are in line with relatively high $\alpha_{\text{alkenone-sw}}$ and $\delta^{18}\text{O}_{\text{ic-sw}}$, for example at 33 and 42 ka.

To assess if salinity variability in the eastern equatorial Atlantic is linked to AMOC strength, we compare the $\alpha_{\text{alkenone-sw}}$ and $\delta^{18}\text{O}_{\text{ic-sw}}$ to the $\delta^{13}\text{C}_{\text{benthic}}$ record from the benthic foraminifera *C. wuellerstorfi* from the same core (Castañeda et al., 2009) (Figure 2f). The latter is a proxy for deep water ventilation and AMOC strength and minima in $\delta^{13}\text{C}_{\text{benthic}}$ correspond to reduced AMOC strength (Duplessy and Shackleton, 1985; Vidal et al., 1997). Low values in $\delta^{13}\text{C}_{\text{benthic}}$, such as throughout MIS6, MIS4 and late MIS3 correspond to elevated $\delta^{18}\text{O}_{\text{ic-sw}}$ and $\alpha_{\text{alkenone-sw}}$, except for MIS4 which is only recognizable in $\alpha_{\text{alkenone-sw}}$ (Figure 2i). This correspondence suggests that weakened AMOC coincided with elevated salinity in the eastern tropical Atlantic.

Comparison of the $\alpha_{\text{alkenone-sw}}$ and $\delta^{18}\text{O}_{\text{ic-sw}}$ salinity records from core GeoB9528-3 with a $\delta^{18}\text{O}_{\text{ic-sw}}$ record from a core (ODP-999A) in the Caribbean (Figure 2e) (Schmidt et al., 2004) shows some similarities between the two records. For example, both show elevated values towards ca. 16 ka, and during MIS4 and MIS6, suggesting that salinity increased simultaneously across the tropical Atlantic during glacials (Schmidt et al., 2004; Carlson et al., 2008). The decreasing $\delta^{18}\text{O}_{\text{ic-sw}}$ values

during the transition between MIS6/MIS5 and MIS4/MIS3 in the Caribbean record suggest a freshening of ca. 2 according to the $\delta^{18}\text{O}$ - salinity relationship of Watanabe et al. (2001) in the western tropical Atlantic (Schmidt et al., 2004). This compares favorably with estimations based on $\delta^{18}\text{O}_{\text{ic-sw}}$ and $\alpha_{\text{alkenone-sw}}$ for MIS6/MIS5 and $\alpha_{\text{alkenone-sw}}$ for MIS4/MIS3 (Table 1). We also observe a substantial minimum in $\delta^{13}\text{C}_{\text{benthic}}$ during MIS4 (at ca. 65 ka), which occurs simultaneously with high $\delta^{18}\text{O}_{\text{ic-sw}}$ in the Caribbean and high $\alpha_{\text{alkenone-sw}}$ in the eastern Atlantic suggesting a tropical Atlantic salinity increase related to an AMOC slow down. However, this increase in salinity during MIS 4 is not reflected to the same extent in the eastern Atlantic $\delta^{18}\text{O}_{\text{ic-sw}}$. Nevertheless, our results suggest that AMOC variability likely had not only an impact on temperature (Lopes dos Santos, 2012), but also on sea surface salinity across the tropical North Atlantic.

4.4. Conclusions

In this study, we analyzed a sediment core (GeoB9528-3) from the Guinea Plateau in the eastern tropical Atlantic Ocean for $\delta^{18}\text{O}_{\text{ruber}}$ and $\delta\text{D}_{\text{alkenone}}$ covering the period between 12 – 190 ka. We reconstructed relative salinity shifts from $\delta^{18}\text{O}_{\text{ic-sw}}$ of $\delta^{18}\text{O}_{\text{ruber}}$ and fractionation factors $\alpha_{\text{alkenone-sw}}$ from $\delta\text{D}_{\text{alkenone}}$. Both records show increased salinity during glacial period MIS6 and a subsequent freshening into MIS5e. Reconstructed relative salinity shifts during the transition from MIS6 to MIS5 suggest a roughly 2 - 4 decrease in salinity. The $\delta^{18}\text{O}_{\text{ic-sw}}$ shows only little variation during the period between MIS5 - MIS2, whereas $\alpha_{\text{alkenone-sw}}$ indicates more pronounced variability. Salinity reconstructions based on $\delta^{18}\text{O}_{\text{ic-sw}}$ from the Caribbean compare reasonably well in amplitude and timing with $\delta^{18}\text{O}_{\text{ic-sw}}$ and $\alpha_{\text{alkenone-sw}}$ for MIS6/MIS5, suggesting that changes in salinity occurred basin-wide in the tropical Atlantic. During MIS4/MIS3 the agreement of $\alpha_{\text{alkenone-sw}}$ with $\delta^{18}\text{O}_{\text{ic-sw}}$ is weaker at the GeoB9528-3 core site, for reasons which are presently unclear. Comparison of the salinity records with a benthic foraminifera $\delta^{13}\text{C}$ record, as indicator for AMOC strength, indicates a possible connection between AMOC strength variability and relative salinity shifts during different isotope stages suggesting that AMOC strength has affected sea surface salinity.

Acknowledgment

We acknowledge financial support from The Seventh Framework Programme PEOPLE Work Programme, Grant 238512 (Marie Curie Initial Training Network 'GATEWAYS'). The Netherlands Organization for Scientific Research (NWO) is acknowledged for funding M.v.d.M (VIDI). D. Chivall is thanked for his input on the manuscript.

Chapter 5

Evaluating the impact of lateral transport on alkenones using sea surface temperature reconstructions and D/H ratios in the Atlantic sector of the Southern Ocean

Sebastian Kasper, Marcel T.J. van der Meer, Raquel A. Lopes dos Santos, Claire Waelbroeck, Julia Gottschalk, Luke Skinner, Jung-Hyun Kim, Jaap S. Sinninghe Damsté, Stefan Schouten, in preparation

Abstract

It is known that both organic and inorganic paleoproxies can be subject to pre- and post-depositional processes, which may lead to erroneous interpretations of past oceanic and climatic records. In particular, the resuspension and lateral transport of alkenones has been demonstrated to occur in the Indian Ocean Sector of the Southern Ocean and the Argentine Basin, resulting in anomalous $U^{k'}_{37}$ temperatures. Here, we generated a 25 ka long record for $U^{k'}_{37}$ and sea surface temperatures (SST) from a marine sediment core MD07-3076Q from the sub-Antarctic Atlantic and compared it with temperature reconstructions from planktonic foraminifera Mg/Ca and Modern Analogue Technique temperature estimates. In order to unravel potential provenance variations of the alkenone biomarkers, a record of the hydrogen isotope composition of the alkenones ($\delta D_{\text{alkenone}}$), an indicator for the hydrogen isotope composition of sea water (δD_{sw}) and salinity, was generated. Anomalously warm $U^{k'}_{37}$ temperatures during the last glacial, diverging from TEX^L_{86} and foraminifer-based temperature reconstructions, suggest that alkenones were potentially synthesized in a different water mass and subsequently transported to the core site. These anomalous temperatures coincide with enriched $\delta D_{\text{alkenone}}$, potentially indicating elevated salinity, and elevated alkenone accumulation rates. The glacial-interglacial shift in $\delta D_{\text{alkenone}}$ is only slightly larger than the shift expected based on the ice volume effect alone, suggesting that the alkenones were synthesized in warmer water masses with similar or slightly higher salinity than at the core site during the last glacial and are therefore probably partly allochthonous. Our results, therefore, suggest that the divergence of $U^{k'}_{37}$ -based SST from TEX^L_{86} - and foraminifera-based SST estimates results from lateral transport processes of the fine grained sediment fraction at the boundary between the South Atlantic and the Southern Ocean.

5.1. Introduction

Paleoceanographic climate proxies for ocean temperature and salinity are often used to reconstruct long-term natural climate variability on millennial time scales and can be obtained from the measurement of sedimentary organic (e.g. lipid biomarker) and inorganic material (e.g. calcareous foraminifer shells). For example, the foraminiferal carbonate oxygen isotope composition ($\delta^{18}\text{O}_{\text{foram}}$) is related to temperature (Shackleton, 1967; Bemis et al., 1998), and so are the Mg/Ca ratio of foraminiferal carbonate (Lea et al., 1999; Mashiotta et al., 1999; Lear et al., 2002), the ratio between di- and tri-unsaturated C_{37} long-chain alkenones produced by haptophyte algae (U^k_{37}) (Marlowe et al., 1984a; Brassell et al., 1986) and the number of cyclopentane moieties in glycerol dialkyl glycerol tetraethers (GDGTs) of archaea (TEX_{86}) (Schouten et al., 2002; Kim et al., 2008; 2010). The reconstruction of past ocean salinity often relies on the reconstruction of the past sea water oxygen isotope composition ($\delta^{18}\text{O}_{\text{sw}}$) derived from measurements of stable oxygen isotope ratios of, for example, $\delta^{18}\text{O}_{\text{foram}}$ corrected for calcifying temperatures, [e.g Duplessy et al. (1991); Rostek et al. (1993)]. More recently, as the biological hydrogen isotope fractionation in alkenones is correlated to salinity (Schouten et al., 2006; Chivall et al., 2014; M'Boule et al., 2014), the hydrogen isotopic composition of alkenones ($\delta\text{D}_{\text{alkenone}}$) has also been used to estimate past ocean salinity variability [e.g. van der Meer et al. (2007); (2008); Pahnke et al. (2007); Coolen et al. (2013); Leduc et al. (2013)].

It is well known that the composition of sedimentary organic and inorganic material can be affected by pre-depositional processes, for example lateral transport of particles (Benthien and Müller, 2000; Mollenhauer et al., 2006; Kim et al., 2009a), as well as post-depositional alterations, such as preferential degradation (Hoefs et al., 1998), dissolution (Brown and Elderfield, 1996), re-suspension and bioturbation (Guinasso and Schink, 1975; Thomsen and Gust, 2000). These processes can substantially bias proxy records, and subsequently lead to erroneous interpretations of past oceanic processes. In particular, fine-grained organic and inorganic particles can be subject to lateral advection, leading to mixing with large-sized particles of a different origin and thus introducing spatial and/or temporal offsets between sedimentary proxy records (Ohkouchi et al., 2002; Kim et al., 2009a). For instance, Benthien and Müller (2000) and Rühlemann and Butzin (2006) showed that the anomalously low alkenone temperatures in surface sediments south of the Brazil-Malvinas Confluence in the western Argentine Basin between 30° and 45°S are related to lateral displacement of suspended particles originating from colder source waters further south of their study site due to particle transport in the upper water column. Lateral transport of fine-grained particles was also demonstrated to cause differences between alkenone, TEX_{86} and foraminiferal temperature records resulting in the reconstruction of anomalously warm glacial conditions in the Indian sector of the Southern Ocean based on alkenones (Sicre et al., 2005; Kim et al., 2009a). However, it is unknown if sediment redistribution mechanisms affect lipid biomarker sea surface temperature (SST) reconstructions in the central sub-Antarctic Atlantic.

Here we investigate a sediment core from sub-Antarctic Atlantic, MD07-3076Q, spanning the last 25 ka (Figure 1). The site is located in between the subtropical and sub-polar fronts, which form a temperature and salinity boundary between the South Atlantic Gyre and the Antarctic Circumpolar Current (Smythe-Wright et al., 1998). Based on planktonic foraminifera

census counts it was shown that the sub-polar fronts migrated from a more northern position towards the present day position during the marine isotope stage (MIS) 2 – Holocene transition (Gottschalk et al., 2015). At the same time the retraction of Antarctic sea ice (Skinner et al., 2013) and changing surface wind stress (Klinck and Smith, 1993) substantially modified hydrological conditions and ocean currents at the core location.

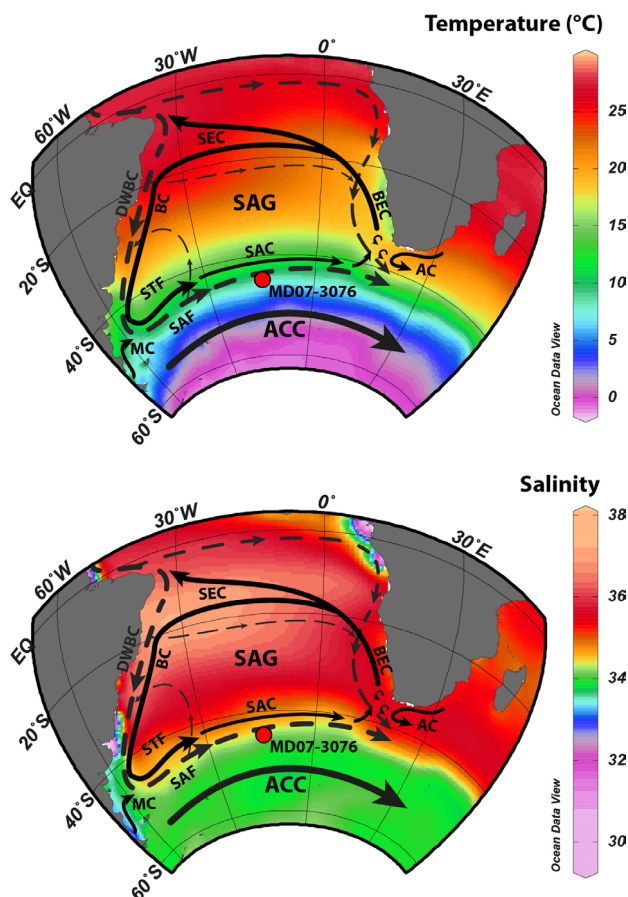


Figure 1. Maps of modern surface salinity (top panel) and temperature (lower panel) from Locarnini (2010), showing the location of core MD07-3076 (red dot) together with the predominant surface ocean currents (black solid lines), a simplified representation of the large scale North Atlantic Deep Water (NADW) flow at 2000 m depth (grey dashed lines) after Stramma and England (1999) and oceanic fronts prevailing in the Atlantic Sector of the Southern Ocean; DWBC – Deep Water Western Boundary Current; AC – Agulhas Current; BEC – Benguela Current; BC – Brazil Current; SEC – Southern Equatorial Current; SAG – South Atlantic Gyre; STF - Subtropical Front; SAC – South Atlantic Current; SAF – Sub Antarctic Front; MC – Malvinas current.

In this study we analyzed TEX_{86}^L and U_{37}^k temperature records and compared them to the previously published foraminiferal Mg/Ca and modern analog technique (MAT), based on foraminiferal community composition, temperature records (Skinner et al., 2010; Vázquez Riveiros et al., 2010). Comparison of these organic- and inorganic-based proxies as well as measuring the δD of alkenones, which can be used to trace allochthonous input of alkenones (Englebrecht and Sachs, 2005), were used to evaluate lateral transport effects on organic proxies in sediment records from the Atlantic sector of the Southern Ocean.

5.2. Material and Methods

5.2.1. Core location

Sediment core MD07-3076 (44° 4.46 'S, 14°12.47'W; 3770 m water depth) was retrieved from the eastern flank of the mid-Atlantic ridge in the Atlantic sector of the Southern Ocean (Figure 1) (Skinner et al., 2010). The age model for core MD07-3076 was established previously and is based on ^{14}C measurements of planktonic foraminifera corrected for variable age reservoir effects (Skinner et al., 2010).

5.2.2. Sample preparation

Sediment samples were freeze dried and homogenized with a mortar and pestle. The homogenized material was then extracted using the accelerated solvent extractor method (ASE) with dichloromethane (DCM):methanol (9:1, v:v) and a pressure of 1000 psi in 3 extraction cycles. The total lipid extract was separated over an Al_2O_3 column into apolar, ketone and polar fractions using hexane:DCM (9:1, v:v), hexane:DCM (1:1, v:v) and DCM:methanol (1:1, v:v), respectively.

5.2.3. Alkenone analysis

The alkenone-containing ketone fractions were analyzed by gas chromatography (GC) using an Agilent 6890 gas chromatograph with a flame ionization detector and a Agilent CP Sil-5 fused silica capillary column (50 m x 0.32 mm, film thickness=0.12 μm) with helium as the carrier gas. The GC-oven was programmed to subsequently increase the temperature from 70 to 200°C at 20°C min^{-1} , and then at 3°C min^{-1} to 320°C, at which it was held isothermally for 10 min. U_{37}^k values were calculated according to Prahl and Wakeham (1987). Subsequently, SST was calculated using the core top calibration against annual mean SST ($U_{37}^k = 0.033 * \text{SST} + 0.044$) established by Müller et al. (1998).

5.2.4. Analysis for δD of alkenone

GC/high-temperature conversion/isotope ratio mass spectrometry (GC/TC/irMS) was used to measure the combined hydrogen isotope composition of the combined C_{37} di- and tri-unsaturated alkenones. Alkenone hydrogen isotope analyses were carried out on a Thermo – Finnigan DELTA^{Plus} XL GC/TC/irMS. The temperature of the GC was increased from 70 to 145°C at 20°C min^{-1} , then to 200°C at 8°C min^{-1} and eventually to 320°C at 4°C min^{-1} , at which it was held isothermally for 20 min. An Agilent CP Sil-5 column (25 m x 0.32 mm) with a film thickness of 0.4 μm and helium as carrier gas at 1 ml min^{-1} (constant flow) was used. The high temperature conversion reactor was set at a temperature of 1425°C. The H_3^+ correction factor

was determined daily and was constant at 6.1 ± 0.4 . A set of standard n-alkanes with known isotopic composition (Mixture B prepared by Arndt Schimmelmann, University of Indiana) was analyzed daily prior to analyzing samples in order to monitor the system performance. Samples were only analyzed when the n-alkanes in Mix B had an average deviation from their off-line determined value of <5 ‰. Squalane was co-injected as an internal standard with each sample to monitor the precision and accuracy of the alkenone isotope values. The squalane standard yielded an average δD value of -158 ± 5 ‰, which is relatively high compared with its offline determined δD -value of -170 ‰ potentially due to sample background and/or co-elution with compounds from the sample itself. Alkenone δD values were measured as the combined peak of the $C_{37:2-3}$ alkenones (van der Meer et al., 2013) and analyzed in duplicate. Standard deviations of replicate analyses were on average ± 4 ‰.

5.2.5. Analysis of isoprenoidal GDGTs

The polar (DCM:MeOH, 1:1, v:v) fraction was concentrated under N_2 , dissolved in hexane:isopropanol (99:1, v:v), and filtered using a 0.4 mm PTFE filter prior to injection. Analyses for GDGTs were performed according to Schouten et al. (2007) using an Agilent 1100 series HPLC/MS equipped with an auto-injector and Agilent Chemstation chromatography manager software. Separation was achieved on an Alltech Prevail Cyano column (2.1 x 150 mm, $3\mu m$), maintained at $30^\circ C$. GDGTs were eluted with 99 % hexane and 1% propanol for 5 min, followed by a linear gradient to 1.8% propanol in 45 min, followed by back-flushing hexane/propanol (9:1, v/v) at 0.2ml/min for 10 min. Detection was attained by using atmospheric pressure positive ion chemical ionization mass spectrometry (APCI-MS) of the eluent. The Agilent 1100 APCI-MS were set to the following conditions: nebulizer pressure of 60 psi, vaporizer temperature of $400^\circ C$, drying gas (N_2) flow of 6 L/min and temperature $200^\circ C$, capillary voltage of -3 kV and a corona of $5 \mu A$ (~ 3.2 kV). GDGTs were detected by Single Ion Monitoring (SIM) of their $[M+H]^+$ ions (dwell time = 234 ms) (Schouten et al., 2007) and quantified by integration of the peak areas. In this setting TEX_{86}^L index ($TEX_{86}^L = \log([GDGT-2]/[GDGT-1]+[GDGT-2]+[GDGT-3])$), rather than the TEX_{86} index, was used to calculate absolute temperatures. The TEX_{86}^L index is specifically calibrated for annual mean SST reconstructions below $15^\circ C$ ($SST = 67.5 * TEX_{86}^L + 46.9$) in (sub)polar oceans (Kim et al., 2010).

5.3. Results

5.3.1. U_{37}^k and TEX_{86}^L

The U_{37}^k SST record (Figure 2e) showed values of $10.3 \pm 1.0^\circ C$ during MIS2 with a temperature minimum of ca. $7^\circ C$ at 19.5 ka BP. During the transition from MIS2 to MIS1, the U_{37}^k SSTs gradually decreased to ca. $6.5^\circ C$ at 5 ka BP. After this period, the U_{37}^k SST record reached a temperature maximum of ca. $10^\circ C$ at 4.1 ka BP before it decreased to $6^\circ C$ at 2.5 ka BP. From 2.5 ka BP onward the U_{37}^k SSTs showed a warming to ca. $9^\circ C$ again. In contrast, the TEX_{86}^L record

(Figure 2d) showed a completely different trend, i.e. relatively cool conditions (ca. 2.5°C) during MIS2 from 24.1 to 17.1 ka BP, followed by a gradual warming with ca. 8°C from 17 to 12.3 ka BP to the average MIS1 temperature 10.6±1°C, which were relatively constant during the Holocene.

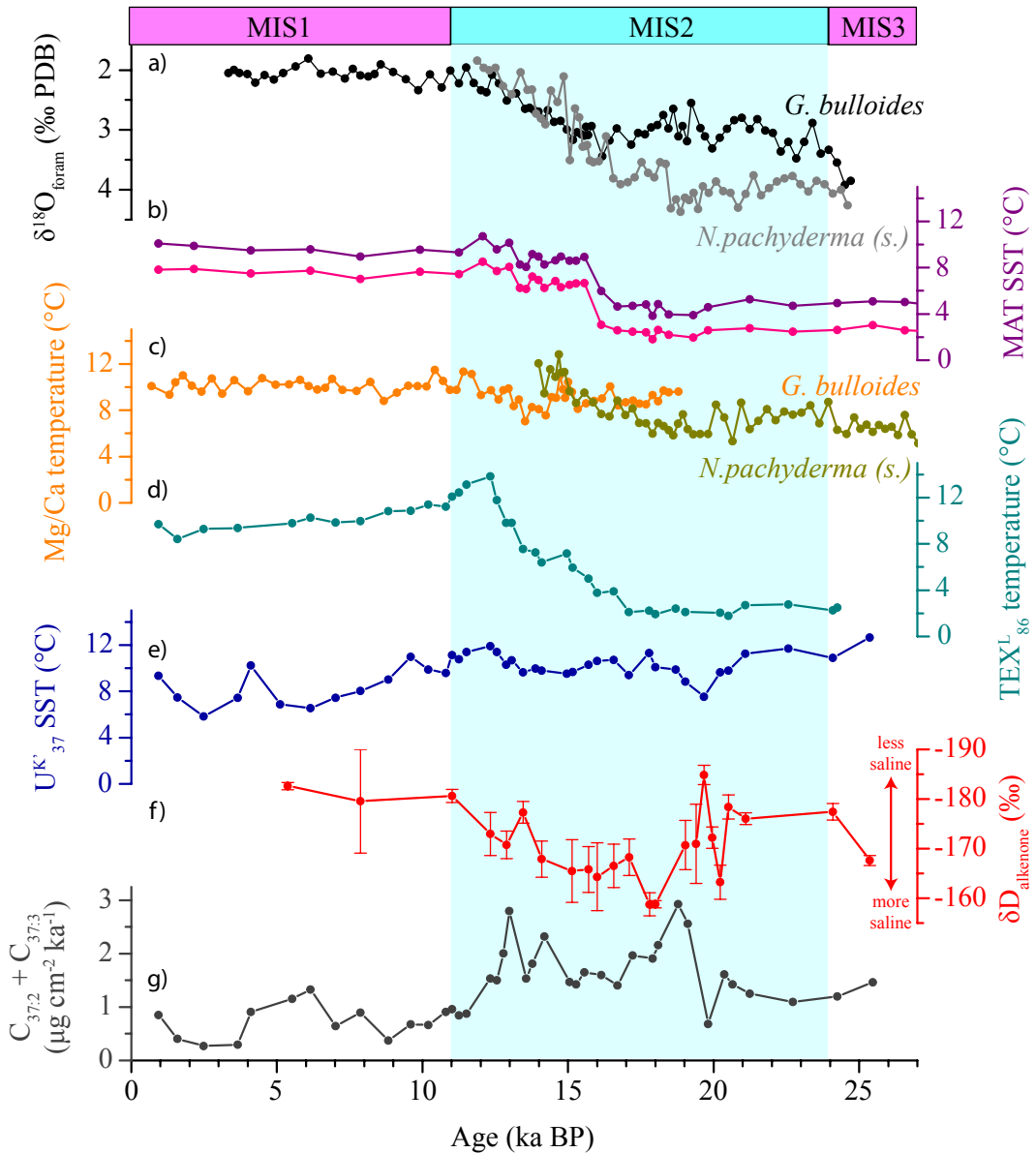


Figure 2. Paleoproxy records for core MD07-3076 showing (a) the $\delta^{18}\text{O}$ of *G. bulloides* (black) and *N. pachyderma* (s.) (grey) (y-axis reversed) (Vázquez Riveiros et al., 2010; Gottschalk et al., 2015); (b) foraminiferal assemblage based austral summer months estimates (purple) and austral winter months estimates (pink) for MAT SST (Skinner et al., 2010); (c) combined records of Mg/Ca temperature of *G. bulloides* (orange) and *N. pachyderma* (light green) (Skinner et al., 2010; Vázquez Riveiros et al., 2010; Gottschalk et al., 2015); (d) $\text{TEX}_{86}^{\text{L}}$ temperature record (green); (e) U^{K}_{37} SST (blue); (f) $\delta\text{D}_{\text{alkenone}}$ (red) with 1σ error bars (y-axis reversed) and (g) $C_{37:2} + C_{37:3}$ alkenone accumulation rates (grey). The blue shaded area indicates the glacial MIS2.

5.3.2 Alkenone δD

Values for $\delta D_{\text{alkenone}}$ ranged between -159 and -185 ‰ (Figure 2f; note the reversed scale). At 25 ka BP $\delta D_{\text{alkenone}}$ was -167 ‰ and decreased to -177 at 24 ka BP. Between 20.5 to 18 ka BP $\delta D_{\text{alkenone}}$ was highly variable with a maximum of -159 ‰ at 18 ka BP and a minimum of -185‰ at 19.7 ka BP after which it increased to -158‰. From 18 ka BP onward $\delta D_{\text{alkenone}}$ gradually decreased to approximately -180 ‰ at 11 ka BP and remained stable until 5.3 ka BP. The number of data points in the Holocene part of the core is unfortunately low due to the low abundance of alkenones (Figure 2g), which prohibited reliable measurements of their δD value.

5.4. Discussion

5.4.1. Temperature proxy records

To evaluate the potential impact of lateral transport on alkenone temperature reconstruction, we compare it with other proxies, which were suggested to be less affected by this, i.e. foraminiferal temperature records and TEX_{86}^L temperature records (Shah et al., 2008; Kim et al., 2009a; Kim et al., 2009b). Indeed, temperature estimates based on TEX_{86}^L show a similar pattern as Mg/Ca temperatures of the planktonic foraminifera *N. pachyderma* (*s.*) and austral summer month based MAT temperatures as described by Skinner et al. (2010) (Figure 2b, c). Average late Holocene (0–5 ka BP) temperatures are nearly identical for TEX_{86}^L ($9.2 \pm 0.5^\circ\text{C}$) and summer month MAT estimates ($9.8 \pm 0.3^\circ\text{C}$), and agree with present day austral summer months (Jan-Feb-Mar) SST of $10.7 \pm 0.6^\circ\text{C}$ for this region (Locarnini, 2010) (Figure 1). This suggests that TEX_{86}^L temperature reconstructions likely represent summer SST during the Holocene. The temperature records of TEX_{86}^L , Mg/Ca of *N. pachyderma* (*s.*) and MAT temperature show the start of deglacial warming occurring within a timeframe of ca. 1 ka, beginning with the *N. pachyderma* (*s.*) Mg/Ca SST record at ca. 18 ka BP, followed by TEX_{86}^L and MAT SST warming, which starts at ca. 17 ka BP. However, the average TEX_{86}^L temperature values in the last glacial ($2.3 \pm 0.3^\circ\text{C}$) approximate MAT temperature estimates for austral winter months ($2.4 \pm 0.4^\circ\text{C}$) (Figure b, d). The TEX_{86}^L -based glacial-interglacial SST gradient (8°C) is higher than for either summer or winter months based MAT temperature (ca. 4–5°C). This change in TEX_{86}^L temperatures, reflecting summer month MAT temperatures during the Holocene and winter month MAT temperatures during the last glacial, could indicate a change in growth season and/or depth habitat of the GDGT producers from the glacial to the Holocene (Castañeda et al., 2010; Huguët et al., 2011; Lopes dos Santos et al., 2013b).

In contrast to the TEX_{86}^L and foraminiferal temperature records, no pronounced MIS2-Holocene warming trend is seen in the alkenone U^{k}_{37} SST record (Figure 2e). Reconstructed U^{k}_{37} SST shows relatively warm conditions of up to 12°C throughout the glacial MIS2 compared to ca. 8°C from Mg/Ca of *N. pachyderma* (*s.*), 2°C from TEX_{86}^L and winter months MAT SST, and 5°C in summer MAT SST estimates (Figure 2). The average late Holocene U^{k}_{37} SST (0–5 ka BP) of $8 \pm 2^\circ\text{C}$ is lower than TEX_{86}^L -derived temperatures and those of the foraminiferal temperature

proxies, but corresponds well with the modern day annual mean SST of ca. 8°C for the region (Locarnini, 2010). Clearly, the high glacial U_{37}^k SST compare to Holocene values similar to < the glacial SST estimates from TEX_{86}^L , MAT and Mg/Ca. Furthermore, the absolute temperature differences in the glacial exceed the cumulative calibration uncertainty of 3°C between the U_{37}^k index ($\pm 1.5^\circ\text{C}$; Müller et al. (1998) on the one hand and foraminifera Mg/Ca ($\pm 1.2^\circ\text{C}$, Mashiotta et al. (1999) and the TEX_{86}^L index ($\pm 2.5^\circ\text{C}$; (Kim et al., 2010) proxies on the other. The anomalous Glacial U_{37}^k values coincide with relatively high alkenone accumulation rates between 19.1 and 12.8 ka BP (Figure 2g), suggesting increased haptophyte productivity at the core site (Volkman et al., 1980; Marlowe et al., 1984b; Ikehara et al., 2000). A possible source for the stimulation of algal productivity is the enhanced glacial expansion of polar waters, as suggested by Gottschalk et al. (2015) or enhanced ocean fertilization via increased wind-driven iron supply (Martin, 1990; Martínez-García et al., 2014). Studies of Prahl et al. (2003) and Prahl et al. (2006), indicated that ecological changes in the surface waters, such as nutrient limitation, can cause temperature unrelated variability in the U_{37}^k and subsequently lead to differences with other temperature proxies. Differences in haptophyte growth could contribute to the observed differences in reconstructed alkenone temperatures between the glacial and interglacial, however the most deviating temperatures seem to occur during more optimal haptophyte growth. Another, more likely, explanation for the diverging U_{37}^k SST trend might be re-suspension and lateral transport of the fine grain size particles, containing alkenones, originating from an area of warmer glacial SST than the core site. This has been observed previously in the Indian sector of the Southern Ocean (Sicre et al., 2005; Kim et al., 2009a) as well as in the Argentine Basin (Benthien and Müller, 2000; Rühlemann and Butzin, 2006). Indeed, model experiments on biases between water and alkenone temperatures in response to particle residence time and lateral transport showed that warm SST anomalies of up to 4°C, i.e. alkenone temperatures higher than water temperatures, are likely to occur at our core site during austral spring and summer months (Rühlemann and Butzin, 2006). Thus, the U_{37}^k record likely represents a signal that is not only reflecting glacial temperature conditions at the core site, but represents potentially also a signal transported from a remote area with warmer SST of up to 4°C than at the core site during glacial MIS2.

5.4.2. $\delta D_{\text{alkenone}}$ record

To investigate the potential source of the warm glacial U_{37}^k values, we measured the hydrogen isotopic composition of the alkenones. The $\delta D_{\text{alkenone}}$ values of the late glacial alkenones are relatively positive, ca. -166 ‰, compared to values during the early Holocene (Figure 2f). Several explanations can be put forward to explain these relatively positive values. The δD of alkenones can be affected by changes in the haptophyte species composition (M'Boule et al., 2014). However, the ratio of C_{37}/C_{38} alkenones, a proxy for haptophyte species composition (Marlowe et al., 1984b; Prahl et al., 1988; Schulz et al., 2000; Liu et al., 2011), remains relatively constant at 1.0 ± 0.2 over the entire record (data not shown), suggesting that no significant haptophyte species composition changes occurred. Potential effects of growth rate changes, conversely, are more difficult to constrain. We find elevated alkenone accumulation rates particularly between 19.1 and 12.8 ka, potentially indicating higher haptophyte productivity (Figure 2g). However, if higher

alkenone accumulation rates would reflect increased haptophyte growth rates, then the $\delta D_{\text{alkenone}}$ would be expected to become generally more negative (Schouten et al., 2006; M'Boule et al., 2014), in contrast to the more positive values observed in this time interval.

One likely explanation for the more positive values is the global change in δD of sea water (δD_{sw}) due to the preferential accumulation of H in large ice sheets during the Glacial, consequently leading to a relative enrichment of D in the sea water. Using the global mean ocean $\delta^{18}\text{O}_{\text{sw}}$ curve of Waelbroeck et al. (2002) and the global meteoric waterline ($\delta D_{\text{sw}} = 8 * \delta^{18}\text{O}_{\text{sw}} + 10$) (Craig, 1961), this ice volume effect on δD_{sw} is estimated to cause a 8 - 10 ‰ shift in $\delta D_{\text{alkenone}}$ during the glacial – interglacial transition. Since the overall glacial-interglacial $\delta D_{\text{alkenone}}$ shift is ca. -13 ‰, the remaining shift of ca. 3 -5 ‰ in the $\delta D_{\text{alkenone}}$ could be caused by a relatively small salinity shift of ± 1 salinity unit (Schouten et al., 2006). This suggests that the anomalous glacial alkenones were derived from sediments relatively enriched in alkenones and deposited in a warm, somewhat more saline water mass. We speculate that a possible transport mechanism for alkenones from warmer and marginally more saline conditions could be the sediment drift of fine grained particles caused by winnowing and focusing processes from South Atlantic waters north of the subtropical fronts to the core site. Such mechanism has been described from the Southern Cape Basin (Tucholke and Embley, 1984; Sachs and Anderson, 2003). However, in the Southern Cape Basin multiple U^{k}_{37} SST records from drift and non-drift locations showed a coherent regional temperature signal for the Cape Basin (Sachs and Anderson, 2003). For our record we speculated that sediment drift of winnowed fine grained particles, including alkenones, to the core site might provide a transport mechanism to explain anomalously higher U^{k}_{37} , as also modeled by Rühlemann and Butzin (2006), especially with multiple, significantly different water masses in the vicinity. Besides the proposed increased glacial ocean iron fertilization as a driver for algae productivity (Martínez-García et al., 2014), an increased lateral displacement of the fine grained material might have additionally contributed to higher alkenone accumulation rates (Sachs and Anderson, 2003) as observed during the last Glacial (Figure 2g).

Interestingly in the older part of the record between 24 and 19 ka BP, the $\delta D_{\text{alkenone}}$ values are more negative again and accumulation rates are also lower, suggesting that the alkenones may be more locally derived, albeit that the U^{k}_{37} temperatures are still relatively high. The values for $\delta D_{\text{alkenone}}$ are lower than those reported in other glacial records at the southern tip of the African continent (Kasper et al., 2014). For the same interval Gottschalk et al. (2015) observed a divergence between the $\delta^{18}\text{O}$ records of the surface dwelling planktonic foraminifera *G. bulloides* and *N. pachyderma* (s.) in core MD07-3076 (Figure 2a), which was explained by a shift in the depth habitat of *N. pachyderma* (s.) to the deeper thermocline as a response to the increasing influence of polar waters and the development of salinity-driven density stratification towards the LGM, consistent with the predicted enhanced sea ice summer melt in the South Antarctic Zone during this period (Gersonde et al., 2003). The relatively depleted $\delta D_{\text{alkenone}}$ values during the first half of MIS2 could, thus, reflect the enhanced salinity-density driven upper water layer stratification as proposed by Gottschalk et al. (2015) and the resulting relatively fresh water layer at the surface. After stratification disappears, as indicated by the converging oxygen isotopic composition for both, *G. bulloides* and *N. pachyderma* (s.) (Figure 2a), the alkenones reflect the relatively D-enriched sea water typically expected for glacial conditions. This salinity-driven density stratification during

early MIS2 could potentially also help explain the large glacial-interglacial temperature shift reconstructed by $\text{TEX}_{86}^{\text{L}}$ by also pushing the preferred niche of *Thaumarchaeota* to a deeper water depth.

5.5. Conclusion

During the transition between the last Glacial and the Holocene, we observe a clear increase in the temperatures based on the $\text{TEX}_{86}^{\text{L}}$ and foraminiferal assemblage-based MAT estimates as well as in the Mg/Ca of *N. pachyderma* (s.). This can be explained by the southward migration of the subtropical fronts as response to changes in Antarctic sea ice extent and changes in the wind fields dominating the ocean current regime and the global change to a warmer climate. In contrast to these proxy records, anomalously warm glacial conditions followed by a cooling trend into the Holocene is recorded by the U_{37}^{k} paleothermometer. This suggests that the fine-grained particles containing alkenones were laterally transported from a warmer glacial area to the core site, as observed previously in the Indian sector of the Southern ocean. The record of $\delta\text{D}_{\text{alkenone}}$, as indicator for salinity and $\delta\text{D}_{\text{sw}}$ changes, shows enriched values during the glacial when the alkenone accumulation rates are also high and a glacial-interglacial shift is only slightly higher than expected based on ice volume changes alone. This can be explained by the input of allochthonous alkenones, which were synthesized in warmer water masses with similar or slightly higher salinity during the glacial. Accordingly, our study highlights that alkenone based U_{37}^{k} SST and $\delta\text{D}_{\text{alkenone}}$ records need to be interpreted with caution in Southern Ocean sediment records but that combined they can yield information on the lateral transport processes of the fine grained sediment fraction at the boundary between the South Atlantic and the Southern Ocean.

Acknowledgments

We acknowledge financial support from The Seventh Framework Programme PEOPLE Work Programme, Grant 238512 (Marie Curie Initial Training Network ‘GATEWAYS’). The Netherlands Organization for Scientific Research (NWO) is acknowledged for funding M.v.d.M. (VIDI). The European Research Council ERC under the European Union’s Seventh Framework Program (FP7/2007-2013)/ERC grant agreement No. [226600] is acknowledged for financial support for J.-H.K. and J.S.D..

Chapter 6

Testing the alkenone D/H ratio as a paleo indicator of sea surface salinity in a coastal ocean margin (Mozambique Channel)

Sebastian Kasper, Marcel T.J. van der Meer, Isla S. Castañeda, Rik Tjallingii, Geert-Jan A. Brummer, Jaap S. Sinninghe Damsté, Stefan Schouten, 2015, *Organic Geochemistry* 78, 62-68

Abstract

Reconstructing past ocean salinity is important for assessing paleoceanographic change and therefore past climatic dynamics. Commonly, sea water salinity reconstruction is based on planktonic foraminifera oxygen isotope values combined with sea surface temperature reconstruction. However, the approach relies on multiple proxies, resulting in rather large uncertainty and, consequently, relatively low accuracy of salinity estimates. An alternative tool for past ocean salinity reconstruction is the hydrogen isotope composition of long chain (C_{37}) alkenones ($\delta D_{\text{alkenone}}$). Here, we have applied $\delta D_{\text{alkenone}}$ to a 39 ka sedimentary record from the Eastern South African continental shelf in the Mozambique Channel, close to the Zambezi River mouth. Despite changes in global seawater δD related to glacial – interglacial ice volume effects, no clear changes were observed in the $\delta D_{\text{alkenone}}$ record throughout the entire 39 ka. The BIT index record from the same core, which provides information on relative contributions of soil organic matter (OM) vs. marine input, indicates high soil OM input during the glacial and low input during the Holocene. This suggests a more pronounced freshwater influence at the core location during the glacial, resulting in alkenones depleted in D during that time, thereby explaining the lack of a clear glacial-interglacial alkenone δD shift. The correlation between the BIT index and $\delta D_{\text{alkenone}}$ during the glacial period suggests that increased continental runoff potentially changed the growth conditions of the alkenone-producing haptophytes, promoting coastal haptophyte species with generally more enriched $\delta D_{\text{alkenone}}$ values. We therefore suggest that the application of $\delta D_{\text{alkenone}}$ for reconstructing past salinity in coastal settings may be complicated by changes in the alkenone-producing haptophyte community.

6.1. Introduction

The interaction and feedback mechanisms at the interface between oceanic and atmospheric circulation on glacial – interglacial timescales are largely unknown, but are thought to play an important role in the global transmission of climate change (Manabe, 1969; Rahmstorf, 2002). Accurate reconstruction of past oceanic and atmospheric changes is crucial for a better understanding of these mechanisms and should eventually improve prediction of future climate development (Esper et al., 2005). Reconstruction of ocean circulation requires an estimate of seawater density, which is determined by salinity and temperature. Therefore, in order to understand past ocean circulation in relation to climate change it is essential to be able to reconstruct paleosalinity and temperature with reasonable accuracy.

Ocean salinity and the oxygen isotope composition of seawater are linearly correlated (Epstein and Mayeda, 1953) and this can be utilized for reconstruction of past seawater salinity using the $\delta^{18}\text{O}$ record of carbonate shells of foraminifera (Duplessy et al., 1991; Rostek et al., 1993) under the assumption of temporal consistency of the relationship between $\delta^{18}\text{O}$ and salinity (Rohling and Bigg, 1998; Rohling et al., 2000). However, salinity reconstruction based on $\delta^{18}\text{O}$ values of foraminiferal carbonate requires accurate correction for the global ice volume (Rostek et al., 1993) and knowledge of the temperature during calcification (Erez and Luz, 1983). The global ice volume can be estimated from the mean ocean $\delta^{18}\text{O}$ record (Waelbroeck et al., 2002), whereas the temperature is mostly obtained from Mg/Ca ratio values of foraminifera (Nürnberg et al., 1996; Lea et al., 1999; Mashiotta et al., 1999) or the alkenone-based $\text{U}^{\text{K}'}_{37}$ Index (Brassell et al., 1986; Rostek et al., 1993; Nürnberg et al., 1996). However, the correlation between $\delta^{18}\text{O}$ and salinity is affected by mixing and evaporation processes (Craig and Gordon, 1965), seasonality (Strain and Tan, 1993) and likely changes over glacial – interglacial periods (Rohling and Bigg, 1998). Consequently, salinity reconstruction based on $\delta^{18}\text{O}$ values of foraminiferal carbonate is subject to uncertainty and is difficult to calibrate (Rohling and Bigg, 1998; Rohling, 2000).

In addition to the correlation between oxygen isotopes and salinity, there is also a strong correlation between the hydrogen isotope composition of seawater ($\delta\text{D}_{\text{sw}}$) and salinity (Craig, 1961; Friedman et al., 1964). $\delta\text{D}_{\text{sw}}$ is recorded in the non-exchangeable hydrogen of organic matter (OM; Sessions et al., 1999; Sauer et al., 2001; Sachse et al., 2012) and can potentially be used for reconstructing past $\delta\text{D}_{\text{sw}}$. The hydrogen isotope composition of long chain alkenones, in particular C_{37} alkenones ($\delta\text{D}_{\text{alkenone}}$) appears well suited for reconstructing past δD values of seawater (Englebrecht and Sachs, 2005; Schouten et al., 2006). The isotopic composition of covalently bound hydrogen is thought to be preserved over long geological timescales (Sessions et al., 2004). Culture studies have shown that $\delta\text{D}_{\text{alkenone}}$ of two common marine haptophytes, *Emiliania huxleyi* and *Gephyrocapsa oceanica*, depends mainly on salinity and the hydrogen isotope composition of the growth medium and, to a lesser extent, growth rate (Schouten et al., 2006). Attempts to reconstruct past salinity change based on $\delta\text{D}_{\text{alkenone}}$ has led to reasonable results for the eastern Mediterranean Sea and Black Sea (van der Meer et al., 2007, 2008; Coolen et al., 2013) and the Panama Basin (Pahnke et al., 2007). Recently, the approach has also been applied to open marine sediments to evaluate relative salinity changes in the Agulhas Leakage area at the southern tip of the African continent over two glacial termination periods (Kasper

et al., 2014). However, the lack of a clear correlation between $\delta D_{\text{alkenone}}$ and seawater salinity in the Chesapeake Bay estuary suggests that the interpretation of this salinity proxy may become problematic for coastal environments (Schwab and Sachs, 2011). A possible explanation for the absence of a clear correlation relates to change in species composition since different haptophytes may have specific D/H fractionation characteristics. Comparison of the coastal haptophyte alga *Isochrysis galbana* with the open ocean species *E. huxleyi* in a culture experiment (M'Boule et al., 2014) revealed a strong fractionation difference between the two species. *I. galbana* fractionated to an extent of ca. 90‰ less than *E. huxleyi*, although the rate of change in D/H fractionation per salinity unit remained similar for both species (M'Boule et al., 2014, Chivall et al., 2014). This raises the question as to which extent $\delta D_{\text{alkenone}}$ is applicable as a paleosalinity proxy in coastal settings, where differences in haptophyte communities are to be expected (Marlowe et al., 1990; Noble et al., 2003; Örnólfssdóttir et al., 2004; Schwab and Sachs, 2011). To investigate the $\delta D_{\text{alkenone}}$ -based sea surface salinity proxy in a freshwater runoff-influenced continental margin, we analyzed a 39,000 year (39 ka) long record of $\delta D_{\text{alkenone}}$ from a marine sediment core (64PE304-80) from the Mozambique Channel near the Zambezi River mouth inside the Zambezi River fan (Fig. 1; Beiersdorf et al., 1980). The core site is off the continental shelf in the channel, which is traversed by the Mozambique Current, a branch of the South Equatorial Current (SEC; Fig. 1). The Mozambique Current is dominated by large anti-cyclonic eddies passing through the Mozambique Channel, with an annual net flow rate of ca. 15 Sv (de Ruijter et al., 2002; Schouten et al., 2003; Ullgren et al., 2012). However, interannual net flow rate varies substantially by up to 9 Sv in volume transport (Ridderinkhof et al., 2010). Additionally, there is a substantial input of continental freshwater to the Mozambique Channel (Siddorn et al., 2001). A main contributor is the Zambezi River, with a runoff of ca. 224 km³/yr (7.1 x 10⁻³Sv; Meybeck, 1982). Due to the location of the core site within the Zambezi River fan and independent reconstruction of high freshwater outflow by the BIT index, we would expect variation in freshwater runoff and therefore in salinity at the core site over time, suggesting it as a promising record for testing $\delta D_{\text{alkenone}}$ as a paleo sea surface salinity proxy at a river dominated ocean margin.

6.2. Material and methods

6.2.1. Core and chronology

Samples were taken from core 64PE304-80 (18° 14' 26.6274"S; 37° 52' 8.6874" E, 1329 m water depth), located north of the Zambezi River Delta at the Mozambique shelf (Fig. 1). The core was taken during the RV Pelagia cruise "64PE304, INATEX - GEO" (Brummer et al., 2009). The chronology was established from ¹⁴C dating of 20 samples consisting of ca.10 mg mixed surface-dwelling planktonic foraminifera (*Globigerinoides acculifer*, *G. trilobus* and *G. ruber*). These samples were collected from the washed and sieved > 250 μm sediment fraction by selecting individual foraminifera specimens under a microscope (Fig. 2). The age model for the upper 6 m, spanning the last 20 ka, was constrained by 11 ¹⁴C dates and by stratigraphic correlation with

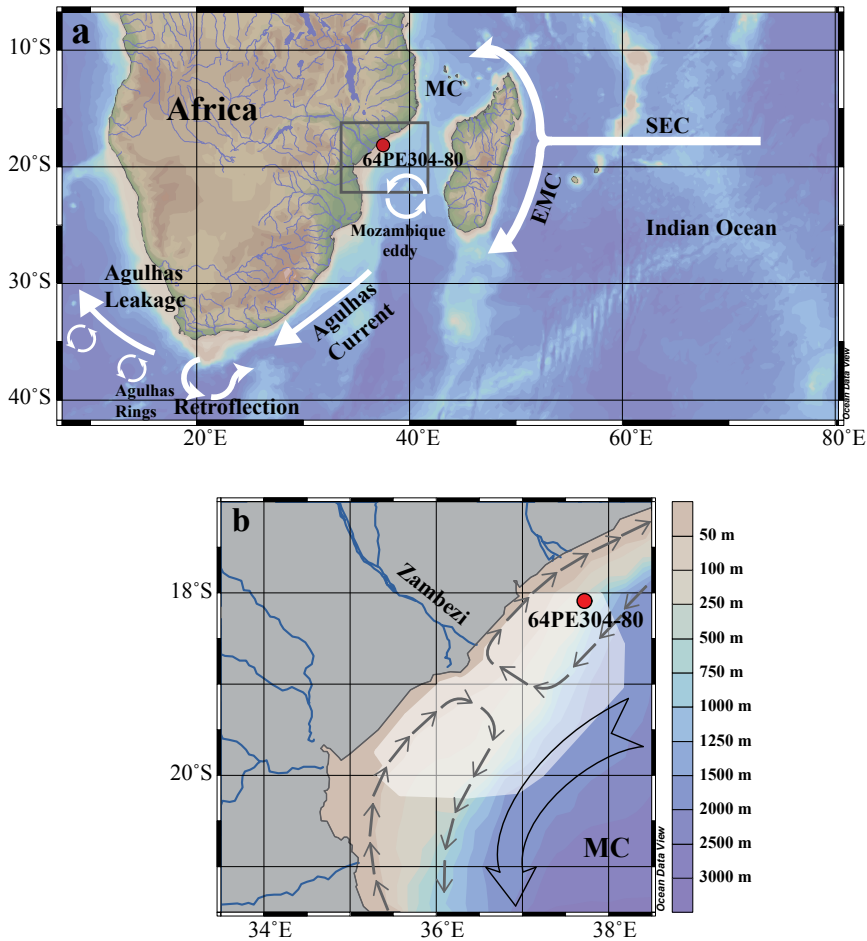


Figure 1. Map of oceanic currents in the study region and core location. (a) Main ocean current systems in the Western Indian Ocean (white arrows), showing the South Equatorial Current (SEC), the Eastern Madagascar Current (EMC), the Mozambique Current (MC) and the greater Agulhas Current (Beal et al., 2011). The location of core 64PE304-80 is given by the red circle in the Mozambique Channel. Fig. (b) Shows an enlargement of the Mozambique Channel and the location of the Zambezi River mouth; the large gray arrow indicates the general current direction of the Mozambique Current, small gray arrows coastal circulation cells, and white shaded area represents the sediment distribution of Zambezi River fan (Sætre and Da Silva, 1984).

a parallel core (GIK16160-3; Wang et al., 2013b; Van der Lubbe et al., 2014). The age model between 20 and 39.5 ka BP was constrained by 9 additional ^{14}C dating points. The ^{14}C age values were converted to calendar age using the MARINE09 calibration curve that applies a standard reservoir correction of ca. 400 yr (Reimer et al., 2011).

6.2.2. Extraction

Sediment samples were freeze dried and homogenized with a mortar and pestle. The homogenized material was extracted using accelerated solvent extraction (ASE) with dichloromethane (DCM):MeOH 9:1 (v/v) and a pressure of 6895 kPa in 3 extraction cycles.

The extract was separated over an Al_2O_3 column into apolar, ketone and polar fractions using hexane:DCM 9:1 (v/v), hexane:DCM 1:1 (v/v) and DCM:MeOH 1:1 (v/v), respectively. Column chromatography was carried out using about 4 cm activated Al_2O_3 (MPO Chemicals; technical quality, basic A) as stationary phase in a Pasteur pipette. Fractions were eluted with 3 column volumes of eluent.

6.2.3. Branched isoprenoid tetraether (BIT) index

The polar fraction was analyzed for the BIT index, a proxy originally thought to reflect the input of soil OM (Hopmans et al., 2004) but which has recently been shown to be affected by in situ production of branched glycerol dibiphytanyl glycerol tetraethers (br GDGTs) in rivers (Zell et al., 2013; De Jonge et al., 2014). Analysis was performed using high performance liquid chromatography-mass spectrometry (HPLC-MS) with an Agilent 1100 series instrument equipped with an auto-injector. Separation was achieved with an Alltech Prevail Cyano column (2.1 x 150 mm, 3 μm), maintained at 30 °C. GDGTs were eluted with 99% hexane and 1% propanol for 5 min, followed by a linear gradient to 1.8% propanol in 45 min, followed by back-flushing with hexane/propanol (9:1, v/v) at 0.2ml/min for 10 min. Detection was achieved using atmospheric pressure positive ion chemical ionization MS (APCI-MS). APCI-MS settings were: nebulizer 414 kPa, vaporizer 400 °C, drying gas (N_2) at 6 l/min and 200 °C, capillary voltage -3 kV and a corona 5 μA (ca. 3.2 kV). GDGTs were detected using selected ion monitoring (SIM) of the $[\text{M}+\text{H}]^+$ ions (m/z 1292 for crenarchaeol and m/z 1050, 1036 and 1022 for br GDGTs, respectively, dwell time 234 ms; Schouten et al., 2007) and integrated peak areas were used for quantification. BIT values were calculated according to the formula of Hopmans et al. (2004).

6.2.4. $\text{C}_{37}/\text{C}_{38}$ alkenone ratio

The ketone fraction, containing long chain alkenones, was analyzed using an Agilent 6890 gas chromatography (GC) instrument with a flame ionization detection (FID) and an Agilent CP Sil-5 fused silica column (50 m x 0.32 mm, film thickness 0.12 μm) with He as carrier gas. The GC oven was programmed from 70 to 200 °C at 20 °C/min and then at 3°C/min to 320 °C (held 25 min). Peak integration for the calculation of ratio values for the total abundance of the $\text{C}_{37}/\text{C}_{38}$ alkenones was performed using the Atlas 8.2 Chromatography Data System software from Thermo Electron Cooperation.

6.2.5. Alkenone δD analysis

The ketone fraction was analyzed using GC-high temperature conversion-isotope ratio MS (GC-TC-irMS) to determine the combined hydrogen isotope composition of the di- and triunsaturated C_{37} alkenones (van der Meer et al., 2013). Isotope analyses were carried out with a Thermo – Scientific DELTA V GC-TC-irMS instrument. The GC temperature conditions were: 70 to 145 °C at 20 °C/min, then heated at 8 °C/min to 200 °C and to 320 °C (held 20

min) at 4°C/min. An Agilent CP Sil-5 column (25 m x 0.32 mm) with a film thickness of 0.4 µm was used with He as carrier gas at 1 ml/min (constant flow). The high temperature conversion reactor was at 1420 °C. The H₃⁺ correction factor was determined daily and was constant at 5.6 ± 0.5. The δD_{alkenone} values were calculated with the Isodat software relative to pulses of H₂ reference gas. A set of standard *n*-alkanes with known isotopic composition (Mix B prepared by A. Schimmelmann, University of Indiana) was analyzed daily prior to analyzing samples in order to monitor system performance. Samples were only analyzed when the alkanes in Mix B had an average deviation from their off-line determined value of < 5‰. Squalane was co-injected as internal standard with each sample to monitor the accuracy and precision of alkenone isotope values. The standard had an average δD value of -165 ± 3.6‰, which compared favorably with that of -170‰ determined offline. The alkenone fraction was analyzed in duplicate if sufficient amount of material was available. Standard deviation of replicate analyses varied from ± 0.1‰ to ± 5.9‰.

6.3. Results

6.3.1. BIT index

To trace the relative importance of the river outflow at the core location we determined the BIT index, indicating riverine transported soil OM (Hopmans et al., 2004; Kim et al., 2007; Walsh et al., 2008; Schouten et al., 2013) as well as in situ produced crenarcheol from the river system (Zell et al., 2013; De Jonge et al., 2014). Values ranged between 0 and 1- a value near 0 indicates marine dominated OM and values near 1 a dominance of soil/river OM. Values were relatively high at ca. 0.50 between 39 and 38 ka and decreased to ca. 0.3 at 37 ka (Fig. 2). Between 37 and 16 ka they increased continuously to a maximum of ca. 0.7 during Heinrich Event 1 (HE1). Subsequently, they decreased to a plateau of ca. 0.25 between 15 and 12 ka in the Younger Dryas (YD). At ca. 12 ka they decreased to the Holocene level of ca. 0.1.

6.3.2. δD_{alkenone}

The δD_{alkenone} values were measured as the combined signal from C_{37:2} and C_{37:3}, as this has been suggested to yield a more robust water δD and salinity signal and to reduce additional biosynthetic effects related to the synthesis of C_{37:3} alkenone from the C_{37:2} alkenone (van der Meer et al., 2013). The total variability in the δD_{alkenone} record was ca. 23‰, with absolute values ranging between -181 and -204‰. They varied around a mean of -191‰ ± 5‰ (1σ standard deviation) over the entire record (Fig. 2). No trend from glacial Marine Isotope Stage (MIS) 3, through the Last Glacial Maximum (LGM) to the Holocene, was observed. Instead, the record was highly variable, showing a minor tendency of ca. 5‰ to increasingly D-depleted values with decreasing age during the Holocene. The record showed several periods of relatively D-enriched values of ca. -185‰ to -180‰ at 31 ka, 23 ka and during HE1, and more D-depleted values of ca. -200‰ at 37 ka, 27 ka and the LGM.

6.3.3. C_{37}/C_{38} alkenone ratio

The ratio ranged between 0.8 and 1.7, with an average of 1.3 ± 0.2 over the entire record (Fig. 2). During the period between 39–21 ka, it was 1.3 ± 0.1 , and after 21 ka it increased to a maximum of 1.7 at 19 ka, followed by a decrease to 1.3 at 10 ka. After this, it increased slightly to 1.4 at 9 ka and then rapidly decreased to the minimum value of ca. 0.8 at 8 ka. It was generally lower at 1.1 ± 0.1 during the Holocene compared with the glacial period.

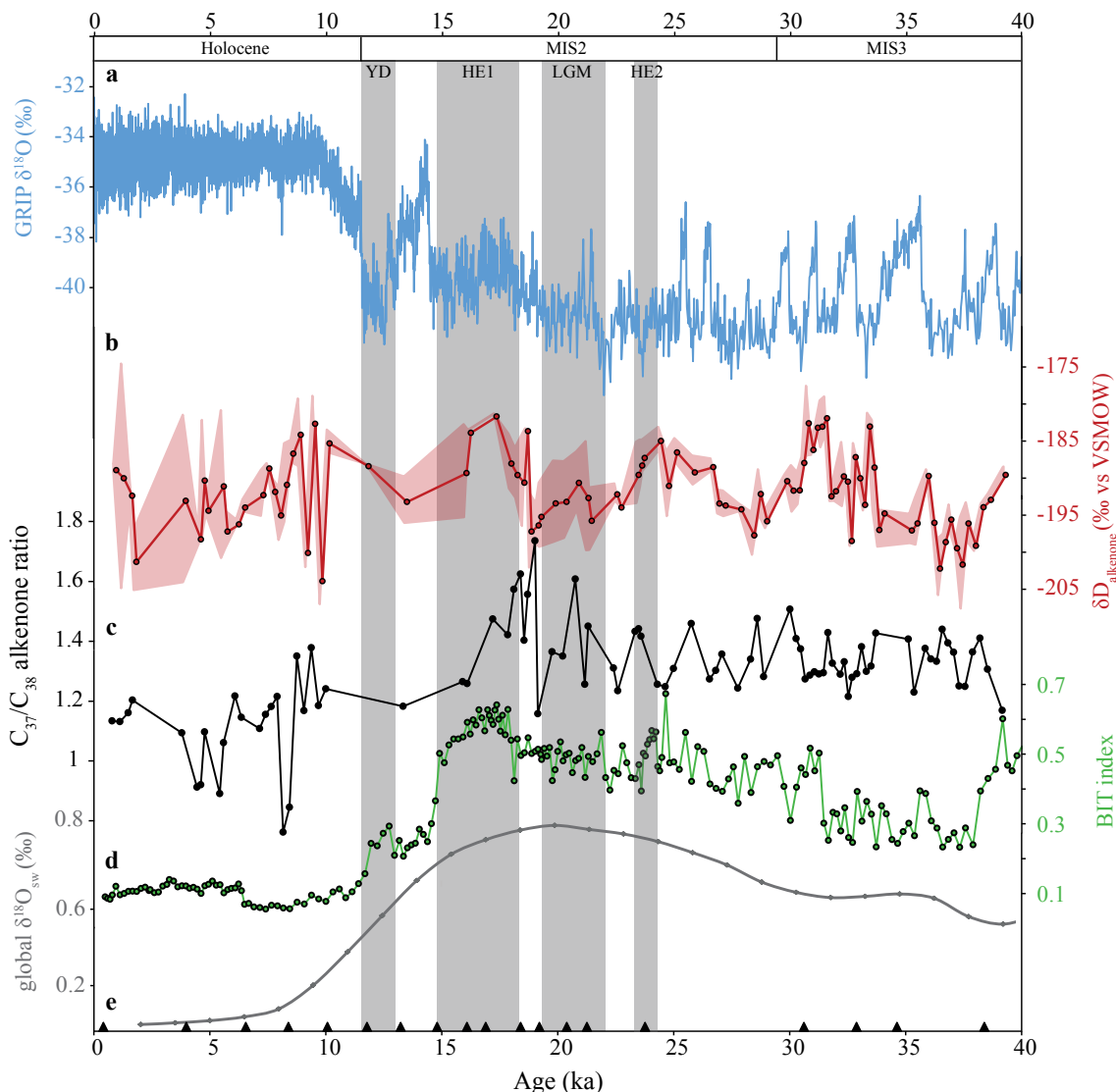


Figure 2. (a) Temperature variation over Greenland indicated by the $\delta^{18}\text{O}$ record of GRIP ice core (blue; Greenland Ice-core Project, 1993); (b) $\delta\text{D}_{\text{alkenone}}$ record (red line) with analytical error (1σ), (c) C_{37}/C_{38} alkenone ratio (black line) and (d) BIT index (green) for core 64PE304-80; (e) mean global benthic $\delta^{18}\text{O}_{\text{sw}}$ curve (Waelbroeck et al., 2002). Gray shaded bars indicate Younger Dryas (YD) (ca. 12.5-11 ka), Heinrich Event 1 (HE1) (ca. 19-14.6 ka), Last Glacial Maximum (LGM; ca. 23-19 ka) and Heinrich Event 2 (HE2; ca. 24 ka). Radiocarbon samples are indicated as black triangles.

6.4. Discussion

The transition from glacial to interglacial periods is marked by a significant decrease in the stable oxygen isotope ratio ($\delta^{18}\text{O}_{\text{sw}}$) and the stable hydrogen isotope ratio ($\delta\text{D}_{\text{sw}}$) of seawater as a consequence of melting of a large ice volume accumulated during the glacial (Shackelton, 1987). Global change in $\delta^{18}\text{O}_{\text{sw}}$ was obtained from a mean global benthic isotope record (Waelbroeck et al., 2002) and indicates a gradual increase in $\delta^{18}\text{O}_{\text{sw}}$ values from 0.53 to 1.02‰ between 39 and 20 ka BP (Fig. 2e). The values decrease linearly between 18 and 8 ka by almost 1‰. Based on a meteoric water line for the Indian Ocean (Srivastava et al., 2010), this record suggests an increase in the mean global $\delta\text{D}_{\text{sw}}$ of ca. 4‰ during the last glacial and a decrease of nearly 8‰ during the deglaciation. In contrast, the $\delta\text{D}_{\text{alkenone}}$ record from the upstream Mozambique slope showed fairly constant average values of -191 ± 5 ‰, with no trend that could be attributed to the inferred change related to the glacial – interglacial transition (Fig. 2b). The absence of a clear glacial-interglacial change related to the changing global ice volume is unlike that for a $\delta\text{D}_{\text{alkenone}}$ record obtained for open ocean sediments in the Agulhas Leakage area (Kasper et al., 2014). This suggests that additional environmental factors affect the δD values of alkenones in the Mozambique Channel. This could be related to the change in salinity, in combination with the input of relatively D-depleted freshwater via the Zambezi River outflow (Schefuß et al., 2011). An impact of temperature induced change in the U^{K}_{37} ratio on the fractionation of hydrogen isotopes seems unlikely as this effect has not been observed in marine haptophyte algae (Schouten et al., 2006; van der Meer et al., 2013). Furthermore, the temperature change in this region has found to be relatively small (3.5 °C; Wang et al., 2013b) and we did not find any correlation between $\delta\text{D}_{\text{alkenone}}$ and local U^{K}_{37} sea surface temperature (SST; data not shown).

In order to assess changes in freshwater input, we examined the BIT index for the same core (64PE304-80). The values indicate a relative increase in continental OM input during MIS2/3, with a relative maximum at ca. 17 ka during HE1 and at ca. 12 ka during the Younger Dryas, suggesting an increased influence of river outflow (Fig. 2; Van der Lubbe et al., 2014). These events were followed by a rapid decrease in the index during the deglaciation phase between 15-12 ka and the period between 11-8 ka, showing reduced input of continent-derived OM. This could indicate a strongly reduced river outflow, consistent with the rising sea level at the time and the subsequent transgression of the shelf (Walford et al., 2005; März et al., 2008), moving the Zambezi River mouth further away from the core site. Based on δD values of leaf wax alkanes, Schefuß et al. (2011) demonstrated that, during northern hemisphere cold events, such as the Younger Dryas and HE1, rainfall was enhanced in the Zambezi catchment area in response to a southwards forcing of the intertropical convergence zone (ITCZ). In contrast, a northward shift of the ITCZ in the Holocene would have resulted in reduced rainfall and decreasing river discharge as compared with glacial conditions (Schefuß et al., 2011; Wang et al., 2013a). The BIT record covering the last 17 ka from the Zambezi River mouth presented by Schefuß et al. (2011) is in good agreement with the BIT record here. The constant high BIT values during the glacial indicate an increased impact of freshwater input at the study site compared with the Holocene when BIT values were low. Increased freshwater input, either via closer proximity to the coast or increased precipitation or a combination of both, would lead to a relative depletion in $\delta\text{D}_{\text{sw}}$ at the

core site and subsequently to a decrease in $\delta D_{\text{alkenone}}$ during the glacial. The combination of lower salinity, resulting in increased biosynthetic hydrogen isotope fractionation (Schouten et al., 2006) and the more negative δD_{sw} values from the freshwater runoff may have resulted in production of relatively D-depleted alkenones during the glacial; this may have counteracted the global ice volume-induced increase in δD_{sw} , potentially leading to relatively constant values of alkenone δD during the glacial-interglacial transition.

During MIS 2/3, positive excursions in $\delta D_{\text{alkenone}}$ of up to 10‰ correspond with elevated BIT values (Fig. 2), such as between 34 and 31ka, between 26 and 24 ka, and during HE1 (19-16 ka) (Fig. 2). In fact, a crossplot of BIT values vs. $\delta D_{\text{alkenone}}$ showed (Fig. 3) that, during the glacial period (39.4 to 16.2 ka), BIT index and $\delta D_{\text{alkenone}}$ correlated significantly ($R^2 = 0.209$, p value = 0.0001), whilst during the Holocene no statistically significant relationship was observed ($R^2 = 0.0186$, p value = 0.5249). This suggests that variation in freshwater input had a significant impact on the variability in $\delta D_{\text{alkenone}}$ during the glacial. However, a negative correlation between BIT and $\delta D_{\text{alkenone}}$ would be expected, as an increasing freshwater input would lead to an input of D-depleted water, as well as increasing fractionation due to a decrease in salinity. Thus, the trend cannot be explained by a salinity effect or by an increasing influx of D-depleted water.

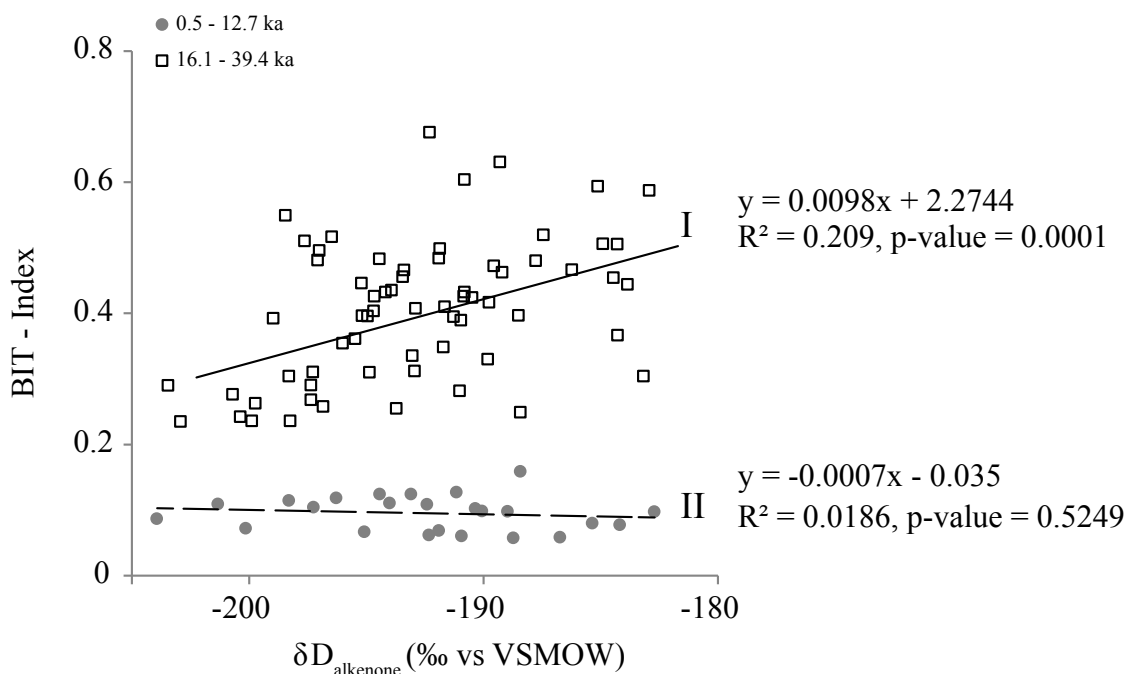


Figure 3. Cross plot of $\delta D_{\text{alkenone}}$ vs. BIT index. Values for Holocene (ca.12.7 – 0.5 ka) are indicated by closed gray circles, regression II (dashed line). Values for pre-LGM (ca. 39.4 – 16.1 ka) are indicated by open squares, regression I (solid line).

Alternative factors, which could lead to the apparent positive correlation between BIT values and δD of alkenones during the glacial period, are changes in growth rate or in haptophyte species composition (Schouten et al., 2006; Wolhowe et al., 2009; M'Boule et al., 2014). The reason why this effect is apparent in the glacial and not in the interglacial, may be because the core site was in much closer proximity to the coast during glacial sea level low stands (Walford et al., 2005; März et al., 2008; van der Lubbe et al., 2014), thereby allowing a potential proliferation of coastal haptophyte species as well as an increased impact of river-transported nutrients on growth rate. Regarding the latter hypothesis, although high freshwater input might have provided nutrients to the core site, thereby promoting algal growth (Verity et al., 1993; Pedersen and Borum, 1996; Gillanders and Kingsford, 2002), increased growth rate would be expected to lead to a depletion in $\delta D_{\text{alkenone}}$ (Schouten et al., 2006) and so cannot explain the positive excursions in $\delta D_{\text{alkenone}}$. Since coastal haptophytes produce alkenones 90‰ enriched in D compared with open ocean haptophytes (M'Boule et al., 2014; Chivall et al., 2014), changes in marine vs. coastal haptophytes in the alkenone producing community could explain the positive excursions of ca. 10‰ in hydrogen isotopic composition during the glacial period. The relative amount of the $C_{37:4}$ alkenone has been suggested as a marker for low salinity haptophyte algae (Schulz et al., 2000; Liu et al., 2008; 2011), but its abundance was very low in the sediment record (data not shown). However, the hypothesis of a changing contribution to the alkenone pool is supported by the observed change in the ratio between C_{37} and C_{38} alkenones (Fig. 2). This ratio has been reported to be more elevated for coastal haptophytes than for open ocean species (Marlowe et al., 1984b; Prah et al., 1988; Schulz et al., 2000; Liu et al., 2011). No significant positive anomalies in the C_{37}/C_{38} ratio were apparent between 39 and 22 ka. Nevertheless, C_{37}/C_{38} ratio indicated elevated values during the glacial, with the highest at ca. 18.5 ka (Fig. 2), which coincides with relatively more enriched $\delta D_{\text{alkenone}}$ values and elevated BIT values (Fig. 2). After 18.5 ka the ratio generally decrease to values of ca. 1.1 throughout the Holocene. This suggests that, during these periods of elevated C_{37}/C_{38} alkenone ratio, coastal haptophyte species may have contributed more to the alkenone pool and consequently shifted $\delta D_{\text{alkenone}}$ towards more positive values at times of increased freshwater input. Changing haptophyte assemblages in coastal settings in response to changing environmental conditions appear, therefore, to have a strong effect on $\delta D_{\text{alkenone}}$. This highlights the care that has to be taken when using the $\delta D_{\text{alkenone}}$ as a proxy for freshwater input in coastal settings or other environments where changes in the dominant alkenone producer(s) are likely to have occurred.

6.5. Conclusion

Despite changes in global seawater δD related to glacial – interglacial ice volume effects, no long term change in the 39 ka record of $\delta D_{\text{alkenone}}$ off the Mozambique shelf was observed. We suggest that glacial – interglacial changes in the $\delta D_{\text{alkenone}}$ were masked by changing freshwater input to the core site, as evidenced by the BIT index. During the glacial, the site was in closer proximity to the coast, when there was likely also larger river outflow. These conditions probably led to locally more D-depleted water and increased fractionation of hydrogen isotopes during

alkenone biosynthesis due to decreased salinity. The correlation between periods of enriched $\delta D_{\text{alkenone}}$ and elevated BIT values during the glacial is possibly related to an increased contribution from coastal alkenone-producing haptophyte species coinciding with elevated river outflow. This complicates the application of $\delta D_{\text{alkenone}}$ as a proxy for freshwater input in coastal settings. However, the technique appears promising in more open ocean settings.

Acknowledgments

We thank the two anonymous reviewers for their comments, which improved the manuscript. D. Chivall (Royal NIOZ) is thanked for input to the manuscript. We acknowledge financial support from The Seventh Framework Programme PEOPLE Work Programme, Grant 238512 (Marie Curie Initial Training Network 'GATEWAYS'). The Netherlands Organization for Scientific Research (NWO) is acknowledged for funding M.v.d.M (VIDI), S.S. (VICI), I.S.C. (NEBROC II) and R.T. (INATEX program, G.-J. B.; project number 839.08.434). R.T. acknowledges the SCAN2 program on advanced instrumentation. A. Mets is thanked for laboratory assistance. We thank the Captain and crew of the R/V Pelagia and participants of the INATEX cruise for collecting core 64PE304-80. Y. Wang at Kiel University is acknowledged for extracting some of the 64PE304-80. Data presented here can be found at Pangaea.de; doi:10.1594/PANGAEA.836271.

Chapter 7

A 135 ka long record of ocean salinity as recorded by C_{37} alkenone hydrogen isotope ratios from offshore Southeast Australia

Sebastian Kasper, Marcel T.J. van der Meer, Raquel A. Lopes dos Santos, Patrick De Deckker, Jaap S. Sinninghe Damsté, Stefan Schouten, in preparation

Abstract

Reconstructions of past salinity are presently mainly done using the oxygen isotope composition of sea water ($\delta^{18}O_{sw}$) reconstructed by correcting the oxygen isotope composition of foraminifera ($\delta^{18}O_{foram}$) for calcification temperatures and the ice volume effect. However, these corrections are subject to uncertainties in the assumption of temporal and spatial consistency, which are difficult to constrain. Alternatively, the hydrogen isotope composition of long chain alkenones ($\delta D_{alkenone}$), produced by a limited number of haptophyte algae, has been used to estimate past ocean salinity variability. Here we apply both the $\delta^{18}O_{foram}$ and $\delta D_{alkenone}$ to a 135 ka long sedimentary record from the upper Sprigg Canyon, south of Australia to reconstruct past ocean salinity. This location is influenced by both Southern and Indian Ocean water, of which the latter is transported via the warm and low salinity Leeuwin Current (LC) while, during sea level low stand, river discharge via the River Murray increasingly affects conditions at the core site. The records of $\delta D_{alkenone}$, $\delta^{18}O_{foram}$ and sea surface temperature (SST) based on the alkenone unsaturation index ($U^{K'}_{37}$) correspond well with each other showing parallel glacial-interglacial variability. Comparison of $\delta D_{alkenone}$ with the BIT index, a proxy for riverine transported soil/riverine derived organic matter in the marine environment, suggests that freshwater discharge via the Murray Darling River, has not had a major impact on the variability in $\delta D_{alkenone}$. Instead, glacial – interglacial variability in the ice volume corrected $\delta D_{alkenone}$ ($\delta D_{ic-alkenone}$) is likely to be related to the transport of lower salinity water via the Leeuwin Current, which reaches the core site during deglaciations and interglacials. However, the ice volume corrected $\delta^{18}O_{sw}$ ($\delta^{18}O_{ic-sw}$) shows a somewhat opposite trend from the $\delta D_{ic-alkenone}$, suggesting fresher ocean salinity conditions during glacial periods. This diverging trend in $\delta^{18}O_{ic-sw}$ is probably due to the use of alkenone based $U^{K'}_{37}$ SST, derived from haptophyte algae as a proxy for calcification temperatures of the planktonic foraminifera *G. bulloides*, which are likely to have different growth seasons and depth habitats, potentially leading to an overcorrection of calcification temperatures of the planktonic foraminiferal carbonate.

7.1. Introduction

The reconstruction of ocean salinity and temperature is a prerequisite for setting boundary conditions for modelling past ocean dynamics (Esper et al., 2005). Therefore, information on past sea surface salinity and temperature can help to understand past ocean circulation and the interaction between oceans and the atmosphere, which is an important modulator for the global climate (Manabe, 1969; Rahmstorf, 2002). While modern-day salinity and temperature measurements are relatively simple to obtain with a high level of accuracy, reconstruction of past variations, e.g. over glacial – interglacial cycles, is more complex and relies on paleoceanographic proxies. For temperature, these proxies include the Mg/Ca ratios of foraminifera (Nürnberg et al., 1996; Lea et al., 1999; Lear et al., 2002), the alkenone unsaturation index ($U_{37}^{K'}$) of haptophyte algae (Marlowe et al., 1984a; Brassell et al., 1986) and the relative number of cyclopentane moieties in glycerol dialkyl glycerol tetraethers (GDGTs) of archaea (TEX_{86}) (Schouten et al., 2002; Kim et al., 2010).

Although there are multiple temperature proxies, fewer tools are available for past ocean salinity reconstruction. Thus far, the oxygen isotopic composition of carbonate shells of foraminifera ($\delta^{18}O_{\text{foram}}$) has been used to reconstruct ocean salinity (Duplessy et al., 1991; Rostek et al., 1993), utilizing the close correlation between the oxygen isotopic composition of seawater ($\delta^{18}O_{\text{sw}}$) and salinity (Epstein and Mayeda, 1953). The $\delta^{18}O_{\text{sw}}$ can be calculated from the $\delta^{18}O_{\text{foram}}$ by correcting for calcification temperature of the foraminifera, which can be estimated, for example from foraminiferal Mg/Ca (Pahnke et al., 2003). However, the reconstruction of past salinities from $\delta^{18}O_{\text{sw}}$ is based on the assumption of temporal and spatial consistency of the relationship between $\delta^{18}O$ and salinity over glacial-interglacial intervals (Rohling and Bigg, 1998; Rohling, 2000). Furthermore, salinity reconstruction based on $\delta^{18}O$ of foraminiferal carbonate over longer time scales, such as glacial – interglacial cycles, requires accurate correction for the global ice volume effect caused by accumulation of the lighter ^{16}O isotopes in ice sheets and the relative enrichment of ^{18}O in the seawater during glacials (Rostek et al., 1993; Waelbroeck et al., 2002).

More recently it has been suggested that the hydrogen isotopic composition of the non-exchangeable hydrogen of organic compounds can be used to reconstruct the hydrogen isotope composition of seawater (δD_{sw}) (Paul, 2002; Englebrecht and Sachs, 2005; Sessions and Hayes, 2005), which is, similar to $\delta^{18}O_{\text{sw}}$, linearly related to ocean salinity (Craig, 1961; Friedman et al., 1964). In particular, the hydrogen isotopic composition of the C_{37} long chain alkenones ($\delta D_{\text{alkenone}}$), produced by a limited number of haptophyte species (Marlowe et al., 1984b), appears well suited for reconstructing past ocean salinity (Englebrecht and Sachs, 2005; Schouten et al., 2006). Culture experiments demonstrated that the hydrogen fractionation factor α ($\alpha_{\text{alkenone-sw}}$) of hydrogen in alkenones versus sea water of the algae mainly depends on salinity and the hydrogen isotope composition of the sea water and, to a lesser extent, growth rate and growth phase of the algae (Schouten et al., 2006; Wolhowe et al., 2009; Chivall et al., 2014; M'Boule et al., 2014). First applications of $\delta D_{\text{alkenone}}$ as a tool for reconstructing past ocean salinity have led to reasonable results for the eastern Mediterranean and Black Sea (van der Meer et al., 2007, 2008; Coolen et al., 2013), the Panama Basin (Pahnke et al., 2007) and the Agulhas Leakage area, south of Africa

(Kasper et al., 2015). In marine records that are influenced by freshwater runoff, the $\delta D_{\text{alkenone}}$ has been shown to reflect reduced salinity during high runoff episodes (Leduc et al., 2013). However, application of the $\delta D_{\text{alkenone}}$ in Pleistocene sediments from the Mozambique Channel showed that during the last glacial, a period of high runoff at the core site as indicated by a high branched and isoprenoid tetraether (BIT) index and relatively low $\delta D_{\text{alkenone}}$ values, $\delta D_{\text{alkenone}}$ indicated increased salinity at times of even higher runoff as indicated by the BIT index (Kasper et al., 2015). This was explained by an increased contribution of alkenones derived from coastal haptophyte species to the algae community at lower salinities, as alkenones derived from coastal haptophyte species have been shown to be relatively more D-enriched than marine haptophyte species (M'Boule et al., 2014). Furthermore, no clear correlation between $\delta D_{\text{alkenone}}$ and seawater salinity in the Chesapeake Bay estuary was found (Schwab and Sachs, 2011). Together, these observations suggest that the interpretation of $\delta D_{\text{alkenone}}$ as a salinity proxy may be complex in coastal environments.

To further investigate the potential of $\delta D_{\text{alkenone}}$ as a tool for salinity reconstructions in coastal environments, we generated a $\delta D_{\text{alkenone}}$ record spanning the last 135 thousand years (ka) in a setting close to the southeastern Australian coast line in front of the large Murray Darling River system. Today the core site is located approximately 200 km away from the southern Australian coast line and is not substantially influenced by fluvial discharge (Gingele et al., 2004). However, during glacial sea level low stands the coast line was much closer to the core location and terrestrial runoff was more influential (Gingele et al., 2004). Several biomarker studies on this core have been done previously, showing the abundant presence of alkenones as well as an input of terrestrial biomarkers, partly derived from the Murray Darling River system (Lopes dos Santos et al., 2012; Lopes dos Santos et al., 2013a; Lopes dos Santos et al., 2013b). Furthermore, a $\delta^{18}\text{O}$ record of the planktonic foraminifera *Globigerina bulloides* (Gingele et al., 2004; Lopes dos Santos et al., 2012) is available, which can be utilized as an independent proxy for the isotopic composition of sea water, and, accordingly, salinity. This makes the location ideal for the testing of $\delta D_{\text{alkenone}}$ as tool for past ocean salinity variability on millennial scale in coastal conditions under the influence of freshwater runoff.

7.2. Materials and Methods

7.2.1. Core location and oceanographic setting

Core MD03-2607 (36°57.64 'S; 137°24.39 'E; 865 m water depth) was retrieved from a plateau south of the upper Sprigg Canyon, offshore South Australia (Figure 1) during the AUSCAN 2003 cruise with the French research vessel *Marion Dufresne*, also known as MD 131. The chosen core location is separated from the main shelf break in order to avoid significant erosion or turbidite depositions interfering with the record (Hill et al., 2004; Gingele and De Deckker, 2005). The age model for core MD03-2607 was previously published in Lopes dos Santos et al. (2012) and is based on Optically Stimulated Luminescence (OSL) of single grains of sand-sized quartz and ^{14}C dating on planktonic foraminifera *Globigerina bulloides* and *Globigerina ruber* for the past 35 ka and

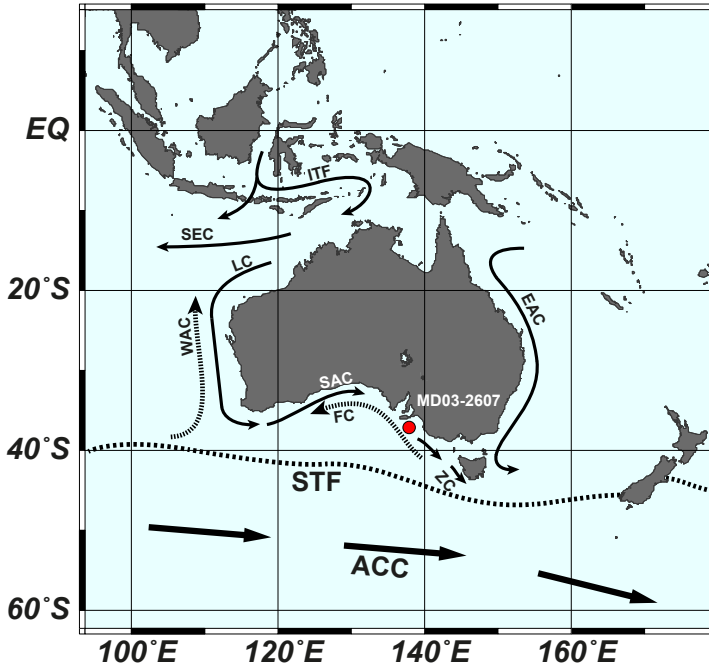


Figure 1. Map showing the location for core MD03-2607 (red dot), based on Lopes dos Santos et al. (2013b). Main surface currents are indicated by solid lines: ITF – Indonesian Throughflow; SEC – Southern Equatorial Current; LC – Leeuwin Current; EAC – Eastern Australia Current; SAC – Southern Australian Current; ZC – Zeehan Current; ACC – Antarctic Circumpolar Current. Subsurface currents are indicated by dashed lines: WAC – Western Australia Current; FC – Flinders Current; STF – Subtropical Front.

also by correlating tie points between planktonic foraminifera $\delta^{18}\text{O}$ of *Globigerina bulloides* and the stack isotope records of Lisiecki and Raymo (2005) for the older part of the record.

7.2.2. Alkenone δD analysis

Alkenone fractions for hydrogen isotopic analysis were used from samples previously extracted by Lopes dos Santos et al. (2013b). A Thermo – Scientific DELTA V gas chromatography/high-temperature conversion/isotope ratio mass spectrometry (GC/TC/irMS) was used to measure the combined hydrogen isotope composition of the di- and tri-unsaturated C_{37} alkenones (van der Meer et al., 2013) using the method described in M'Boule et al. (2014). Samples were only analyzed when the set of standard *n*-alkanes (Mixture B, Arndt Schimmelmann, University of Indiana) had an average deviation from their off-line determined value of $<5\%$. Squalane was co-injected as an internal standard with each sample to monitor the precision and accuracy of the alkenone isotope values. The squalane standard yielded an average δD - value of $-163 \pm 2.4\%$, which compared reasonably with its offline determined δD -value of -170% . Alkenone δD values and analyzed in duplicate with a maximum standard deviation of replicate analyses of $\pm 6 \%$.

7.3. Results and Discussion

7.3.1. δD of C_{37} alkenones and comparison with $\delta^{18}O$ of *G. bulloides*

In core MD03-2607 the $\delta D_{\text{alkenone}}$ shows millennial scale variability corresponding with the different Marine Isotope Stages (MIS): relatively positive $\delta D_{\text{alkenone}}$ values are observed during glacial MIS2 ($-165 \pm 2\%$) and the penultimate glacial MIS6 ($-171 \pm 4\%$; Figure 2c). The alkenone hydrogen isotope composition becomes more D-depleted during the transition from MIS6 to late MIS5 (118 ka) and from MIS 2 to MIS 1, and remains relatively stable during interglacials MIS5 and MIS1 at values of $-179 \pm 2\%$ and $-181 \pm 1\%$, respectively. When plotting the $\delta D_{\text{alkenone}}$ we see a good correspondence with the $\delta^{18}O$ record of *G. bulloides* ($\delta^{18}O_{\text{bull}}$) ($R^2 = 0.63$, p-value = 1.714×10^{-11}) and the U^{K}_{37} sea surface temperature record ($R^2 = 0.85$, p-value $< 2.2 \times 10^{-16}$) (both from Lopes dos Santos et al. (2012) for the same samples as our $\delta D_{\text{alkenone}}$ record (Figure 2a, g). D- or ^{18}O -enriched values and low sea surface temperature (SST) are observed during glacials and depleted values and high SST during interglacials, as expected. The matching pattern for $\delta D_{\text{alkenone}}$ and $\delta^{18}O_{\text{bull}}$ suggests they may be driven by the same environmental parameters, in particular the isotopic composition of sea water and, therefore, salinity. If so, then the records suggest higher salinities and/or isotopically-enriched sea water during glacials and lower salinities/isotopically-depleted seawater during interglacials. However, both the $\delta D_{\text{alkenone}}$ and $\delta^{18}O_{\text{bull}}$ proxies can also be affected by other factors (e.g. temperature, growth rate and species composition of the alkenone producers, depth habitats, and growth seasons) which may have also varied on glacial-interglacial scales and thus may also be the cause for the similar enrichment patterns in $\delta D_{\text{alkenone}}$ and $\delta^{18}O_{\text{bull}}$.

To investigate whether salinity and the isotopic composition of local sea water were the main driving factors behind the synchronous behaviour of $\delta D_{\text{alkenone}}$ and $\delta^{18}O_{\text{bull}}$, we performed several corrections on both records. Firstly, we corrected the $\delta^{18}O_{\text{bull}}$ for calcification temperature using the U^{K}_{37} SST record (Lopes dos Santos et al., 2012) and the isotopic fractionation equation for *G. bulloides* ($\delta^{18}O_{\text{sw}} = \delta^{18}O_{\text{foram}} - ((13.13 - \text{SST})/4.91)$; Bemis et al., 2002). The resulting record should reflect the oxygen isotopic composition of the seawater ($\delta^{18}O_{\text{sw}}$). Subsequently, $\delta D_{\text{alkenone}}$ and $\delta^{18}O_{\text{sw}}$ records were corrected for the changes in global ice volume by subtracting the global mean $\delta^{18}O$ record of Waelbroeck et al. (2002). The ice-volume correction on the $\delta D_{\text{alkenone}}$ ($\delta D_{\text{ic-alkenone}}$) is calculated by subtracting a mean global δD_{sw} , which is derived from the mean global $\delta^{18}O$ record of Waelbroeck et al. (2002) using a local meteoric water line (LMWL) for the modern River Murray region ($\delta D = 7.6 * \delta^{18}O + 8$; Simpson and Herczeg, 1991). Both $\delta D_{\text{ic-alkenone}}$ and the ice volume corrected $\delta^{18}O_{\text{sw}}$ ($\delta^{18}O_{\text{ic-sw}}$) should reflect local variations in salinity and the isotopic composition of sea water.

The $\delta D_{\text{ic-alkenone}}$ shows a similar glacial – interglacial pattern as the uncorrected $\delta D_{\text{alkenone}}$ record with slightly more D depleted values ranging between -193 to -174% (Figure 2b). We observe the most D-depleted values (ca. -188 to -191%) during interglacials MIS 5 and MIS 1 and relatively D-enriched values (ca. -175 to -181%) during the glacials, especially towards the end of MIS6 and MIS3. In contrast, the reconstructed $\delta^{18}O_{\text{ic-sw}}$ (Figure 2h) shows much less clear variation and even a somewhat opposite trend to $\delta D_{\text{ic-alkenones}}$ with ^{18}O depleted values during

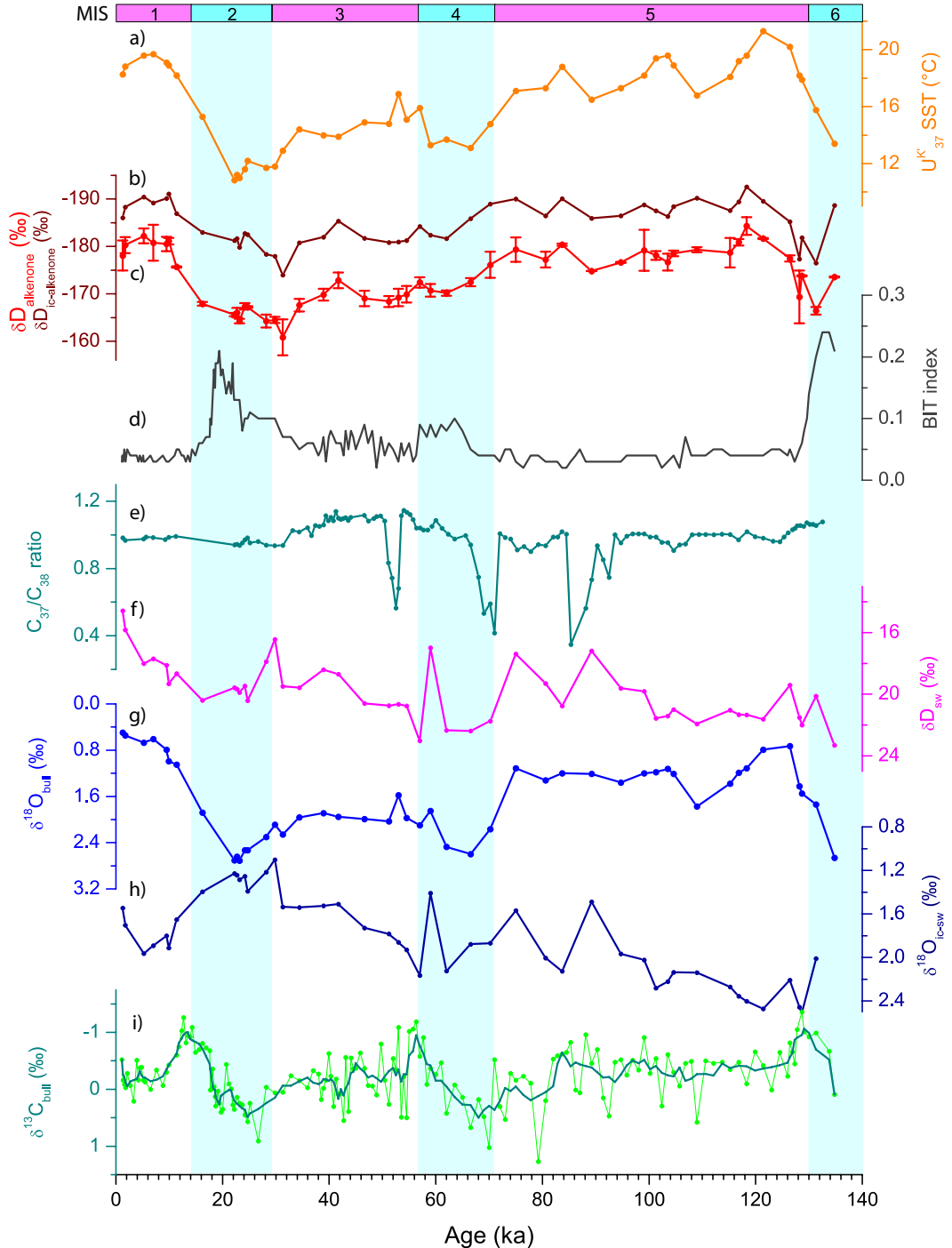


Figure 2: Records of core MD03-2607 (a) U^{k}_{37} SST (orange) (Lopes dos Santos et al., 2012); (b) ice volume corrected $\delta D_{ic-alkenone}$ following Waelbroeck et al. (2002) (brown); (c) $\delta D_{alkenone}$ with 1σ error (red); (d) BIT index (Lopes dos Santos et al., 2013a) (black); (e) alkenone C_{37}/C_{38} ratios (olive); (f) δD_{sw} (pink) calculated from U^{k}_{37} temperature (Lopes dos Santos et al., 2012) corrected $\delta^{18}\text{O}_{sw}$ of $\delta^{18}\text{O}_{foram}$ of *G. bulloides* (Lopes dos Santos et al., 2012); (g) *G. bulloides* $\delta^{18}\text{O}$ (blue) (Lopes dos Santos et al., 2012); (h) ice volume corrected $\delta^{18}\text{O}_{ic-sw}$ (dark blue) from $\delta^{18}\text{O}_{sw}$ of *G. bulloides*; (i) *G. bulloides* $\delta^{13}\text{C}$ (light green) with a three point running mean (dark green) (Lopes dos Santos et al., 2012).

glacials and enriched values during interglacials. Since oxygen and hydrogen isotopes in seawater are strongly positively correlated (Craig and Gordon, 1965), it is unlikely that changes in the isotopic composition of the seawater itself explains this apparent opposite behavior. In the same way, salinity should induce similar variations in both proxies with increases in salinity leading to D- and ^{18}O -enriched isotopic composition of sea water and vice versa as well as decreased hydrogen isotopic fractionation of alkenones versus sea water (Schouten et al., 2006; Wolhowe et al., 2009a; Chivall et al., 2014; M'Boule et al., 2014). Below we explore possible explanations for the apparently different behavior of the two salinity proxies.

7.3.2. Factors influencing $\delta\text{D}_{\text{alkenone}}$

Several factors other than the isotopic composition of sea water and salinity may impact variability in $\delta\text{D}_{\text{alkenone}}$ such as the variability in growth rates of the alkenone producers (Schouten et al., 2006), as well as changes in their species composition (Chivall et al., 2014; M'Boule et al., 2014). Potentially lower salinity, changing light conditions and nutrient availability in a shallower and more coastal environment during the sea level low stand in the glacial period might have promoted the growth of coastal alkenone producers over open marine haptophytes (Marlowe et al., 1990; Noble et al., 2003; Örnólfssdóttir et al., 2004) and thus may have led to an increasing contribution of coastal haptophyte derived alkenones. Since alkenones produced by coastal species have been shown to be more deuterium enriched by up to 90‰ than alkenones produced by open ocean species (M'Boule et al., 2014), a moderate change in the haptophyte composition could substantially affect the δD of the alkenones. To test whether species composition changes occurred, we calculated the ratio for the total abundance of $\text{C}_{37}/\text{C}_{38}$ alkenones (Figure 2e). This ratio has been reported to be higher in coastal haptophyte algae compared to open marine species (Marlowe et al., 1984b; Prahl et al., 1988; Schulz et al., 2000; Liu et al., 2011). Indeed, Kasper et al. (2015) found in a core in the Mozambique Channel elevated $\text{C}_{37}/\text{C}_{38}$ alkenone ratios for periods when $\delta\text{D}_{\text{alkenone}}$ shifted towards more positive values, thus suggesting an increasing contribution of coastal haptophyte species. However, in our Australian sediment record the $\text{C}_{37}/\text{C}_{38}$ ratio remains generally constant around ca. 1 ± 0.1 and does not seem to follow a glacial interglacial trend (Figure 2e). Only during three periods, at ca. 85 - 90 ka, 69 - 71 ka and ca. 52 ka, significantly decreased $\text{C}_{37}/\text{C}_{38}$ ratios are observed which are, however, not reflected in any shifts in the $\delta\text{D}_{\text{ic-alkenone}}$. Consequently, these relatively short lived events appear not to be related to a change in the species composition. Instead the shifts in $\text{C}_{37}/\text{C}_{38}$ ratios might reflect environmental adaptations of the alkenone producer community (Conte et al., 1998). The effect of growth rate was tested by correlating the $\delta\text{D}_{\text{alkenone}}$ with reported alkenone accumulation rates (Lopes dos Santos et al., 2012), as a proxy for haptophyte productivity (Volkman et al., 1980; Marlowe et al., 1984b). However, no correlation, ($R^2 = 0.02$, p-value = 0.934) was observed suggesting that the effect of growth rate on $\delta\text{D}_{\text{alkenone}}$ variability was likely to be minor. Thus, the data suggests that the $\delta\text{D}_{\text{alkenone}}$ was not substantially affected by haptophyte species and growth rate changes of the alkenone producers and therefore is likely to reflect mainly salinity variability at the core site.

7.3.3. Factors affecting the $\delta^{18}\text{O}$ salinity records

As stated above, $\delta^{18}\text{O}_{\text{bull}}$ and $\delta\text{D}_{\text{alkenones}}$ show a similar trend but this trend becomes opposite once $\delta^{18}\text{O}_{\text{bull}}$ is corrected for calcification temperature and global ice volume. In fact, the reconstructed $\delta^{18}\text{O}_{\text{sw}}$ shows very little variation ($1.6 \pm 0.3 \text{ ‰}$) and only by subtracting the global mean $\delta^{18}\text{O}_{\text{sw}}$ record of benthic foraminifera (which has a typical glacial – interglacial pattern) the residual $\delta^{18}\text{O}_{\text{ic-sw}}$ shows an opposite trend to $\delta^{18}\text{O}_{\text{bull}}$ and $\delta\text{D}_{\text{ic-alkenones}}$ (Figure 2b, g, h). The cause for this change in correlation is apparently the large temperature correction of planktonic foraminifera $\delta^{18}\text{O}$ using the haptophyte derived temperatures. However, using temperature estimates from an organism different than the planktonic foraminifer itself is potentially problematic. *G. bulloides* is not strictly representing ocean surface conditions (Berger, 1968; Bard et al., 1989) and typically calcifies in a depth range of 50 – 100 m in the ocean subsurface (Niebler et al., 1999; De Deckker et al., 2012), whereas the photosynthesizing alkenone producers are restricted to the photic zone (Marlowe et al., 1984b). Furthermore, studies showed that SST likely represent an annual mean SST in this region (Lopes dos Santos et al., 2013b), whereas *G. bulloides* generally has the tendency to record winter conditions (Elderfield and Ganssen, 2000; Fraile et al., 2009). Temperature gradients in the upper 100 m of the water column are up to 4 °C in the modern day ocean of southern Australia (Rintoul et al., 1997; Middleton et al., 2007; Foster et al., 2014) with a seasonal variability of up to 8 °C in the ocean surface layer (Belkin and Gordon, 1996; Sikes et al., 2009; Foster et al., 2014). Potentially, and perhaps even likely, the temperatures, and changes therein, registered by the $\text{U}^{k'}_{37}$ are not those experienced by *G. bulloides*. Reduced temperature variability would result in a much reduced calcification temperature correction on the $\delta^{18}\text{O}_{\text{bull}}$ and effectively lead to $\delta^{18}\text{O}_{\text{ic-sw}}$ variability with similar trends as found in $\delta\text{D}_{\text{ic-alkenone}}$. Therefore, our results suggest that using proxies derived from organisms with potentially different growth habitats and/or growth seasons may result in deviating estimates for calcification temperatures and subsequently lead to confounding salinity estimations. Based on this, we suggest that $\delta\text{D}_{\text{ic-alkenone}}$ likely better reflects the variations in isotopic composition of sea water and salinity at this site than the $\delta^{18}\text{O}_{\text{ic-sw}}$ obtained using temperatures.

7.3.4. Paleoceanographic implications

Assuming that our $\delta\text{D}_{\text{ic-alkenone}}$ reflects local variations in salinity and isotopic composition of water, we can explore the causes for the observed glacial-interglacial variations. At present, the core site is located about 200 km away from the Australian coastline (Gingele et al., 2004). However, reconstructions for the past 135 ka indicate that during the last glacial maximum the paleo coastline was in close proximity of ca. 20 km to the core site and increased river discharge of D- and ^{18}O - depleted freshwater occurred at the edge of the continental shelf via the Murray Darling River system (Gingele et al., 2004). To investigate the effect of freshwater runoff on our $\delta\text{D}_{\text{ic-alkenone}}$, we compared it with the record of BIT index (Lopes dos Santos et al., 2013a) (Figure 2d). The BIT index is based on bacterial branched tetraether membrane lipids (Hopmans et al., 2004), produced in soils, lakes and rivers, and their relative abundance compared to crenarchaeol,

mainly produced in the marine environment. It is frequently used as a proxy for riverine transported soil/riverine derived organic matter (OM) in the marine environment (Herfort et al., 2006; Ménot et al., 2006; Zell et al., 2013; De Jonge et al., 2014). BIT values range between 0, indicating marine dominated OM, and 1, indicating a dominance of river transported continental OM. In core MD03-2607, the BIT index reaches the maximum of 0.22 during late MIS6 and MIS2 and shows lower values of ca. 0.10 during MIS4. During interglacial periods BIT values are below 0.10 and close to 0.05 (Lopes dos Santos et al., 2013a), indicating no substantial soil/riverine derived OM at the core site. This pattern generally agrees with the studies on terrigenous sediments from the Murray Canyons, suggesting reduced input of terrigenous material during periods of high sea level (Gingele et al., 2004). We find a relatively weak positive correlation ($R^2 = 0.24$, p -value = 0.0002) between the BIT index and $\delta D_{ic-alkenone}$ (Figure 3), however, with a temporal mismatch (Figure 2b, d). This suggests that the river runoff from the River Murray might not have been sufficient to substantially affect the hydrogen isotopic composition and salinity of the sea water at our core site as would be expected during periods of close proximity of the coastline to the core site, such as the LGM. This could be explained by particularly drier conditions experienced by Australia during the LGM leading to a drying of most lakes (Williams et al., 1998; Lopes dos Santos et al., 2013a). Furthermore, we find a positive, rather than a negative correlation (Figure 3), which is difficult to understand as enhanced discharge of D-depleted fresh water from the paleo Murray Darling River system would be expected to result in relatively more D-depleted surface waters as well as lower salinities and thus depleted $\delta D_{ic-alkenone}$, rather than the observed more D enriched $\delta D_{ic-alkenone}$ values during these glacial periods.

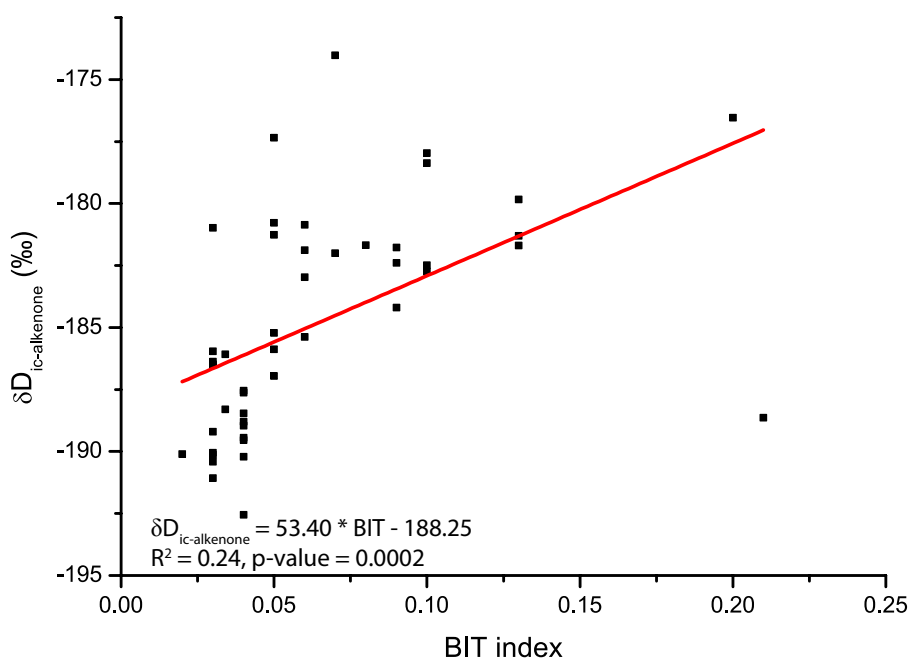


Figure 3. Regression for the BIT index versus $\delta D_{ic-alkenone}$ for core MD03-2607.

Lopes dos Santos et al. (2012) suggested, based on the carbon isotope composition of *G. bulloides* ($\delta^{13}\text{C}_{\text{bull}}$), that there was an enhanced influence of ^{13}C -depleted Southern Ocean waters occurring particularly during deglaciation phases from MIS6 to MIS5e and from MIS 2 to MIS1 as well as at the transition from MIS4 to MIS3 (Figure 2i). This enhanced influence of Southern Ocean waters might contribute cooler and fresher water masses as shown east of Tasmania by Nürnberg and Groeneveld (2006) with a different, likely more depleted, water isotope signature. It is likely that the contribution of Southern Ocean water with a different isotopic composition has altered the relationship of δD to $\delta^{18}\text{O}$ of the meteoric water line as well as the relationship for salinity versus $\delta^{18}\text{O}$ (Tiwari et al., 2013), which have been used to calculate $\delta\text{D}_{\text{sw}}$ equivalents from $\delta^{18}\text{O}_{\text{sw}}$ and relative salinity shifts calculated from $\delta^{18}\text{O}_{\text{ic-sw}}$. However, comparison of the records of $\delta^{13}\text{C}_{\text{bull}}$ with $\delta\text{D}_{\text{ic-alkenone}}$ (as well as by direct correlation; $R^2 = 0.02$, $p\text{-value} = 0.92$) shows only little correspondence as the negative excursions in $\delta^{13}\text{C}_{\text{bull}}$ are mainly during terminations of glacial episodes. This suggests that Southern Ocean water had a relatively minor influence on the salinity and isotopic composition of the seawater at the core site.

An important current reaching the core site is the Leeuwin Current (LC) (Figure 1; Spooner et al., 2011). This shallow surface current is characterized by warm water with a lower salinity of ca. 34 (Cresswell, 1990; Ignacio Martinez et al., 1997), compared to an average ocean surface salinity of ca. 35.6 at the core site (Levitus et al., 2013). Several studies suggested that the influence of the LC at the core site was particularly enhanced during deglaciations, interglacials and to some extent during MIS3, whereas during glacials the LC was prevented from reaching southern Australia due to the northward displacement of the Subtropical Front (Sikes et al., 2009; De Deckker et al., 2012; Lopes dos Santos et al., 2013b). Indeed, the deglacial periods between MIS6/MIS5 and MIS2/MIS1 as well as the interglacial periods MIS5 and MIS1 are characterized by relatively D-depleted $\delta\text{D}_{\text{alkenone}}$ suggesting less saline water at these times. Thus, our δD record may have mainly been influenced by the strength of the LC at the core site.

7.4. Conclusion

A 135 ka long $\delta\text{D}_{\text{alkenone}}$ record for sediment core MD03-2607 off the continental shelf of South Australia in front of the River Murray shows a strong glacial – interglacial pattern, which is also observed in the SST and *G. bulloides* $\delta^{18}\text{O}$ records. In general, the glacial periods (late MIS6, MIS4 and MIS2) are marked by more D-enriched $\delta\text{D}_{\text{alkenone}}$ values compared to interglacial periods. This pattern persists after ice volume correction of the $\delta\text{D}_{\text{alkenone}}$ record, suggesting a freshening during glacial terminations. Comparison with records of the alkenone $\text{C}_{37}/\text{C}_{38}$ ratio and alkenone accumulation rates suggest that species composition or growth rate changes in the haptophyte producers did not affect the $\delta\text{D}_{\text{alkenone}}$ record. In contrast, the record of $\delta^{18}\text{O}$ of the planktonic foraminifer *G. bulloides* corrected for ice volume shows less clear changes in temperature glacial – interglacial variation and an even opposite trend to $\delta\text{D}_{\text{ic-alkenones}}$. However, the temperature correction of $\delta^{18}\text{O}$ of *G. bulloides* based on temperature estimates may be inappropriate as alkenone producing haptophytes and planktonic foraminifera likely thrive in different growth seasons and/or depth habitats leading to inaccurate estimations of $\delta^{18}\text{O}_{\text{sw}}$. The

lack of a clear correlation between the records of $\delta D_{\text{alkenone}}$ and the BIT index, as proxy for river discharge of terrestrial OM, suggests that salinity of ocean water at the core site was not substantially influenced by freshwater runoff. Glacial – interglacial variability in $\delta D_{\text{ic-alkenone}}$ is more likely derived from changing salinity related to the input of low salinity water transported to the core site by the Leeuwin Current during deglaciations and interglacials.

Acknowledgment

We acknowledge financial support from the Seventh Framework Programme PEOPLE Work Programme, grant 238512 (Marie Curie Initial Training Network GATEWAYS) and the Netherlands Organization for Scientific Research (NWO) for funding S.S. (VICI) and M.v.d.M. (VIDI). Core MD03-2607 was obtained with a National Oceans Office and Australian Research Council grant, both awarded to P.D.D.. Y. Balut from IPEV was instrumental in obtaining the core.

Chapter 8

Synthesis and Outlook

In this thesis several sedimentary records of the hydrogen isotopic composition of the C_{37} di- and tri-unsaturated alkenones ($\delta D_{\text{alkenone}}$) have been generated from both coastal and open ocean settings, to test its potential as a proxy for paleo sea surface salinity (SSS) reconstructions. In general the $\delta D_{\text{alkenone}}$ records obtained from open ocean settings showed a similar glacial-interglacial pattern as oxygen isotope records of foraminifera ($\delta^{18}O_{\text{foram}}$) (Duplessy et al., 1981; Niebler et al., 1999) with more D-enriched values during glacial periods and relatively more D-depleted $\delta D_{\text{alkenone}}$ values during the interglacials (Chapter 2-4). Moreover, $\delta D_{\text{alkenone}}$ records correspond well with records of $\delta^{18}O$ of sea water ($\delta^{18}O_{\text{sw}}$) reconstructions, based on temperature corrected $\delta^{18}O_{\text{foram}}$, with respect to the timing of the isotopic shifts in the Agulhas Leakage area (Chapter 2), the upstream Agulhas Current (Chapter 3) and the Tropical Eastern Atlantic Ocean (Chapter 4). This suggest that similar factors that are affecting the oxygen isotopic composition of foraminifera shells are also affecting the hydrogen isotopic composition of long chain alkenones, in particular salinity and the isotopic composition of the water, which fits with culture studies (Schouten et al., 2006; Chivall et al., 2014; M'Boule et al., 2014).

Although $\delta^{18}O_{\text{sw}}$ and $\delta D_{\text{alkenone}}$ often show similar patterns, they also differ sometimes such as during the period between MIS5 - MIS2 in the Tropical Eastern Atlantic (Chapter 4). This could be due to several issues affecting the different proxies. Calculation of $\delta^{18}O_{\text{sw}}$ based on $\delta^{18}O_{\text{foram}}$ requires a correction for calcification temperatures (Duplessy et al., 1991; Rostek et al., 1993). This can be achieved by using temperature proxies such as the Mg/Ca ratios of foraminifera carbonate or alternatively the U^{k}_{37} or TEX_{86} index. While the Mg/Ca ratios are derived from the same organism as $\delta^{18}O$, the use of the organic proxies potentially introduce uncertainties in the correction for calcification temperatures due to differences in the depth habitat and growth season of the proxy organisms (Chapter 7). Furthermore, there are uncertainties associated with the correction for the isotopic ice volume effect, which is done by subtracting an estimation of the global $\delta^{18}O_{\text{sw}}$ from the temperature corrected $\delta^{18}O_{\text{foram}}$. This requires an accurate alignment of the global $\delta^{18}O_{\text{sw}}$ record with the temperature corrected $\delta^{18}O_{\text{foram}}$ in order to avoid temporal mismatches in the resulting local $\delta^{18}O_{\text{sw}}$ reconstructions. Moreover, some planktonic foraminifera species, e.g. *Globigerina bulloides*, may not strictly represent solely ocean surface conditions, but also subsurface conditions, which needs to be considered when reconstructing SSS (Chapter 2).

Relatively salinity changes can be inferred from ice-volume corrected $\delta D_{\text{alkenone}}$ or by calculating the stable hydrogen isotope fractionation factor α between the alkenones and the seawater ($\alpha_{\text{alkenone-sw}}$). However, the latter approach requires an estimate for past δD_{sw} , which can be calculated from planktonic foraminifera based $\delta^{18}O_{\text{sw}}$ reconstructions using the meteoric water line, each associated with uncertainties. Culture experiments have also shown that $\alpha_{\text{alkenone-water}}$ is not only salinity driven, but is also affected by growth rate (Schouten et al., 2006), growth phase (Wolhowe et al., 2009; Chivall et al., 2014), and the haptophyte species composition (M'Boule et al., 2014).

Regarding growth phase, batch culture experiments of different haptophyte algae showed that the sensitivity of the fractionation factor $\alpha_{\text{alkenone-water}}$ was largest for cells harvested in the exponential growth phase and decreased at the onset of the stationary phase (Chivall et al., 2014). For environmental studies this may become particularly important in case of nutrient

stress related growth phase changes of the alkenone producers (Prah et al., 2003). However, the importance of growth phase for alkenones eventually preserved in sediments is largely unclear (Volkman, 2000; Harada et al., 2003). It is assumed that the majority of sedimentary alkenones is coming from haptophyte blooms and are effectively transported to the sediment through grazing and packaging in fecal pellets or large size particle transport by, for example, particle aggregation (Sawada et al., 1998; Ternois et al., 1998; Fischer and Karakaş, 2009).

Another factor possibly affecting the use of $\alpha_{\text{alkenone-sw}}$ as a salinity proxy is growth rate. In contrast to the positive correlation of $\alpha_{\text{alkenone-water}}$ with salinity, growth rate changes are negatively correlated with $\alpha_{\text{alkenone-water}}$, meaning that higher growth rates will result in lower $\alpha_{\text{alkenone-water}}$ values (Schouten et al., 2006). Therefore, growth rate changes could interfere with salinity reconstructions based on $\delta D_{\text{alkenone}}$. Unfortunately, reconstruction of past growth rate is not straight forward and relies on other proxies. For instance, the carbon isotope composition of alkenones ($\delta^{13}C_{\text{alkenone}}$) has been shown to largely depend on growth rate (Rau et al., 1996; Bidigare et al., 1997; Benthien et al., 2002; 2005), but can also be affected by the concentration of CO_2 , which has likely varied over glacial-interglacial transitions (Curry and Crowley, 1987). A sediment record for $\delta^{13}C_{\text{alkenone}}$ from the Agulhas leakage area (Chapter 2) showed only relatively small changes, pointing towards little change in growth rate during the last two glacial terminations. However, the effect of growth rate on $\delta D_{\text{alkenone}}$ and $\alpha_{\text{alkenone-sw}}$ could be more important where changes in salinity are relatively small, as might be the case for the observed $\alpha_{\text{alkenone-sw}}$ variability during MIS5-2 in the Tropical Eastern Atlantic Ocean (Chapter 4). This was supported by a record of alkenone accumulation rates, another possible indicator for paleoproductivity and, indirectly, growth rate of the alkenone producers (Volkman et al., 1980; Marlowe et al., 1984b), which showed elevated and more variable alkenone accumulation rates during this period (Chapter 4). It is, therefore, important to further constrain the effect of growth rate on the $\delta D_{\text{alkenone}}$ in modern natural settings and eventually in down core $\delta D_{\text{alkenone}}$ records.

Apart from growth phase and growth rate changes, the species composition, in particular the contribution of coastal species, can also affect the $\delta D_{\text{alkenone}}$ signal (M'Boule et al., 2014). While this scenario is less likely in open ocean settings (Chapter 2-4), near coastal settings could certainly be affected (Schwab and Sachs, 2011). Indeed, application of the $\delta D_{\text{alkenone}}$ in a coastal ocean margin setting within the Mozambique Channel does not show the typical glacial-interglacial variability observed at other sites (Chapter 6). The good correlation of $\delta D_{\text{alkenone}}$ with the BIT index, as well as changes in the ratio of C_{37} and C_{38} alkenones as indicator for haptophyte species composition changes, points towards contribution of alkenones produced by coastal species during the glacial. On the other hand, a $\delta D_{\text{alkenone}}$ record from the River Murray Canyon south of Australia shows, despite a terrestrial influence via the Murray Darling River system, a clear glacial-interglacial variability (Chapter 7). Here BIT values show no correspondence with the $\delta D_{\text{alkenone}}$ record, possibly suggesting that the continental freshwater discharge was not substantial enough to affect $\delta D_{\text{alkenone}}$, while also the C_{37}/C_{38} alkenone ratio indicates no changes that correspond to variability in the $\delta D_{\text{alkenone}}$ record.

In summary, findings presented in this thesis suggest that $\delta D_{\text{alkenone}}$ is a suitable proxy for past ocean SSS. Results suggest that relative salinity shifts can be inferred from ice volume corrected $\delta D_{\text{alkenone}}$ or, alternatively, from reconstructed $\alpha_{\text{alkenone-water}}$. In open ocean settings, the $\delta D_{\text{alkenone}}$ generally agrees with the planktonic foraminifera derived $\delta^{18}O_{\text{sw}}$ reconstructions and in particular $\delta^{18}O_{\text{foram}}$. Application of $\delta D_{\text{alkenone}}$ in coastal ocean margin settings indicate that this proxy can become complicated by factors such as continental freshwater discharge or changes in the haptophyte species composition.

Despite these results, it is clear that other factors need to be studied in more detail in order to more confidently apply $\delta D_{\text{alkenone}}$ as a salinity proxy. For example, the transfer of the $\delta D_{\text{alkenone}}$ signal from living haptophytes in the ocean surface through the water column into the sedimentary record needs to be better constrained (Sessions et al., 2004; Sachse et al., 2012). This can be achieved by analyzing suspended material obtained by *in situ* pump, efficient use of sediment traps (preferentially remotely triggered) to capture different stages of a haptophyte bloom, and multicores to accurately sample the most recent sediments. Preferentially, these studies should be carried out in an area with a relatively large natural salinity gradient in combination with *in situ* measurements for salinity and the hydrogen isotope composition of the seawater. Such studies of modern day field situations, covering the distribution of alkenones along a surface as well as a depth gradient, will be beneficial to translate the results obtained from culture experiments into the natural environment and help to constrain uncertainties in factors other than salinity affecting $\delta D_{\text{alkenone}}$.

An approach for absolute salinity reconstructions from $\delta D_{\text{alkenone}}$

The results in this thesis have also shown that it is problematic to obtain absolute salinity estimates from both $\delta^{18}O_{\text{foram}}$ (Rohling, 2000) as well as $\delta D_{\text{alkenone}}$. For $\delta^{18}O$, substantial uncertainties for the calculation of absolute past ocean salinity comes from corrections for temperature and ice volume of $\delta^{18}O_{\text{foram}}$ as discussed above. In addition, the correlation between $\delta^{18}O$ and salinity needs to be constrained and has likely varied over the geological past. In order to reconstruct absolute salinity from the $\delta D_{\text{alkenone}}$, it is necessary to calculate the hydrogen isotope fractionation factor α between the alkenones and the ambient seawater and use the correlations between α and salinity observed in culture studies (Schouten et al., 2006; M'Boule et al., 2014). As discussed above, this requires an estimate for past δD_{sw} from $\delta^{18}O_{\text{sw}}$ reconstructions using the meteoric water line, estimates that are associated with large uncertainties. Indeed, it is striking that even though initially there is often a good relationship between $\delta D_{\text{alkenone}}$ and $\delta^{18}O_{\text{foram}}$ in these sediment records, the $\delta^{18}O_{\text{sw}}$ and $\alpha_{\text{alkenone-sw}}$ obtained after the abovementioned corrections often show large scatter and a poor relationship (Chapter 4, 7). This suggests that these corrections lead to large errors in salinity estimates.

In the following a novel approach is presented that avoids the use of estimated δD_{sw} . This approach involves the combination of different relationships of $\alpha_{\text{compound-water}}$ versus salinity for multiple lipid biomarkers. As culture studies on alkenones suggest, the relationship between the hydrogen isotope fractionation during lipid biosynthesis, $\alpha_{\text{compound-water}}$, and salinity S can be

described by a linear relationship (Eq.1):

$$\alpha_{\text{compound-water}} = m * S + q \quad (\text{Eq. 1})$$

with m representing the slope and q the intercept (Schouten et al., 2006). If the relationship for the stable hydrogen isotope fractionation factor α and salinity is known for at least two biomarker lipids, a and b , than Eq.1 can be substituted and rearranged for S (Eq.2):

$$S = \frac{(1000 + \delta D_b) q_a - (1000 + \delta D_a) q_b}{(1000 + \delta D_a) m_b - (1000 + \delta D_b) m_a} \quad (\text{Eq.2})$$

Thus, salinity can be calculated using the hydrogen isotopic composition of two biomarker lipids without the need to reconstruct the δD of seawater. Potentially suitable biomarkers for this approach are those compounds that occur ubiquitously and in sufficient amounts in sediments, that are species specific, and are not prone to the exchange of labile hydrogen and degradation. Furthermore, the biomarker lipids have to be synthesized by source organisms sharing the same ecological niche, in this case surface waters.

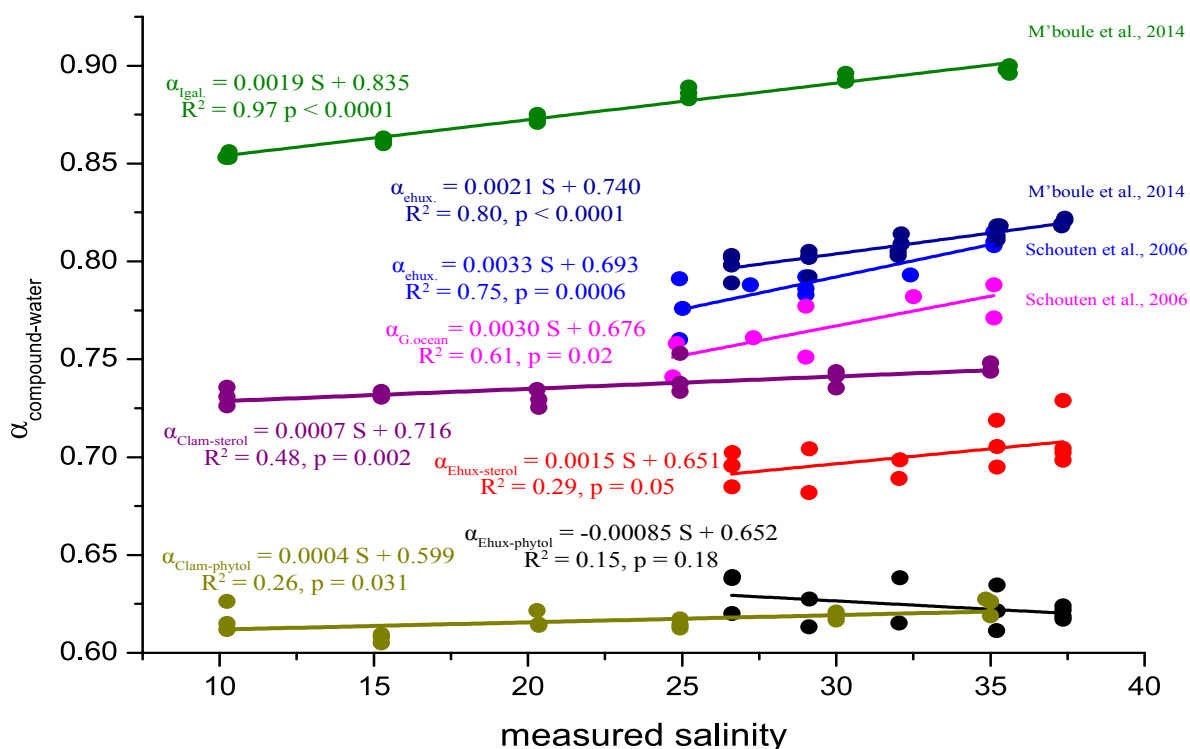


Figure 1. Correlations between $\alpha_{\text{compound-water}}$ and salinity for phytol of *E. huxleyi* (black, this study) and *C. lamellosa* (Chivall et al., in prep; dark yellow); brassicasterol of *E. huxleyi* (red, this study) and *C. lamellosa* (Chivall et al., in prep.; purple); *G. oceanica* (pink, Schouten et al, 2006); *E. huxleyi* (light blue, M'Boule et al., 2014); *E. huxleyi* (dark blue, Schouten et al., 2006); *I. galbana* (green, M'Boule et al., 2014).

Here, I investigated the potential of phytol and sterols, together with alkenones, as suitable compounds for the application of this multiple $\alpha_{\text{compound-water}}$ approach. Phytol is an isoprenoid alcohol, that is the main esterifying alcohol of chlorophyll (Boon et al., 1975; Johns et al., 1980). It is ubiquitous in the marine environment and has been frequently used as biomarker for chemical and biological processes (Volkman and Maxwell, 1986; Rontani and Volkman, 2003). Because of its link with photosynthesis it is synthesized in surface waters and thus in the same water where alkenones are produced, although it is much less specific than alkenones. Sterols might be a second potentially suitable compound class as it has been shown that there is a good correlation between $\alpha_{\text{sterol-water}}$ and salinity for brassicasterol (Figure 1, red dots) (Nelson and Sachs, 2014). Brassicasterol is, similar to phytol, less specific and synthesized ubiquitously by phytoplankton (Goad and Withers, 1982; Volkman, 1986).

To test this approach, $\alpha_{\text{phytol-water}}$ and $\alpha_{\text{sterol-water}}$ were evaluated for biomass of *E. huxleyi*, grown at salinities ranging from 27 to 37 at constant temperatures and known δD of the culture water (Table 1) and of *Chrysolita lamellosa* grown at salinities between 10 to 35 (Chivall et al., in prep.). For the analyses of δD of phytol and brassicasterol, samples were base-hydrolyzed and subsequently acetylated with acetic anhydride at 60 °C for 30 min using silver triflate as acetylation catalyst (Das and Chakraborty, 2011). Interestingly, the $\alpha_{\text{sterol-water}}$ of brassicasterol shows a relatively weak relationship with salinity for *E. huxleyi* ($\alpha_{\text{Ehux-sterol}} = 0.0015 * S + 0.651$; $R^2 = 0.29$, p-value = 0.05) and *C. lamellosa* ($\alpha_{\text{Clam-sterol}} = 0.0007 * S + 0.761$; $R^2 = 0.48$, p-value = 0.002; Figure 1). However, the relationship of $\alpha_{\text{sterol-water}}$ versus salinity for *C. lamellosa* is in good agreement with the reported relationship for $\alpha_{\text{sterol-water}}$ of brassicasterol obtained from globally distributed saline and hypersaline lakes [$\alpha_{\text{sterol-water}} = 0.0007 * S + 0.732$; $R^2 = 0.73$, p-value = 0.0002 (Nelson and Sachs, 2014)].

Table 1. Initial results for measurements of δD_{phytol} and δD_{sterol} (brassicasterol) and the respective hydrogen fractionation factors α from batch cultured *E. huxleyi* at constant temperature and measured δD of the culture water (δD_{water}).

salinity	δD_{phytol}	$\pm 1\sigma$ error	δD_{sterol}	$\pm 1\sigma$ error	δD_{water}	$\alpha_{\text{phytol-water}}$	$\alpha_{\text{sterol-water}}$
37.3	-379	1	-266	4	6	0.617	0.729
37.3	-377	9	-293	7	6	0.619	0.702
37.4	-371	2	-290	1	7	0.624	0.704
37.3	-374	0	-297	2	7	0.622	0.698
35.2	-387	0	-279	0	3	0.611	0.719
35.2	-364	1	-293	0	3	0.635	0.705
35.2	-377	1	-303	1	3	0.621	0.695
32.1	-364	2	-304	1	-3	0.638	0.699
32.0	-385	4	-311	10	0	0.615	0.689
29.1	-376	1	-300	1	-6	0.627	0.704
29.1	-391	0	-322	0	-6	0.613	0.682
26.6	-386	1	-321	3	-9	0.620	0.685
26.6	-369	8	-311	1	-10	0.638	0.696
26.6	-368	13	-306	13	-11	0.639	0.702

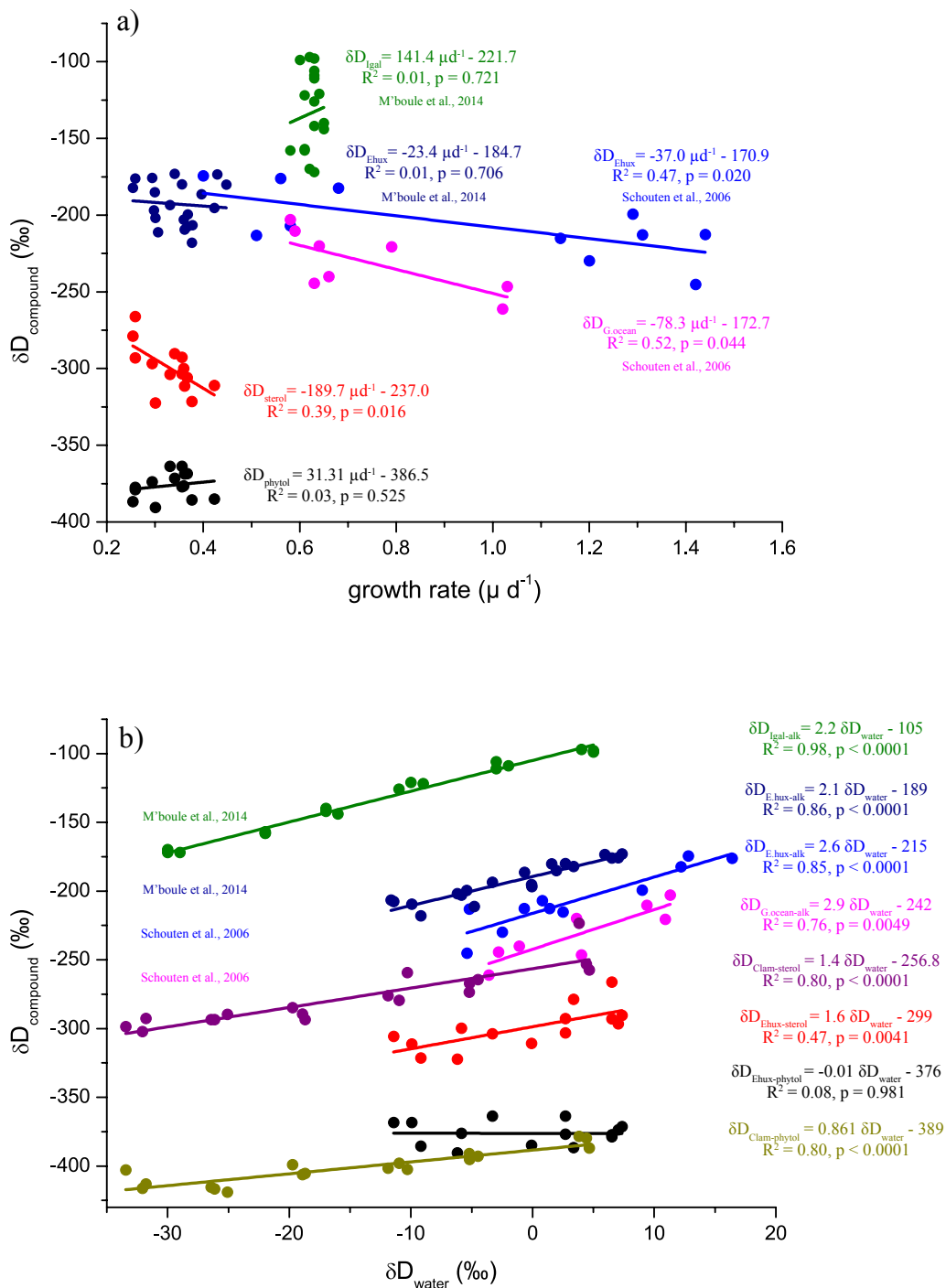


Figure 2. Correlations between δD of the compound with (a) growth rate and (b) the δD of the culture water for phytol of *E. huxleyi* (black, this study) and *C. lamellosa* (Chivall et al., in prep; dark yellow); brassicasterol of *E. huxleyi* (red, this study) and *C. lamellosa* (Chivall et al., in prep; purple); *G. oceanica* (pink, Schouten et al, 2006); *E. huxleyi* (light blue, M'Boule et al., 2014); *E. huxleyi* (dark blue, Schouten et al., 2006); *I. galbana* (green, M'Boule et al., 2014).

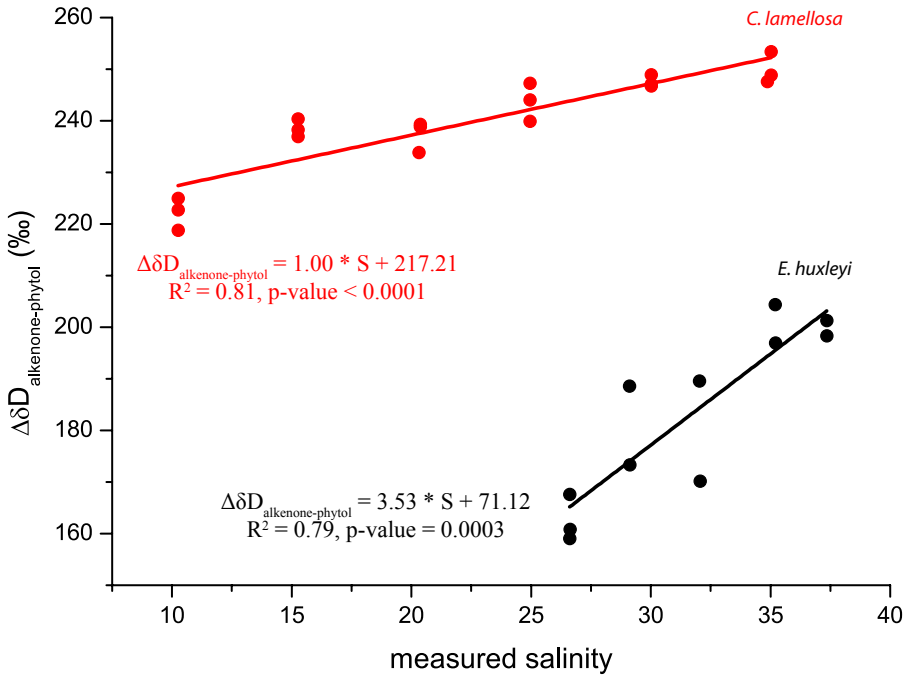


Figure 3. Correlation of the difference between the $\delta D_{\text{alkenone}}$ and δD_{phytol} ($\Delta\delta D_{\text{alkenone-phytol}}$) versus salinity for *E. huxleyi* (black) and *C. lamellosa* (red, Chivall et al., in prep.).

The slope for the $\alpha_{\text{sterol-water}}$ salinity relationship is generally smaller than for alkenones (Schouten et al., 2006; M'Boule et al., 2014). Brassicasterol and alkenones could thus be suitable candidates for the application in the multi fractionation factor approach described above.

The relationship of $\alpha_{\text{phytol-water}}$ for *E. huxleyi* on the other hand shows no significant change with salinity ($\alpha_{\text{phytol-water}} = -0.00085 * S + 0.652$; $R^2 = 0.15$, $p\text{-value} = 0.18$) and is not statistically significantly different (ANCOVA: $df = 1$, $F = 0$, $p\text{-value} = 0.995$) from the weak relationship for $\alpha_{\text{phytol-water}}$ versus salinity of *C. lamellosa* ($\alpha_{\text{Clam-phytol}} = 0.0004 * S + 0.599$, $R^2 = 0.26$, $p\text{-value} = 0.031$; Figure 1). Interestingly, there is also no significant relationship of δD_{phytol} from *E. huxleyi* with growth rate (Figure 2a). Although this suggests that phytol is not suitable for the dual isotope approach, it does suggest an alternative approach involving phytol. The independence of hydrogen isotope fractionation in phytol from salinity (Figure 1) and growth rate (Figure 2a) may make it a potentially suitable compound for tracking δD of the water (Figure 2b). Indeed, $\delta D_{\text{Clam-phytol}}$ shows a strong correlation with δD_{water} ($\delta D_{\text{Clam-phytol}} = 0.861 * \delta D_{\text{water}} - 389$, $R^2 = 0.80$, $p\text{-value} < 0.0001$) (Figure 2) with a slope slightly below 1 as can be expected from hydrogen isotopic fractionation (Sessions et al., 2005). This suggests that $\delta D_{\text{Clam-phytol}}$ mainly is correlated with δD_{water} and not affected by salinity (Schouten et al., 2006). However, δD_{phytol} for *E. huxleyi* shows no significant relationship with δD_{water} although this may be due to the small range in δD_{water} values. Indeed, the two δD_{phytol} datasets are not statistically different (ANCOVA: $df = 1$, $F = 0.063$, $p\text{-value} = 0.806$). Additional δD_{phytol} analyses, including those of other species, are required to validate these initial results. Nevertheless, if we plot the difference between $\delta D_{\text{alkenone}}$ and δD_{phytol}

against salinity we observe a significant correlation for the dataset of *E. huxleyi* ($\Delta\delta D_{\text{alkenone-phytol}} = 3.53 * S + 71.12$, $R^2 = 0.79$, p-value = 0.0003) and *C. lamellosa* ($\Delta\delta D_{\text{alkenone-phytol}} = 1.00 * S + 217.21$, $R^2 = 0.81$, p-value < 0.0001; Figure 3), indicating the potential to reconstruct salinity using the δD of two biomarker lipids. However, since phytol is a constituent of chlorophyll, which is produced by nearly all photosynthesizing organisms, this relationship may become obscured in natural settings with a large contribution of organic material from a great variety of photosynthesizing organisms. However, the positive side to this could be the averaging of $\alpha_{\text{phytol-water}}$ over multiple organisms, and therefore different biological and species specific fractionation effects, in the end reflecting mainly changes in the δD_{sw} .

In summary, the initial results for the relationship of $\alpha_{\text{phytol-water}}$ and salinity for the cultured haptophyte algae *E. huxleyi* and *C. lamellosa* suggest the hydrogen isotope fractionation in phytol may be independent of salinity and growth rate changes. This might indicate that $\alpha_{\text{phytol-water}}$ could be applied to track the δD of the water. A promising compound for the use in a multi- α approach for reconstructing past absolute salinity independent of δD_{sw} reconstructions could be brassicasterol, which showed a significant correlation of α with salinity as found for the alkenones, yet with a different sensitivity.

- Adkins, J.F., McIntyre, K., Schrag, D.P., 2002. The salinity, temperature, and $\delta^{18}\text{O}$ of the Glacial Deep Ocean. *Science* 298, 1769-1773.
- Adkins, J.F., Schrag, D.P., 2001. Pore fluid constraints on deep ocean temperature and salinity during the Last Glacial Maximum. *Geophysical Research Letters* 28, 771-774.
- Alley, R.B., Clark, P.U., 1999. The Deglaciation of the Northern Hemisphere: A Global Perspective. *Annual Review of Earth and Planetary Sciences* 27, 149-182.
- Anand, P., Elderfield, H., Conte, M.H., 2003. Calibration of Mg/Ca thermometry in planktonic foraminifera from a sediment trap time series. *Paleoceanography* 18, 1050.
- Andersen, N., Paul, H.A., Bernasconi, S.M., McKenzie, J.A., Behrens, A., Schaeffer, P., Albrecht, P., 2001. Large and rapid climate variability during the Messinian salinity crisis: Evidence from deuterium concentrations of individual biomarkers. *Geology* 29, 799-802.
- Antonov, J.I., R. A. Locarnini, T. P. Boyer, A. V. Mishonov, Garcia, H.E., 2006. World Ocean Atlas 2005, Volume 2: Salinity, S. Levitus, Ed. NOAA Atlas NESDIS 62, U.S. Government Printing Office, Washington, DC, p. 182 pp.
- Arbuszewski, J., deMenocal, P., Kaplan, A., Farmer, E.C., 2010. On the fidelity of shell-derived $\delta^{18}\text{O}_{\text{sw}}$ estimates. *Earth and Planetary Science Letters* 300, 185-196.
- Bard, E., 1988. Correction of accelerator mass spectrometry ^{14}C ages measured in planktonic foraminifera: Paleoceanographic implications. *Paleoceanography* 3, 635-645.
- Bard, E., 2001. Comparison of alkenone estimates with other paleotemperature proxies. *Geochemistry, Geophysics, Geosystems* 2, 1002.
- Bard, E., Fairbanks, R., Arnold, M., Maurice, P., Duprat, J., Moyes, J., Duplessy, J.-C., 1989. Sea-level estimates during the last deglaciation based on $\delta^{18}\text{O}$ and accelerator mass spectrometry ^{14}C ages measured in *Globigerina bulloides*. *Quaternary Research* 31, 381-391.
- Bard, E., Rickaby, R.E.M., 2009. Migration of the subtropical front as a modulator of glacial climate. *Nature* 460, 380-U393.
- Barker, S., Cacho, I., Benway, H., Tachikawa, K., 2005. Planktonic foraminiferal Mg/Ca as a proxy for past oceanic temperatures: a methodological overview and data compilation for the Last Glacial Maximum. *Quaternary Science Reviews* 24, 821-834.
- Barker, S., Diz, P., 2014. Timing of the descent into the last Ice Age determined by the bipolar seesaw. *Paleoceanography* 29, 2014PA002623.
- Barker, S., Elderfield, H., 2002. Foraminiferal Calcification Response to Glacial-Interglacial Changes in Atmospheric CO_2 . *Science* 297, 833-836.
- Barker, S., Greaves, M., Elderfield, H., 2003. A study of cleaning procedures used for foraminiferal Mg/Ca paleothermometry. *Geochemistry, Geophysics, Geosystems* 4, 8407.
- Barker, S., Knorr, G., Edwards, R.L., Parrenin, F., Putnam, A.E., Skinner, L.C., Wolff, E., Ziegler, M., 2011. 800,000 Years of Abrupt Climate Variability. *Science* 334, 347-351.
- Beal, L.M., Chereskin, T.K., Lenn, Y.D., Elipot, S., 2006. The Sources and Mixing Characteristics of the Agulhas Current. *Journal of Physical Oceanography* 36, 2060-2074.
- Beal, L.M., De Ruijter, W.P.M., Biastoch, A., Zahn, R., 2011. On the role of the Agulhas system in ocean circulation and climate. *Nature* 472, 429-436.
- Beiersdorf, H.K.H.-R.S.U.v., 1980. Placer deposits of ilmenite and zircon on the Zambezi shelf. Schweizerbart, Stuttgart.
- Belkin, I.M., Gordon, A.L., 1996. Southern Ocean fronts from the Greenwich meridian to Tasmania. *Journal of Geophysical Research: Oceans* 101, 3675-3696.

- Bemis, B.E., Spero, H.J., Bijma, J., Lea, D.W., 1998. Reevaluation of the oxygen isotopic composition of planktonic foraminifera: Experimental results and revised paleotemperature equations. *Paleoceanography* 13, 150-160.
- Bemis, B.E., Spero, H.J., Thunell, R.C., 2002. Using species-specific paleotemperature equations with foraminifera: a case study in the Southern California Bight. *Marine Micropaleontology* 46, 405-430.
- Benthien, A., Andersen, N., Schulte, S., Müller, P.J., Schneider, R.R., Wefer, G., 2005. The carbon isotopic record of the C_{37:2} alkenone in the South Atlantic: Last Glacial Maximum (LGM) vs. Holocene. *Palaeogeography, Palaeoclimatology, Palaeoecology* 221, 123-140.
- Benthien, A., Andersen, N., Schulte, S., Müller, P.J., Schneider, R.R., Wefer, G., 2002. Carbon isotopic composition of the C_{37:2} alkenone in core top sediments of the South Atlantic Ocean: Effects of CO₂ and nutrient concentrations. *Global Biogeochemical Cycles* 16, 12.
- Benthien, A., Müller, P.J., 2000. Anomalously low alkenone temperatures caused by lateral particle and sediment transport in the Malvinas Current region, western Argentine Basin. *Deep Sea Research Part I: Oceanographic Research Papers* 47, 2369-2393.
- Berger, W.H., 1968. Planktonic Foraminifera: selective solution and paleoclimatic interpretation. *Deep Sea Research and Oceanographic Abstracts* 15, 31-43.
- Bertrand, P., 1997. Les rapport de campagne a la mer a bord du Marion Dufresne - Campagne NAUSICAA - Images II - MD105 du 20/10/96 au 25/11/96. Inst. Fr. pour la Rech. et la Technol. Polaires, France, Plouzane.
- Biaostoch, A., Böning, C.W., 2013. Anthropogenic impact on Agulhas leakage. *Geophysical Research Letters* 40, 1138-1143.
- Biaostoch, A., Boning, C.W., Lutjeharms, J.R.E., 2008. Agulhas leakage dynamics affects decadal variability in Atlantic overturning circulation. *Nature* 456, 489-492.
- Bidigare, R.R., Fluegge, A., Freeman, K.H., Hanson, K.L., Hayes, J.M., Hollander, D., Jasper, J.P., King, L.L., Laws, E.A., Milder, J., Millero, F.J., Pancost, R., Popp, B.N., Steinberg, P.A., Wakeham, S.G., 1997. Consistent fractionation of ¹³C in nature and in the laboratory: Growth-rate effects in some haptophyte algae. *Global Biogeochem. Cycles* 11, 279-292.
- Bony, S., Dufresne, J.-L., 2005. Marine boundary layer clouds at the heart of tropical cloud feedback uncertainties in climate models. *Geophysical Research Letters* 32, L20806.
- Boon, J.J., Rijpstra, W.I.C., De Leeuw, J.W., Schenck, P.A., 1975. Phytanic acid in sediments. *Nature* 258, 414-416.
- Bourles, B., Molinari, R.L., Johns, E., Wilson, W.D., Leaman, K.D., 1999. Upper layer currents in the western tropical North Atlantic (1989–1991). *Journal of Geophysical Research: Oceans* 104, 1361-1375.
- Bowen, G.J., Winter, D.A., Spero, H.J., Zierenberg, R.A., Reeder, M.D., Cerling, T.E., Ehleringer, J.R., 2005. Stable hydrogen and oxygen isotope ratios of bottled waters of the world. *Rapid Communications in Mass Spectrometry* 19, 3442-3450.
- Brassell, S.C., Eglinton, G., Marlowe, I.T., Pflaumann, U., Sarnthein, M., 1986. Molecular stratigraphy: a new tool for climatic assessment. *Nature* 320, 129-133.
- Brasseur, P., Beckers, J.M., Brankart, J.M., Schoenauen, R., 1996. Seasonal temperature and salinity fields in the Mediterranean Sea: Climatological analyses of a historical data set. *Deep Sea Research Part I: Oceanographic Research Papers* 43, 159-192.
- Broecker, W., Clark, E., 2001. An evaluation of Lohmann's foraminifera weight dissolution index. *Paleoceanography* 16, 531-534.
- Broecker, W.S., 1991. The great ocean conveyor. *Oceanography* 4, 79-89.

- Broecker, W.S., 1998. Paleocan circulation during the Last Deglaciation: A bipolar seesaw? *Paleoceanography* 13, 119-121.
- Broecker, W.S., Bond, G., Klas, M., Bonani, G., Wolffi, W., 1990. A salt oscillator in the glacial Atlantic? 1. The concept. *Paleoceanography* 5, 469-477.
- Brohan, P., Kennedy, J.J., Harris, I., Tett, S.F.B., Jones, P.D., 2006. Uncertainty estimates in regional and global observed temperature changes: A new data set from 1850. *Journal of Geophysical Research: Atmospheres* 111, D12106.
- Brown, S.J., Elderfield, H., 1996. Variations in Mg/Ca and Sr/Ca ratios of planktonic foraminifera caused by postdepositional dissolution: Evidence of shallow Mg-dependent dissolution. *Paleoceanography* 11, 543-551.
- Brummer, G.-J.A., participants, a., 2009. RV Pelagia Cruise Report: Cruise 64PE304, INATEX-GEO, SE African margin, 10 March - 2 April, NIOZ, Royal Netherlands Institute for Sea Research, Texel, The Netherlands.
- Bryden, H.L., Longworth, H.R., Cunningham, S.A., 2005. Slowing of the Atlantic meridional overturning circulation at 25°N. *Nature* 438, 655-657.
- Caley, T., Giraudeau, J., Malaizé, B., Rossignol, L., Pierre, C., 2012. Agulhas leakage as a key process in the modes of Quaternary climate changes. *Proceedings of the National Academy of Sciences* 109, 6835-6839.
- Carlson, A.E., Oppo, D.W., Came, R.E., LeGrande, A.N., Keigwin, L.D., Curry, W.B., 2008. Subtropical Atlantic salinity variability and Atlantic meridional circulation during the last deglaciation. *Geology* 36, 991-994.
- Castañeda, I.S., Mulitza, S., Schefuß, E., Lopes dos Santos, R.A., Sinninghe Damsté, J.S., Schouten, S., 2009. Wet phases in the Sahara/Sahel region and human migration patterns in North Africa. *Proceedings of the National Academy of Sciences*.
- Castañeda, I.S., Schefuß, E., Pätzold, J., Sinninghe Damsté, J.S., Weldeab, S., Schouten, S., 2010. Millennial-scale sea surface temperature changes in the eastern Mediterranean (Nile River Delta region) over the last 27,000 years. *Paleoceanography* 25, PA1208.
- Chang, P., Zhang, R., Hazeleger, W., Wen, C., Wan, X., Ji, L., Haarsma, R.J., Breugem, W.-P., Seidel, H., 2008. Oceanic link between abrupt changes in the North Atlantic Ocean and the African monsoon. *Nature Geoscience* 1, 444-448.
- Chiang, J.C.H., Cheng, W., Bitz, C.M., 2008. Fast teleconnections to the tropical Atlantic sector from Atlantic thermohaline adjustment. *Geophysical Research Letters* 35, L07704.
- Chivall, D., M'Boule, D., Sinke-Schoen, D., Sinninghe Damsté, J.S., Schouten, S., van der Meer, M.T.J., 2014. The effects of growth phase and salinity on the hydrogen isotopic composition of alkenones produced by coastal haptophyte algae. *Geochimica et Cosmochimica Acta* 140, 381-390.
- Clark, P.U., Pisias, N.G., Stocker, T.F., Weaver, A.J., 2002. The role of the thermohaline circulation in abrupt climate change. *Nature* 415, 863-869.
- Conte, M.H., Thompson, A., Lesley, D., Harris, R.P., 1998. Genetic and Physiological Influences on the Alkenone/Alkenoate Versus Growth Temperature Relationship in *Emiliania huxleyi* and *Gephyrocapsa Oceanica*. *Geochimica et Cosmochimica Acta* 62, 51-68.
- Coolen, M.J., Orsi, W.D., Balkema, C., Quince, C., Harris, K., Sylva, S.P., Filipova-Marinova, M., Giosan, L., 2013. Evolution of the plankton paleome in the Black Sea from the Deglacial to Anthropocene. *Proceedings of the National Academy of Sciences* 110, 8609-8614.
- Craig, H., 1961. Isotopic Variations in Meteoric Waters. *Science* 133, 1702-1703.

- Craig, H., Gordon, L.I., 1965. Deuterium and oxygen 18 variations in the ocean and marine atmosphere, Proceedings of a Conference on Stable Isotopes in Oceanographic Studies and Paleotemperatures. Pisa: V. Lischi & Figli., Spoleto, Italy, pp. 9 - 130.
- Cresswell, G., 1990. The Leeuwin Current. *Corella* 14, 113-118.
- Cunningham, S.A., Kanzow, T., Rayner, D., Baringer, M.O., Johns, W.E., Marotzke, J., Longworth, H.R., Grant, E.M., Hirschi, J.J.-M., Beal, L.M., Meinen, C.S., Bryden, H.L., 2007. Temporal variability of the Atlantic Meridional Overturning Circulation at 26.5°N. *Science* 317, 935-938.
- Curry, W.B., Crowley, T.J., 1987. The $\delta^{13}\text{C}$ of equatorial Atlantic surface waters: Implications for Ice Age pCO₂ levels. *Paleoceanography* 2, 489-517.
- D'Andrea, W.J., Liu, Z., Alexandre, M.D.R., Wattley, S., Herbert, T.D., Huang, Y., 2007. An efficient method for isolating individual long-chain alkenones for compound-specific hydrogen isotope analysis. *Analytical Chemistry* 79, 3430-3435.
- Das, R., Chakraborty, D., 2011. Silver Triflate Catalyzed Acetylation of Alcohols, Thiols, Phenols, and Amines. *Synthesis* 2011, 1621-1625.
- Dávila, P.M., Figueroa, D., Müller, E., 2002. Freshwater input into the coastal ocean and its relation with the salinity distribution off austral Chile (35–55°S). *Continental Shelf Research* 22, 521-534.
- De Deckker, P., Moros, M., Perner, K., Jansen, E., 2012. Influence of the tropics and southern westerlies on glacial interhemispheric asymmetry. *Nature Geoscience* 5, 266-269.
- De Jonge, C., Stadnitskaia, A., Hopmans, E.C., Cherkashov, G., Fedotov, A., Sinninghe Damsté, J.S., 2014. In situ produced branched glycerol dialkyl glycerol tetraethers in suspended particulate matter from the Yenisei River, Eastern Siberia. *Geochimica et Cosmochimica Acta* 125, 476-491.
- de Ruijter, W.P.M., Biastoch, A., Drijfhout, S.S., Lutjeharms, J.R.E., Matano, R.P., Pichevin, T., van Leeuwen, P.J., Weijer, W., 1999. Indian-Atlantic interocean exchange: Dynamics, estimation and impact. *Journal of Geophysical Research: Oceans* 104, 20885-20910.
- de Ruijter, W.P.M., Ridderinkhof, H., Lutjeharms, J.R.E., Schouten, M.W., Veth, C., 2002. Observations of the flow in the Mozambique Channel. *Geophysical Research Letters* 29, 140-141-140-143.
- Dessier, A., Donguy, J.R., 1994. The sea surface salinity in the tropical Atlantic between 10°S and 30°N—seasonal and interannual variations (1977–1989). *Deep Sea Research Part I: Oceanographic Research Papers* 41, 81-100.
- Diffenbaugh, N.S., Pal, J.S., Trapp, R.J., Giorgi, F., 2005. Fine-scale processes regulate the response of extreme events to global climate change. *Proceedings of the National Academy of Sciences of the United States of America* 102, 15774-15778.
- Duplessy, J.-C., Shackleton, N.J., 1985. Response of global deep-water circulation to Earth's climatic change 135,000-107,000 years ago. *Nature* 316, 500-507.
- Duplessy, J., Bé, A., Blanc, P., 1981. Oxygen and carbon isotopic composition and biogeographic distribution of planktonic foraminifera in the Indian Ocean. *Palaeogeography, Palaeoclimatology, Palaeoecology* 33, 9-46.
- Duplessy, J.C., Bard, E., Labeyrie, L., Duprat, J., Moyes, J., 1993. Oxygen isotope records and salinity changes in the Northeastern Atlantic Ocean during the Last 18,000 Years. *Paleoceanography* 8, 341-350.
- Duplessy, J.C., Labeyrie, L., Juilletleclerc, A., Maitre, F., Duprat, J., Sarnthein, M., 1991. Surface salinity reconstruction of the north-Atlantic ocean during the last glacial maximum. *Oceanologica Acta* 14, 311-324.

- Dyez, K.A., Zahn, R., Hall, I.R., 2014. Multicentennial Agulhas leakage variability and links to North Atlantic climate during the past 80,000 years. *Paleoceanography* 29, 2014PA002698.
- Elderfield, H., Ganssen, G., 2000. Past temperature and $\delta^{18}\text{O}$ of surface ocean waters inferred from foraminiferal Mg/Ca ratios. *Nature* 405, 442-445.
- Elliot, M., Labeyrie, L., Duplessy, J.-C., 2002. Changes in North Atlantic deep-water formation associated with the Dansgaard-Oeschger temperature oscillations (60–10ka). *Quaternary Science Reviews* 21, 1153-1165.
- Englebrecht, A.C., Sachs, J.P., 2005. Determination of sediment provenance at drift sites using hydrogen isotopes and unsaturation ratios in alkenones. *Geochimica et Cosmochimica Acta* 69, 4253-4265.
- Epstein, S., Mayeda, T., 1953. Variation of ^{18}O content of waters from natural sources. *Geochimica et Cosmochimica Acta* 4, 213-224.
- Erez, J., Luz, B., 1983. Experimental paleotemperature equation for planktonic foraminifera. *Geochimica et Cosmochimica Acta* 47, 1025-1031.
- Esper, J., Wilson, R.J.S., Frank, D.C., Moberg, A., Wanner, H., Luterbacher, J., 2005. Climate: past ranges and future changes. *Quaternary Science Reviews* 24, 2164-2166.
- Fallet, U., Ullgren, J.E., Castañeda, I.S., van Aken, H.M., Schouten, S., Ridderinkhof, H., Brummer, G.-J.A., 2011. Contrasting variability in foraminiferal and organic paleotemperature proxies in sedimenting particles of the Mozambique Channel (SW Indian Ocean). *Geochimica et Cosmochimica Acta* 75, 5834-5848.
- Ferguson, J.E., Henderson, G.M., Kucera, M., Rickaby, R.E.M., 2008. Systematic change of foraminiferal Mg/Ca ratios across a strong salinity gradient. *Earth and Planetary Science Letters* 265, 153-166.
- Fischer, G., Karakaş, G., 2009. Sinking rates and ballast composition of particles in the Atlantic Ocean: implications for the organic carbon fluxes to the deep ocean. *Biogeosciences* 6, 85-102.
- Fischer, G., Wefer, G., 1999. *Use of Proxies in Paleoceanography: Examples from the South Atlantic; with 43 Tables*. Springer Science & Business Media.
- Flores, J.A., Bárcena, M.A., Sierro, F.J., 2000. Ocean-surface and wind dynamics in the Atlantic Ocean off Northwest Africa during the last 140 000 years. *Palaeogeography, Palaeoclimatology, Palaeoecology* 161, 459-478.
- Flores, J.A., Gersonde, R., Sierro, F.J., 1999. Pleistocene fluctuations in the Agulhas Current Retroflection based on the calcareous plankton record. *Marine Micropaleontology* 37, 1-22.
- Foster, S.D., Griffin, D.A., Dunstan, P.K., 2014. Twenty years of high-resolution Sea Surface Temperature imagery around Australia: Inter-annual and annual variability. *PLoS ONE* 9, e100762.
- Fraile, I., Mülitz, S., Schulz, M., 2009. Modeling planktonic foraminiferal seasonality: Implications for sea-surface temperature reconstructions. *Marine Micropaleontology* 72, 1-9.
- Franzese, A.M., Hemming, S.R., Goldstein, S.L., Anderson, R.F., 2006. Reduced Agulhas Leakage during the Last Glacial Maximum inferred from an integrated provenance and flux study. *Earth and Planetary Science Letters* 250, 72-88.
- Friedman, I., Redfield, A.C., Schoen, B., Harris, J., 1964. The variation of the deuterium content of natural waters in the hydrologic cycle. *Reviews of Geophysics* 2, 177-224.
- Ganachaud, A., Wunsch, C., 2003. Large-scale ocean heat and freshwater transports during the World Ocean Circulation Experiment. *Journal of Climate* 16, 696-705.

- Gemmeke, B., 2010. Spätquartäre Variationen der Sauerstoffsotopenzusammensetzung des Oberflächenwassers im östlichen tropischen Nordatlantik, Department of Geoscience. University of Bremen, p. 39 pp.
- Gersonde, R., Abelmann, A., Brathauer, U., Becquey, S., Bianchi, C., Cortese, G., Grobe, H., Kuhn, G., Niebler, H.S., Segl, M., Sieger, R., Zielinski, U., Fütterer, D.K., 2003. Last glacial sea surface temperatures and sea-ice extent in the Southern Ocean (Atlantic-Indian sector): A multiproxy approach. *Paleoceanography* 18, 1061.
- Gillanders, B.M., Kingsford, M.J., 2002. Impact of changes in flow of freshwater on estuarine and open coastal habitats and the associated organisms. CRC Press, Boca Raton, FL, ETATS-UNIS.
- Gingele, F.X., De Deckker, P., 2005. Late Quaternary fluctuations of palaeoproductivity in the Murray Canyons area, South Australian continental margin. *Palaeogeography, Palaeoclimatology, Palaeoecology* 220, 361-373.
- Gingele, F.X., De Deckker, P., Hillenbrand, C.-D., 2004. Late Quaternary terrigenous sediments from the Murray Canyons area, offshore South Australia and their implications for sea level change, palaeoclimate and palaeodrainage of the Murray–Darling Basin. *Marine Geology* 212, 183-197.
- Giraudeau, J., Balut, Y., Hall, I.R., Mazaud, A., Zahn, R., 2003. SWAF-MDI128 Scientific Report, Rep. OCE/2003/01. Inst. Polaire Fr., Plouzané, France, p. 108 pp.
- Goad, L.J., Withers, N., 1982. Identification of 27-nor-(24R)-24-methylcholesta-5,22-dien-3 β -ol and brassicasterol as the major sterols of the marine dinoflagellate *Gymnodinium simplex*. *Lipids* 17, 853-858.
- Gordon, A.L., 1985. Indian-Atlantic Transfer of Thermocline Water at the Agulhas Retroflexion. *Science* 227, 1030-1033.
- Gordon, A.L., 1986. Interocean exchange of thermocline water. *Journal of Geophysical Research: Oceans* 91, 5037-5046.
- Gordon, A.L., 2001. Interocean exchange, in: Siedler, G., Church, J., Gould, J. (Eds.), *Ocean circulation and climate: observing and modelling the global ocean*. Academic Press, New York, pp. 303-314.
- Gordon, A.L., Lutjeharms, J.R.E., Gründlingh, M.L., 1987. Stratification and circulation at the Agulhas Retroflexion. *Deep Sea Research Part A. Oceanographic Research Papers* 34, 565-599.
- Gottschalk, J., Skinner, L.C., Waelbroeck, C., 2015. Contribution of seasonal sub-Antarctic surface water variability to millennial-scale changes in atmospheric CO₂ over the last deglaciation and Marine Isotope Stage 3. *Earth and Planetary Science Letters* 411, 87-99.
- Govin, A., Varma, V., Prange, M., 2014. Astronomically forced variations in western African rainfall (21°N–20°S) during the Last Interglacial period. *Geophysical Research Letters* 41, 2013GL058999.
- Grant, K.M., Rohling, E.J., Bar-Matthews, M., Ayalon, A., Medina-Elizalde, M., Ramsey, C.B., Satow, C., Roberts, A.P., 2012. Rapid coupling between ice volume and polar temperature over the past 150,000 years. *Nature* 491, 744-747.
- Greenland Ice-core Project, M., 1993. Climate instability during the last interglacial period recorded in the GRIP ice core. *Nature* 364, 203-207.
- Gross, M.G., 1987. *Oceanography, a view of the earth*, 4th ed. ed. Prentice-Hall, Englewood Cliffs, N.J.
- Guinasso, N.L., Schink, D.R., 1975. Quantitative estimates of biological mixing rates in abyssal sediments. *Journal of Geophysical Research* 80, 3032-3043.

- Haarsma, R.J., Campos, E.J.D., Drijfhout, S., Hazeleger, W., Severijns, C., 2011. Impacts of interruption of the Agulhas leakage on the tropical Atlantic in coupled ocean-atmosphere simulations. *Climate Dynamics* 36, 989-1003.
- Harada, N., Shin, K.H., Murata, A., Uchida, M., Nakatani, T., 2003. Characteristics of alkenones synthesized by a bloom of *Emiliania huxleyi* in the Bering Sea. *Geochimica et Cosmochimica Acta* 67, 1507-1519.
- Heinrich, H., 1988. Origin and consequences of cyclic ice rafting in the Northeast Atlantic Ocean during the past 130,000 years. *Quaternary Research* 29, 142-152.
- Herfort, Lydie, Schouten, Stefan, Boon, Jan, P., Woltering, Martijn, Baas, Marianne, Weijers, Johan, W.H., Sinninghe, D., Jaap, S., 2006. Characterization of transport and deposition of terrestrial organic matter in the southern North Sea using the BIT index. *American Society of Limnology and Oceanography*, Waco, TX, ETATS-UNIS.
- Hill, P.J., De Deckker, P., Australia, G., 2004. AUSCAN seafloor mapping and geological sampling survey on the Australian southern margin by RV Marion Dufresne in 2003: final project report. *Geoscience Australia*.
- Hoefs, M.J.L., Versteegh, G.J.M., Rijpstra, W.I.C., de Leeuw, J.W., Damsté, J.S.S., 1998. Postdepositional oxic degradation of alkenones: Implications for the measurement of palaeo sea surface temperatures. *Paleoceanography* 13, 42-49.
- Hönisch, B., Allen, K.A., Lea, D.W., Spero, H.J., Eggins, S.M., Arbuszewski, J., deMenocal, P., Rosenthal, Y., Russell, A.D., Elderfield, H., 2013. The influence of salinity on Mg/Ca in planktic foraminifers – Evidence from cultures, core-top sediments and complementary $\delta^{18}\text{O}$. *Geochimica et Cosmochimica Acta* 121, 196-213.
- Hopmans, E.C., Weijers, J.W.H., Schefuß, E., Herfort, L., Sinninghe Damsté, J.S., Schouten, S., 2004. A novel proxy for terrestrial organic matter in sediments based on branched and isoprenoid tetraether lipids. *Earth and Planetary Science Letters* 224, 107-116.
- Huguet, C., Martrat, B., Grimalt, J.O., Damsté, J.S.S., Schouten, S., 2011. Coherent millennial-scale patterns in U^{K}_{37} and $\text{TEX}^{\text{H}}_{86}$ temperature records during the penultimate interglacial-to-glacial cycle in the western Mediterranean. *Paleoceanography* 26.
- Hut, G., 1987. Consultants' group meeting on stable isotope reference samples for geochemical and hydrological investigations. International Atomic Energy Agency, Vienna (Austria).
- Ignacio Martinez, J., Deckker, P.D., Chivas, A.R., 1997. New estimates for salinity changes in the Western Pacific Warm Pool during the Last Glacial Maximum: Oxygen-isotope evidence. *Marine Micropaleontology* 32, 311-340.
- Ikehara, M., Kawamura, K., Ohkouchi, N., Murayama, M., Nakamura, T., Taira, A., 2000. Variations of terrestrial input and marine productivity in the Southern Ocean (48°S) during the last two deglaciations. *Paleoceanography* 15, 170-180.
- IPCC, 2007. Contribution of Working Group I to the Fourth Assessment Report of the Intergovernmental Panel on Climate Change, 2007 in: Solomon, S., D. Qin, M. Manning, Z. Chen, M. Marquis, K.B. Averyt, M. Tignor and H.L. Miller (Ed.), *Climate Change 2007*. Cambridge University Press, Cambridge, United Kingdom and New York, NY, USA.
- Johns, R.B., Gillan, F.T., Volkman, J.K., 1980. Early diagenesis of phytol esters in a contemporary temperate intertidal sediment. *Geochimica et Cosmochimica Acta* 44, 183-188.
- Jungclaus, J.H., Keenlyside, N., Botzet, M., Haak, H., Luo, J.J., Latif, M., Marotzke, J., Mikolajewicz, U., Roeckner, E., 2006. Ocean Circulation and Tropical Variability in the Coupled Model ECHAM5/MPI-OM. *Journal of Climate* 19, 3952-3972.
- Karl, T.R., Trenberth, K.E., 2003. Modern Global Climate Change. *Science* 302, 1719-1723.

- Karner, M.B., DeLong, E.F., Karl, D.M., 2001. Archaeal dominance in the mesopelagic zone of the Pacific Ocean. *Nature* 409, 507-510.
- Kasper, S., van der Meer, M.T.J., Castañeda, I.S., Tjallingii, R., Brummer, G.-J.A., Sinninghe Damsté, J.S., Schouten, S., 2015. Testing the alkenone D/H ratio as a paleo indicator of sea surface salinity in a coastal ocean margin (Mozambique Channel). *Organic Geochemistry* 78, 62-68.
- Kasper, S., van der Meer, M.T.J., Mets, A., Zahn, R., Sinninghe Damsté, J.S., Schouten, S., 2014. Salinity changes in the Agulhas leakage area recorded by stable hydrogen isotopes of C₃₇ alkenones during Termination I and II. *Clim. Past* 10, 251-260.
- Keeling, R.F., Stephens, B.B., 2001. Antarctic sea ice and the control of Pleistocene climate instability. *Paleoceanography* 16, 112-131.
- Kim, J.-H., Crosta, X., Michel, E., Schouten, S., Duprat, J., Sinninghe Damsté, J.S., 2009a. Impact of lateral transport on organic proxies in the Southern Ocean. *Quaternary Research* 71, 246-250.
- Kim, J.H., Buscaill, R., Bourrin, F., Palanques, A., Sinninghe Damsté, J.S., Bonnin, J., Schouten, S., 2009b. Transport and depositional process of soil organic matter during wet and dry storms on the Têt inner shelf (NW Mediterranean). *Palaeogeography, Palaeoclimatology, Palaeoecology* 273, 228-238.
- Kim, J.-H., Ludwig, W., Schouten, S., Kerhervé, P., Herfort, L., Bonnin, J., Sinninghe Damsté, J.S., 2007. Impact of flood events on the transport of terrestrial organic matter to the ocean: A study of the Têt River (SW France) using the BIT index. *Organic Geochemistry* 38, 1593-1606.
- Kim, J.H., Schouten, S., Hopmans, E.C., Donner, B., Damsté, J.S.S., 2008. Global sediment core-top calibration of the TEX₈₆ paleothermometer in the ocean. *Geochimica et Cosmochimica Acta* 72, 1154-1173.
- Kim, J.H., van der Meer, J., Schouten, S., Helmke, P., Willmott, V., Sangiorgi, F., Koc, N., Hopmans, E.C., Damsté, J.S.S., 2010. New indices and calibrations derived from the distribution of crenarchaeal isoprenoid tetraether lipids: Implications for past sea surface temperature reconstructions. *Geochimica et Cosmochimica Acta* 74, 4639-4654.
- Kim, S.-T., O'Neil, J.R., 1997. Equilibrium and nonequilibrium oxygen isotope effects in synthetic carbonates. *Geochimica et Cosmochimica Acta* 61, 3461-3475.
- Kinkel, H., Baumann, K.H., Čepok, M., 2000. Coccolithophores in the equatorial Atlantic Ocean: response to seasonal and Late Quaternary surface water variability. *Marine Micropaleontology* 39, 87-112.
- Klinck, J.M., Smith, D.A., 1993. Effect of wind changes during the Last Glacial Maximum on the circulation in the Southern Ocean. *Paleoceanography* 8, 427-433.
- Knoll, M., Hernández-Guerra, A., Lenz, B., López Laatzén, F., Machín, F., Müller, T.J., Siedler, G., 2002. The Eastern Boundary Current system between the Canary Islands and the African Coast. *Deep Sea Research Part II: Topical Studies in Oceanography* 49, 3427-3440.
- Knorr, G., Lohmann, G., 2003. Southern Ocean origin for the resumption of Atlantic thermohaline circulation during deglaciation. *Nature* 424, 532-536.
- Knorr, G., Lohmann, G., 2007. Rapid transitions in the Atlantic thermohaline circulation triggered by global warming and meltwater during the last deglaciation. *Geochemistry, Geophysics, Geosystems* 8, Q12006.
- Krishnamurthy, R.V., Meyers, P.A., Lovan, N.A., 2000. Isotopic evidence of sea-surface freshening, enhanced productivity, and improved organic matter preservation during sapropel deposition in the Tyrrhenian Sea. *Geology* 28, 263-266.

- Kucera, M., Weinelt, M., Kiefer, T., Pflaumann, U., Hayes, A., Weinelt, M., Chen, M.-T., Mix, A.C., Barrows, T.T., Cortijo, E., Duprat, J., Juggins, S., Waelbroeck, C., 2005. Reconstruction of sea-surface temperatures from assemblages of planktonic foraminifera: multi-technique approach based on geographically constrained calibration data sets and its application to glacial Atlantic and Pacific Oceans. *Quaternary Science Reviews* 24, 951-998.
- Kuhlbrodt, T., Griesel, A., Montoya, M., Levermann, A., Hofmann, M., Rahmstorf, S., 2007. On the driving processes of the Atlantic meridional overturning circulation. *Reviews of Geophysics* 45, RG2001.
- Le Vine, D.M., Kao, M., Garvine, R.W., Sanders, T., 1998. Remote Sensing of Ocean Salinity: Results from the Delaware Coastal Current Experiment. *Journal of Atmospheric and Oceanic Technology* 15, 1478-1484.
- Lea, D.W., Mashiotta, T.A., Spero, H.J., 1999. Controls on magnesium and strontium uptake in planktonic foraminifera determined by live culturing. *Geochimica et Cosmochimica Acta* 63, 2369-2379.
- Lear, C.H., Rosenthal, Y., Slowey, N., 2002. Benthic foraminiferal Mg/Ca-paleothermometry: a revised core-top calibration. *Geochimica et Cosmochimica Acta* 66, 3375-3387.
- Leduc, G., Sachs, J.P., Kawka, O.E., Schneider, R.R., 2013. Holocene changes in eastern equatorial Atlantic salinity as estimated by water isotopologues. *Earth and Planetary Science Letters* 362, 151-162.
- Lee, K.E., Kim, J.-H., Wilke, I., Helmke, P., Schouten, S., 2008. A study of the alkenone, TEX₈₆, and planktonic foraminifera in the Benguela Upwelling System: Implications for past sea surface temperature estimates. *Geochemistry, Geophysics, Geosystems* 9, Q10019.
- Lehman, S.J., Keigwin, L.D., 1992. Sudden changes in North Atlantic circulation during the last deglaciation. *Nature* 356, 757-762.
- Levitus, S., Antonov, J.I., Baranova, O., Boyer, T., Coleman, C., Garcia, H.E., Grodsky, A., Johnson, D., Locarnini, R., Mishonov, A., 2013. The World Ocean Database Data Science Journal 12, WDS229-WDS234.
- Libes, S., 2009. Introduction to marine biogeochemistry. Academic Press.
- Lippold, J., Luo, Y., Francois, R., Allen, S.E., Gherardi, J., Pichat, S., Hickey, B., Schulz, H., 2012. Strength and geometry of the glacial Atlantic Meridional Overturning Circulation. *Nature Geosci* 5, 813-816.
- Lisiecki, L.E., Raymo, M.E., 2005. A Pliocene-Pleistocene stack of 57 globally distributed benthic $\delta^{18}\text{O}$ records. *Paleoceanography* 20, PA1003.
- Liu, W., Liu, Z., Fu, M., An, Z., 2008. Distribution of the C₃₇ tetra-unsaturated alkenone in Lake Qinghai, China: A potential lake salinity indicator. *Geochimica et Cosmochimica Acta* 72, 988-997.
- Liu, W., Liu, Z., Wang, H., He, Y., Wang, Z., Xu, L., 2011. Salinity control on long-chain alkenone distributions in lake surface waters and sediments of the northern Qinghai-Tibetan Plateau, China. *Geochimica et Cosmochimica Acta* 75, 1693-1703.
- Locarnini, R.A., A. V. Mishonov, J. I. Antonov, T. P. Boyer, H. E. Garcia, O. K. Baranova, M. M. Zweng, and D. R. Johnson, 2010. World Ocean Atlas 2009, Volume 1: Temperature. S. Levitus, Ed. NOAA Atlas NESDIS 68, U.S. Government Printing Office, Washington, D.C. 1, 184 pp.
- Lohmann, G., 2003. Atmospheric and oceanic freshwater transport during weak Atlantic overturning circulation. *Tellus A* 55, 438-449.
- Lohmann, G.P., 1995. A model for variation in the chemistry of planktonic foraminifera due to secondary calcification and selective dissolution. *Paleoceanography* 10, 445-457.

- Lopes dos Santos, R., 2012. Reconstruction of late Quarternary marine and terrestrial environmental conditions of Northwest Africa and Southeast Australia: a multiple organic proxy study using marine sediments. University of Utrecht.
- Lopes dos Santos, R.A., De Deckker, P., Hopmans, E.C., Magee, J.W., Mets, A., Sinninghe Damsté, J.S., Schouten, S., 2013a. Abrupt vegetation change after the Late Quaternary megafaunal extinction in southeastern Australia. *Nature Geoscience* 6, 627-631.
- Lopes dos Santos, R.A., Prange, M., Castañeda, I.S., Schefuß, E., Mulitza, S., Schulz, M., Niedermeyer, E.M., Sinninghe Damsté, J.S., Schouten, S., 2010. Glacial–interglacial variability in Atlantic meridional overturning circulation and thermocline adjustments in the tropical North Atlantic. *Earth and Planetary Science Letters* 300, 407-414.
- Lopes dos Santos, R.A., Spooner, M.I., Barrows, T.T., De Deckker, P., Sinninghe Damsté, J.S., Schouten, S., 2013b. Comparison of organic ($U^{K'}$, TEX_{86}^H , LDI) and faunal proxies (foraminiferal assemblages) for reconstruction of late Quaternary sea surface temperature variability from offshore southeastern Australia. *Paleoceanography* 28, 377-387.
- Lopes dos Santos, R.A., Wilkins, D., De Deckker, P., Schouten, S., 2012. Late Quaternary productivity changes from offshore Southeastern Australia: A biomarker approach. *Palaeogeography, Palaeoclimatology, Palaeoecology* 363–364, 48-56.
- Lutjeharms, J.R.E., 1988. Remote sensing corroboration of retroflexion of the East Madagascar Current. *Deep Sea Research Part A. Oceanographic Research Papers* 35, 2045-2050.
- Lutjeharms, J.R.E., 2006. *The Agulhas Current*. Springer, Berlin.
- Lutjeharms, J.R.E., Anson, I.J., 2001. The Agulhas Return Current. *Journal of Marine Systems* 30, 115-138.
- M'Boule, D., Chivall, D., Sinke-Schoen, D., Sinninghe Damsté, J.S., Schouten, S., van der Meer, M.T.J., 2014. Salinity dependent hydrogen isotope fractionation in alkenones produced by coastal and open ocean haptophyte algae. *Geochimica et Cosmochimica Acta* 130, 126-135.
- Manabe, S., 1969. Climate and the ocean circulation 1. *Monthly Weather Review* 97, 739-774.
- Manabe, S., Bryan, K., Spelman, M.J., 1979. A global ocean-atmosphere climate model with seasonal variation for future studies of climate sensitivity. *Dynamics of Atmospheres and Oceans* 3, 393-426.
- Manabe, S., Stouffer, R.J., 1997. Coupled ocean-atmosphere model response to freshwater input: Comparison to Younger Dryas Event. *Paleoceanography* 12, 321-336.
- Marino, G., Zahn, R., Ziegler, M., Purcell, C., Knorr, G., Hall, I.R., Ziveri, P., Elderfield, H., 2013. Agulhas salt-leakage oscillations during abrupt climate changes of the Late Pleistocene. *Paleoceanography*, 599-606.
- Marlowe, I.T., Brassell, S.C., Eglinton, G., Green, J.C., 1984a. Long chain unsaturated ketones and esters in living algae and marine sediments. *Organic Geochemistry* 6, 135-141.
- Marlowe, I.T., Brassell, S.C., Eglinton, G., Green, J.C., 1990. Long-chain alkenones and alkyl alkenoates and the fossil coccolith record of marine sediments. *Chemical Geology* 88, 349-375.
- Marlowe, I.T., Green, J.C., Neal, A.C., Brassell, S.C., Eglinton, G., Course, P.A., 1984b. Long chain ($n-C_{37}$ - C_{39}) alkenones in the Prymnesiophyceae. Distribution of alkenones and other lipids and their taxonomic significance. *British Phycological Journal* 19, 203 - 216.
- Martin, J.H., 1990. Glacial-interglacial CO_2 change: The Iron Hypothesis. *Paleoceanography* 5, 1-13.
- Martínez-García, A., Sigman, D.M., Ren, H., Anderson, R.F., Straub, M., Hodell, D.A., Jaccard, S.L., Eglinton, T.I., Haug, G.H., 2014. Iron Fertilization of the Subantarctic Ocean During the Last Ice Age. *Science* 343, 1347-1350.

- Martinez-Mendez, G., Zahn, R., Hall, I.R., Peeters, F.J.C., Pena, L.D., Cacho, I., Negre, C., 2010. Contrasting multiproxy reconstructions of surface ocean hydrography in the Agulhas Corridor and implications for the Agulhas Leakage during the last 345,000 years. *Paleoceanography* 25, 12.
- Martinez-Mendez, G., Zahn, R., Hall, I.R., Pena, L.D., Cacho, I., 2008. 345,000-year-long multiproxy records off South Africa document variable contributions of Northern versus Southern Component Water to the Deep South Atlantic. *Earth and Planetary Science Letters* 267, 309-321.
- März, C., Hoffmann, J., Bleil, U., de Lange, G.J., Kasten, S., 2008. Diagenetic changes of magnetic and geochemical signals by anaerobic methane oxidation in sediments of the Zambezi deep-sea fan (SW Indian Ocean). *Marine Geology* 255, 118-130.
- Mashiotta, T.A., Lea, D.W., Spero, H.J., 1999. Glacial-interglacial changes in Subantarctic sea surface temperature and $\delta^{18}\text{O}$ -water using foraminiferal Mg. *Earth and Planetary Science Letters* 170, 417-432.
- Mazeika, P.A., 1967. Thermal domes in the eastern tropical Atlantic Ocean. *Limnology and Oceanography* 12, 537-539.
- McIntyre, A., Cline, R., 1981. Seasonal reconstructions of the earth's surface at the last glacial maximum. Geological Society of America.
- McManus, J.F., Francois, R., Gherardi, J.M., Keigwin, L.D., Brown-Leger, S., 2004. Collapse and rapid resumption of Atlantic meridional circulation linked to deglacial climate changes. *Nature* 428, 834-837.
- Ménot, G., Bard, E., Rostek, F., Weijers, J.W.H., Hopmans, E.C., Schouten, S., Damsté, J.S.S., 2006. Early Reactivation of European Rivers During the Last Deglaciation. *Science* 313, 1623-1625.
- Meybeck, M., 1982. Carbon, nitrogen, and phosphorus transport by world rivers. *American Journal of Science* 282, 401-450.
- Middleton, J.F., Arthur, C., Van Ruth, P., Ward, T.M., McClean, J.L., Maltrud, M.E., Gill, P., Levings, A., Middleton, S., 2007. El Niño Effects and Upwelling off South Australia. *Journal of Physical Oceanography* 37, 2458-2477.
- Mix, A.C., Bard, E., Schneider, R., 2001. Environmental processes of the ice age: land, oceans, glaciers (EPILOG). *Quaternary Science Reviews* 20, 627-657.
- Mohtadi, M., Steinke, S., Groeneveld, J., Fink, H.G., Rixen, T., Hebbeln, D., Donner, B., Herunadi, B., 2009. Low-latitude control on seasonal and interannual changes in planktonic foraminiferal flux and shell geochemistry off south Java: A sediment trap study. *Paleoceanography* 24, PA1201.
- Mollenhauer, G., McManus, J.F., Benthien, A., Müller, P.J., Eglinton, T.I., 2006. Rapid lateral particle transport in the Argentine Basin: Molecular ^{14}C and ^{230}Th evidence. *Deep Sea Research Part I: Oceanographic Research Papers* 53, 1224-1243.
- Mulitza, S., Boltovskoy, D., Donner, B., Meggers, H., Paul, A., Wefer, G., 2003. Temperature: $\delta^{18}\text{O}$ relationships of planktonic foraminifera collected from surface waters. *Palaeogeography, Palaeoclimatology, Palaeoecology* 202, 143-152.
- Mulitza, S., Bouimtarhan, I., Brüning, M., Freeseemann, A., Gussone, N., Filipson, H., Heil, G., Hessler, S., Jaeschke, A., Johnstone, H., Klann, M., Klein, F., Küster, K., März, C., McGregor, H., Minning, M., Müller, H., Ochsenhirt, W., Paul, A., Schewe, F., Schulz, M., Steinlöchner, J., Stuetz, J., Tjallingii, R., Dobeneck, T., Wiesmaier, S., Zabel, M., Zonneveld, K., 2006. Report and preliminary results of Meteor-Cruise M65/1, Dakar-Dakar, 11.06.-01.07.2005, Berichte aus dem Fachbereich Geowissenschaften der Universität Bremen. Fachbereich Geowissenschaften, Universität Bremen, pp. 1-149.

- Mulitza, S., Prange, M., Stuut, J.-B., Zabel, M., von Dobeneck, T., Itambi, A.C., Nizou, J., Schulz, M., Wefer, G., 2008. Sahel megadroughts triggered by glacial slowdowns of Atlantic meridional overturning. *Paleoceanography* 23, PA4206.
- Müller, P.J., Kirst, G., Ruhland, G., von Storch, I., Rosell-Melé, A., 1998. Calibration of the alkenone paleotemperature index $U^{K'_{37}}$ based on core-tops from the eastern South Atlantic and the global ocean (60°N-60°S). *Geochimica et Cosmochimica Acta* 62, 1757-1772.
- Nelson, D.B., Sachs, J.P., 2014. The influence of salinity on D/H fractionation in dinosterol and brassicasterol from globally distributed saline and hypersaline lakes. *Geochimica et Cosmochimica Acta* 133, 325-339.
- NGRIP, 2004. High-resolution record of Northern Hemisphere climate extending into the last interglacial period. *Nature* 431, 147-151.
- Niebler, H.S., Hubberten, H.W., Gersonde, R., 1999. Oxygen isotope values of planktic foraminifera: A tool for the reconstruction of surface water stratification, in: Fischer, G., Wefer, G. (Eds.), *Use of Proxies in Paleoceanography*. Springer Berlin Heidelberg, pp. 165-189.
- Noble, P.A., Tymowski, R.G., Fletcher, M., Morris, J.T., Lewitus, A.J., 2003. Contrasting patterns of phytoplankton community pigment composition in two salt marsh estuaries in southeastern United States. *Applied and Environmental Microbiology* 69, 4129-4143.
- Nürnberg, D., Bijma, J., Hemleben, C., 1996. Assessing the reliability of magnesium in foraminiferal calcite as a proxy for water mass temperatures. *Geochimica et Cosmochimica Acta* 60, 803-814.
- Nürnberg, D., Groeneveld, J., 2006. Pleistocene variability of the Subtropical Convergence at East Tasman Plateau: Evidence from planktonic foraminiferal Mg/Ca (ODP Site 1172A). *Geochemistry, Geophysics, Geosystems* 7, Q04P11.
- Nürnberg, D., Müller, A., Schneider, R.R., 2000. Paleo-sea surface temperature calculations in the equatorial east Atlantic from Mg/Ca ratios in planktic foraminifera: A comparison to sea surface temperature estimates from $U^{K'_{37}}$ oxygen isotopes, and foraminiferal transfer function. *Paleoceanography* 15, 124-134.
- Ohkouchi, N., Eglinton, T.I., Keigwin, L.D., Hayes, J.M., 2002. Spatial and Temporal Offsets Between Proxy Records in a Sediment Drift. *Science* 298, 1224-1227.
- Örnólfssdóttir, E.B., Lumsden, S.E., Pinckney, J.L., 2004. Phytoplankton community growth-rate response to nutrient pulses in a shallow turbid estuary, Galveston Bay, Texas. *Journal of Plankton Research* 26, 325-339.
- Pahnke, K., Sachs, J.P., Keigwin, L., Timmermann, A., Xie, S.-P., 2007. Eastern tropical Pacific hydrologic changes during the past 27,000 years from D/H ratios in alkenones. *Paleoceanography* 22, PA4214.
- Pahnke, K., Zahn, R., Elderfield, H., Schulz, M., 2003. 340,000-year centennial-scale marine record of southern hemisphere climatic oscillation. *Science* 301, 948-952.
- Parnell, A.C., Buck, C.E., Doan, T.K., 2011. A review of statistical chronology models for high-resolution, proxy-based Holocene palaeoenvironmental reconstruction. *Quaternary Science Reviews* 30, 2948-2960.
- Parnell, A.C., Haslett, J., Allen, J.R.M., Buck, C.E., Huntley, B., 2008. A flexible approach to assessing synchronicity of past events using Bayesian reconstructions of sedimentation history. *Quaternary Science Reviews* 27, 1872-1885.
- Paul, H.A., 2002. Application of novel stable isotope methods to reconstruct paleoenvironments: Compound-specific hydrogen isotope and pore-water oxygen isotopes. Swiss Federal Institute of Technology.

- Pawlowicz, R., 2013. Key physical variables in the ocean: temperature, salinity, and density. *Nature Education Knowledge* 4, 13.
- Pedersen, M.F., Borum, J., 1996. Nutrient control of algal growth in estuarine waters. Nutrient limitation and the importance of nitrogen requirements and nitrogen storage among phytoplankton and species of macroalgae. *Marine ecology progress series. Oldendorf* 142, 261-272.
- Peeters, F.J.C., Acheson, R., Brummer, G.J.A., de Ruijter, W.P.M., Schneider, R.R., Ganssen, G.M., Ufkes, E., Kroon, D., 2004. Vigorous exchange between the Indian and Atlantic oceans at the end of the past five glacial periods. *Nature* 430, 661-665.
- Penven, P., Lutjeharms, J.R.E., Florenchie, P., 2006. Madagascar: A pacemaker for the Agulhas Current system? *Geophysical Research Letters* 33, L17609.
- Peterson, R.G., Stramma, L., 1991. Upper-level circulation in the South Atlantic Ocean. *Progress in Oceanography* 26, 1-73.
- Prahl, F.G., Muehlhausen, L.A., Zahnle, D.L., 1988. Further evaluation of long-chain alkenones as indicators of paleoceanographic conditions. *Geochimica et Cosmochimica Acta* 52, 2303-2310.
- Prahl, F.G., Rontani, J.-F., Volkman, J.K., Sparrow, M.A., Royer, I.M., 2006. Unusual C₃₅ and C₃₆ alkenones in a paleoceanographic benchmark strain of *Emiliania huxleyi*. *Geochimica et Cosmochimica Acta* 70, 2856-2867.
- Prahl, F.G., Sparrow, M.A., Wolfe, G.V., 2003. Physiological impacts on alkenone paleothermometry. *Paleoceanography* 18, 1025.
- Prahl, F.G., Wakeham, S.G., 1987. Calibration of unsaturation patterns in long-chain ketone compositions for paleotemperature assessment. *Nature* 330, 367-369.
- Purcell, C., Knorr, G., Hall, I.R., Lohmann, G.P., Stepanek, C., in review. Warm and cold water route gateway transport changes during abrupt climate shifts. *Paleoceanography*.
- Rackebrandt, N., Kuhnert, H., Groeneveld, J., Bickert, T., 2011. Persisting maximum Agulhas leakage during MIS 14 indicated by massive *Ethmodiscus* oozes in the subtropical South Atlantic. *Paleoceanography* 26, PA3202.
- Rahmstorf, S., 1995. Bifurcations of the Atlantic thermohaline circulation in response to changes in the hydrological cycle. *Nature* 378, 145-149.
- Rahmstorf, S., 1996. On the freshwater forcing and transport of the Atlantic thermohaline circulation. *Climate Dynamics* 12, 799-811.
- Rahmstorf, S., 2000. The thermohaline ocean circulation: A system with dangerous thresholds? *Climatic Change* 46, 247-256.
- Rahmstorf, S., 2002. Ocean circulation and climate during the past 120,000 years. *Nature* 419, 207-214.
- Rahmstorf, S., 2003. Thermohaline circulation: The current climate. *Nature* 421, 699-699.
- Ramanathan, V., 1981. The role of ocean-atmosphere interactions in the CO₂ Climate Problem. *Journal of the Atmospheric Sciences* 38, 918-930.
- Rau, A.J., Rogers, J., Lutjeharms, J.R.E., Giraudeau, J., Lee-Thorp, J.A., Chen, M.T., Waelbroeck, C., 2002. A 450-kyr record of hydrological conditions on the western Agulhas Bank Slope, south of Africa. *Marine Geology* 180, 183-201.
- Rau, G.H., Riebesell, U., Wolf Gladrow, D., 1996. A model of photosynthetic ¹³C fractionation by marine phytoplankton based on diffusive molecular CO₂ uptake. *Marine Ecology Progress Series* 133, 275-285.

- Reichler, T., Kim, J., 2008. How Well Do Coupled Models Simulate Today's Climate? *Bulletin of the American Meteorological Society* 89, 303-311.
- Reimer, P., Baillie, M., Bard, E., Bayliss, A., Beck, J., Blackwell, P., Bronk Ramsey, C., Buck, C., Burr, G., Edwards, R., 2009. IntCal09 and Marine09 radiocarbon age calibration curves, 0-50,000 years cal BP. *Radiocarbon* 51, 1111-1150.
- Reimer, P.J., Baillie, M.G.L., Bard, E., Bayliss, A., Beck, J.W., Blackwell, P.G., Ramsey, C.B., Buck, C.E., Burr, G.S., Edwards, R.L., Friedrich, M., Grootes, P.M., Guilderson, T.P., Hajdas, I., Heaton, T.J., Hogg, A.G., Hughen, K.A., Kaiser, K.F., Kromer, B., McCormac, F.G., Manning, S.W., Reimer, R.W., Richards, D.A., Southon, J.R., Talamo, S., Turney, C.S.M., van der Plicht, J., Weyhenmeyer, C.E., 2011. IntCal09 and Marine09 Radiocarbon Age Calibration Curves, 0-50,000 Years cal BP.
- Renold, M., Raible, C.C., Yoshimori, M., Stocker, T.F., 2010. Simulated resumption of the North Atlantic meridional overturning circulation – Slow basin-wide advection and abrupt local convection. *Quaternary Science Reviews* 29, 101-112.
- Richardson, P.L., Reverdin, G., 1987. Seasonal cycle of velocity in the Atlantic North Equatorial Countercurrent as measured by surface drifters, current meters, and ship drifts. *Journal of Geophysical Research: Oceans* 92, 3691-3708.
- Ridderinkhof, H., van der Werf, P.M., Ullgren, J.E., van Aken, H.M., van Leeuwen, P.J., de Ruijter, W.P.M., 2010. Seasonal and interannual variability in the Mozambique Channel from moored current observations. *Journal of Geophysical Research: Oceans* 115, C06010.
- Rintoul, S.R., Donguy, J.R., Roemmich, D.H., 1997. Seasonal evolution of upper ocean thermal structure between Tasmania and Antarctica. *Deep Sea Research Part I: Oceanographic Research Papers* 44, 1185-1202.
- Rohling, E.J., 2000. Paleosalinity: confidence limits and future applications. *Marine Geology* 163, 1-11.
- Rohling, E.J., 2007. Progress in paleosalinity: Overview and presentation of a new approach. *Paleoceanography* 22, PA3215.
- Rohling, E.J., Bigg, G.R., 1998. Paleosalinity and $\delta^{18}\text{O}$: A critical assessment. *Journal of Geophysical Research-Oceans* 103, 1307-1318.
- Rohling, E.J., Grant, K., Bolshaw, M., Roberts, A.P., Siddall, M., Hemleben, C., Kucera, M., 2009. Antarctic temperature and global sea level closely coupled over the past five glacial cycles. *Nature Geoscience* 2, 500-504.
- Roman, R.E., Lutjeharms, J.R.E., 2009. Red Sea Intermediate Water in the source regions of the Agulhas Current. *Deep Sea Research Part I: Oceanographic Research Papers* 56, 939-962.
- Rontani, J.-F., Prahl, F.G., Volkman, J.K., 2006. Re-examination of the double bond positions in alkenones and derivatives: biosynthetic implications *Journal of Phycology* 42, 800-813.
- Rontani, J.-F., Volkman, J.K., 2003. Phytol degradation products as biogeochemical tracers in aquatic environments. *Organic Geochemistry* 34, 1-35.
- Rosenthal, Y., Perron-Cashman, S., Lear, C.H., Bard, E., Barker, S., Billups, K., Bryan, M., Delaney, M.L., deMenocal, P.B., Dwyer, G.S., Elderfield, H., German, C.R., Greaves, M., Lea, D.W., Marchitto, T.M., Pak, D.K., Paradis, G.L., Russell, A.D., Schneider, R.R., Scheiderich, K., Stott, L., Tachikawa, K., Tappa, E., Thunell, R., Wara, M., Weldeab, S., Wilson, P.A., 2004. Interlaboratory comparison study of Mg/Ca and Sr/Ca measurements in planktonic foraminifera for paleoceanographic research. *Geochemistry, Geophysics, Geosystems* 5, Q04D09.

- Rosenthal, Y., et al. (2004), Interlaboratory comparison study of Mg/Ca and Sr/Ca measurements in planktonic foraminifera for paleoceanographic research, *Geochemistry, Geophysics, Geosystems*, 5(4), Q04D09. doi: 10.1029/2003gc000650
- Rostek, F., Ruhlandt, G., Bassinot, F.C., Muller, P.J., Labeyrie, L.D., Lancelot, Y., Bard, E., 1993. Reconstructing sea surface temperature and salinity using $\delta^{18}\text{O}$ and alkenone records. *Nature* 364, 319-321.
- Rouault, M., Penven, P., Pohl, B., 2009. Warming in the Agulhas Current system since the 1980's. *Geophysical Research Letters* 36, L12602.
- Rudnick, D.L., Ferrari, R., 1999. Compensation of horizontal temperature and salinity gradients in the ocean mixed layer. *Science* 283, 526-529.
- Rühlemann, C., Butzin, M., 2006. Alkenone temperature anomalies in the Brazil-Malvinas Confluence area caused by lateral advection of suspended particulate material. *Geochemistry, Geophysics, Geosystems* 7, Q10015.
- Ruhlemann, C., Mulitza, S., Muller, P.J., Wefer, G., Zahn, R., 1999. Warming of the tropical Atlantic Ocean and slowdown of thermohaline circulation during the last deglaciation. *Nature* 402, 511-514.
- Rühs, S., Durgadoo, J.V., Behrens, E., Biastoch, A., 2013. Advective timescales and pathways of Agulhas leakage. *Geophysical Research Letters* 40, 3997-4000.
- Sachs, J.P., Anderson, R.F., 2003. Fidelity of alkenone paleotemperatures in southern Cape Basin sediment drifts. *Paleoceanography* 18, 1082.
- Sachse, D., Billault, I., Bowen, G.J., Chikaraishi, Y., Dawson, T.E., Feakins, S.J., Freeman, K.H., Magill, C.R., McInerney, F.A., van der Meer, M.T.J., Polissar, P., Robins, R.J., Sachs, J.P., Schmidt, H.-L., Sessions, A.L., White, J.W.C., West, J.B., Kahmen, A., 2012. Molecular paleohydrology: Interpreting the hydrogen-isotopic composition of lipid biomarkers from photosynthesizing organisms. *Annual Review of Earth and Planetary Sciences* 40, 221-249.
- Sætre, R., Da Silva, A.J., 1984. The circulation of the Mozambique channel. *Deep Sea Research Part A. Oceanographic Research Papers* 31, 485-508.
- Saher, M.H., Rostek, F., Jung, S.J.A., Bard, E., Schneider, R.R., Greaves, M., Ganssen, G.M., Elderfield, H., Kroon, D., 2009. Western Arabian Sea SST during the penultimate interglacial: A comparison of U^{K}_{37} and Mg/Ca paleothermometry. *Paleoceanography* 24, PA2212.
- Sarnthein, M., Winn, K., Jung, S.J.A., Duplessy, J.-C., Labeyrie, L., Erlenkeuser, H., Ganssen, G., 1994. Changes in East Atlantic Deepwater Circulation over the last 30,000 years: Eight time slice reconstructions. *Paleoceanography* 9, 209-267.
- Sauer, P.E., Eglinton, T.I., Hayes, J.M., Schimmelmann, A., Sessions, A.L., 2001. Compound-specific D/H ratios of lipid biomarkers from sediments as a proxy for environmental and climatic conditions. *Geochimica et Cosmochimica Acta* 65, 213-222.
- Sawada, K., Handa, N., Nakatsuka, T., 1998. Production and transport of long-chain alkenones and alkyl alkenoates in a sea water column in the northwestern Pacific off central Japan. *Marine Chemistry* 59, 219-234.
- Schefuss, E., Kuhlmann, H., Mollenhauer, G., Prange, M., Patzold, J., 2011. Forcing of wet phases in southeast Africa over the past 17,000 years. *Nature* 480, 509-512.
- Schimmelmann, A., Lewan, M.D., Wintsch, R.P., 1999. D/H isotope ratios of kerogen, bitumen, oil, and water in hydrous pyrolysis of source rocks containing kerogen types I, II, IIS, and III. *Geochimica et Cosmochimica Acta* 63, 3751-3766.
- Schmid, C., Boebel, O., Zenk, W., Lutjeharms, J.R.E., Garzoli, S.L., Richardson, P.L., Barron, C., 2003. Early evolution of an Agulhas Ring. *Deep Sea Research Part II: Topical Studies in Oceanography* 50, 141-166.

- Schmidt, G.A., 1999a. Error analysis of paleosalinity calculations. *Paleoceanography* 14, 422-429.
- Schmidt, G.A., G. R. Bigg and E. J. Rohling, 1999b. Global Seawater Oxygen-18 Database - v1.21, <http://data.giss.nasa.gov/o18data/>
- Schmidt, M.W., Spero, H.J., Lea, D.W., 2004. Links between salinity variation in the Caribbean and North Atlantic thermohaline circulation. *Nature* 428, 160-163.
- Schneider, R.R., Muller, P.J., Ruhland, G., 1995. Late Quaternary surface circulation in the east equatorial South Atlantic: Evidence from Alkenone sea surface temperatures. *Paleoceanography* 10, 197-219.
- Schouten, M.W., de Ruijter, W.P.M., van Leeuwen, P.J., Ridderinkhof, H., 2003. Eddies and variability in the Mozambique Channel. *Deep Sea Research Part II: Topical Studies in Oceanography* 50, 1987-2003.
- Schouten, S., Hopmans, E.C., Pancost, R.D., Sinninghe Damsté, J.S., 2000. Widespread occurrence of structurally diverse tetraether membrane lipids: Evidence for the ubiquitous presence of low-temperature relatives of hyperthermophiles. *Proceedings of the National Academy of Sciences of the United States of America* 97, 14421-14426.
- Schouten, S., Hopmans, E.C., Schefuß, E., Sinninghe Damsté, J.S., 2002. Distributional variations in marine crenarchaeotal membrane lipids: a new tool for reconstructing ancient sea water temperatures? *Earth and Planetary Science Letters* 204, 265-274.
- Schouten, S., Hopmans, E.C., Sinninghe Damsté, J.S., 2013. The organic geochemistry of glycerol dialkyl glycerol tetraether lipids: A review. *Organic Geochemistry* 54, 19-61.
- Schouten, S., Hugué, C., Hopmans, E.C., Kienhuis, M.V.M., Sinninghe Damsté, J.S., 2007. Analytical methodology for TEX₈₆ paleothermometry by high-performance liquid chromatography/atmospheric pressure chemical ionization-mass spectrometry. *Analytical Chemistry* 79, 2940-2944.
- Schouten, S., Ossebaar, J., Schreiber, K., Kienhuis, M.V.M., Langer, G., Benthien, A., Bijma, J., 2006. The effect of temperature, salinity and growth rate on the stable hydrogen isotopic composition of long chain alkenones produced by *Emiliania huxleyi* and *Gephyrocapsa oceanica*. *Biogeosciences* 3, 113-119.
- Schrag, D.P., Adkins, J.F., McIntyre, K., Alexander, J.L., Hodell, D.A., Charles, C.D., McManus, J.F., 2002. The oxygen isotopic composition of seawater during the Last Glacial Maximum. *Quaternary Science Reviews* 21, 331-342.
- Schulz, H.-M., Schöner, A., Emeis, K.-C., 2000. Long-chain alkenone patterns in the Baltic sea--an ocean-freshwater transition. *Geochimica et Cosmochimica Acta* 64, 469-477.
- Schwab, V.F., Sachs, J.P., 2009. The measurement of D/H ratio in alkenones and their isotopic heterogeneity. *Organic Geochemistry* 40, 111-118.
- Schwab, V.F., Sachs, J.P., 2011. Hydrogen isotopes in individual alkenones from the Chesapeake Bay estuary. *Geochimica et Cosmochimica Acta* 75, 7552-7565.
- Scussolini, P., Marino, G., Brummer, G.-J.A., Peeters, F.J.C., 2015. Saline Indian Ocean waters invaded the South Atlantic thermocline during glacial termination II. *Geology* 43, 139-142.
- Scussolini, P., Peeters, F.J.C., 2013. A record of the last 460 thousand years of upper ocean stratification from the central Walvis Ridge, South Atlantic. *Paleoceanography* 28, 426-439.
- Scussolini, P., van Sebille, E., Durgadoo, J.V., 2013. Paleo Agulhas rings enter the subtropical gyre during the penultimate deglaciation. *Climate of the Past* 9, 2631-2639.
- Sessions, A.L., Burgoyne, T.W., Schimmelmann, A., Hayes, J.M., 1999. Fractionation of hydrogen isotopes in lipid biosynthesis. *Organic Geochemistry* 30, 1193-1200.

- Sessions, A.L., Hayes, J.M., 2005. Calculation of hydrogen isotopic fractionations in biogeochemical systems. *Geochimica et Cosmochimica Acta* 69, 593-597.
- Sessions, A.L., Sylva, S.P., Summons, R.E., Hayes, J.M., 2004. Isotopic exchange of carbon-bound hydrogen over geologic timescales. *Geochimica et Cosmochimica Acta* 68, 1545-1559.
- Shackleton, N., 1974. Attainment of isotopic equilibrium between ocean water and the benthonic foraminifera genus *Uvigerina*: isotopic changes in the ocean during the last glacial. *Colloques Internationaux du Centre national de la recherche scientifique*.
- Shackleton, N.J., 1967. Oxygen isotope analyses and Pleistocene temperatures re-assessed. *Nature* 215, 15-17.
- Shackleton, N.J., 1987. Oxygen isotopes, ice volume and sea level. *Quaternary Science Reviews* 6, 183-190.
- Shah, S.R., Mollenhauer, G., Ohkouchi, N., Eglinton, T.I., Pearson, A., 2008. Origins of archaeal tetraether lipids in sediments: Insights from radiocarbon analysis. *Geochimica et Cosmochimica Acta* 72, 4577-4594.
- Sicre, M.A., Labeyrie, L., Ezat, U., Duprat, J., Turon, J.L., Schmidt, S., Michel, E., Mazaud, A., 2005. Mid-latitude Southern Indian Ocean response to Northern Hemisphere Heinrich events. *Earth and Planetary Science Letters* 240, 724-731.
- Siddorn, J.R., Bowers, D.G., Hoguane, A.M., 2001. Detecting the Zambezi River plume using observed optical properties. *Marine Pollution Bulletin* 42, 942-950.
- Sijp, W.P., England, M.H., 2009. Southern hemisphere Westerly wind control over the ocean's thermohaline circulation. *Journal of Climate* 22, 1277-1286.
- Sikes, E.L., Howard, W.R., Samson, C.R., Mahan, T.S., Robertson, L.G., Volkman, J.K., 2009. Southern Ocean seasonal temperature and Subtropical Front movement on the South Tasman Rise in the late Quaternary. *Paleoceanography* 24, PA2201.
- Simon, M.H., Arthur, K.L., Hall, I.R., Peeters, F.J.C., Loveday, B.R., Barker, S., Ziegler, M., Zahn, R., 2013. Millennial-scale Agulhas Current variability and its implications for salt-leakage through the Indian–Atlantic Ocean Gateway. *Earth and Planetary Science Letters* 383, 101-112.
- Simpson, H.J., Herczeg, A.L., 1991. Stable isotopes as an indicator of evaporation in the River Murray, Australia. *Water Resources Research* 27, 1925-1935.
- Sinninghe Damsté, J.S.S., Schouten, S., Hopmans, E.C., van Duin, A.C.T., Geenevasen, J.A.J., 2002. Crenarchaeol: the characteristic core glycerol dibiphytanyl glycerol tetraether membrane lipid of cosmopolitan pelagic crenarchaeota. *Journal of Lipid Research* 43, 1641-1651.
- Skinner, L.C., Fallon, S., Waelbroeck, C., Michel, E., Barker, S., 2010. Ventilation of the Deep Southern Ocean and Deglacial CO₂ Rise. *Science* 328, 1147-1151.
- Skinner, L.C., Scrivner, A.E., Vance, D., Barker, S., Fallon, S., Waelbroeck, C., 2013. North Atlantic versus Southern Ocean contributions to a deglacial surge in deep ocean ventilation. *Geology* 41, 667-670.
- Smythe-Wright, D., Chapman, P., Rae, C.D., Shannon, L.V., Boswell, S.M., 1998. Characteristics of the South Atlantic subtropical frontal zone between 15°W and 5°E. *Deep Sea Research Part I: Oceanographic Research Papers* 45, 167-192.
- Soden, B.J., Held, I.M., 2006. An assessment of climate feedbacks in coupled ocean–atmosphere models. *Journal of Climate* 19, 3354-3360.
- Speich, S., Blanke, B., Madec, G., 2001. Warm and cold water routes of an O.G.C.M. thermohaline conveyor belt. *Geophysical Research Letters* 28, 311-314.

- Spooner, M.I., De Deckker, P., Barrows, T.T., Fifield, L.K., 2011. The behaviour of the Leeuwin Current offshore NW Australia during the last five glacial–interglacial cycles. *Global and Planetary Change* 75, 119-132.
- Srivastava, R., Ramesh, R., Jani, R.A., Anilkumar, N., Sudhakar, M., 2010. Stable oxygen, hydrogen isotope ratios and salinity variations of the surface Southern Indian Ocean waters. *Current Science* 99, 1395-1399.
- Stocker, T.F., Johnsen, S.J., 2003. A minimum thermodynamic model for the bipolar seesaw. *Paleoceanography* 18, 1087.
- Stocker, T.F., Schmittner, A., 1997. Influence of CO₂ emission rates on the stability of the thermohaline circulation. *Nature* 388, 862-865.
- Strain, P.M., Tan, F.C., 1993. Seasonal evolution of oxygen isotope-salinity relationships in high-latitude surface waters. *Journal of Geophysical Research: Oceans* 98, 14589-14598.
- Stramma, L., England, M., 1999. On the water masses and mean circulation of the South Atlantic Ocean. *Journal of Geophysical Research: Oceans* 104, 20863-20883.
- Stramma, L., Lutjeharms, J.R.E., 1997. The flow field of the subtropical gyre of the South Indian Ocean. *Journal of Geophysical Research: Oceans* 102, 5513-5530.
- Ternois, Y., Sicre, M.-A., Boireau, A., Beaufort, L., Miquel, J.-C., Jeandel, C., 1998. Hydrocarbons, sterols and alkenones in sinking particles in the Indian Ocean sector of the Southern Ocean. *Organic Geochemistry* 28, 489-501.
- Thomsen, L., Gust, G., 2000. Sediment erosion thresholds and characteristics of resuspended aggregates on the western European continental margin. *Deep Sea Research Part I: Oceanographic Research Papers* 47, 1881-1897.
- Tiwari, M., Nagoji, S.S., Kartik, T., Drishya, G., Parvathy, R.K., Rajan, S., 2013. Oxygen isotope-salinity relationships of discrete oceanic regions from India to Antarctica vis-à-vis surface hydrological processes. *Journal of Marine Systems* 113–114, 88-93.
- Tucholke, B.E., Embley, R.W., 1984. Cenozoic regional erosion of the abyssal sea floor off South Africa. *American Association of Petroleum Geologists, Tulsa, Oklahoma*.
- Ullgren, J.E., van Aken, H.M., Ridderinkhof, H., de Ruijter, W.P.M., 2012. The hydrography of the Mozambique Channel from six years of continuous temperature, salinity, and velocity observations. *Deep Sea Research Part I: Oceanographic Research Papers* 69, 36-50.
- Urey, H.C., Lowenstam, H.A., Epstein, S., McKinney, C.R., 1951. Measurement of paleotemperatures and temperatures of the Upper Cretaceous of England, Denmark, and the southeastern United States. *Geological Society of America Bulletin* 62, 399-416.
- van Aken, H.M., van Veldhoven, A.K., Veth, C., de Ruijter, W.P.M., van Leeuwen, P.J., Drijfhout, S.S., Whittle, C.P., Rouault, M., 2003. Observations of a young Agulhas ring, Astrid, during MARE in March 2000. *Deep Sea Research Part II: Topical Studies in Oceanography* 50, 167-195.
- van Ballegooyen, R.C., Gründlingh, M.L., Lutjeharms, J.R.E., 1994. Eddy fluxes of heat and salt from the southwest Indian Ocean into the southeast Atlantic Ocean: A case study. *Journal of Geophysical Research: Oceans* 99, 14053-14070.
- Van der Lubbe, J.J.L., Tjallingii, R., Prins, M.A., Brummer, G.-J.A., Jung, S.J.A., Kroon, D., Schneider, R.R., 2014. Sedimentation patterns off the Zambezi River over the last 20.000years. *Marine Geology*.
- van der Meer, M.T.J., Baas, M., Rijkstra, W.I.C., Marino, G., Rohling, E.J., Sinninghe Damsté, J.S., Schouten, S., 2007. Hydrogen isotopic compositions of long-chain alkenones record freshwater flooding of the Eastern Mediterranean at the onset of sapropel deposition. *Earth and Planetary Science Letters* 262, 594-600.

- van der Meer, M.T.J., Benthien, A., Bijma, J., Schouten, S., Sinninghe Damsté, J.S., 2013. Alkenone distribution impacts the hydrogen isotopic composition of the C_{37:2} and C_{37:3} alkan-2-ones in *Emiliana huxleyi*. *Geochimica et Cosmochimica Acta* 111, 162-166.
- van der Meer, M.T.J., Sangiorgi, F., Baas, M., Brinkhuis, H., Sinninghe Damsté, J.S., Schouten, S., 2008. Molecular isotopic and dinoflagellate evidence for Late Holocene freshening of the Black Sea. *Earth and Planetary Science Letters* 267, 426-434.
- van Sebille, E., Beal, L.M., Johns, W.E., 2011. Advective Time Scales of Agulhas Leakage to the North Atlantic in Surface Drifter Observations and the 3D OFES Model. *Journal of Physical Oceanography* 41, 1026-1034.
- van Sebille, E., Biastoch, A., van Leeuwen, P.J., de Ruijter, W.P.M., 2009. A weaker Agulhas Current leads to more Agulhas leakage. *Geophysical Research Letters* 36, 4.
- van Sebille, E., van Leeuwen, P.J., Biastoch, A., de Ruijter, W.P.M., 2010. On the fast decay of Agulhas rings. *Journal of Geophysical Research: Oceans* 115, C03010.
- Vázquez Riveiros, N., Waelbroeck, C., Skinner, L., Roche, D.M., Duplessy, J.-C., Michel, E., 2010. Response of South Atlantic deep waters to deglacial warming during Terminations V and I. *Earth and Planetary Science Letters* 298, 323-333.
- Vellinga, M., Wood, R., 2002. Global climatic impacts of a collapse of the Atlantic Thermohaline Circulation. *Climatic Change* 54, 251-267.
- Veres, D., Bazin, L., Landais, A., Toyé Mahamadou Kele, H., Lemieux-Dudon, B., Parrenin, F., Martinerie, P., Blayo, E., Blunier, T., Capron, E., 2013. The Antarctic ice core chronology (AICC2012): an optimized multi-parameter and multi-site dating approach for the last 120 thousand years. *Climate of the Past* 9, 1733-1748.
- Verity, P.G., Yoder, J.A., Stephen Bishop, S., Nelson, J.R., Craven, D.B., Blanton, J.O., Robertson, C.Y., Tronzo, C.R., 1993. Composition, productivity and nutrient chemistry of a coastal ocean planktonic food web. *Continental Shelf Research* 13, 741-776.
- Vidal, L., Labeyrie, L., Cortijo, E., Arnold, M., Duplessy, J.C., Michel, E., Becqué, S., van Weering, T.C.E., 1997. Evidence for changes in the North Atlantic Deep Water linked to meltwater surges during the Heinrich events. *Earth and Planetary Science Letters* 146, 13-27.
- Volkman, J.K., 1986. A review of sterol markers for marine and terrigenous organic matter. *Organic Geochemistry* 9, 83-99.
- Volkman, J.K., 2000. Ecological and environmental factors affecting alkenone distributions in seawater and sediments. *Geochemistry, Geophysics, Geosystems* 1, 1036.
- Volkman, J.K., Eglinton, G., Corner, E.D.S., Forsberg, T.E.V., 1980. Long-chain alkenes and alkenones in the marine coccolithophorid *Emiliana huxleyi*. *Phytochemistry* 19, 2619-2622.
- Volkman, J.K., Maxwell, J.R., 1986. Acyclic isoprenoids as biological markers. *Methods in geochemistry and geophysics* 24, 1-42.
- Waelbroeck, C., Labeyrie, L., Michel, E., Duplessy, J.C., McManus, J.F., Lambeck, K., Balbon, E., Labracherie, M., 2002. Sea-level and deep water temperature changes derived from benthic foraminifera isotopic records. *Quaternary Science Reviews* 21, 295-305.
- Walford, H.L., White, N.J., Sydow, J.C., 2005. Solid sediment load history of the Zambezi Delta. *Earth and Planetary Science Letters* 238, 49-63.
- Walsh, E.M., Ingalls, A.E., Keil, R.G., 2008. Sources and transport of terrestrial organic matter in Vancouver Island fjords and the Vancouver-Washington Margin: A multiproxy approach using delta C-13(org), lignin phenols, and the ether lipid BIT index. *Limnology and Oceanography* 53, 1054-1063.

- Wang, Y.V., Larsen, T., Leduc, G., Andersen, N., Blanz, T., Schneider, R.R., 2013a. What does leaf wax δD from a mixed C_3/C_4 vegetation region tell us? *Geochimica et Cosmochimica Acta* 111, 128-139.
- Wang, Y.V., Leduc, G., Regenbergh, M., Andersen, N., Larsen, T., Blanz, T., Schneider, R.R., 2013b. Northern and southern hemisphere controls on seasonal sea surface temperatures in the Indian Ocean during the last deglaciation. *Paleoceanography* 28, 2013PA002458.
- Watanabe, T., Winter, A., Oba, T., 2001. Seasonal changes in sea surface temperature and salinity during the Little Ice Age in the Caribbean Sea deduced from Mg/Ca and $^{18}O/^{16}O$ ratios in corals. *Marine Geology* 173, 21-35.
- Webster, P.J., Moore, A.M., Loschnigg, J.P., Leben, R.R., 1999. Coupled ocean-atmosphere dynamics in the Indian Ocean during 1997-98. *Nature* 401, 356-360.
- Weijer, W., De Ruijter, W.P.M., Sterl, A., Drijfhout, S.S., 2002. Response of the Atlantic overturning circulation to South Atlantic sources of buoyancy. *Global and Planetary Change* 34, 293-311.
- Williams, M., Dunkerley, D., De Deckker, P., Kershaw, P., Chappell, J., 1998. Quaternary environments, 2nd edition ed. Arnold, London.
- Wolhowe, M.D., Prah, F.G., Probert, I., Maldonado, M., 2009. Growth phase dependent hydrogen isotopic fractionation in alkenone-producing haptophytes. *Biogeosciences* 6, 1681-1694.
- Wood, R.A., Keen, A.B., Mitchell, J.F.B., Gregory, J.M., 1999. Changing spatial structure of the thermohaline circulation in response to atmospheric CO_2 forcing in a climate model. *Nature* 399, 572-575.
- Wuchter, C., Schouten, S., Wakeham, S.G., Sinninghe Damsté, J.S., 2006. Archaeal tetraether membrane lipid fluxes in the northeastern Pacific and the Arabian Sea: Implications for TEX_{86} paleothermometry. *Paleoceanography* 21, PA4208.
- Xie, S., Nott, C., Avsejs, L., Volders, F., Maddy, D., Chambers, F., Gledhill, A., Carter, J., Evershed, R., 2000. Palaeoclimate records in compound-specific δD values of a lipid biomarker in ombrotrophic peat. *Organic Geochemistry* 31, 1053-1057.
- Zell, C., Kim, J.-H., Moreira-Turcq, P., Abril, G., Hopmans, E.C., Bonnet, M.-P., Sobrinho, R.L., Sinninghe Damsté, J.S., 2013. Disentangling the origins of branched tetraether lipids and crenarchaeol in the lower Amazon River: Implications for GDGT-based proxies. *Limnol. Oceanogr* 58, 343-353.

Summary

The extent of the general warming related to increasing anthropogenic CO₂ emission and its implications for the global climate system are currently under heavy debate. In particular the extrapolation of long term climatic trends relies on complex climate models for the interaction between the atmosphere, the oceans and the land surface. In turn these models require validation based on continuous time series of observational data. However, instrumental based data records only extend as far back as approximately 150 years and thus make the validation of long-term modelling experiments difficult. To obtain information on past climate beyond the instrumental period, so-called paleoceanographic proxies are used. Two of the most targeted paleoceanographic parameters are the sea surface temperature (SST) and sea surface salinity, which determine water density. While past ocean temperatures can be reconstructed relatively accurately from various independent methods, the accurate reconstruction of past ocean salinity has proven to be more difficult. A promising new method for the reconstruction of past ocean salinity has been suggested to come from the hydrogen isotope composition of long chain alkenones ($\delta D_{\text{alkenone}}$) derived from marine haptophyte algae. Culture studies have shown a strong correlation between hydrogen isotope fractionation and salinity, with decreasing fractionation with increasing salinity. In order to test the applicability of the $\delta D_{\text{alkenone}}$ as a salinity proxy, this thesis presents studies on sedimentary records obtained from various open ocean settings including the greater Agulhas System south of the African continent, the Eastern Tropical Atlantic and the Atlantic sector of the Southern Ocean, as well as coastal ocean margin settings in the Mozambique Channel and offshore Southeast Australia.

The $\delta D_{\text{alkenone}}$ from two sediment records located in the Agulhas Leakage area, covering the last two glacial terminations, showed substantial hydrogen isotopic shifts from more D-enriched alkenones during the glacial towards relatively more D-depleted alkenones during the interglacials. This pattern was in good agreement with planktonic foraminiferal based sea water oxygen isotope ($\delta^{18}\text{O}_{\text{sw}}$) records, suggesting a glacial-interglacial freshening in the Agulhas leakage area. This trend could be explained by the generally weaker Agulhas Leakage during glacial periods as a response to changing wind field stress, the expansion of sea ice and the northward displacement of the subtropical fronts. As a result, the transport of Indian Ocean water into the Atlantic was likely less efficient and a potentially increased back transport of the Indian Ocean water occurred via the Agulhas Return Current, possibly leading to more saline conditions during glacials and subsequent freshening during the glacial terminations.

Application of the $\delta D_{\text{alkenone}}$ salinity proxy in the upstream region of the Agulhas Current provided evidence that upper water mass salinities in the Agulhas leakage signal might have been controlled by upstream dynamics in the southern Agulhas Current without a significant change in the actual Agulhas leakage into the South Atlantic. Instead, more saline southern Agulhas Current waters were potentially propagated to the Agulhas Leakage area during glacial termination periods implying that periods of higher salinity in the source region did not necessarily entail a greater fraction of Indian Ocean water entering the South Atlantic Ocean, as initially inferred from the salinity proxy records in the Agulhas Leakage area.

A comparison of the hydrogen isotope fractionation factor $\alpha_{\text{alkenone-sw}}$ with $\delta^{18}\text{O}_{\text{sw}}$ reconstructions in the eastern tropical Atlantic Ocean showed similar patterns, suggesting both proxy records reflected salinity. Differences were observed for the period between marine isotope stage (MIS) 5 - MIS2 where $\delta^{18}\text{O}_{\text{sw}}$ reconstructions showed only little variation, while $\alpha_{\text{alkenone-sw}}$ indicated more pronounced variability. This is potentially related to variability in growth rate of the alkenone producers. However, a comparison of the $\delta\text{D}_{\text{alkenone}}$ record with $\delta^{18}\text{O}_{\text{sw}}$ reconstructions from the western subtropical Atlantic showed a fairly good agreement during this time period, suggesting that changes in salinity occurred basin-wide in the tropical Atlantic. The relatively good agreement of the $\delta\text{D}_{\text{alkenone}}$ with the carbon isotope record of benthic foraminifera suggest a connection between AMOC strength variability and relative salinity shifts during MIS5 and MIS6 as well as during MIS3 and MIS4 at the core site.

The $\delta\text{D}_{\text{alkenone}}$ was used to trace allochthonous input of alkenones in the Atlantic Sector of the Southern Ocean. Here, SSTs reconstructed using the distribution of alkenones indicate a relatively warm glacial, in contrast to distinctively cold glacial SST conditions indicated temperature records based upon planktonic foraminiferal $\delta^{18}\text{O}$ values and distribution of Thaumarchaeotal lipids. The observed shift towards more negative values in $\delta\text{D}_{\text{alkenone}}$ during the glacial – interglacial transition was only slightly higher than expected based on global ice volume changes. This suggests that indeed the alkenones might have been allochthonous and synthesized in warmer water masses with similar or slightly higher salinity during the glacial and transported to the core site.

A 39 kyr record of $\delta\text{D}_{\text{alkenone}}$ values obtained from the Eastern African continental shelf in the Mozambique Channel showed, in contrast to open ocean records, no clear glacial – interglacial trend. In contrast to present day, the core site was in closer proximity to the continent during glacial sea level low stand, resulting in a much larger effect of freshwater run off. These conditions probably led to relatively low salinity and therefore an increased isotopic fractionation of hydrogen during alkenone biosynthesis, resulting in the apparent lack of glacial-interglacial trend in the $\delta\text{D}_{\text{alkenone}}$ record. On top of that a positive correlation between $\delta\text{D}_{\text{alkenone}}$ and values for the branched isoprenoid tetraether (BIT) index, a proxy for the input of soil organic matter, is observed during the glacial period. This possibly indicated an increasing contribution to alkenone production by coastal haptophyte species, which is supported by elevated ratios of C_{37}/C_{38} alkenones.

In contrast, a coastal marine 135 kyr $\delta\text{D}_{\text{alkenone}}$ record off the continental shelf of South Australia in front of the River Murray did show a strong glacial – interglacial pattern, in good agreement with a planktonic foraminiferal $\delta^{18}\text{O}$ record. Despite increased terrestrial influence, as inferred from elevated BIT values, during sea level low stands via the Murray river, records of alkenone accumulation rate and the alkenone C_{37}/C_{38} ratio suggested that species composition or growth rate changes in the haptophyte producers did not substantially affect the $\delta\text{D}_{\text{alkenone}}$ variability in this record. This suggests that $\delta\text{D}_{\text{alkenone}}$ record at this core site was influenced by freshwater runoff to a lesser extent than that in the Mozambique Channel. In general, the glacial periods (i.e. late MIS6, MIS4 and MIS2) were marked by more D-enriched alkenones compared to interglacial periods, indicating a freshening during glacial terminations. This input of low salinity water is likely derived from the southwards flowing Leeuwin Current, which was elevated during deglaciations and interglacials.

In summary, results described in this thesis have shown that the hydrogen isotope fractionation as reflected in long chain alkenones is a promising proxy for assessing changes in past ocean salinity. Multi-millennial sediment records of $\delta D_{\text{alkenone}}$ generally agreed well with planktonic foraminifera $\delta^{18}O$ records from open ocean and near coastal settings. Estimation of absolute salinity shifts, based on culture derived salinity $\alpha_{\text{alkenone-sw}}$ relationships also corresponded reasonably well with estimations based on planktonic foraminifera $\delta^{18}O_{\text{sw}}$ reconstructions. However, using $\alpha_{\text{alkenone-sw}}$ for calculating absolute salinities requires an estimation of the hydrogen isotope composition of the past ocean, which results in larger uncertainties. This problem may be resolved in the future by using multiple relationships of α for different compounds, e.g. sterols.

Samenvatting

De mate van opwarming van de Aarde als gevolg van de uitstoot van broeikasgassen en de gevolgen hiervan voor het klimaat is onderwerp van hevige discussie. Toekomstvoorspellingen van het klimaat zijn voornamelijk gebaseerd op complexe computermodellen die de interactie tussen de atmosfeer, de oceanen en het landoppervlak beschrijven. Deze klimaatmodellen worden gevalideerd met behulp van lange termijn observaties van bijvoorbeeld temperatuur. Instrumentale klimaatgegevens zijn echter alleen beschikbaar voor ongeveer de laatste 150 jaar, hetgeen het testen van klimaatmodellen lastig maakt. Om klimaatinformatie van voor deze (instrumentale) periode te verkrijgen, worden zogenaamde proxies gebruikt. Twee van de meest belangrijke klimaatparameters voor reconstructie zijn de oppervlakte zeevatertemperatuur (OZT) en het zoutgehalte van oppervlaktewater. Deze factoren bepalen samen de dichtheid van zeewater. Terwijl de OZT relatief nauwkeurig kan worden gereconstrueerd met behulp van verschillende onafhankelijke methoden, is een nauwkeurige reconstructie van het zoutgehalte erg lastig. Een veelbelovende nieuwe aanpak voor de reconstructie van het zoutgehalte van oceanen is gebaseerd op de waterstofisotopensamenstelling van lang-ketige alkenonen ($\delta D_{\text{alkenone}}$), organische verbindingen die worden geproduceerd door mariene Haptophyte algen. Cultuurstudies hebben aangetoond dat er een sterke relatie bestaat tussen de waterstofisotoopfractionering en het zoutgehalte van het kweekmedium tijdens de productie deze alkenonen; met toenemend zoutgehalte werd een afname in de isotoopfractionering waargenomen. In dit proefschrift is de toepassing van $\delta D_{\text{alkenone}}$ als een proxy voor zoutgehalte in mariene milieus getest. Hiervoor zijn meerdere sedimentafzettingen onderzocht van verschillende tijdsperiodes en uit verschillende mariene milieus, namelijk de Agulhas stroom ten zuiden van het Afrikaanse continent, de oostelijke tropische Atlantische Oceaan en de Atlantische sector van de Zuidelijke Oceaan. Naast deze open oceaangebieden werd de proxy voor zoutgehalte ook getest in sedimentafzettingen uit grensgebieden tussen de kust en open oceaan, zoals in de Straat van Mozambique en in het gebied net buiten de kust van Zuidoost-Australië.

De $\delta D_{\text{alkenone}}$ werd bepaald van twee sedimentkernen genomen in het gebied waar de Agulhas stroom, een stroming in de zuidwestelijke Indische Ocean langs de kust van zuidelijk Afrika, uitstroomt in de zuidelijke Atlantische Oceaan (zogenaamde Agulhas uitstroomgebied). De $\delta D_{\text{alkenone}}$ records, die de laatste twee glaciale terminaties (i.e. de overgang van een glaciaal naar een interglaciaal) beslaan, laten aanzienlijke verschuivingen zien in de waterstofisotoopsamenstelling van de alkenonen met relatief zware of D-verrijkte alkenonen tijdens de glacialen en relatief lichte of D-verarmde alkenonen tijdens de interglacialen. Dit patroon in waterstofisotoopsamenstelling is erg vergelijkbaar met reconstructies van de zuurstofisotoopsamenstelling van zeewater ($\delta^{18}O_{\text{zw}}$) gebaseerd op planktonische foraminiferen. Dit suggereert dat tijdens glaciale terminaties het zoutgehalte in het gebied van de uitstroom van de Agulhas is afgenomen. Een mogelijke verklaring daarvoor is het verminderde transport van Agulhas water tijdens de glacialen naar de zuidelijke Atlantische Oceaan als gevolg van verandering in het windveld, de uitbreiding van zeeijs vanuit het zuiden en de verschuiving van het subtropische front naar het noorden. Hierdoor was het transport van water uit de Indische Oceaan naar de Atlantische Oceaan minder efficiënt en

dat leidde mogelijk tot een verhoogde terugstroom van water van de Indische oceaan naar het oosten via de Agulhas terugstroom. Deze relatief zwakke Agulhasstroom zou kunnen resulteren in een algemene verhoging van het zoutgehalte in het gehele gebied waar de Agulhas doorheen stroomt, inclusief het uitstroomgebied, tijdens het glaciaal en een afname van het zoutgehalte tijdens de glacial terminatie.

De toepassing van $\delta D_{\text{alkenone}}$ als indicator voor zoutgehalte stroomopwaarts van het Agulhasgebied laat zien dat het zoutgehalte van de bovenste watermassa in het uitstroomgebied mogelijk direct gerelateerd is aan de dynamiek stroomopwaarts van de Agulhasgebied. Het zoutere water uit het Zuid Agulhasgebied is waarschijnlijk de oorzaak van het zoutere water in het uitstroomgebied tijdens de glaciaal terminaties. Dit houdt mogelijk in dat perioden met hogere zoutgehaltes in de Agulhas brongebieden niet automatisch ook leidden tot een grotere fractie Indische Oceaan water dat de Zuidelijk Atlantische Oceaan binnenkomt, zoals oorspronkelijk gedacht.

Veranderingen in de waterstofisotopfractionatiefactor $\alpha_{\text{alkenone-zw}}$ en $\delta^{18}\text{O}_{\text{zw}}$ in een sedimentkern uit de oostelijke tropische Atlantische Oceaan laten vergelijkbare patronen zien. Dit suggereert dat beide proxies het zoutgehalte weerspiegelen. Er werden echter verschillen waargenomen tussen deze parameters in de tijdsperiode tussen de mariene isotopstadia (MIS) 5 en MIS 2, waar de gereconstrueerde $\delta^{18}\text{O}_{\text{sw}}$ minder varieerde dan de $\alpha_{\text{alkenone-sw}}$. De relatief hoge variabiliteit in $\alpha_{\text{alkenone-sw}}$ in deze periode zou te wijten kunnen zijn aan veranderingen in de groeisnelheden van de algen die de alkenonen produceerde. Echter, de variabiliteit in $\delta D_{\text{alkenone}}$ komt goed overeen met gereconstrueerde $\delta^{18}\text{O}_{\text{sw}}$ van de westerse tropische Atlantische Oceaan. Dit suggereert dat de $\delta D_{\text{alkenone}}$ veranderingen in het zoutgehalte van zeewater registreerde en dat deze over de gehele tropische Atlantische Oceaan hebben plaatsgevonden. De relatief goede correlatie tussen $\delta D_{\text{alkenone}}$ en de stabiele koolstofisotopsamenstelling ($\delta^{13}\text{C}$) van benthische foraminiferen uit dezelfde kern suggereert een connectie tussen de sterkte van de zogenaamde Atlantische Meridionale Omslaande Circulatie (AMOC) en de verandering in zoutgehalte, vooral in de tijdsperiodes tussen MIS5 en MIS6 en tussen MIS3 en MIS4.

In de Atlantische sector van de Zuidelijke Oceaan werd de $\delta D_{\text{alkenone}}$ gebruikt om een inschatting te maken of de alkenonen in het sediment lokaal geproduceerd waren of van verder weg naar de locatie van de kern waren getransporteerd. Temperatuurreconstructies op basis van alkenonen gaven aan dat de ijstijd relatief warm was, in tegenstelling met temperatuurreconstructies op basis van andere proxies zoals de $\delta^{18}\text{O}$ van planktonische foraminiferen en de distributie van de lipiden van Thaumarchaeota (TEX_{86}). De verandering naar meer negatieve $\delta D_{\text{alkenone}}$ waarden tijdens de overgang van het glaciaal naar het interglaciaal was iets groter dan op basis van het isotopeneffect als gevolg van ijsvolume veranderingen werd verwacht. Dit alles suggereert dit dat alkenonen in dit gebied niet lokaal zijn geproduceerd maar waarschijnlijk oorspronkelijk werden gesynthetiseerd in warmere watermassa's met een vergelijkbare of iets hoger zoutgehalte, waarna ze getransporteerd werden naar de studielocatie.

Een $\delta D_{\text{alkenone}}$ sedimentarchief uit de Straat van Mozambique op het continentaal plat voor de Oost-Afrikaanse kust, dat de laatste 39 duizend jaar beslaat, laat, in tegenstelling tot open mariene sedimentkernen, geen duidelijke glaciaal-interglaciaal trend zien. In tegenstelling tot vandaag de dag was de locatie van de sedimentkern tijdens de relatief lage zeespiegelstand in het laatste glaciaal

dichter bij het continent. Dit resulteerde in een toegenomen invloed van zoetwater, voornamelijk door aanvoer via rivieren, resulterend in een relatief laag zoutgehalte. Dit ging gepaard met een toename in de waterstofisotopfractionatie tijdens de biosynthese van alkenonen. Deze toename heeft waarschijnlijk de schijnbare afwezigheid van de typische glaciaal-interglaciaal trend in de $\delta D_{\text{alkenone}}$ veroorzaakt. Daarnaast is er een duidelijk positieve correlatie tussen de $\delta D_{\text{alkenone}}$ en de vertakte Isoprenoïde Tetraether (BIT) index, een indicator voor organisch materiaal afkomstig uit bodems, in sedimenten afgezet in het glaciaal. Dit is mogelijk een indicatie voor een grotere bijdrage van alkenonen afkomstig van meer kustgebonden Haptophyte algensoorten. Dit wordt ondersteund door een hogere C_{37}/C_{38} alkenonen verhouding gedurende deze periode.

In tegenstelling tot de sedimentkern uit de Straat van Mozambique, laat de $\delta D_{\text{alkenone}}$ uit een sedimentkern van het continentaal plat voor Zuid-Australië, dicht bij de rivier Murray, wel een sterk glaciaal-interglaciaal patroon zien, vergelijkbaar met de $\delta^{18}O$ van de planktonische foraminiferen. Ondanks de verhoogde aanvoer van terrestrisch materiaal via de Murray rivier tijdens de glaciale laagstand van de zeespiegel, zoals verhoogde BIT waarden aangeven, laten de accumulatiesnelheid van alkenonen en de C_{37}/C_{38} alkenonenverhouding zien dat veranderingen in soortsaamenstelling of groeisnelheid van de Haptophyten slechts geringe invloed hebben op de variabiliteit van $\delta D_{\text{alkenone}}$. Dit betekent dat de $\delta D_{\text{alkenone}}$ in deze sedimenten minder door zoetwatertoevoer werd beïnvloed dan in de Straat van Mozambique. In het algemeen worden de glaciale periodes (laat MIS6, MIS4, en MIS2) vooral gekenmerkt door een verrijking van D in de alkenonen ten opzichte van de interglaciale periodes, hetgeen wijst op lagere zoutgehaltes. Deze lagere zoutgehaltes kunnen veroorzaakt zijn door relatief meer toevoer van zoeter water afkomstig van de Leeuwin stroom, die het gebied tijdens het interglaciaal beïnvloed heeft.

Samenvattend laten de resultaten die worden beschreven in dit proefschrift zien dat de stabiele waterstofisotopsamenstelling van lang-ketige alkenonen een veelbelovende proxy is voor het reconstrueren van veranderingen in het zoutgehalte van de zee water. Metingen van $\delta D_{\text{alkenone}}$ in sedimentkernen uit open zee- en kustgebieden laten goede overeenkomsten met de zuurstofisotopsamenstelling van planktonische foraminiferen zien. Gereconstrueerde veranderingen in het zoutgehalte, gebaseerd op de relatie tussen zoutgehalte en de waterstofisotopfractionering gemeten in het laboratorium, komen redelijk goed overeen met de gereconstrueerde waarden op basis van de $\delta^{18}O$ van planktonische foraminiferen. Voor het berekenen van de absolute zoutgehaltes is echter de waterstofisotopsamenstelling van zee water nodig en dat is momenteel nog steeds een grote bron van onzekerheid in de berekening van absolute saliniteit. Dit probleem kan mogelijk in de toekomst worden opgelost door het bepalen van waterstofisotopfractionaties bij variërende saliniteit voor meerdere lipiden, zoals bij voorbeeld sterolen.

Zusammenfassung

Das Ausmaß der im Zusammenhang mit ansteigender CO₂ Emissionen stehenden allgemeinen Erderwärmung und dessen Implikationen für das globale Klima stehen derzeit unter heftiger Debatte. Dabei stützt sich im Besonderen die Extrapolation von klimatischen Langzeittrends auf komplexe Modelle zur Interaktion zwischen der Atmosphäre, den Ozeanen und der Landoberfläche. Diese Langzeitklimamodelle benötigen wiederum eine Validierung durch Langzeitbeobachtungen, z.B. der Temperatur. Kontinuierliche Aufzeichnungen solcher Messwerte reichen jedoch nur etwa 150 Jahre zurück in die Vergangenheit und verkomplizieren somit die Validierung von Langzeitmodellen. Um an Informationen über diese instrumentelle Periode hinaus zu gelangen, werden unter anderem so genannte paläozeanographische Proxies herangezogen. Zwei der am häufigsten genutzten paläozeanographischen Proxies dienen zur Rekonstruktion der Meeresoberflächentemperatur (Englischen sea surface temperatures: SST), sowie des Salzgehalt (=Salinität; Englisch sea surface salinity: SSS). Beide Faktoren zusammen bestimmen maßgeblich die Dichte des Meeresswassers und schließlich dessen Strömungsverhalten. Während SST relativ präzise mit verschiedenen unabhängigen Methoden rekonstruiert werden kann, gestaltet sich die Rekonstruktion der Salinität aufwendiger. Ein vielversprechender neuer Ansatz zur Salinitätsrekonstruktion vergangener Ozeane basiert auf der Wasserstoffisotopenzusammensetzung von langkettigen Alkenonen ($\delta D_{\text{alkenone}}$), welche durch marinen Haptophyten Algen produziert werden. Laborstudien an Kulturen dieser Algen haben gezeigt, dass beim Einbau der Wasserstoffisotope in die Alkenone ein enger Zusammenhang zwischen der Wasserstoffisotopenfraktionierung sowie des Salzgehaltes im Wachstumsmediums besteht. Dabei wurde mit zunehmendem Salzgehalt eine Abnahme in der Isotopenfraktionierung während des Einbaus von Wasserstoff in die Alkenone beobachtet. Um die Anwendbarkeit des $\delta D_{\text{alkenone}}$ als Proxy für Salinität in natürlicher Umgebung zu testen, werden in der vorliegenden Arbeit Studien an Sedimentkernen aus verschiedenen marinen Umgebungen vorgestellt. Dazugehören Lokalitäten im offenen Ozean, wie dem Agulhas System im Süden des Afrikanischen Kontinents, dem östlichen tropischen Atlantik und dem Atlantischen Sektor des Südlichen Ozeans; sowie in Randbereichen zwischen dem offenen und küstennahen Ozean im Mozambique Kanal und im Offshore-Bereich vor der Küste von Südost Australien.

Messwerte für $\delta D_{\text{alkenone}}$ aus zwei Sedimentkernen aus dem Agulhas Austrittsbereiches, während des Übergangs zwischen den letzten zwei Glaziale - Interglazialen, zeigte substantielle Verschiebungen in der Wasserstoffisotopenzusammensetzung ausgehend von Deuterium (D) angereicherten Alkenonen während der Glaziale zu D abgereicherten Alkenonen während der Interglaziale. Dieses Muster in der Isotopenzusammensetzung zeigte gute Übereinstimmung mit Rekonstruktionen zur Sauerstoffisotopenzusammensetzungen des Ozeanwassers ($\delta^{18}O_{\text{sw}}$) basierend auf planktonischen Foraminiferen. Das deutet darauf hin, dass während des Übergangs zwischen den Glazialen und Interglazialen der Salzgehalt im Agulhas Austrittsgebiet abgenommen hat. Eine Erklärung dafür könnte eine generell reduzierte Agulhas Strömung in den Südatlantik sein, die von Änderungen in der Konfiguration des Windspannungsfeldes, der Expansion von

Eismassen aus dem Süden und der Verschiebung der Subtropischen Barriere während des Glaziales verursacht wurde. Daraus resultierend wäre der Transport aus dem Indischen Ozean in den Atlantik weniger effizient gewesen und führte möglicherweise zu einem erhöhten Rückfluss des generell wärmeren und salzigeren dem Indischen Ozeanwasser mittels der Agulhas Rückflusströmung zurück in den Indischen Ozean. Demzufolge könnte eine generelle Erhöhung der Salinität im Agulhas Austrittsbereich während des Glaziales resultieren. Mit Wiederherstellung Interglazialer Bedingungen könnte darauffolgend der ansteigende Abtransport von Indischem Ozeanwasser in den Südatlantik wieder zu einer Verringerung der Salinität nach Abbruch des Glaziales geführt haben.

Die Anwendung des $\delta D_{\text{alkenone}}$ als Salinitäts-Proxy stromaufwärts im Agulhas System erbrachte Belege dafür, dass die Salinität im Übergangsbereich zwischen Indischem und Atlantischen Ozean maßgeblich von der Dynamik des Südlichen Agulhas Stroms kontrolliert wurde, ohne signifikante Änderungen in der Bilanz der in den Südatlantik transportierten Wassermassen, wie ursprünglich angenommen.

Der Vergleich zwischen dem Wasserstoffsotopenfraktionierungsfaktor $\alpha_{\text{alkenone-sw}}$ und rekonstruierten Werten für $\delta^{18}O_{\text{sw}}$ aus dem östlichen tropischen Atlantik zeigte vergleichbare Verteilungsmuster. Das deutet darauf hin, dass beide Proxies zu einem großen Teil Salinität widerspiegeln. Zwischen beiden Proxies konnten jedoch auch Unterschiede während den Marinen Isotopen Stadien (MIS) 5 – MIS 2 beobachtet werden. Diese Perioden zeigten geringe Variabilität im rekonstruierten $\delta^{18}O_{\text{sw}}$, wohingegen $\alpha_{\text{alkenone-sw}}$ eine stärker ausgeprägte Variabilität zeigte. Möglicherweise ist diese erhöhte Variabilität in $\alpha_{\text{alkenone-sw}}$ auf Schwankungen in der Wachstumsrate der Alkenonproduzenten zurückzuführen. Demgegenüber zeigte ein Vergleich des $\delta D_{\text{alkenone}}$ mit rekonstruiertem $\delta^{18}O_{\text{sw}}$ aus dem westlichen tropischen Atlantik relativ gute Übereinstimmungen während der Periode zwischen MIS5 - MIS2. Das lässt darauf schließen, dass Änderungen in der Salinität über den gesamten tropischen Atlantik stattgefunden haben könnten. Eine relative gute Übereinstimmung des $\delta D_{\text{alkenone}}$ mit der Kohlenstoffsotopenzusammensetzung ($\delta^{13}C$) aus benthischen Foraminiferen, deutet darauf hin, dass eine Verbindung zwischen der Stärke der thermohalinen Zirkulation im Nordatlantik (Englisch: Atlantic Meridional Overturning Circulation; AMOC) und der Änderung der relativen Salinität sowohl zwischen dem MIS5 und MIS6, als auch zwischen MIS3 und MIS4 bestanden hat.

Im Atlantischen Sektor des Südlichen Ozeans wurde das $\delta D_{\text{alkenone}}$ benutzt, um den Eintrag von allochthonen Alkenonen zurückzuverfolgen. Hier zeigten SST Rekonstruktionen basierend auf Alkenonen vergleichsweise warme Temperaturen während des Glaziales. Dieses steht im starken Kontrast zu niedrigen Temperaturen konstruiert auf Basis von $\delta^{18}O$ von planktonischen Foraminiferen und der Verteilung von Thaumarchaeoten Lipiden (TEX_{86}). Der zu beobachtende Trend hin zu mehr negativen Werten im $\delta D_{\text{alkenone}}$ während des Übergangs vom Glazial zum Interglazial zeigte sich nur geringfügig höher als eine zu erwartende Änderung hervorgerufen durch den isotopischen Effekt der globalen Eisvolumenänderung. Das deutet darauf hin, dass Alkenone an dieser Lokalität in der Tat allochthonen Ursprungs sind und wahrscheinlich ursprünglich in wärmeren Wassermassen mit ähnlicher oder nur leicht erhöhter Salinität synthetisiert und zur Studienlokation verfrachtet wurden.

Ein 39 ka langes Archiv von $\delta D_{\text{alkenone}}$ aus dem Mozambique Kanal am Kontinentalen Schelf vor der Küste Ostafrikas zeigt, im Gegenteil zu den vorher betrachteten vollmarinen Sedimentkernen, keinen klaren Glazial-Interglazialen Trend. Im Gegensatz zu heute lag die Lokation des Sedimentkerns während des Meeresspiegeltiefstandes im letzten Glazial sehr viel näher am Kontinent. Daraus resultierte ein erhöhter Einfluss von Süßwasser durch Flusseintrag, wie z.B. dem Sambesi Fluss. Diese Bedingungen führten höchstwahrscheinlich zu relative niedrigen Salzgehalten und einem daraus resultierenden Anstieg der Isotopenfraktionierung von Wasserstoffisotopen in den Haptophyten während der Alkenonbiosynthese. Dieses wiederum könnte das anscheinende Ausbleiben des Trends im $\delta D_{\text{alkenone}}$ während des Glazial-Interglazials erklären. Hinzu kommt eine erkennbare positive Korrelation während des Glaziales zwischen dem $\delta D_{\text{alkenone}}$ und Werten für den verzweigten Isoprenoide Tetraether Index (BIT), als Proxy für den Eintrag von terrestrischem organischem Material. Dies könnte möglicherweise auf den Anstieg einer Alkenonproduktion durch Küstenspezies der Haptophyten hindeuten. Unterstützt wird diese Hypothese durch erhöhte Werte für das Verhältnis von C_{37}/C_{38} Alkenonen, als Anzeichen für Änderungen in der Algenpezieszusammensetzung.

Im Gegensatz dazu, zeigen Werte für $\delta D_{\text{alkenone}}$ vom kontinentalen Schelf vor Südastralien in der Nähe zum River Murray für die letzten 135.000 Jahre ein ausgeprägtes Glazial-Interglazial Muster. Ein solches Muster findet sich ebenfalls im $\delta^{18}O$ aus planktonischen Foraminiferen. Trotz des verstärkten terrestrischen Einflusses, wie aus erhöhten BIT Werten zu schließen ist, schlagen Werte für Alkenonakkumulationsraten und dem Verhältnis zwischen den C_{37}/C_{38} Alkenone vor, dass Änderungen in den Wachstumsraten der Haptophyten Algen die Variabilität des $\delta D_{\text{alkenone}}$ nur geringfügig beeinflusst haben. Dies würde bedeuten, dass das $\delta D_{\text{alkenone}}$ in diesem Sedimentkern weniger durch Süßwassereintrag beeinflusst wurde als im Mozambique Kanal. Im Allgemeinen sind hier die Glazialen Perioden (spätes MIS6, MIS4 und MIS2) besonders durch Anreicherungen von D in den Alkenonen im Vergleich zu den Interglazialen gekennzeichnet, was auf einen Trend zu geringerer Salinität im Verlaufe der Glazialen Terminationen hindeutet. Der Eintrag von Wasser mit geringerer Salinität könnte dabei möglicherweise von dem südwärts fließenden Leeuwin Strom herrühren, welcher die Lokation während der Interglaziale zunehmend erreichte.

Zusammenfassend lässt sich sagen, dass die Ergebnisse, wie sie in dieser Arbeit beschrieben werden, zeigen, dass die Wasserstoffisotopenzusammensetzung aus langkettigen Alkenonen ein vielversprechender Proxy zur Beurteilung der Änderungen in der Salinität vergangener Ozeane ist. Messungen von $\delta D_{\text{alkenone}}$ an Jahrtausenden alten Sedimenten zeigen prinzipielle Übereinstimmungen mit der Sauerstoffisotopenzusammensetzung von planktonischen Foraminiferen aus offenmarinen und küstennahen Umgebungen. Rekonstruktionen von relativen Änderungen in der Salinität auf Basis der Ergebnisse aus Laborversuchen, korrespondieren relativ gut mit errechneten Werten aus dem $\delta^{18}O$ von planktonischen Foraminiferen. Dennoch werden zur Berechnung der absoluten Salinität mittels $\alpha_{\text{alkenone-sw}}$ einen Schätzwert für die Wasserstoffisotopenzusammensetzung des Meerwassers benötigt, was zurzeit noch mit großen Unsicherheiten in der Berechnung verbunden ist. Dieses Problem könnte in Zukunft mit Hilfe von multiplen Gleichungen für α von verschiedenen Komponenten, wie z.B. dem Sterol, gelöst werden.

Acknowledgment

At this point I would like to take a moment to thank all the people who were crucial for assembling this thesis. “You are nearly finished”, as I was told many times, increasingly the very last months, was what kept me pushing (Thanks Dave, Sandra and Kevin). However, I would have never reached this final stage without the guidance, input and support of Jaap and Stefan especially in the sometimes complex environment of European sciences. Further, I would like to thank all my co-authors, who put a huge amount of work and dedication into their contributions.

Although I really tried to have all graphs printed for the numerous meetings on new δD data, somehow there was always a graph missing. This brings me to an advice that goes along the lines of “don’t think too much and focus on the important things”. Marcel, I am deeply grateful for the relentless work you put into sometimes long and let’s call it “multi-focused” manuscripts of an occasionally overwhelmed PhD student. I am still trying to follow your advice, admittedly with more or less success at times. Also, I would like to thank you for all the discussions we had on the data and ideas and manuscripts and posters. I think it was a great fortune for me that you moved right next to my office and to have you as my day to day contact and supervisor.

Next I would like to thank the δD -group, mainly consisting of Dave, Sandra and Danielle. It was great fun to work with you. Dave, I would like to acknowledge all the fruitful discussions and input to the manuscripts, if you know what I mean. Danielle, thank you for helping out with preparing samples and fixing the machines. The recipe for the sugar free ontbijtkoek was pretty good I have to admit. Sandra, was soll ich sagen? Vielleicht sollten wir mal ein Bier trinken und Pizza mit viel Käse essen gehen?

Of course, I not only have to thank the δD -group, but also the entire BGC department. I really enjoyed working amongst and with you. I also would like to thank my office mates that I had over the past years for creating such a great working atmosphere. Thank you Darci, Els, Zhenia, Luke, Martina (I hope I did not forget anyone). Despite the stubborn ideas of the general public of me not showing up at parties, which apparently led to bets involving money on my (none-)appearance, I would like to thank Jort & Sharyn, Sandra, Marcel, Kevin, Craig and Jeroen for the fun evenings out in Den Helder. Een dank u gaat ook naar familie Kerseboom en alle lieve mensen die hebben geholpen me thuis voelen.

An dieser Stelle will ich mich auch bei Laura bedanken, besonders für die Hilfe zu guter Letzt. Und last but certainly not least will ich mich bei meinen Eltern Beatrix und Reinhard und meinen Brüdern Christian und Gordian bedanken. Ihr habt mir doch sehr geholfen auf viele verschiedenen Arten und Weisen. Nur um ein paar zu nennen: schnelle Umzüge, Bereitstellen eines fahrbaren Untersatzes und nicht zu unterschätzende moralische Unterstützung und viele Besuche am Meer. I had a great time working at NIOZ, which will always be a part of me.

Thank you! Bedankt! Danke!

Curriculum Vitae

Sebastian Kasper was born on the 25th of September 1983 in Heinsberg, Germany. After finishing secondary school, he went on to study Geology with focus on geochemistry and sedimentology at the Technical University of Aachen in Germany. For his graduation project, he worked on coral sclerochronology and trace element based climate reconstructions in a joint project between the RWTH Aachen University and the marine geology department of the Royal NIOZ on Texel. After his graduation in 2010, Sebastian went on to pursue his PhD research on the compound specific hydrogen isotope composition of lipids as paleo-salinity proxy in the department of marine organic biogeochemistry (BGC) at the Royal NIOZ on Texel. Currently, Sebastian works as analytical service manager at Eurofins Umwelt West in Germany.

